A TECHNICAL EVALUATION OF CONCENTRATING SOLAR THERMAL POWER GENERATION TECHNOLOGIES FOR THE UPINGTON AREA OF SOUTH AFRICA

Jonathan C. Tempies

In partial fulfillment of

Master of Science in Engineering (Electric Power and Energy Systems)

School of Engineering
University of KwaZulu-Natal

October 2012

Examiner's Copy

Supervisor: Michael J. Brooks
Co-supervisor: Professor Nelson M. Ijumba

As the candidate's Supervisor I agree/do not agree to the submission of this thesis.

Signed: _____ Date: _____
Michael J. Brooks

DECLARATION

I Jonathan C. Tempies declare that

(i) The research reported in this dissertation/thesis, except where otherwise indicated, is my original work.
(ii) This dissertation/thesis has not been submitted for any degree or examination at any other university.
(iii) This dissertation/thesis does not contain other persons' data, pictures, graphs or other information, unless specifically acknowledged as being sourced from other persons.
(iv) This dissertation/thesis does not contain other persons' writing, unless specifically acknowledged as being sourced from other researchers. Where other written sources have been quoted, then:
a) their words have been re-written but the general information attributed to them has been referenced;
b) where their exact words have been used, their writing has been placed inside quotation marks, and referenced.
(v) Where I have reproduced a publication of which I am an author, co-author or editor, I have indicated in detail which part of the publication was actually written by myself alone and have fully referenced such publications.
(vi) This dissertation/thesis does not contain text, graphics or tables copied and pasted from the Internet, unless specifically acknowledged, and the source being detailed in the dissertation/thesis and in the References sections.

Signed: _____ Date: _____

ACKNOWLEDGEMENTS

I am indebted to Michael J. Brooks for his excellent feedback and guidance as supervisor of this work. His eye for detail and ability to suggest alternative approaches are deeply appreciated. The extra hours he invested in checking this work even over weekends and in his personal time are recognised with gratitude.

Thanks to Professor Nelson M. Ijumba for his assistance with refinement of the study.

A special thanks to my wife, Christy Tempies, for professionally laying out certain diagrams, redrawing others and proof-reading. Her assistance with the nomenclature table is also deeply appreciated.

ABSTRACT

Studies undertaken by Eskom in 2001 identified three sites near the Northern Cape town of Upington which are suitable for a 100 MW Concentrating Solar Power (CSP) generating plant. Of the CSP technologies investigated, the central receiver option was identified as best for the Northern Cape, however almost none of Eskom's analysis was made public. The basis of the central receiver's suitability versus other CSP options is not publicly known. Given recent advances in concentrating systems, an argument exists for reassessing the suitability of various solar thermal technologies for bulk power generation.

This study first characterises the incident solar radiation (insolation) levels at Upington from six data sources and assesses their quality. The data are then used to model performance of the parabolic trough, compact linear Fresnel reflector, central receiver, and dish-engine technologies. A software modelling tool of the United States National Renewable Energy Laboratory (System Advisor Model) is used to facilitate the comparison. Simulation results are compared with data from similar studies to ensure consistency of the CSP model inputs and performance outputs.

Constraining the results to the environmental conditions of Upington, it is found that while central receiver technology produces less electricity per square kilometre of collector area, it uses less water than parabolic trough technology to obtain a higher annual electric output. Dish-engine technology has the most favourable annual electricity production to water-usage ratio, however, its modest annual electricity output and lack of energy storage capability weaken the case for it to match South Africa's national load profile substantively. Examining the modelled month-to-month electricity output characteristic, the central receiver technology delivers significantly more electricity during the lower insolation winter period of the year than the competing technologies. This results in the central receiver technology achieving the highest annual electric output of the four technologies compared under the same insolation levels, strengthening the case for its implementation.

As a whole, this work characterises the insolation levels at Upington, provides an analysis of the technical performance of competing CSP technologies for the proposed Northern Cape site, and argues quantitatively in favour of the central receiver option.

TABLE OF CONTENTS

LIST OF TABLES

LIST OF FIGURES

NOMENCLATURE

A	Parabolic trough collector aperture area	m^2
a_1	Linear Fresnel coefficient for primary collector determined by experiments	-
a_2	Linear Fresnel coefficient for primary collector determined by experiments	-
A_{app}	Dish-engine concentrator aperture area	m^2
A_{col}	Linear Fresnel primary mirror collector area	m^2
A_{field}	Central receiver heliostat field surface area	m^2
A_i	Linear Fresnel collector aperture area	m^2
A_{proj}	Projected area of dish-engine concentrator mirror	m^2
A_{rec}	Dish-engine receiver aperture area	m^2
B	Gross land area	m^2
$Beale\#_{curve}$	Beale number curve fit polynomial	-
B_{CC}	Beale constant coefficient	-
B_{1st}	Beale first-order coefficient	-
B_{2nd}	Beale second-order coefficient	-
B_{3rd}	Beale third-order coefficient	-
B_{4th}	Beale fourth-order coefficient	-
C_1	Constant required for Stirling engine efficiency curve-fit polynomial	-
C_2	First-order coefficient required for Stirling engine efficiency curve-fit polynomial	-
C_3	Second-order coefficient required for Stirling engine efficiency curve-fit polynomial	-
CR_g	Dish-engine concentrator geometric concentration ratio	-
d_i	Space between linear Fresnel primary collectors	m^2
E	Fraction of dish-engine concentrator aperture area not shaded by receiver struts and other dish-engine components	-
E_b	Direct normal radiation	W/m^2

e_c	Carnot efficiency	-
F	Dish-engine receiver equivalent radiative conductance	W/mK
G_{on}	Extraterrestrial radiation striking a plane perpendicular to the radiation on the *n*th day of any given year.	MJ/m^2
G_{sc}	The solar constant	W/m^2
H	Daily solar radiation on a horizontal surface	kWh/m^2/day
$\overline{H}$	Monthly daily solar radiation on a horizontal surface	kWh/m^2/day
H_b	Daily beam radiation	kWh/m^2/day
$\overline{H}_b$	Monthly beam radiation	kWh/m^2/day
H_d	Daily diffuse radiation	kWh/m^2/day
$\overline{H}_d$	Monthly diffuse radiation	kWh/m^2/day
h_{in}	Temperature of working fluid entering the linear Fresnel HCE	ºC
H_o	Daily global extraterrestrial radiation	kWh/m^2/day
$\overline{H}_o$	Monthly-averaged daily extraterrestrial radiation	kWh/m^2/day
h_{out}	Temperature of working fluid leaving the linear Fresnel HCE	ºC
I	Total hourly solar radiation	kWh/m^2
I_b	Hourly direct normal radiation	kWh/m^2
$I_{b,n}$	Incident horizontal beam radiation	W/m^2
I_d	Hourly diffuse radiation	kWh/m^2
I_{DNI}	Direct normal insolation	W/m^2
I_o	Hourly extraterrestrial radiation	kWh/m^2
$IAM(\theta_i)$	Incident Angle Modifier - Angular dependent losses of collector in longitudinal direction due to growing beam expansion and rising end losses	-
$IAM_{\parallel}$	Angular dependent losses of collector in longitudinal direction	-
$IAM_{\perp}$	Angular dependent losses of collector in transversal direction	-
k_T	Hourly clearness index	-
K_T	Daily clearness index	-
$\overline{K}_T$	Monthly average clearness index	-

$\dot{m}$	Linear Fresnel total collector flow rate	kg/s
n	Day number	-
P_{coll}	Useful power given by parabolic trough collector	W
$P_{controls}$	Tracking controls parasitic power consumption	W
P_{fan}	Dish-engine cooling fan parasitic power consumption	W
P_{gross}	Dish-engine net power from manufacturer or test data less a parasitic power loss estimate	kW
$P_{Gross,op}$	Gross output power of a Stirling engine	kW
$P_{in,SE}$	Power output of dish-engine receiver delivered to the Stirling engine	kW_{th}
$P_{in,rec}$	Solar power intercepted by dish-engine receiver	kW_{th}
P_{Net}	Net dish-engine system power	kW
P_{out_SE}	Electrical output power of a Stirling engine	kW_e
$P_{parasitics}$	Power used for dish-engine tracking motors, cooling fans, control instruments and other parasitic power consumption	kW
P_{pump}	Dish-engine cooling fluid pump parasitic power consumption	W
P_{ThL}	Sum of the parabolic trough collector thermal or heat losses	kW_{th}
P_u	Useful power extracted from a set of parabolic solar collectors	W
$\dot{q}_{cond}$	Dish-engine receiver conduction losses	W
$\dot{q}_{conv,tot}$	Dish-engine receiver heat loss by natural and forced convection	W
$\dot{q}_{rad,emit}$	Radiation emitted out of dish-engine receiver aperture	W
$\dot{q}_{rad,reflect}$	Radiation reflected out of dish-engine receiver aperture	W
Q_{useful}	Dish-engine useful heat	kW_{th}
R_b	Geometric factor	-
T_m^*	Reduced mean temperature of linear Fresnel HCE	^oC
T_{amb}	Ambient temperature	^oC
T_H	Hot reservoir temperature of Carnot cycle	K
T_L	Cold reservoir temperature of Carnot cycle	K
T_m	Mean fluid temperature of linear Fresnel HCE	^oC

T_{rec}	Dish-engine receiver operating temperature	K
U	Convection-conduction heat-loss coefficient for air currents within the dish-engine receiver cavity, and conduction through receiver walls	W/m^2K
$wind_{cut,out}$	Dish-engine wind cut-out velocity	m/s

GREEK SYMBOLS

α	Dish-engine receiver absorptance	-
α_s	Solar altitude angle	degrees
β	Angle between plane of surface and horizontal	degrees
β_{Carnot}	Ratio of actual engine efficiency to Carnot cycle efficiency	-
γ	Surface azimuth angle	degrees
γ_s	Solar azimuth angle	degrees
Γ	Fraction of heliostat field tracking the sun and not having control problems, being fixed or being cleaned	-
δ	Declination	degrees
η	Efficiency of a parabolic trough collector	-
η_{alt}	Dish-engine alternator efficiency	-
η_{conc}	Dish-engine concentrator efficiency	-
$\eta_{conv,gross}$	Dish-engine system gross efficiency	-
$\eta_{conv,net}$	Dish-engine system net efficiency	-
η_{eng}	Stirling engine efficiency	-
η_{field}	Total heliostat field efficiency	-
η_{opt}	Parabolic trough collector optical efficiency	-
η_{opt^*}	Optimum linear Fresnel optical efficiency minus all optical influences	-
$\eta_{opt,0}$	Linear Fresnel collector efficiency for perpendicular irradiation and no heat loss	-
η_{rec}	Dish-engine receiver efficiency	-
η_{SE}	Stirling engine efficiency	-

$\eta_{SE,curve}$	Stirling engine efficiency curve-fit	-
θ	Angle of incidence	degrees
$\theta_{\parallel}$	Longitudinal angle	degrees
$\theta_{\perp}$	Transverse angle	degrees
θ_i	Incidence angle	degrees
θ_z	Zenith angle	degrees
λ	Solar radiation wavelength	μm
ρ	Dish-engine concentrator surface reflectance	-
ρ_{field}	Heliostat mirror reflectivity	-
ρ_{ref}	Dish-engine concentrator mirror reflectivity	-
σ	Stefan-Boltzmann constant (5.67×10^{-8} W/m^2-K^2)	W/m^2-K^2
τ	Transmittance of any interface between a dish-engine concentrator and receiver	-
$\varphi_{int,fac}$	Dish-engine concentrator intercept factor	-
φ_{shade}	Dish-engine concentrator shading factor	-
φ_{wind}	Dish-engine concentrator wind stow factor	-
ϕ	Latitude	-
ω	Hour angle	degrees
ω_s	Sunset hour angle	degrees

ABBREVIATIONS

3D	Three Dimensional
APS	Arizona Public Service
BP:DPO	Biphenyl:Diphenyl Oxide
BSRN	Baseline Surface Radiation Network
CO_2	Carbon Dioxide
$Ca(NO_3)_2$	Calcium Nitrate

CFSR	Climate Forecast System Reanalysis
CIEMAT	Spanish Research Centre for Energy, Environment and Technology
CLFR	Compact Linear Fresnel Reflector
CPC	Compound Parabolic Concentrator
CRS	Central Receiver Systems
CRSES	Centre for Renewable and Sustainable Energy Studies
CSP	Concentrating Solar Power
CSR	Climatological Solar Radiation
CSV	Comma Separated File
DC	Direct Current
DHI	Direct Horizontal Insolation
DISS	Direct Solar Steam
DLR	German Aerospace Centre
DME	South African Department of Minerals and Energy
DNI	Direct Normal Insolation
DNR	Direct Normal Radiation
DoE	South African Department of Energy
DOE	United States Department of Energy
DSG	Direct Steam Generation
EIA	Environmental Impact Assesment
EPC	Engineering, Procurement and Construction
EPW	EnergyPlus Weather
FSI	FLABEG Solar International
GEWEX	Global Energy and Water Cycle Experiment
GHI	Global Horizontal Insolation
GMT	Greenwich Meridian Time
GWh	Gigawatt hour
H_2O	Water

HCE	Heat Collector Element
HTF	Heat Transfer Fluid
IAM	Incidence Angle Modifier
ID	Identity
IEA	International Energy Agency
ISCCS	Integrated Solar Combined Cycle System
ISE	Fraunhofer Institute for Solar Energy Systems
IST	Industrial Solar Technology
$KN0_3$	Potassium Nitrate
LCOE	Levelised Cost of Electricity
LFR	Linear Fresnel Reflector
LTR	Linear Tubular Receiver
METSTAT	Meteorological Statistical Model
Mtoe	Million tons of oil equivalent
$NaNO_2$	Sodium Nitrite
$NaNO_3$	Sodium Nitrate
NASA	National Aeronautics and Space Administration
NCEP	United States National Centers for Environmental Prediction
NERSA	National Energy Regulator of South Africa
NOAA	United States National Oceanic and Atmospheric Administration
NREL	National Renewable Energy Laboratory
O&M	Operation and Maintenance
O_3	Ozone
ORC	Organic Rankine Cycle
PCM	Phase Change Material
PMOD	Physikalisch-Meteorologisches Observatorium, Davos
PSA	Plataforma Solar de Almería
PSE	Projects in Solar Energy

PV	Photovoltaic
REFIT	Renewable Energy Feed-in Tariff
REN21	Renewable Energy Policy Network for the 21st Century
SAM	System Advisor Model
SANBI	South African National Biodiversity Institute
SAWS	South African Weather Service
SBP	Schlaich Bergermann und Partner
SCA	Solar Collector Assembly
SEGS	Solar Electric Generating Systems
SES	Stirling Energy Systems
SIA	Social Impact Assessment
SRB	Surface Radiation Budget
SSE	Surface Meteorology of Solar Energy
SST	Siemens Steam Turbine
STORES	Solar Trough Organic Rankine Cycle Electricity System
SWERA	Solar and Wind Energy Resource Assessment
TES	Thermal Energy Storage
TMY	Typical Meteorological Year
USA	United States of America
UV	Ultraviolet
UVAC	Universal Vacuum Air Collector
WGA	Wilkinson, Goldberg, and Associates, Inc.
WRC	World Radiation Center
WRDC	World Radiation Data Centre
WRR	World Radiometric Reference

1. INTRODUCTION

1.1 Project summary

Solar thermal electricity generation is normally understood as the concentration of sunlight using solar collectors to heat a working fluid which passes through a heat exchanger to produce steam for powering a turbine. High-temperature solar energy replaces fossil fuel as the heat source. This concept is often denoted as concentrating solar power (CSP) and can be suitable for centralized power production in areas with high levels of insolation. With sufficient thermal energy storage (TES), CSP can be an efficient, CO_2-free, dispatchable power supply independent of weather conditions.

In a CSP power plant, mirrors concentrate sunlight on to a heat exchanger, referred to as the receiver or absorber. Here the absorbed heat is transmitted to a heat transfer fluid (HTF). Then the HTF either transfers the heat *directly* to a suitable power cycle or *indirectly* to a TES stage before the power cycle to provide a buffer for transient weather conditions.

Concentrating solar power systems may be distinguished by the arrangement of their reflective elements. Line focusing systems like parabolic troughs or linear Fresnel systems only require single-axis tracking to localise insolation on an absorber tube. Concentration factors of up to 100 can be achieved in practice. Point focusing systems like parabolic dish concentrators or central receiver systems (using a 3D paraboloid to focalise insolation onto a local receiver, or a large number of individually tracking heliostats to concentrate the insolation onto a distant, elevated receiver) may attain a higher concentration factor (on the order of a thousand) with the additional burden of tracking on two axes.

With an abundance of solar potential in the arid regions of South Africa, this dissertation investigates bulk solar power generating options for one of the more densely populated areas of the Northern Cape province, namely Upington (28°4'S, 21°3'E).

A pre-environmental scoping study and pre-feasibility study undertaken in 2001 by the South African utility Eskom identified three sites near Upington which are suitable for a 100 MW CSP generating plant (Eskom and Bohlweki Environmental, 2006). Of the CSP technologies investigated, Eskom concluded that the central receiver option was best for the Northern Cape, however, almost none of their analysis was made public and implementation of the project has now stalled due to funding constraints. Questions remain about the suitability of the central receiver versus other CSP options, given recent advances in concentrating systems.

A strong argument exists for reassessing the plan to determine whether other technologies may presently be more suitable for bulk power generation.

Thus the following research question may be posed:
Which CSP technology, from a technical performance perspective, is most suitable for bulk power generation given the solar resource available in Upington?

The objective of this research is twofold. Firstly the solar resource available in Upington must be quantified. Secondly, the most technically suitable CSP technology for implementation in the Upington area must be identified.

The project is divided into two parts. First, the solar resource at Upington is assessed. Upington's usable radiation is quantified and its characteristics in terms of seasonal variation, component breakdown and magnitude are compared with other CSP sites globally. Secondly, four solar energy power generating technologies (parabolic trough, central receiver, linear Fresnel concentrator and dish concentrator), are compared with respect to output for the given radiometric conditions, efficiency, durability, and suitability in the South African context, to establish which is currently most appropriate for implementation in the Upington region. The comparison is facilitated by the System Advisor Model software modelling tool (SAM) of the United States National Renewable Energy Laboratory (NREL). Although economics are important to the final selection of a CSP technology, this study is concerned primarily with a technical evaluation of four CSP options, and an analysis of the economics is therefore omitted. Recommendations are made as to the most suitable CSP technology for bulk power generation. The recommendations may be used as a basis for more detailed investigation or a feasibility-level study.

1.2 Motivation for project

The world's economy is upheld by reliable or "firm" supplies of electrical energy. It is clear that sustaining economic advancement will require more energy in light of the world's growing population. ExxonMobil's (2011) most recent research advises that

> "By 2040, global electricity demand will be about 80 percent higher than today. Broken down by sector, this growth will come from industrial (45 percent), residential (30 percent) and commercial (20 percent)."
> (ExxonMobil, 2011: 28)

Van Wyk *et al*. (2006) report that South Africa has almost an undivided reliance on fossil fuels as a primary energy source (approximately 92%), where coal provides 74% of the fossil fuel derived energy. Furthermore, coal fired power stations generate approximately 93% of South Africa's electricity (National Energy Regulator of South Africa, 2007). The International Energy Agency (IEA) (2011) cited coal combustion as South Africa's fundamental contributor to its carbon dioxide (CO_2) emissions. The majority of the scientific community report CO_2 as a large contributor to the greenhouse effect which can result in climate change.

Indeed, according to the United Nations Statistics Division (2004):

> "South Africa has one of the highest levels of carbon dioxide emissions per capita in the world."

In recognition of this the South African government drafted and published a white paper on renewable energy in November 2003 (DME, 2003). This white paper presented a "medium-term (10-year) target" of "10 000 GWh (0.8 Mtoe) renewable energy contribution to final energy consumption by 2013". This approximates to "4% (1667 MW) of the projected electricity demand for 2013". This contribution was to be "mainly from biomass, wind, solar and small-scale hydro". (DME, 2003: ix)

In December 2009 the South African Department of Energy (DoE) released an Integrated Resource Plan (IRP 1) reiterating the 2003 renewable energy target as a policy objective (DoE, 2009). This plan then entered a public consultation and policy-adjustment process which resulted in the medium-term target being replaced by a new target of renewable energy comprising 42% of all new electricity generation capacity by 2030 (DoE, 2011). This revised plan, termed IRP 2010 was promulgated and approved by Cabinet in May 2011 (DoE, 2011).

Within these visions and targets, solar energy generation plays an important role. In the next section, background information on solar energy and the differing methods employed in converting it into electricity will be discussed.

1.3 Solar energy technologies

Solar energy may be captured directly as radiation or indirectly in green plants, wind, and ocean currents.

Bansal (2000) provided an extensive summary of direct and indirectly harnessed solar energy. He defines direct solar energy as the usable energy harnessed after only one transformation of sunlight in its native form. Examples of direct solar energy in line with this definition would be electricity generated by sunlight irradiating a photovoltaic cell or heat converted from light interacting with a material.

Likewise he defines indirect solar energy as the usable energy harnessed after more than one transformation of sunlight in its native form. An example of this idea would be how solar energy that was captured in plants which died and were compacted by many layers of soil over many thousands of years resulted in a transformation of the energy captured in the plant matter into coal or oil. This energy is then released via combusting the coal or oil.

This study investigates the application of direct solar energy to bulk electricity generation. A useful method of classifying direct solar energy harnessing systems is furnished by Bansal (2000). Bansal (2000) classifies solar power systems as either passive or active. If a solar power system only needs incoming sunlight to operate, and does not require any other energy input, he terms it a passive solar system. If, however, the system requires additional energy to be applied to it to circulate a working fluid, or track the sun, then he labels it an active solar system. A solar system is more efficient if it can track the sun and maintain high levels of insolation on its working surface, however, this requires supplementary energy. Therefore, a trade-off exists between optimally utilizing solar energy and avoiding excessive parasitic energy loss from the additional mechanisms.

From the work of Bansal (2000), and Pitz-Paal (2008), a scheme of solar energy utilisation can be made. A generalised solar energy utilisation scheme is displayed in Figure 1-1.

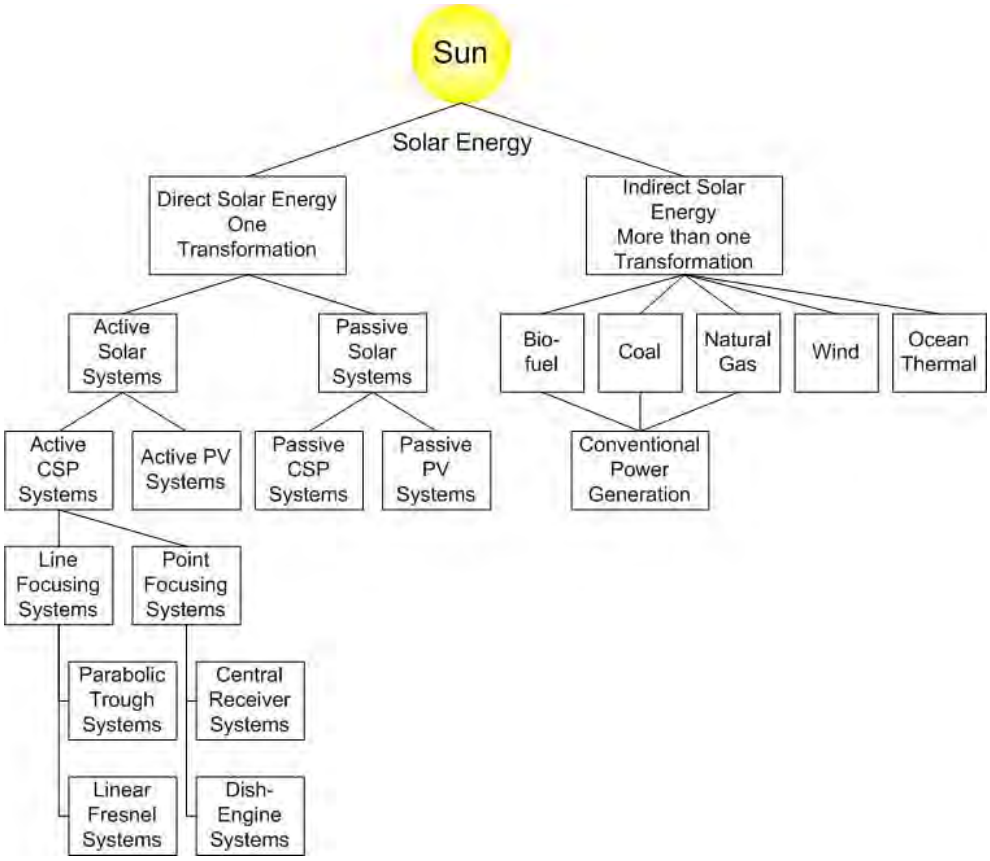

Figure 1-1: Solar energy utilisation

The two major direct solar power systems contending for acceptance as the preferred electricity generation technology are photovoltaic (PV) systems and solar thermal systems.

Photovoltaic systems use photons to agitate electrons of variably unpurified silicon from their valence bands to the conduction band. This causes a Direct Current (DC) to flow. This process is termed the photovoltaic effect (Zobaa, 2006). By adding many silicon segments together in series significant DC can be obtained. Silicon segments are generally arranged in arrays which are called PV modules in the solar industry. Due to the static nature of PV modules (no moving parts) they can operate for periods on the order of twenty to thirty years according to Zobaa (2006).

Photovoltaic systems can be divided into three major categories, namely crystalline silicon systems, thin-film systems and concentrating PV systems. The most established PV system is the crystalline silicon type. It is in essence single-crystal (monocrystalline) or polycrystalline (multicrystalline) silicon with strategically introduced impurities to promote current flow. This silicon is portioned into cells and placed in arrays. These arrays are termed “flat-plate collectors”, and do not make use of lenses to concentrate incident sunlight.

By depositing a homogenous layer of silicon onto a glass or metal stratum a thin-film system is produced. Due to thin-film systems not having such a developed crystal-lattice structure they are not as efficient as crystalline systems in producing electricity, however, their fabrication is more cost effective.

A concentrating PV system utilises a lens or reflector to concentrate insolation on a PV cell. This increases the energy in the photovoltaic reaction and results in a higher power output. Due to the concentration of insolation on the PV cell, a less specialised PV material can be used. This material may be produced at lower cost than both crystalline silicon systems and thin-film systems. However, most recent advancement has occurred with high optical concentration PV systems using high-efficiency (in the 40% range) multijunction solar cells (Kurtz, 2012). Installation of these CPV panels with solar trackers is starting to increase with one supplier, Amonix, completing a 30 MW installation in Alamosa, CO, USA for Cogentrix in 2011 (Kurtz, 2012). This is currently the largest CPV power plant in the world and started commercial operation in May 2012 (Cogentrix, 2012).

Solar thermal systems transfer the energy from direct sunlight to heat. Kreider (2006) indicates that the production of heat is the prime use of solar energy. He reports an upper temperature limit of 1800°C can be achieved from solar radiation due to manufacturing, optical, and thermodynamic constraints. He states that many thermal collector designs are used between temperatures near ambient and this upper limit to generate heat at the required temperature.

Solar thermal systems consist primarily of collectors or concentrators and receivers. The collectors focus direct sunlight onto the receivers which then transfer the energy to a high temperature working fluid. The working fluid energy is either converted to mechanical energy directly or used to generate steam which is then used to generate mechanical energy. The mechanical energy is then converted into electricity via a turbine (generator). This is the CSP concept.

Each technology fulfills a slightly different niche. PV systems are an economical means of providing modest quantities of electricity to remote off-grid applications. Many millions of PV systems have been installed in applications ranging from calculators to water-pumping installations. Duffie and Beckman (2006) provide a range of energy problems where PV generators are the most suitable approach. The solutions presented confirm that the most practical application of PV is to generate small amounts of electricity to match modest, specialised or residential loads. Nobesol has constructed the largest PV power plant in the

world in Olmedilla de Alarcón, Spain. The plant can produce 60 MWp (Megawatts peak) and provides 87 500 MWh of electricity annually from its 270 000 PV panels (Nobesol, 2008).

With a global total of approximately 1095 MW installed capacity (REN21, 2011), solar thermal energy generation technologies present the most cost-effective, practical and proven approach when considering bulk solar energy generation. The Solar Electric Generating Systems (SEGS) plants of southern California are frequently held up as examples of CSP technology since they have been in operation the longest of all solar thermal plants and are regarded as having successfully demonstrated the bulk solar thermal power concept commercially.

Two factors make solar thermal electricity generation in the Northern Cape province of South Africa attractive. Firstly South Africa has a dominant peak in its electricity usage in the evenings between 6 pm to 9 pm both in summer and winter (Eskom, 2010a). CSP plants with TES can dispatch electricity to service that peak load after the sun has set. Secondly, Meyer and van Niekerk (2011) noted that shale gas could be present in areas that overlap with viable CSP plant locations in the Northern Cape. CSP plants can be hybridised with Brayton cycle power plants to provide base load power (Schwarzbözl *et al*., 2006).

The National Energy Regulator of South Africa (NERSA) approved and published a Renewable Energy Feed-in Tariff (REFIT) on 29 March 2009 (NERSA, 2009a,b). Within the regulatory guidelines of the REFIT only landfill gas power plants, small hydro power plants (less than 10 MW), wind power plants and CSP plants were listed as qualifying as a renewable energy power generator. The CSP technology proposed at this stage was a parabolic trough plant with 6 hours of daily thermal storage. This set of documents is often referred to as REFIT Phase I.

On 29 October 2009 NERSA approved REFIT Phase II (NERSA, 2009c). Within this document additional solar energy generation technologies were added to the REFIT programme. These included parabolic trough plants without thermal storage, large scale grid connected PV systems (≥1 MW) and central receiver system (tower) plants with 6 hours of daily thermal storage. This phase of the programme excluded concentrating photovoltaic (CPV) “due to high economic cost” (NERSA, 2009c: 1).

In March 2011 NERSA issued a consultation paper titled: “Review of Renewable Energy Feed - In Tariffs” (NERSA, 2011). This consultation paper confirmed that only the technologies approved under REFIT Phase I and II would be considered and proposed lower

feed-in tariffs. It also provided more detailed eligibility criteria for the qualifying technologies.

The DoE has since selected preferred bidders for several CSP and PV projects (DoE, 2012).

1.4 Concentrating solar power technologies

Concentrating solar power systems concentrate solar radiation to produce steam or hot air to generate electricity in a conventional power cycle. Only direct radiation can be concentrated in optical systems (Philibert, 2004). The concentration of sunlight is accomplished by mirrors directing the sunlight onto a heat exchanger (receiver or absorber), where the energy absorbed is transferred to a HTF. A CSP system can be presented schematically as shown in Figure 1-2.

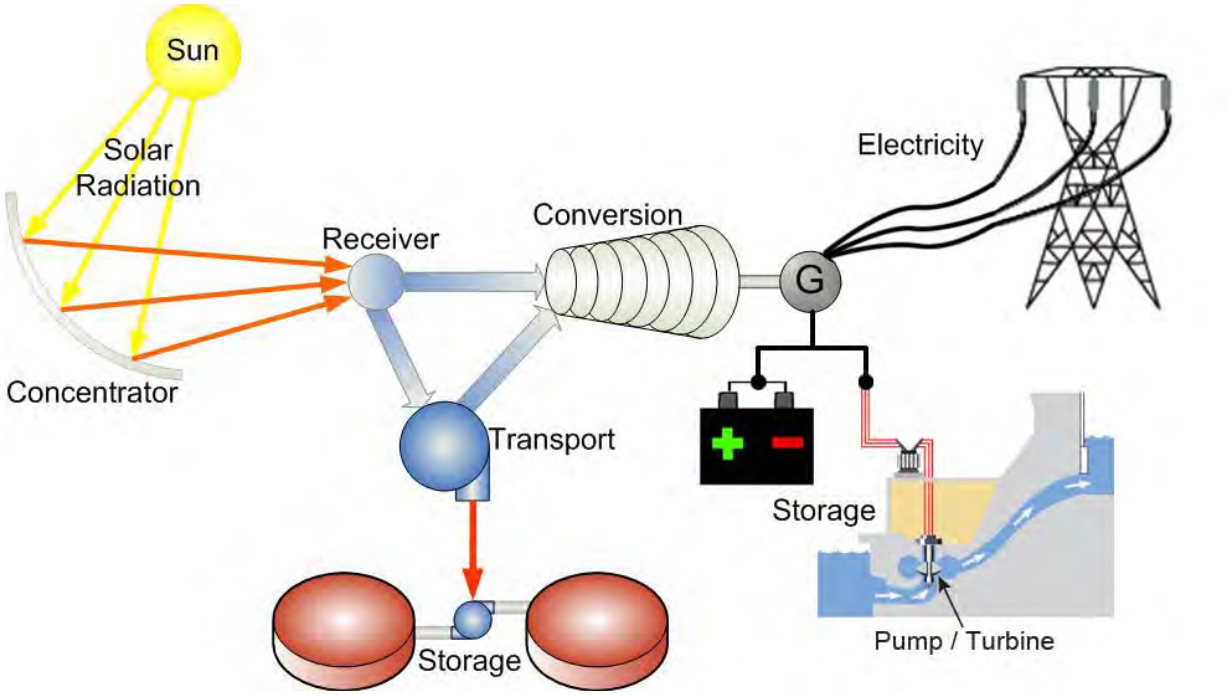

Figure 1-2: Schematic representation of the component parts of a CSP system

A variety of different CSP concepts exist in which the HTF of steam or gas is either used in the power cycle directly or a thermal oil or molten salt is circulated in an intermediate secondary cycle, in which case an additional heat transfer to the power cycle is required (Pitz-Paal, 2008).

Pitz-Paal (2008) distinguishes CSP systems by the arrangement of their concentrator mirrors. Line focusing systems like parabolic troughs or linear Fresnel systems only require single-axis tracking in order to concentrate solar radiation onto an absorber tube. Concentration factors of up to 100 can be achieved in practice. Point focusing systems like parabolic dish concentrators or central receiver systems (CRS) use two-axis tracking to concentrate incident insolation several thousands of times.

1.4.1 Parabolic trough systems

With approximately 985 MW of installed capacity globally (REN21, 2011), parabolic trough systems embody the most mature CSP electricity generation technology. They generally consist of large arrays of solar collector assemblies (tracking groups of parabolic collectors with metal support structure, receiver tubes and tracking systems), a HTF or direct steam generation (DSG) system, a Rankine steam cycle turbine and optional thermal storage and/or fossil fuelled accompaniment (Price *et al*., 2002).

1.4.2 Linear Fresnel systems

Linear Fresnel Reflector (LFR) technology is a variation on the parabolic trough system. Hence, its major components are very similar to parabolic trough components. A linear Fresnel system uses a series of narrow, long, flat or shallow-curvature mirrors to focus beam insolation onto one or several linear absorber pipes above the mirrors.

Compact Linear Fresnel Reflector (CLFR) technology is an enhancement on the LFR concept by increasing the amount of linear absorbers in the array such that each reflector can reflect solar radiation to at least two absorbers (Mills and Morrison, 2000). This reduces the likelihood of reflectors shadowing each other and hence results in a more compactly packed array.

CLFR power plants generally consist of large arrays of tracking groups of primary reflectors straddled by several static receivers a few meters above each group, a DSG system, a Rankine steam cycle turbine and optional fossil fuelled accompaniment (Novatec Biosol, 2011).

1.4.3 Central receiver systems

Central receiver systems (CRS) consist of a large number of two-axis tracking mirrors (heliostats), each with a surface of between 20 m^2 and 200 m^2 and a heat exchanger (receiver) located at the top of a central tower. The heliostats focus light onto the central receiver. The receiver then either transfers the heat to a TES system or directly to a Rankine steam cycle with optional fossil fuelled accompaniment. The higher temperatures attainable by CRS result in a more efficient steam cycle and open the advent of using a Brayton gas cycle turbine (Heller *et al*., 2006).

1.4.4 Dish-engine systems

The major components of dish-engine systems are a dish-shaped concentrating collector, a high-temperature solar receiver, and a Stirling or Brayton cycle engine. A dish-engine plant is qualitatively different to the three technologies discussed above as each dish-engine is an autonomous system delivering electricity the plant's main substation in contrast to the above plants which transport a HTF through the plant to the power block.

1.5 Solar energy technology assessment methods

In this study System Advisor Model is used to evaluate four CSP technologies using meteorological data for Upington. System Advisor Model is a performance and economic model designed to facilitate technology comparisons for decision-makers in the renewable energy industry. It was developed by NREL in collaboration with Sandia National Laboratories and in partnership with the United States Department of Energy (DOE) Solar Energy Technologies Program (SETP) (Gilman *et al*., 2008). It is maintained and updated by NREL. Using TRNSYS (a validated, time-series simulation program developed at the University of Wisconsin) with custom component-models, SAM simulates system performance using hourly resource data.

System Advisor Model can model PV, parabolic trough, central receiver, linear Fresnel, dish-engine, fossil fuel, solar water heating, wind, geothermal and biomass systems.

The use of SAM to model solar energy technologies is not unprecedented. Lew *et al.* (2009) utilised SAM to model the CSP component of the Western Wind and Solar Integration Study –one of the largest regional wind and solar integration studies to date. Cameron *et al.* (2008) compared measured PV system performance with the performance-model predictions from SAM and concluded that the results displayed reasonable agreement. Turchi *et al.* (2011) presented a novel gas turbine / parabolic trough hybrid design using SAM to compare the performance and cost of the hybrid system to a solar-only parabolic trough system.

1.6 Structure of dissertation

This dissertation consists of five chapters. Chapter 1 provides a high level summary of the work undertaken, the motivation for the project, an introduction of the competing CSP technologies, assessment methods and the structure of the dissertation. A review of the technical characteristics of the considered CSP technologies is performed in chapter 2. In chapter 3 the solar resource availability at Upington is presented. Using SAM each CSP

technology is modelled and the results compared in chapter 4. The solar resource assessment and modelling results are discussed in chapter 5, which then inform the conclusions and recommendations made in chapter 6.

2. LITERATURE REVIEW

2.1 Introduction

The following sections contain a description of each of the CSP electricity generation systems considered in this study. The major components are identified and analysed in terms of performance and latest advances in technology. Practical operational issues are highlighted. Efficiencies and operational issues are then compared to inform the selection of the most suitable technology given the insolation levels determined in chapter 3. Subsystems are then related to the underlying workings of the performance modelling executed in SAM in chapter 4.

Certain concepts are common among CSP technologies, one of which is the solar multiple which represents the solar field aperture as a multiple of the turbine-generator's nameplate capacity (System Advisor Model, 2011).

The solar field of a parabolic trough, linear Fresnel or central receiver system should be sized so that it produces enough thermal energy to drive the turbine-generator of the plant at rated capacity as much as possible, so that its installation and operating costs are minimized, and it makes efficient use of TES.

An inherent trade-off exists in the above requirements. The solar multiple can be used to analyse the tradeoff between a larger field producing more electricity and a smaller field reducing project capital and operational costs.

The following discussion is an adaptation of solar multiple explanation in SAM (System Advisor Model, 2011). A solar multiple of one means that the solar field's aperture area is sized so that it will deliver enough thermal energy to drive the turbine-generator at rated capacity when it receives the DNR-level it was designed for. It is clear that a CSP plant will not receive its design DNR-level for many consecutive hours in a year. Therefore, a plant with a solar multiple of 1 will run its turbine-generator at part-load most of the year. By increasing the solar multiple to greater than one, the field can produce enough thermal energy to drive the turbine-generator at rated capacity even if lower than design-level DNR is being received. If the solar multiple is too large then more thermal energy will be delivered to the turbine-generator than it can cope with, and the capital and operational costs of the plant will be high. Generally a CSP system with TES will have a higher optimal solar multiple than one without.

2.2 Parabolic trough systems

Parabolic trough systems are considered the most mature CSP electricity generation technology. Mills (2004) estimated more than 100-plant years of experience had been garnered from nine operating plants ranging from 14 MW to 80 MW by 2004. The SEGS plants of southern California are the longest operating parabolic trough plants and are regarded as successful demonstrations of the bulk solar thermal power concept. The nine plants are located at three sites in the Mojave Desert near Barstow, California: Daggett (SEGS I and II), Kramer Junction (SEGS III through VII) and Harper Lake (SEGS VIII and IX) as reported by Duffie and Beckman (2006) and Mills (2004).

A diagram displaying the essentials of a parabolic trough system is shown in Figure 2-1. The solar field is modular and contains numerous parallel rows of single-axis tracking, parabolic trough solar collectors which are usually lined up on a North-South horizontal axis (Müller-Steinhagen and Trieb, 2004). Every solar collector consists of a linear parabolic-shaped reflector that focalises beam insolation onto a linear receiver tube at the focal point of the parabola (Pitz-Paal, 2008).

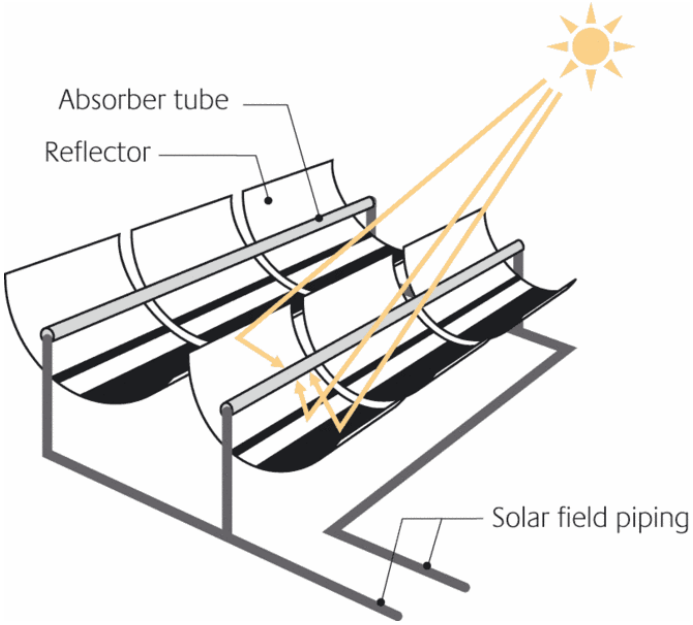

Figure 2-1: Parabolic trough system (German Energy Agency, 2009)

To ensure that the sun is continuously focused on the receiver, the collectors track it from east to west during the day (Wolff *et al.*, 2008). A thermal oil HTF is heated to temperatures above 350°C as it circulates through the receivers and is returned to a steam generator to produce slightly superheated steam at a pressure of around 50 bar to 100 bar which is then fed into a steam turbine as part of a conventional steam cycle power plant (Pitz-Paal, 2008). Often a molten salt TES system is incorporated in-between the solar field and the Rankine cycle steam turbines of the power plant.

Parabolic trough power plants consist of five major components, namely: parabolic reflective collectors (often referred to as reflectors), linear tubular receivers (also called HCEs), HTF or working fluid, energy storage systems and power plants.

2.2.1 Reflective parabolic collectors

In general the useful power (P_u) in Watts extracted from a set of parabolic solar collectors can be characterized by the following equation reported by Hoyer *et al.* (2009) and utilized in FLAGSOL's performance model "PCTrough".

$$P_u = E_b \cdot A \cdot \eta_{opt} - P_{ThL} \tag{2.1}$$

where E_b is the beam insolation measured in W/m^2, A is the aperture area of the parabolic trough collector in m^2, η_{opt} is the optical efficiency multiplied by efficiency derating factors and P_{ThL} is the sum of the thermal or heat losses obtained from a suitable model or measurements. In Equation 2.1 E_b refers to instantaneous beam radiation. In general E_b is used to refer to a summation or integration of beam radiation over an hour.

The aperture area (A) is dependent on the width and length of the collector assembly as determined by manufacturers. SAM has a library of collectors with aperture areas that vary from 235 m² for the Luz LS-2 collector to 817.5 m² for the EuroTrough ET150.

The derating efficiency factors used by SAM to determine the design optical efficiency (η_{opt}) are tracking error, geometry effects, mirror reflectance, dirt on mirror and general optical error. The product of these derating factors is the optical efficiency (η_{opt}).

The heat loss of a collector as a result of radiation, conduction through its structural support members and convection as the wind blows past the collector is difficult to model. Hence, SAM focuses on modelling the heat losses on the linear tubular receiver. These losses are discussed in section 2.2.2.

2.2.1.1 Quantifying reflective parabolic collector efficiency

In order to direct the beam component of solar radiation onto a receiver effectively, a reflective parabolic collector must have a surface with high specular reflectance for radiation in the solar spectrum. Hence, most parabolic trough reflectors are specialized mirrors.

The efficiency of a parabolic trough collector, η, can be defined as the ratio of the useful power given by the collector, P_{coll}, and a solar power reference. Rojas *et al*. (2008) found two main approaches in the literature when defining the reference solar input:

Approach 1 uses the component of direct solar irradiance normal to collector aperture ($E_b cos\theta$; where E_b is the beam irradiance and θ is the solar incidence angle). This approach is mentioned in Kreith and Kreider (1978). The efficiency is calculated as follows:

$$\eta = \frac{P_{coll}}{AE_b cos\theta} \tag{2.2}$$

where A is the aperture of the collector as above in section 2.2.1.

Approach 2 uses the beam or direct solar irradiance (E_b). This approach is followed by many authors and most classical reference texts on solar parabolic troughs according to Rojas *et al*. (2008). It results in an expression of the efficiency as

$$\eta = \frac{P_{coll}}{AE_b} \tag{2.3}$$

It is clear that with a zero solar incident angle both efficiencies are equal. Therefore, in principle, the choice between these two approaches is somewhat arbitrary.

2.2.1.2 Reflective surface technologies

Duffie and Beckman (2006) suggest that back-silvered glass has excellent specular reflectance and durability provided the reflective coating is adequately protected. The transparency of the glass in this application is very important as the radiation will pass through the equivalent of twice the thickness of the glass and twice through the front glass, surface-to-air interface.

The glass mirror range comprises thick, heavier more durable glass and thin, lightweight and more fragile glass. The mirrors may also be front or back surfaced which impacts on the reflectivity. Considering transport, implementation and maintenance of this technology in Upington the thicker glass may be preferable.

Flabeg manufacture low-iron 4 mm float glass mirrors with a solar-weighted transmittance and reflectance of 98% and 93.5% respectively when new. These are used in the SEGS plants on Luz LS-3 parabolic trough concentrators and operational experience with them are

reported to be very good. Despite this they are susceptible to wind-related breakage and are expensive to transport and install.

Glass mirror alternative development and implementation has been occurring for a number of years and Jorgensen reported on a number of these in 2001. ReflecTech, Inc. has co-developed a mirror film with NREL which is used by SkyFuel, Inc. on their SkyTrough parabolic trough concentrator. Before this development most researchers were in agreement that glass alternatives did not demonstrate low cost, good performance and durability characteristics required for commercial trough development, confer with Price *et al*. (2002). However, ReflecTech's most recent technical release (2009) quotes a loss of less than 0.5% across the solar spectrum after 6.25 years of measurements.

ReflecTech mirror film is a 0.10 mm thick pressure sensitive adhesive film made of multiple polymer film layers with one silver layer to give mirror like reflectance while protecting against UV radiation and moisture. It is designed for application to smooth surfaces, has a peel-off back liner to cover the adhesive until application and a peel-off top liner to protect the mirror surface during processing, handling, transportation and installation.

ReflecTech quote a specular reflectance of 94%, a solar-weighted hemispherical reflectance of 94% and a maximum operating temperature of 60°C. The mirror film is laminated onto curved aluminium panels integrated with an aluminium space frame forming the parabolic mirror of SkyFuel's SkyTrough parabolic trough concentrator.

Maintenance of high specular reflectance of parabolic collectors is a challenge as dirt or degradation of the reflective coating result in loss of reflectance. As parabolic collector reflectance directly affects solar field performance, cleaning of parabolic collectors is of vital importance. Cohen *et al*. (1999) experimented with two mechanized cleaning methods and found that a high-pressure, demineralised-water sprayer with rotating heads mounted on a rig that could be operated by one person worked most effectively. SAM has mirror washing input fields which contain the amount of water used to watch each square meter of collector mirror and the number of washes per annum. These inputs are used to calculate the annual wash water usage for the solar field which is presented in the modelling results in chapter 6.

The optical losses and solar absorption of reflective parabolic collector mirrors is difficult to model accurately.

Parabolic collector reflectance has a strong influence on system efficiency. Forristall (2003) reports that at a working fluid temperature of 400°C, a 15% decrease in reflectance results in efficiency decreasing by 24.5%.

2.2.1.3 Parabolic trough support structure technology

The structure supporting the parabolic reflector is an important factor when considering construction of a parabolic trough power plant. The metal support structure for parabolic trough collectors was pioneered by the Luz LS-2 and LS-3 designs implemented at the SEGS plants.

Abengoa Solar Industrial Solar Technology (IST) produced a parabolic trough collector mainly used in low temperature process heat applications called the PT-1. Solúcar, the solar technology business unit of Abengoa then developed the PT-2 based on the PT-1 design. The updated collector's small aperture raises concerns that a larger solar field area may be required to produce the same output as a smaller solar field with larger aperture collectors.

The EuroTrough consortium formed by European research laboratories and companies (CIEMAT, DLR, FSI, CRES, Iberdrola, Inabensa, Fichtner Solar, SBP, Solel) have completed the development and testing of two parabolic trough collector models, namely the ET100 and ET150 (Geyer *et al.*, 2002). These collectors have a torque box design which is light-weight and easy to assemble, which is a significant advantage for installation (Geyer *et al.*, 2002).

FLAGSOL GmbH, a subsidiary of The Solar Millennium Group, has developed two collectors based on the EuroTrough design: the Skal-ET and the new HelioTrough. The differentiating factor between the two collectors is that the Skal-ET uses the torque box design developed by the EuroTrough consortium while the HelioTrough uses a torque tube design developed by Flagsol and Schlaich Bergermann und Partner (SBP) (Flagsol, 2010).

The Skal-ET parabolic collector has been used in the Andasol projects in Granada, Spain as well as the Kuraymat project in Egypt, and as such is a proven design (Herrmann and Nava, 2005). The HelioTrough has recently been integrated into the SEGS V plant (December, 2009) and is undergoing performance and operational tests.

SENER, the Engineering, Procurement and Construction (EPC) contractor for the Andasol projects, has developed its own parabolic collector called the Senertrough. SENER installed and tested a 600 m Senertrough loop at Andasol-1 (Vázquez and Castañeda, 2008) and then implemented the design in the 50 MW Extresol-1 solar thermal plant in Extremadura, Spain

(Vázquez *et al*., 2009). The collector's distinctive elements are its torque tube and 28 stamped cantilever arms attached to the tube, to which the mirrors are directly attached.

Solargenix Energy developed, installed and commissioned their parabolic trough collectors at the 1 MW Arizona Public Service (APS) Saguaro Solar Trough Power Plant. The collector uses an all aluminium space frame and is called the DS1. The design was based on the LS-2 collector but Solargenix Energy claim "superior structural properties, weight, manufacturing simplicity, corrosion resistance, manufactured cost and installation ease." (Solargenix Energy, 2004)

National Renewable Energy Laboratory reported that Solargenix Energy designed a new SGX-1 collector under the U.S. Department of Energy's USA Trough Initiative. The SGX-1's aluminium design is lighter than comparable steel designs and is assembled with fewer fasteners. This avoids the need for specialised manufacturing, welding and component alignment in the field.

In collaboration with NREL, a second generation SGX-2 collector was developed by Solargenix Energy. The SGX-2 collector has an improved space frame design that reduces fabrication time and cost. It is also extremely accurate, light and easy to assemble without a fabrication jig.

The SGX-2 collector has been used in the 64 MW Nevada Solar One project and therefore is considered as successfully proven.

SkyFuel have most recently developed the SkyTrough parabolic trough concentrator. In their own words:

> "The SkyTrough consists of ReflecTech mirror film laminated onto curved aluminum panels; which are integrated into an aluminum space frame to form the parabolic [mirror]. The space frame [is made of] extruded aluminum struts and other components [that] are self-aligning when joined together with fasteners, requiring no welding. The entire assembly is mounted on pylons and attached to a self-locking rotary hydraulic drive enabling the [collector] to pivot and track the sun."
> (SkyFuel, 2009: 2)

SkyFuel have signed an agreement in 2009 to install SkyTrough collectors at SEGS I & II (now known as the Sunray 43 MW parabolic trough generating plant).

To summarise, reflective parabolic receivers consist of a highly reflective glass mirror or a mirror filmed parabolic reflector which is supported by an aluminium frame of varying complexity and weight. A number of manufacturers have developed different designs which can be likened. The latest available data from the most prominent manufacturers are compared in Table 2-1.

Table 2-1: Reflective parabolic receiver metrics (Grey areas indicate data not publicly specified by manufacturer)

Manufacturer	IST Solúcar	Flagsol	Flagsol	SENER	Solargenix Energy	SkyFuel
Collector	PT-2	Skal-ET 150	HelioTrough	Senertrough	SGX-2	SkyTrough
Module aperture length [m]	12	12	19.1	12.27	12*	13.9
Module aperture width [m]	4.4*	5.77	6.77	5.774	5.77*	6
Module aperture area [m^2]	52.8	69.24	129.3	70.8	69.24*	83.4
No. of modules per solar collector assembly	12	12	10		12*	8
Total solar collector assembly length [m]	148.5*	148.5	191		100-150*	115
Net aperture area [m^2]		817.5	1263			667
Mirror type		Glass mirror	Glass mirror	Glass mirror	Glass mirror	Silver polymer film
Solar-weighted reflectance [%]						94
Total mirror area [m^2]						750
Mirror area/aperture area ratio						1.12
Focal length [m]	1.7*	1.71		1.71		1.71
Gemoetric concentration	~63*	82*			82*	75
Structure	Parabolic sheet with front lattice	Torque Box	Torque Tube	Torque Tube	Space-frame	Space-frame
Materials of construction	Sheet metal	Galvanised steel	Recycled aluminium	Pre-galvanized steel sheet	Recycled aluminium	Aluminium
Drive type	Linear actuator/hydraulic	Two hydraulic cylinders	Hydraulic		Hydraulic	Self-locking rotary hydraulic
Rim angle [°]	72*	80*				82.5
Module weight per m^2 [kg]	~17*	~28			~22*	
Erection method	On site factory assembly*	Jig	Concrete jig	Jig	No jig required	
Foundations	Concrete caissons*	Pile	Spread foot foundation			
Wind load design basis [m/s^2]	35.8*	31.5*			~33	40
Control system	Feedback	Flagsol proprietary*			Acciona proprietary*	SkyFuel SkyTrakker
Peak optical efficiency	75*	80			77*	
Overall optical efficiency	--	78				
Geometric concentration (aperture width)/(absorber tube diameter) [sun]	99	Varies with HCE used	Varies with HCE used	Varies with HCE used	Varies with HCE used	Varies with HCE used

*Kearney, DW. 2007. Parabolic Trough Collector Overview. *Parabolic Trough Workshop 2007*. Golden, CO, USA.

2.2.2 Linear tubular receivers

Often referred to as HCEs or simply receivers, linear tubular receivers used in parabolic trough systems typically consist of an internal steel pipe or tube with an absorptive coating covered by a glass envelope with a vacuum or air gap between the pipe and the glass envelope. Thermal tests of the SEGS LS-2 parabolic trough solar collector by Dudley *et al*. (1994) at Sandia National Laboratories demonstrated that the highest efficiency and lowest thermal losses occurred when the linear tubular receiver (LTR) annulus was at vacuum conditions.

Research and modelling by Relloso *et al.* (2008) indicates that the fundamental metric of an LTR affecting the thermal efficiency of a collector assembly is its diameter–specifically the diameter of the metallic tube inside the annulus. Within a range of 65 mm to 100 mm, the larger the diameter, the higher the efficiency will be. This is due to the reduction of 'spillage' of light from the reflective parabolic trough. This improvement in 'spillage' efficiency is greater than the increases of the thermal losses associated with a larger tube so the total thermal efficiency increases within this range.

A variety of absorptive coatings can be applied to the pipes transporting the working fluid. The quality of an absorptive coating is determined by its selectivity. That is how well it absorbs incident radiation and how effectively it limits infrared radiation from its hot surface to surrounding components of the receiver. Therefore, the higher the absorptivity and the lower the emissivity of the coating, the more thermally efficient it is at transferring solar radiation into heating the working fluid. Hence, absorptive coatings are often referred to as selective surface coatings.

Due to its wide adoption for use on solar collectors, black chrome is the selective coating often used as a baseline against which to measure newer coatings. The test results of Dudley *et al*. (1994) suggest that cermet coatings have a lower emissivity than black chrome even at higher temperatures. Although cermet coatings were more efficient and had lower thermal losses than black chrome, the differences were not large. Tests performed on the IST parabolic trough reflector assembly by Dudley *et al*. in 1995 propose that selective coatings of black nickel display better efficiencies and lower thermal losses than black chrome as well. More recent work by Forristall (2003) suggests that cermet coatings developed by Solel Solar Systems Ltd. for their Universal Vacuum Air Collector (UVAC) are improved and are currently being used as a baseline to measure more recently developed coatings.

Another important characteristic of a linear tubular receiver is the type of glass used to transmit incident solar radiation and shield the pipes from radiating their thermal energy to the environment. The glass must have a suitable refractive index and extinction coefficient. That is it should transmit as much incident radiation as possible and absorb or reflect the incident radiation as little as possible. Glass is most often used as its properties do not change with the wavelength of incident solar radiation and hence has a low spectral dependence. Anti-reflective coatings are therefore preferred and widely used. Receiver glass envelopes of solgel anti-reflective coated Pyrex glass have been reported to enhance collector performance (Dudley *et al*., 1995).

A detailed thermal model and efficiency calculation methodology for linear tubular receivers was developed by Forristall (2003). While the efficiency of a reflective parabolic collector is a complex combination of optical losses and solar absorption, a thermal resistance model for a tubular receiver is more conveniently developed and computed. Development of such a model for each technology is beyond the scope of this study.

SAM calculates heat loss using LTR manufacturer's data. The parameters used to determine heat loss include absorber-, envelope- and gas parameters. Variations are also considered, as in the case where some LTRs in the loop have broken glass. The portion of the LTR circuit with broken glass can be modified by the user.

A factor that acutely affects the efficiency of a linear tubular receiver is the stability of the vacuum in the annulus. At typical operation temperatures in parabolic trough plants the HTF slowly decomposes into volatile compounds like furans and hydrogen (Kuckelkorn *et al*., 2009). Free hydrogen can permeate through the absorber tube into the glass annulus, strongly increasing heat losses due to the high heat conductance of hydrogen gas. To resolve this issue, disc-shaped getters are placed in the glass annulus to suppress vacuum loss and maintain vacuum stability. Vacuum stability is dependent on the getter quality and the getter temperature during operation, as hydrogen is mainly gettered physically and capacity is lower at higher temperature.

2.2.3 Heat transfer fluids

A variety of working- or heat-transfer fluids are suitable for use in parabolic trough systems. Variances among the properties of different organic oils or synthetic fluids are small. However, temperature does affect the properties of each fluid significantly. The commonly cited fluids are listed in Table 2-2.

Table 2-2: Heat transfer fluids arranged by manufacturer

Heat transfer fluid	Description	Freeze point [°C]	Minimum temperature [°C]	Maximum operating temperature [°C]	Manufacturer
Therminol VP-1	Low-chloride biphenyl:diphenyl oxide eutectic blend (BP:DPO)	12	50	400	Solutia Inc.
Therminol 59	Alkyl substituted aromatic	-68	-45	315	
Therminol 66	Modified terphenyl	-32	0	345	
Dowtherm RP	Synthetic oil	-40	-20	350	The Dow Chemical Company
Dowtherm Q	Synthetic oil	-50	-35	330	
Syltherm 800	Dimethyl polysiloxane	-60	-40	400	
Xceltherm 600	Hydrogenated paraffinic white oil	-20	10	316	Radco Industries, Inc.
Caloria 500	Mineral hydrocarbon oil	-40	-20	300	Exxon Company USA
Solar Salt	60% $NaNO_3$, 40% KNO_3	220	260	600	Chilean Nitrate
Hitec heat transfer salt	7% $NaNO_3$, 53% KNO_3, 40% $NaNO_2$	142	175	500	Coastal Chemical Company
Hitec XL	48% $Ca(NO_3)_2$, 7% $NaNO_3$, 45% KNO_3	120	150	500	

SAM's HTF library contains Therminol VP-1, Dowtherm Q, Dowtherm RP, Caloria, Solar Salt, Hitec and Hitec XL. Using the HTF viscosity, density, conductivity, temperature and specific heat it calculates the minimum and maximum required velocity of the HTF in the solar field.

Research in direct steam generation (DSG) for parabolic trough collectors is currently being performed by the Spanish Research Centre for Energy, Environment and Technology (CIEMAT) and the German Aerospace Centre (DLR) at the Plataforma Solar de Almería (PSA) test facility. The test facility operates in three modes which generate steam between 300°C and 375°C at 30 bar and 100 bar respectively from its eleven parabolic troughs. Three DSG processes have been developed, as discussed by Zarza *et al*. (2001). The PSA direct solar steam (DISS) facility was operated for over 2000 hours during the first 23 months of the project. However, it has been plagued by failures of its conventional equipment such as the water recirculation pump, thermocouples, and control and instrumentation cards. The facility also has a large thermal inertia due to the steam condensing into water overnight and the solar field being limited in size. Hence more time is required to get the water to boiling point each day than could be expected from a commercial plant.

Langenkamp (1998) proposed that DSG technology along with improvements in collector field design and enhanced system integration could result in levelised cost of electricity (LCOE) reductions of up to 26%. The enhanced solar-to-electric efficiency in DSG systems when compared to traditional plants using an HTF can only be unlocked at temperatures of 450°C and above (García, 2000). Since the PSA facility is unable to operate at temperatures above 400°C, the German-Spanish projects REAL-DISS and GDV-500-PLUS have commissioned a DSG demonstration plant that operates at 500°C (Eck *et al.*, 2009). The chief objective of this plant is to test and develop components at this temperature and ultimately demonstrate feasibility of the concept before the design, construction and commercial operation of a DSG solar thermal power plant in Spain with a capacity of 50 MW is pursued.

Seeing the difficulties of the DSG concept, the physicists at the PSA have very recently started investigating the use of inert gases as HTFs. Rodríguez-García *et al.* (2009) produced experimental results of a parabolic trough plant using CO_2 as the HTF. During simple start-up and shutdown procedures, excellent regulation of the gas outlet temperature (400ºC ±5ºC) under very significant variations of solar radiation was achieved. The start-up time from cold conditions was relatively long compared to plants utilizing conventional HTFs but the team claims that with an optimized layout, the time can be halved.

Carbon dioxide leaks at the rotating joints of the troughs were found to be a significant problem during the experiment. Improved rotating joints or hose connections are being explored to increase the gas outlet temperature to 525ºC (Rodríguez-García *et al.*, 2009).

As it stands the most favourable HTF is the low-chloride (< 10 ppm), biphenyl:diphenyl oxide eutectic blend (BP:DPO) Therminol VP-1, which demonstrated good long-term operation in carbon steel piping systems. Its physical properties allow for excellent heat transfer coefficients, its low viscosity minimizes pump power requirements and its low melting point of 12ºC provides freeze protection for cold plant downtime periods. However, disposal of large volumes of Therminol VP-1 as it ages and its quality deteriorates, needs to be carefully considered due to its benzene content (Bevacqua *et al.*, 2008).

Bevacqua *et al.* (2008) from Solutia Inc. propose the combination of venting low-boiling compounds (which can cause pump cavitation) and distilling high-boiling compounds (which increase viscosity and reduce heat transfer efficiencies) on site to extend the fluid life of Therminol VP-1.

2.2.4 Thermal energy storage

Thermal Energy Storage is of keen interest to parabolic trough operators as it enhances plant operational flexibility and can increase the annual electricity generating capacity of the plant. It also can provide a buffer for transient weather conditions. TES allows the energy converted by the plant to be time-shifted so it aligns with peak electrical load demand. It can even-out electricity production at the plant and allows full load operation of the steam cycle at full load efficiency (Herrmann and Nava, 2006).

Energy storage can be implemented either directly via the HTF or indirectly via a secondary heat exchange and storage system. The direct use of the HTF to both transfer and store thermal energy has the substantial benefit of simplifying plant designs in that no heat exchangers are required. This both reduces the technical risk and cost of the plant. Current research is focused on developing a high-boiling ester with a very low vapour pressure to avoid the requirement of pressure-rated tanks and a boiling point around 0°C to avoid the risk of freezing in the collector fields during cold periods.

Nitrate salts like Hitec XL may be feasible energy storage and HTFs, however, their high boiling point or freeze-onset temperature of around 120°C raise concerns about more expensive piping and materials, as well as the durability of the selective coating on the linear tubular receivers to withstand the increased operating temperatures required (Moens and Blake, 2005). Using a synthetic fluid as mentioned in section 2.2.3 for energy storage and heat transfer is generally considered too expensive for commercial operation (Bradshaw and Siegel, 2008).

In light of the current limitations facing direct TES technology, indirect TES systems utilizing heat exchangers are currently used to reduce the risks involved with direct TES systems such as calcification within pipes if molten salt temperature falls below its melting point.

The use of molten salt to store heat has been relatively widely implemented in the process industry and is the most mature of the indirect TES systems. Andasol 1, a 50 MW_e parabolic trough CSP plant commissioned in Spain in 2009, uses a two-tank molten salt system with seven and a half hours of energy storage (Bürkle, 2009). Andasol 2, currently being commissioned by SENER, uses the same two-tank molten salt system as Andasol 1. Andasol 3, currently under construction, will utilise a two-tank storage system that will attempt to provide nine hours of energy storage (Thompson, 2010). The molten salt thermodynamics in these plants limit the temperature loss in the tanks to 1°C per day.

SAM has a well developed two tank TES model. Based on the turbine's required thermal input and the number of hours of storage required, it sizes a tank pair, calculates the thermal capacity and estimates the heat loss of the system, among other functions.

The thermocline system is a potential low cost alternative to the current two tank system. This is a fluid- and filler-filled tank with a vertical thermal gradient, which results in less dense hot fluid settling in the top of the tank and denser cooler fluid settling in the bottom of the tank. Energy is stored in the potential existing between the hot and cold fluid. As the fluid attempts to reach equilibrium by reducing the thermal gradient across it, this energy is released via conduction, convection and radiation. The filler material reduces the amount of fluid required and provides "thermal capacitance" according to Paccheco *et al*. (2001).

Paccheco *et al*. (2001) built and tested a 2.3 MWh thermocline system using molten-nitrate salt as the HTF to compare with a two-tank molten salt system. Their results suggest that a thermocline indirect storage system may cost less than a two-tank molten salt system.

Laing *et al*. (2009) have started testing a three component thermal storage system for use in a parabolic trough DSG plant. The storage system designed for testing consisted only of a phase change material (PCM) storage module for evaporating water and a concrete storage module for superheating steam. A separate concrete module for preheating liquid water is not installed as the researchers found the super-heating step more critical and challenging to demonstrate successfully. Eventually the system is envisaged to consist of a concrete pre-heater unit, a phase change material evaporator unit and a concrete super-heater unit. The results of their tests will determine the future feasibility of the concept.

2.2.5 Power plants

Three types of power plants or cycles are commonly used for parabolic trough power plants: the steam Rankine cycle, the organic Rankine cycle (ORC) and the combined cycle (which also utilizes a Rankine cycle). There are also differing techniques to integrate the thermal energy generated in the solar field into the power cycle.

The thermal-to-electric energy converter most often used for parabolic trough systems is a turbine. A steam or organic working fluid turbine uses a Rankine cycle to convert heat energy into rotational energy which is then converted to electrical energy via the windings on the shaft (rotor) and the body (stator) of the turbine alternator.

Cumulative temperature measurements by the SAWS report that Upington has a mean temperature of 35°C. Considering that the HTF heats the water used in the Rankine to around 393°C, a theoretical maximum efficiency for any Rankine cycle operating at this temperature can be calculated using the Carnot efficiency (e_c) as follows:

$$e_c = 1 - \frac{T_L}{T_H} \tag{2.4}$$

$$e_c = 1 - \frac{308\ K}{666\ K}$$

$$e_c = 0.54\ or\ 54\%$$

where T_L and T_H are the cold reservoir temperature at ambient and boiler temperature in Kelvin respectively. Adding the parasitic system losses incurred by the major components of a Rankine cycle, namely the pumps, boiler, turbine and condenser will reduce this value significantly. Plants using conventional steam Rankine cycles report efficiencies in the order of 38% (Kelly, 2006a). Also evident from the equation is that the higher the temperature in a Rankine cycle the more efficient the energy conversion. Hence, HTF temperature is a critical contributor to the efficiency of a pure Rankine cycle.

The overall efficiency of a Rankine cycle is characterized mainly by the difference in the temperature and pressure of steam entering a turbine to that of steam exiting it. One of the central design considerations in Rankine cycle CSP applications is the heat rejection system. The two commonly used methods are dry and wet cooling. Wet cooling, which provides a lower condensation temperature, improves the expansion ratio and ultimately the electrical energy derived from work performed by the steam. However, this comes at the cost of using considerable amounts of water. Considering that Upington and its surrounds are arid, this poses an environmental concern. CSP plants utilizing dry cooling are estimated to produce between four and nine percent less electricity annually than plants employing wet cooling (Kelly, 2006b). However, Kelly (2006b) also estimates that dry cooling uses only eight percent of the water required by wet cooling in equivalent CSP plants.

Plant operator experience (Scott and Lee, 2006) suggests that wet cooling is more cost-effective, has lower operation and maintenance (O&M) costs, and provides higher power-cycle efficiencies particularly during the hotter summer months than dry cooling. This along with the higher capital costs of dry-cooling systems requires CSP plant designers to chose

between obtaining higher solar-to-electrical efficiency at lower capital cost, or losing solar-to-electrical efficiency and increasing capital spend to protect water resources in the area.

As parabolic trough- and conventional power plants utilize the same steam turbine technology (with only the steam-heating technology differing), they are easily hybridized. Thus a coal-fired boiler could easily supplement a parabolic trough plant during cloudy periods or overnight if firm base-load power generation is required. However, the startup times of coal-fired boilers often lead to the use of natural gas standby turbines so that the nameplate capacity of the plant can be maintained during peak load times.

2.2.5.1 Steam rankine cycle

All of the SEGS plants and a considerable number of new plant projects entering their Engineering, Procurement and Construction (EPC) phases use steam Rankine cycles. As of 2008 Siemens had secured orders for forty-five of their SST range of steam turbines for CSP plants worldwide (Siemens, 2008).

CSP plants may utilize either high-, intermediate- or low-pressure steam turbines. Kelly (2006a) suggests that intermediate- or low-pressure turbines between 50 MW_e and 140 MW_e provide higher expansion efficiencies than similarly sized high-pressure units. And high-pressure turbines between 140 MW_e and 220 MW_e provide higher expansion efficiencies than similarly sized intermediate- or low-pressure units. Non-uniform aerodynamic loads at the end of the turbine blades from fixed steam leakage in the high-pressure turbine represented a smaller proportion of the total flow past the blades as blade-length was increased. Hence high-pressure turbines are better suited to large CSP plants and intermediate- or low-pressure turbines are more efficient energy converters in intermediate-sized CSP plants.

According to Feldhoff *et al*. (2009) the principal difference between a steam turbine used for a CSP plant, and a steam turbine used for a conventional fossil fired power plant is the cycling rate of start-ups and shut downs. A conventional plant turbine may be shut down several times a year whereas a CSP unit is started up and shut down daily. This daily cycling requires careful monitoring of the main steam temperature and pressure of the turbine.

Steam Rankine cycles are made more efficient by using waste heat to increase the temperature of the steam in the boiler and hence increase the Carnot efficiency. This is commonly termed as reheat technology and most turbines used in CSP applications are reheat steam turbines.

The power cycle model in SAM for parabolic trough plants is a Rankine cycle model. It uses inputs to characterise the power plant's capacity, cycle conversion efficiency, control philosophy and cooling system. It allows for different modes of fossil fuel backup including minimum backup level or supplemental operation. Start up and standby times can also be defined.

2.2.5.2 Organic rankine cycle

In the Organic Rankine Cycle (ORC) an organic chemical is heated to form a gas which drives a turbine. Using refrigerants (e.g. freon, butane, ammonia) which boil at extremely low temperatures of typically 66°C, generating significant pressures, the ORC can occur at much lower temperatures than the steam Rankine cycle. In an ORC an evaporator replaces the boiler and condenser only requires ambient air to cool the gas leaving the turbine into a liquid.

Prabhu (2006) performed a study on the Solar Trough Organic Rankine Cycle Electricity System (STORES) concept and found that even though the steam Rankine cycle has thermal efficiencies of between fifteen and twenty-five percent higher than the ORC; the ORC has other benefits that make it a viable alternative in 1 MW to 10 MW plant sizes. It is more efficient when the ambient temperature is low (this matches the load profile of South African communities which consume more electricity during winter months) and can be operated with minimally skilled operators and maintenance crew which makes it potentially attractive for Upington.

In order to enhance the efficiency of ORC turbines, two ORCs are cascaded with the first higher temperature ORC loop utilising a refrigerant with a higher boiling point and the second lower temperature ORC loop using waste heat from the first loop to evaporate a second refrigerant with a lower boiling point.

Two methods normally used to increase the thermal efficiency of a cascaded ORC are recuperation and selecting an HTF that can operate at a higher temperature. Using the temperature of the gas exiting the turbine's exhaust to preheat the chemical fluid before it is vapourised is termed recuperation. By allowing the HTF temperature to be as high as possible, and hence increasing the temperature at which the ORC occurs, a higher thermal efficiency can be attained.

Prabhu, (2006) states that "the recuperated cascade cycle is the most thermally efficient" ORC. But he also admits that even the efficient ORC systems "are less efficient than extraction steam cycles". They still pose a promising alternative for the Upington area.

2.2.5.3 Combined cycle

Integrating a CSP plant with a conventional coal-fired steam or gas-fired power plant can be an efficient way to combine the base-load reliability of conventional boilers or gas-turbines with the midday peak-load tracking characteristic of a CSP plant provided it has been started up in the morning and is past its thermal inertia.

The steam turbine of a coal fired power plant may be oversized to provide either a gas- or solar-powered supplement to the boiler's capacity and hence run the main turbine at full capacity. During the day and early night the turbine could be supplemented with solar power and stored solar energy respectively. During the later hours of the night the electricity demand may reduce to a level where the turbine need only run at the capacity of the boiler until the next morning. If a morning peak in demand is required before sunrise, the gas turbine could augment the steam supply to the main turbine.

2.3 Linear Fresnel systems

CLFR plants use a series of long, narrow, slightly-curved primary mirrors, to reflect beam radiation to an immobile receiver. The receiver contains a secondary reflector and a linear tubular absorber with a selective coating. The bottom of the receiver structure forms a cavity, which is covered by a glass plate to reduce thermal losses. The receiver is located several meters above the primary mirror field (Figure 2-2).

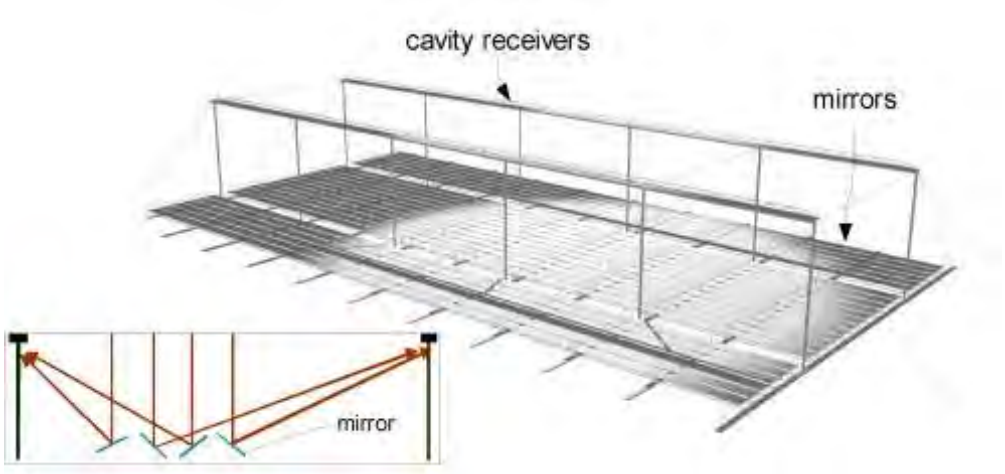

Figure 2-2: Linear Fresnel system (Pye, 2008)

LFR systems differ from parabolic trough systems in optical focusing technology, thermal efficiencies, absorber configuration and power plant implementation method employed.

Linear Fresnel systems do not have the wind loading issues of parabolic trough systems because the mirrors are flat or only very slightly curved. Low-cost flat glass can be used or curved elastically to make each facet. The linear absorber is immobile, therefore, the flexible fluid joints required in trough systems can be omitted. By aiming the mirrors at different linear absorbers at different times of the day, the mirrors can be more densely packed resulting in space-optimisation. However, Pitz-Paal (2008) argues that due to the flat arrangement of the mirrors, intrinsic additional optical (cosine) losses reduce the annual output by 20% to 30% compared with the parabolic trough design. This reduced optical performance needs to be offset by the lower investment cost in order to make linear Fresnel systems a reasonable option.

The most commonly presented mode of operation for a CLFR plant is the direct generation of steam in its absorbers which is then either used to augment the steam generated by a fossil fuel fired boiler in a conventional power plant, or feed hot water into a power plant steam cycle via a heat exchanger. Evidence of this approach can be found in work by Mills and Morrison (2000), Mills *et al*. (2003), Mills (2004), Mills *et al*. (2004a, b), and Bernhard *et al*. (2008).

2.3.1 CLFR optic and thermal efficiencies

While the useful power (P_u) obtained from a CLFR solar collector system can be characterized by exactly the same equation as that used for a parabolic trough collector system, the optical derating factors (losses) are calculated differently due to the existence of two incidence angle modifiers in a CLFR collector.

Bernhard *et al*. (2008) have developed a set of optical and thermal efficiency equations based on the linear Fresnel collector demonstration plant installed and commissioned at PSA in 2008. These were developed during the commissioning and first performance tests of the plant and reported at 14th Biennial CSP SolarPACES Symposium in 2008. Bernhard *et al*. (2009) then presented a refinement of the equations at SolarPACES 2009. It is useful to present both sets of equations with their varying nomenclature for comparison, as given in Table 2-3.

Table 2-3: CLFR efficiency equations (Grey areas indicate no expression listed by Bernhard *et al.)*

Quality	Bernhard *et al*. (2008) definition	Bernhard *et al*. (2009) definition	Discussion
Collector Thermal Efficiency (η)	$\eta = \frac{\dot{m}(h_{out} - h_{in})}{A_{col}E_b}$	$\eta_{therm} = \frac{\dot{Q}_{therm}}{\dot{Q}_{solar}}$	$\dot{Q}_{therm} = \dot{m}(h_{out} - h_{in})$ $\dot{Q}_{therm} = A_{col}E_b$
η expressed in terms of Optical Efficiency	$\eta = \eta_{opt,0} - a_1 T_m^* - a_2 E_b T_m^{*2}$	$\eta = \eta_{opt^*} - c_1 \frac{\Delta T}{DNI} - c_2 DNI \left(\frac{\Delta T}{DNI}\right)^2$	$a_1 = c_1$ $a_2 = c_2$ $E_b = DNI$ $T_m^* = \frac{\Delta \mathrm{T}}{\mathrm{DNI}}$ $\eta_{opt,0}$ – optimum optical efficiency η_{opt^*} – optimum optical efficiency minus all optical influences
η expressed in terms of angular dependent losses	$\eta = \eta_{opt,0} IAM(\theta_i) - a_1 T_m^* - a_2 E_b T_m^{*2}$		

The symbols used in Table 2-3 are defined as follows:

$\dot{m}$ = total collector flow rate

h_{in} = temperature of working fluid entering the collector

h_{out} = temperature of working fluid leaving the collector

A_{col} = collector area defined as cumulative area of the primary mirrors

E_b = direct normal irradiation

$\eta_{opt,0}$ = collector efficiency for perpendicular irradiation and no heat loss (T_m^*= 0)

T_m^* = reduced mean temperature defined as $T_m^* = \frac{T_m - T_{amb}}{E_b}$ where T_{amb} is the ambient temperature; and T_m is the mean of the inlet and outlet temperature of the collector

a_1 and a_2 = particular coefficients for each collector determined by experiments

$IAM(\theta_i)$ = Incidence Angle Modifier (IAM) - angular dependent losses of collector in longitudinal direction; caused mainly by growing beam expansion and rising end losses

In reality the efficiency equations for CLFR collectors are obtained by fitting a polynomial to experimental results. SAM's linear Fresnel model uses a set of polynomial equations in which the user can specify the thermal loss relationships to model the performance of the solar field.

Usually the $IAM(\theta_i)$ is determined via experiments. The data measured from the experiments are either logged or used to develop mathematical approximations.

The sun's rays move both along and across linear Fresnel-collectors during the day. Therefore, two independent angles define the position of the sun relative to the collector, namely the longitudinal angle $\theta_{\parallel}$ and the transversal angle $\theta_{\perp}$ as depicted in Figure 2-3. The incidence angle modifier is dependent on these two angles. In practice a longitudinal $IAM_{\parallel}$ and a transversal $IAM_{\perp}$ are determined by experiments or ray-tracing.

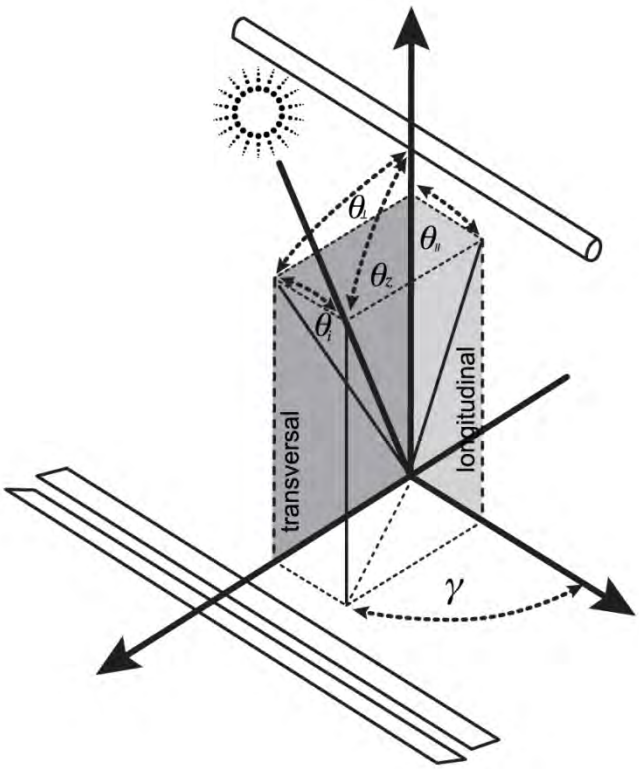

Figure 2-3: CLFR geometry (Bernhard *et al.*, 2008)

The final IAM as a function of zenith angle θ_z and azimuth angle γ: $IAM(\theta_z, \gamma)$ (when a collector orientation is given) or of longitudinal and transversal sun position respectively, $IAM(\theta_i, \theta_{\perp})$ is calculated by factorization.

$$IAM(\theta_i, \theta_{\perp}) = IAM_{\perp}(\theta_{\perp}) IAM(\theta_i) \tag{2.5}$$

Assuming that the $IAM_{\perp}$ and $IAM_{\parallel}$ are given relative to the direct normal irradiance (DNI), the collector efficiency relative to DNI can be calculated as follows:

$$\eta = \eta_{opt,0} IAM(\theta_i, \theta_{\perp}) - a_1 T_m^* - a_2 E_b T_m^{*2} \tag{2.6}$$

The optical performance of a linear Fresnel system in SAM can be characterized either by a solar position table, collector incidence angle table or the incidence angle modifiers listed above. It uses a set polynomial with variable coefficients to calculate both the transverse and longitudinal incidence angle modifier.

2.3.2 Absorber configuration

CLFR linear tubular absorbers are generally a CPC-like structure with a linear tubular absorber running down the centre. The bottom of the absorber is often covered with a glass layer to reduce heat radiation back into the environment. The linear tubular absorber is coated using the same techniques discussed for parabolic troughs.

Two absorber configurations may be used. The first is a vertical linear tubular receiver mounted in the middle of the primary reflectors. The second is a linear tubular receiver in a single-sided CPC-like horizontal receiver above the primary reflectors facing downward.

A detailed study including raytrace and thermal models was performed by Mills and Morrison (2000). The primary results proved horizontal absorber tubes with secondary reflectors to be optimal.

Absorber heat loss is a critical item to consider in CLFR design. Due to the height of the absorber, heat can be lost to wind blowing pass the absorber. The product of this loss and the loss resulting from the temperature difference between the steam temperature inside the absorber and the ambient temperature outside it can be used to quantify this loss. SAM uses either the above-mentioned heat-loss model or an evacuated tube heat loss model to determine the absorber heat loss.

2.3.3 CLFR power plant

Most recent literature on CLFR technology (Mills and Morrison (2000), Mills *et al*. (2003), Mills (2004), Mills *et al*. (2004a, b), Bernhard *et al*. (2008)) suggests its ideal application is DSG in an ISCCS. This is partly due to the CLFR design not having the same difficulties as parabolic trough DSG plants. The top of the absorber tube in a parabolic trough DSG plant can become illuminated, causing overheating during stratified flow when vapour is present inside the tube wall (Mills *et al*., 2003). Certain CLFR designs are more suitable for direct boiling than parabolic trough designs. This is because the top of the linear tubular absorber can be shaded.

First results of CLFR technology being applied as additional steam generation at Liddell Power Station in Australia reported trouble free steam production above 285°C and 69 bar (Mills *et al*., 2004b). This specific array performed as expected and was constructed on budget. Hence, Mills *et al*. (2004b) claimed that CLFR technology was then close to commercial exploitation for the coal saver market.

Mirroxx GmbH, founded in 2008 by PSE AG: a spin-off of the Fraunhofer Institute for Solar Energy Systems (ISE) is setting up serial production and sales cooperation's for CLFR produced industrial process heat in the temperature range of up to 250 °C.

Since 2005 PSE AG has installed four systems, two of them commercial projects (Zahler *et al*., 2009). Mirroxx GmbH has also apparently installed a demonstration system for direct steam production in a linear Fresnel collector in Freiburg. The aperture area of the collector is 132 m^2. Operation pressures should be adjustable in the range from 2 bar to 16 bar. A further demo system for solar cooling was planned to be installed in Abu-Dhabi late 2009.

Zahler *et al*. (2009), state that their Mirroxx linear Fresnel collector with a pressurised water circuit at 16 bars is a cost-effective and efficient way to transfer process heat with temperatures of up to 200 °C. For temperatures above 250 °C, they argue that a thermal oil circuit is the appropriate technology. They further claim that the maximum temperature of their Mirroxx Fresnel collector is only limited by the vacuum absorber tube. Therefore, they argue that the Fresnel approach offers simple, low cost construction, low wind loads and high ground coverage, which makes CLFRs suitable for installation on flat roofs.

While future use in stand-alone solar plants using low temperature turbines was envisaged by earlier proponents of CLFR technology (Mills and Morrison (2000), Mills *et al*. (2003), Mills (2004), Mills *et al*. (2004a), Bernhard *et al*. (2008)), most recent work seems to be focusing on steam production and industrial process heat (Mills *et al*., (2004b), Zahler *et al*., (2009)).

A stand-alone plant model complete with superheated two-stage turbine is provided in SAM. This model is similar to the power cycle model for the parabolic trough system.

2.4 Central receiver systems

A central receiver system may be considered as a large paraboloid, discretised into multiple heliostats, focusing sunlight onto a tower-mounted solar receiver (Figure 2-4). Optical concentration factors ranging from to 200 to 1000 result in high solar fluxes impinging on the receiver which in turn results in relatively high working temperatures in the region of 1000°C. This allows the thermal energy generated to be converted to electricity via either a Rankine or Brayton cycle. This aspect combined with cost-effective TES make central receiver power plants flexible and easy to integrate with fossil fuel plants.

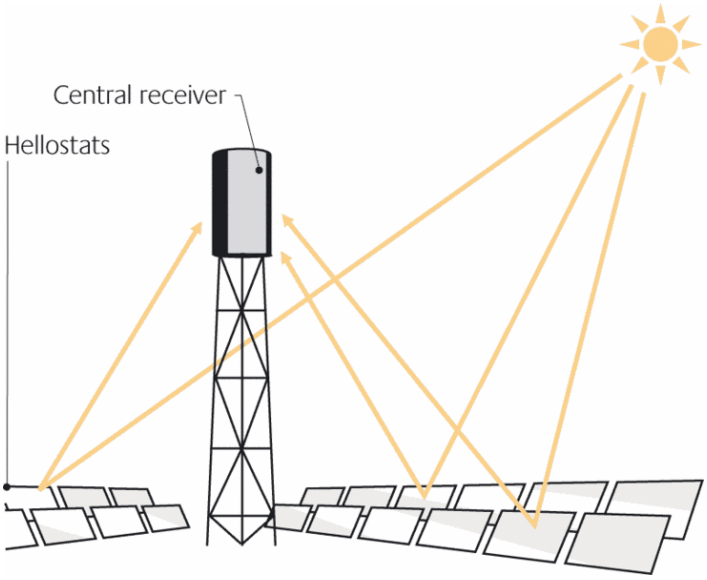

Figure 2-4: Central receiver system (German Energy Agency, 2009)

The main components of CRS power plants are heliostats, a central receiver, a HTF, an energy storage system and a power plant. There are similarities in many of the components and processes of CRS and parabolic trough power plants. However, the higher temperatures generated by CRS affect the overall design and operation of the plants in such a way that their systems are markedly different to parabolic trough systems.

Three technologies are being evaluated for the capture and transport of solar-generated heat: molten salt technology, volumetric air technology, and saturated steam technology. Volumetric air technology may be open or closed loop. Each capture technology may be optimally paired to a power plant technology. For example, molten salt and saturated steam are suited to a Rankine cycle and volumetric air technology lends itself to a Brayton cycle. These technologies will therefore be discussed briefly before investigating the major CRS power plant subsystems.

Table 2-4 provides a listing of experimental CRS power plants that have been commissioned but may not be in current operation, and provides a few useful metrics for high-level analysis of the differing technologies utilised. From these data it is observed that most experimental CRS power plants are small demonstration systems between 0.5 and 10 MW that were built in the 1980's (Romero *et al.*, 2002).

Table 2-4: Central receiver system power plant projects worldwide (Wagner, 2008)

Project	Country	Power (MW_e)	Heat transfer fluid	Storage media	Commencing operation
SSPS	Spain	0.5	Liquid Sodium	Sodium	1981
ERUELIOS	Italy	1	Steam	Nitrate Salt/Water	1981
SUNSHINE	Japan	1	Steam	Nitrate Salt/Water	1981
Solar One	United States	10	Steam	Oil/Rock	1982
CESA-1	Spain	1	Steam	Nitrate Salt	1982
MSEE/Cat B	United States	1	Nitrate Salt	Nitrate Salt	1983
THEMIS	France	2.5	Hitec Salt	Hitec Salt	1984
SPP-5	Russia	5	Steam	Water/Steam	1986
TSA	Spain	1	Air	Ceramic	1993
Solar II	United States	10	Nitrate Salt	Nitrate Salt	1996
Consolar	Israel	0.5(MWth)	Pressurized Air	Fossil Hybrid	2001
PS10	Spain	11	Steam	Steam	2007
PS20	Spain	20	Steam	*	*
Solar Tres	Spain	17	Molten Salt	Molten Salt	*
Solarthermisches Versuchsund Demonstrationskraftwerk Jülich; STJ	Germany	1.5	Steam	Water/Steam	2009

2.4.1 Molten salt technology

A typical molten-salt CRS power plant consists of two molten salt containing tanks. One at a temperature of around 560 ºC termed the hot tank and another around 300 ºC termed the cold tank. The other usual components of any CSP plant also are present. This includes a heliostat field of several hundred or thousand heliostats, a central receiver, a steam turbine and a few pumps to circulate the molten salt working fluid. When sufficient beam insolation exists, molten salt is pumped from the cold tank up the tower to the central receiver. There it is heated to between 500ºC and 600ºC and then gravity fed to the hot tank. Here it is stored until power is required from the plant. Then it is pumped to a superheater and heat-exchanger circuit where steam is generated and fed into a steam turbine generator to produce electricity.

Once the salt has been used to generate steam it is returned to the cold tank so it can start the cycle again.

A useful summary of the operating modes of a molten-salt CRS power plant is provided by Burgaleta *et al*. (2009). This technology is being deployed in the GEMASOLAR plant located in Fuentes de Andalucía, Spain which started operation in 2011.

Wagner (2008) developed components for a molten salt CRS performance model at the University of Wisconsin – Madison. These components are used within the SAM Power Tower Molten Salt model to predict the performance of this system. This model is used in chapter 4 to compare central receiver technology to the other CSP technologies.

2.4.2 Open or closed loop volumetric air technologies

The use of air as a working fluid for CRS power plants has been demonstrated since the early 1980s (Romero *et al*., 2002). The appeal of using air lies in its environmentally friendly characteristics, lack of troublesome phase changes, higher working temperatures, and easy operation and maintenance. Operational problems in several plants like Solar One in the USA, EURELIOS in Italy, and CESA-1 in Spain made it clear that tubular air receivers were not practical.

Volumetric air receivers solve a significant number of the practical short-comings of tubular air receivers. Highly porous structures absorb concentrated solar radiation inside the volume of the volumetric receiver as opposed to the outer surface of a tubular receiver. Air (the heat transfer medium) is forced through the porous structure and is heated by convective heat transfer.

Volumetric absorbers are frequently made from thin heat-resistant wires, or from metallic or ceramic open-cell matrix structures. A good volumetric absorber displays the so-called volumetric effect, where the absorber temperature on the irradiated side of the absorber is lower than the temperature of the heat transfer medium leaving the absorber.

2.4.3 Saturated steam technology

Production of superheated steam from the solar flux impinging on the solar receiver has been demonstrated in several plants like Solar One in the USA, EURELIOS in Italy and CESA-1 in Spain. The operational experience in these plants revealed critical problems in controlling

zones with dissimilar heat transfer coefficients as reported by Romero *et al*. (2002). Romero *et al*. (2002) also state that better results regarding absorber panel life and controllability have been reported for saturated steam receivers. Even though utilizing saturated steam receivers reduces technical risks, the outlet temperatures are significantly lower than those of superheated steam, making it necessary to find applications where saturated steam technology can be integrated into processes where fossil fuel provides superheating.

A drawback of direct steam central receiver technology is that it does not allow for TES. This disadvantages the technology in the South African context, as the national daily load profile (Davis *et al.*, 2011) occurs outside the peak daily DNI window, necessitating TES to meet the demand. Hence, the SAM "Power Tower Direct Steam" performance model was not used to evaluate CRS technology in chapter 5.

2.4.4 The heliostat field

Wagner (2008) states that in order to obtain the required solar flux at the central receiver, heliostats need to reflect solar radiation distances on the order of 1 km or more for large plants. Consequently the considerable average distance between each heliostat and the receiver requires precise construction, installation and control of the heliostats to reduce optical losses. This results in the heliostat field capital cost being disproportionately large with respect to the overall power plant cost. Work by Ortega, *et al.* (2006) notes that the heliostat field capital cost can range from 30% to 40% of the total plant capital costs. As a result, careful optimisation of the capital-intensive heliostat field is essential for an economically viable CRS.

The number of heliostats in each CRS varies but is generally large–on the order of thousands to provide sufficient heat on the receiver. The energy received by the central receiver is a function of the direct normal radiation being reflected by the heliostats onto the receiver. This incident power on the receiver is in turn dependent on a few dynamics within the heliostat field. Wagner (2008) presented the following instructive equation which logically accounts for the heliostat field dynamics influencing the power incident on the receiver:

$$\dot{Q}_{inc} = A_{field} \cdot \rho_{field} \cdot I_{b,n} \cdot \eta_{field} \cdot \Gamma \tag{2.7}$$

Where the total incident power on the central receiver surface, $\dot{Q}_{inc}$; is the product of the surface area, A_{field}; mirror reflectivity, ρ_{field}; incident horizontal beam radiation, $I_{b,n}$; total

field efficiency, η_{field}; and the fraction of the heliostat field that is tracking the sun and not having control problems, being fixed, or being cleaned, Γ.

SAM calculates the heliostat field performance by calculating the total field efficiency and flux distribution on the receiver as a function of solar position. It therefore does not use the above relation to characterize heliostat field performance.

The losses which influence each heliostat's ability to provide maximum reflected solar radiation to the receiver are:

i. Cosine effect losses
ii. Reflection losses
iii. Atmospheric scattering losses
iv. Shading and blocking losses
v. Beam radiation spillage losses
vi. Losses related to the sun-tracking control system

2.4.4.1 Heliostat field design

The layout of the heliostat field is an integral part of the design of a CRS. This is because the heliostat distribution around the receiver determines the required height of the tower, and the type of receiver determines whether heliostats totally surround the receiver or are located only on one side of the receiver (south in the southern hemisphere).

Wagner (2008) provides the correlations for designing a field using the radially staggered method, which is used as a starting point for the circular field optimization wizard employed in the Power Tower model in SAM.

2.4.5 The central receiver

The central receiver must be capable of surviving very high temperatures as well as the environmental conditions. Large thermal gradients that may occur on the receiver face as the plant goes from standby to running in a matter of minutes and as the aiming of the various heliostats settles.

There are two main classes of cavity receivers: external cylindrical-shaped receivers and cavity concave-shaped receivers. Both types have their advantages and disadvantages. External receivers can allow for a larger circular heliostat field while cavity receivers can be

more efficient by being more detached from ambient condition induced losses. Likewise, external receivers are more exposed to the elements and hence have higher convection and radiation losses while cavity receivers limit the amount of sunlight that can be reflected from the heliostat field due to their smaller acceptance angle.

It is also important to note that the solar field layout is determined by the type of receiver. An external receiver can accommodate a 360° heliostat field, while a cavity receiver can only optimally use heliostats placed within a wedge subtending approximately 109° from the center of the receiver.

Both external and cavity receivers can be modelled in SAM. The solar field and receiver optimization wizard within SAM shows that due to the cavity receiver requiring more rows of heliostats in a wedge, as opposed to the shallower, circular row structure for an external receiver, a cavity receiver is required to be located considerably higher from the ground. The cavity receiver's aperture is also required to be significantly wider and higher than an external receiver catering for a heliostat field of the same solar multiple. This suggests that the cost of a cavity receiver will be significantly higher than an equivalent external receiver.

2.4.6 Power cycle technology

Rankine or Brayton cycles are suitable for CRS power plants. The Rankine cycle for a CRS is as described in section 2.2.5. For a more detailed discussion, Wagner (2008) has separated the CRS Rankine cycle into five major components for which he provides mathematical relationships as well as parameters which are used in SAM. Since the HTF entering the super-heater is at a higher temperature than in a parabolic trough system. It is expected that the Rankine cycle of a CRS plant will have lower parasitic loss than that of a parabolic trough plant.

The Brayton cycle may employ either an open-loop system where air is used as the energy transfer medium or a closed-loop system where an inert gas like nitrogen or helium (Forsberg *et al.*, 2007) can be used. SAM does not contain a Brayton cycle model for a CRS power plant.

Kröger (2011) proposed the Stellenbosch University Solar Power Thermodynamic (SUNSPOT) cycle in 2008. The SUNSPOT cycle consists of a primary Brayton cycle and a secondary Rankine cycle. This combined cycle is envisaged for use with a central receiver with a rock bed thermal storage system. Exhaust gasses from the Brayton cycle are used to

run the Rankine cycle and heat the rock bed during the day. After sunset, the hot air from the rock bed is passed through a boiler which generates steam to run the Rankine cycle. The cooling for the Rankine cycle is thus required at night when ambient temperatures are significantly lower, making dry-cooling more effective.

2.5 Dish-engine systems

The major parts of a dish-engine system as shown in Figure 2-5 are the solar concentrator and the power conversion unit. The concentrator typically approximates a 3D paraboloid tracking the sun. Its size is limited to 100 m^2 to 400 m^2 in practice due to wind load constraints (Müller-Steinhagen and Trieb, 2004). The power conversion unit includes the thermal receiver and the heat engine. The thermal receiver absorbs insolation focused on it by the solar concentrator. It then converts the insolation into heat and transfers this heat to the heat engine. A set of helium or hydrogen cooled tubes make up the thermal receiver. The helium or hydrogen serve as the heat engine's working fluid as they transfer heat. Alternative thermal receivers use an intermediate fluid in heat pipes which boil and transfer the heat to the engine as they condense. The engine subsystem takes heat from the thermal receiver and converts it into electricity. The Stirling engine has been the most widely adopted heat engine in dish-engine systems.

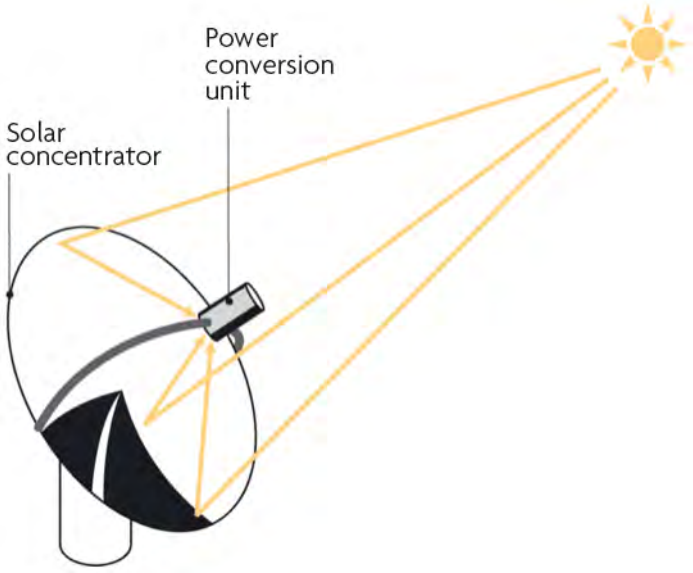

Figure 2-5: Dish-engine system (German Energy Agency, 2009)

Dish-engine systems are efficient, modular, operated autonomously, and can be easily hybridized when a Brayton cycle engine is used. Dish-engine systems utilising a Stirling cycle have demonstrated the highest net solar conversion efficiency of 31.25% net solar

energy conversion to grid-read electricity (Andraka and Powell, 2008). Therefore, dish-engine systems have potential to become a very cost-effective source of solar energy.

An energy balance equation highlights the parameters influencing the design of dish-engine systems. Stine and Diver (1994) present a useful straightforward energy balance equation which unites the expressions more recently listed by Duffie and Beckman (2006) regarding thermal, optical and concentrating performance of concentrating collectors. Stine and Diver (1994) term the following equation "the fundamental solar collection equation", and define it as:

$$Q_{useful} = I_{b,n} A_{app} E(\cos\theta_i)\rho\phi\tau\alpha - A_{rec}[U(T_{rec} - T_{amb}) + \sigma F(T_{rec}^4 - T_{amb}^4)] \qquad (2.8)$$

where Q_{useful} is the useful heat; $I_{b,n}$ the incident horizontal beam radiation; A_{app} the concentrator aperture area; E the fraction of concentrator aperture area not shaded by receiver, struts and other dish-engine components; θ_i the incidence angle (should be 0º as dish tracks sun); ρ the concentrator surface reflectance; ϕ the capture fraction or intercept (fraction of energy reflected by the concentrator into the receiver); τ the transmittance of anything between the concentrator and receiver (like a glass window covering the receiver); α the receiver absorptance; A_{rec} the receiver aperture area; U the convection-conduction heat-loss coefficient for air currents within the receiver cavity and conduction through receiver walls; T_{rec} the receiver operating temperature; T_{amb} the ambient temperature; σ Stefan-Boltzmann radiant-energy transfer constant; and F the equivalent radiative conductance.

While this fundamental equation is useful, Fraser (2008) found that the most accurate modelling results were obtained by creating a detailed model of each major component. His work was incorporated into the "Dish Stirling" model in SAM. In the following sections the major components of a dish-engine system are discussed.

2.5.1 Concentrating dish collector

The ideal shape of a dish-engine solar concentrating collector is a paraboloid of revolution. This shape is sometimes approximated by many, spherically-shaped mirrors mounted on a truss structure.

For the concentrator to effectively focus the DNI it receives onto the solar receiver, it requires a highly reflective surface, which is usually metalized glass or plastic (Stine and Diver, 1994).

For example, Wizard Power in Australia utilises large (approximately 1.2 m x 1.2 m), thin (about 1 mm thick), low iron content, curved (30 m radius) glass mirror panels in their concentrator (Wizard Power, 2011). They claim a reflectivity of greater than 93%.

When considering the design of a concentrator, the geometric concentration ratio is used to estimate the solar flux reflected by the concentrator to the receiver. Stine and Diver (1994) define the geometric concentration ratio (CR_g) as:

$$CR_g = \frac{A_{app}}{A_{rec}} \tag{2.9}$$

This shows the relationship between the accuracy of the optics in the concentrator and its associated cost and the lower concentration ratios achievable by less precise and more cost-effective concentrator optics. An optimal trade-off must be achieved between these two to design an effective concentrator.

The more significant ratio is the optical concentration. This is the flux intensity at a point on the receiver divided by the insolation on the concentrator as reported by Stine and Diver (1994). Stine and Diver (1994) highlight the non-uniform flux produced by real concentrators on receivers. They state three to five times geometric concentration ratio fluxes are normally developed on the receiver in certain areas and lower fluxes in others. This is of concern due to the high DNI levels in Upington. Actual concentrator optics result in complicated high and low flux levels on the receiver. This generates hot-spots which could reduce the operating life of the receiver and possibly damage the solar absorption interface.

The discussion of concentrator optics is incomplete without listing the optical errors which introduce losses for real concentrators. Table 2-5 describes methods of reducing optical errors reported by Stine and Diver (1994).

Table 2-5: Optical errors of dish concentrators

Optical Error	Definition	Source of Error	Possible Amelioration
Slope Error	Angle by which actual concentrator surface slope differs from the ideal	Manufacturing processes	Even precision manufacture will not totally remove this error
Facet Alignment Error	When facets are used to approximate a paraboloid and are not aimed perfectly	Use of facets, and inability to aim all facets perfectly	Precision aiming of facets will help reduce error but not totally remove it
Nonspecular Reflectance	Reflective surface diffusing reflected beam radiation	Reflective material used on concentrator	Use glass-like reflector instead of polished metal or reflective coatings on substrates
Optical Alignment Error	Mechanical alignment of concentrator and receiver and concentrator tracking error	Dish-engine system assembly, tracking algorithm and random error	Precise tolerances and precision tracking algorithms may reduce error but some of the error is random in nature
Sunshape	Apparent width of the sun causing reflected image to spread and pass receiver	The sun is not a point source of light	None

A secondary reflector or concentrator on the receiver (usually a trumpet shaped device placed on the receiver aperture) can reduce optical error, and is seen on many dish-engine prototypes. The support structure for the concentrator requires considerable structural design and variations have been developed by Wizard Power (2011) and Infinia Corporation (2011). The most mentioned designs in the literature are space frame, mirror subframe supports, and using a stretched membrane as the concentrator.

The entire dish-engine assembly is required to track the sun in both azimuth and elevation in order to maintain an insolation incidence angle of $\theta_i = 0°$. Polar tracking is mentioned as an alternative to azimuth-elevation tracking in the literature. The efficiency of the concentrator (η_{conc}) is defined by Stine and Diver (1994) as:

$$\eta_{conc} = E(\cos\theta_i)\rho\phi \tag{2.10}$$

where E is the fraction of concentrator aperture area not shaded by receiver, θ_i the insolation incidence angle, ρ the concentrator surface reflectance and ϕ the fraction of energy reflected by the concentrator into the receiver.

Fraser (2008) developed a collector model which is used in SAM, and described it with the following equations:

$$P_{in,rec} = I_{DNI} \cdot A_{proj} \cdot \rho_{ref} \cdot \varphi_{wind} \cdot \varphi_{int,fac} \cdot \varphi_{shade} \tag{2.11}$$

$$wind, speed \leq wind_{cut,out} \rightarrow \varphi_{wind} = 1.0$$
$$wind, speed > wind_{cut,out} \rightarrow \varphi_{wind} = 0$$

where the solar power intercepted by the receiver ($P_{in,rec}$) is given by:

I_{DNI} = Direct normal insolation

A_{proj} = Projected area of mirror

ρ_{ref} = Mirror reflectivity

φ_{wind} = 1 or 0

$\varphi_{int,fac}$ = Intercept factor

φ_{shade} = Shading factor

The wind cut-out velocity ($wind_{cut,out}$), is the wind velocity at which the concentrator must be moved to the stow position to avoid damage. The intercept factor is constant after the mirrors of a manufactured collector system have been adjusted for a specified receiver aperture diameter (Fraser, 2008).

2.5.2 Solar receiver

The solar receiver absorbs incident radiation reflected by the concentrating dish collector and transfers the concentrated energy to the working fluid of the engine. A solar receiver can either have its absorbing surface open to the solar flux from the concentrator (this is sometimes termed omnidirectional) or have a glass window often termed an aperture between its absorbing surface and the concentrator (these are termed cavity receivers).

External (open) receivers must handle very high solar fluxes and as a result the materials may be thermally overstressed. They are also more susceptible to significant radiation, convection and conduction losses due to wind, altitude and environmental conditions.

Cavity receivers allow the absorber surface to be recessed from the focal point of the concentrator and hence allow the flux to be directed towards the absorber from the reflective cavity walls. This reduces the solar flux gradients across the absorber, which makes for a more uniform flux distribution at a higher more controlled temperature.

Cavity receivers consist of an aperture at the focus of the concentrator to reduce radiation and convection heat losses, and an absorbing interface recessed behind the focus to reduce the flux intensity incident on it. The receiver is the interface between the concentrator and the engine and thus its design is dependent on the engine type.

Two ranges of engine receivers are used in dish-engine systems, namely Stirling engine receivers and Brayton engine receivers. Stirling engine receivers use insolation energy to heat helium or hydrogen working gas under pressure while Brayton engine receivers transfer insolation energy to a conventional combustion cycle.

Stine and Diver (1994) reported that only cavity receivers have been implemented in Stirling-engined dish setups due to their lower heat loss at higher temperatures. They also quote efficiencies of 80% to 90% in energy delivered by the concentrator to the engine.

Brayton engine receivers are less advanced. Buck *et al*. (1996) reported on a short term operation of a volumetric Brayton receiver and postulate an efficiency of over 80% based on their measurements.

Stine and Diver (1994) present a practical receiver thermal performance evaluation equation based on their fundamental solar collection equation which illustrates which attributes of the receiver need to be maximized and which need to be minimized. They define the efficiency of the receiver (η_{rec}) as:

$$\eta_{rec} = \tau\alpha - \frac{U(T_{rec} - T_{amb}) + \sigma F\left(T_{rec}^4 - T_{amb}^4\right)}{\eta_{conc} C R_g I_{b,n}} \tag{2.12}$$

From this equation it can be seen that increasing the cover transmittance and absorbing surface absorptance, while decreasing the operating temperature and conduction, convection and radiation losses will result in an optimal receiver efficiency.

Fraser's (2008) receiver model is used in SAM. Input energy is received from the collector model listed in the previous section, and then accounts for the location- and time-dependent radiation, convection and conduction losses. It can be described with the following equation:

$$P_{in,SE} = P_{in,rec} - \dot{q}_{rad,reflect} - (\dot{q}_{cond} + \dot{q}_{conv,tot} + \dot{q}_{rad,emit})_{losses} \tag{2.13}$$

Where the power output of the receiver delivered to the Stirling engine ($P_{in,SE}$) is given by the previously defined solar power intercepted by the receiver ($P_{in,rec}$) diminished by the rate of-radiation reflected out of the receiver aperture ($\dot{q}_{rad,reflect}$), receiver conduction losses

($\dot{q}_{cond}$), heat loss from the receiver by natural and forced convection ($\dot{q}_{conv,tot}$), and radiation emitted out of the receiver aperture ($\dot{q}_{rad,emit}$).

2.5.3 Engines

Two power cycles can be used to convert the concentrated solar radiation on the receiver to mechanical power: the Stirling and Brayton cycle. The mechanical power is then converted to electrical power by an electric generator or alternator.

The Stirling cycle uses an external source of heat to expand a working gas which then drives a piston in a cylinder or singular displacer. This motion is then converted to electrical energy via either a conventional or linear alternator. According to Stine and Diver (1994) the efficiency of a Stirling engine (η_{eng}) can be computed with the following equation:

$$\eta_{eng} = \beta_{Carnot}(1 - \frac{T_L}{T_H}) \tag{2.14}$$

where β_{Carnot} is the ratio of actual engine efficiency to the Carnot cycle efficiency, T_H the input heat temperature in Kelvin, and T_L the heat rejection temperature in Kelvin.

Fraser (2008) models the efficiency of the Sirling engine using the following relations:

$$\eta_{SE} = \frac{P_{gross}}{P_{in,SE}} \tag{2.15}$$

where engine efficiency (η_{SE}), is given by dividing the net power from manufacturer or test data less a parasitic power loss estimate (P_{gross}) by the power input to the engine predicted by the collector and receiver models listed in the preceding sections ($P_{in,SE}$).

By using radiation data for one day, Fraser (2008) then computes the efficiency curve, which can be obtained with the following curve-fit polynomial:

$$\eta_{SE,curve} = C_1 + C_2 \cdot P_{in,SE} + C_3 \cdot (P_{in,SE})^2 \tag{2.16}$$

where C_1, C_2 and C_3 are constants and coefficients required for this polynomial to fit the curve of the Stirling engine efficiency data from the WGA system taken on 26 April 2004.

The electrical output power of the Stirling engine is then predicted using the following equation:

$$P_{out\_SE} = P_{in,SE} \cdot \eta_{SE,curve} \tag{2.17}$$

Fraser (2008) includes terms for operating pressure, compression space, and expansion space to improve the accuracy of the model and it is used as such in SAM.

The cooling system of a Stirling engine represents a significant parasitic power loss to the Dish-engine system. Fraser (2008) describes the cooling system performance model used in SAM in section 3.4 of his thesis.

The Brayton or gas cycle produces power by the controlled burning of fuel. The Brayton engine therefore compresses air, adds fuel and combusts it in much the same way as an Otto or Diesel cycle engine. A Brayton engine utilised in a dish-engine system replaces or supplements the fuel with solar heat. The expanding hot gas does net work. A turbine and alternator capture the energy produced by the expanding gas.

Brayton engines were predicted to have an engine size dependent thermal-to-electric efficiency of between 28.5% and 33% by Gallup and Kesseli (1994). A model for a dish-engine system with a Brayton cycle does not exist in SAM.

2.5.4 Overall system

The overall dish-engine efficiency is the product of the efficiencies of each component of the system. The term “solar-to-electric conversion efficiency” is often used to describe this attribute of a solar power plant. Gross ($\eta_{conv,gross}$) and net ($\eta_{conv,net}$) efficiencies of a dish-engine system are given by Stine and Diver’s (1994) relations listed below:

$$\eta_{conv,gross} = \eta_{conc}\eta_{rec}\eta_{eng}\eta_{alt} \tag{2.18}$$

$$\eta_{conv,net} = \eta_{conv,gross} - \frac{P_{parasitics}}{I_{b,n}A_{app}} \tag{2.19}$$

Where η_{alt} is the alternator efficiency and $P_{parasitics}$ the amount of power used for tracking motors, cooling fans, control instruments and other parasitic power consumption.

3. SOLAR ENERGY AVAILABILITY AT UPINGTON

3.1 Introduction

South Africa receives very high levels of solar radiation compared to the rest of the World (DME, 2003). South Africa's average daily solar radiation varies between 4.5 kWh/m^2 and 6.5 kWh/m^2 (16 MJ/m^2 and 23 MJ/m^2) (Stassen, 1996). Figure 3-1 depicts the considerable solar resource for CSP generation in South Africa by mapping the annual solar radiation (direct and diffuse) across the country.

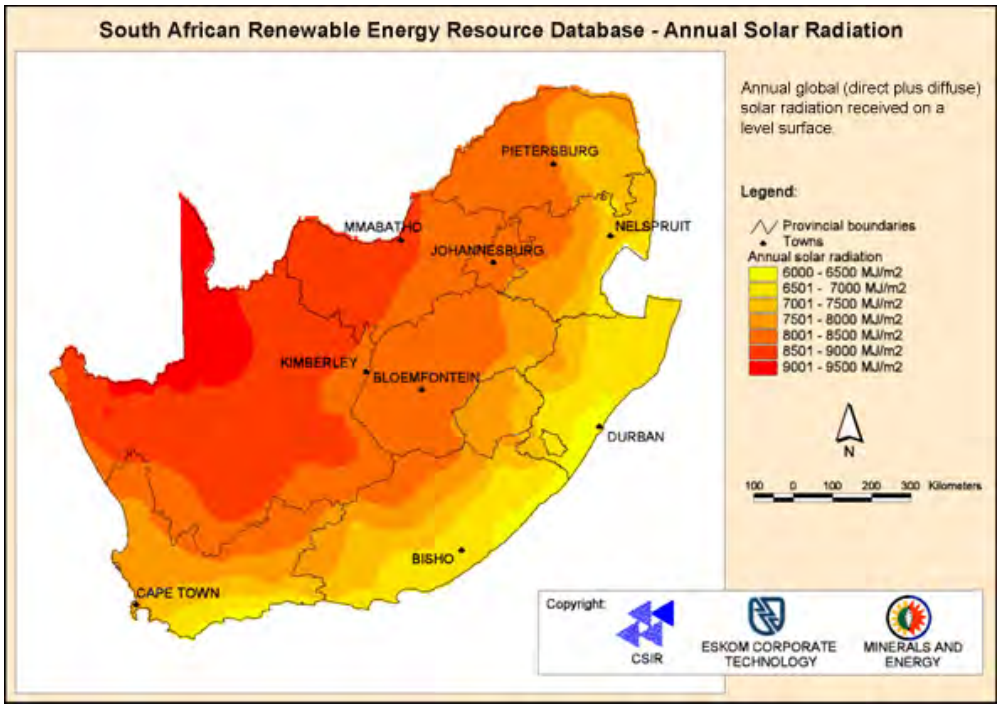

Figure 3-1: Average annual and monthly solar energy received per horizontal square metre [MJ/m2] (SARERD, 2006)

According to the Environmental Impact Assessment (EIA) performed by Eskom, Upington has one of the most favourable, if not the best Direct Normal Radiation (DNR) level in the world as shown in Table 3-1.

Table 3-1: International solar potential relative to South Africa

Location	Site latitude	Annual DNR [kWh/m^2]	Relative solar resource
Upington, Northern Cape, South Africa	28°S	2995	100%
Barstow, California, USA	35°N	2725	92%
Las Vegas, Nevada, USA	36°N	2573	87%
Albuquerque, New Mexico, USA	35°N	2443	83%
Northern Mexico	26 - 30°N	2835	96%
Wadi Rum, Jordan	30°N	2500	85%
Ouarzazate, Morocco	31°N	2364	80%
Crete	35°N	2293	78%
Jodhpur, India	26°N	2200	74%
Spain	34°N	2100	71%

Source: Eskom and Bohlweki Environmental, 2006, p.3

There are multiple sources of data characterizing sun strength in South Africa, including:

i. Pyranometer measurements at a ground station

Here the pyranometer's accuracy, spectral sensitivity and regular calibration determine the correctness of the resulting global and diffuse irradiation data.

ii. Sunshine hour measurements at a ground station

Global irradiation at a specified site can be estimated from the percentage of sunshine measured during an hour. To estimate the diffuse radiation a clearness index must be used which further decreases the accuracy.

iii. Irradiation measurements from a satellite

Where a ground measurement station does not exist satellite measurements are the only indication of the solar resource at a site in question. The disadvantage of satellite observations is that they are unable to account for site-specific microclimate effects.

The period between data points in these irradiation datasets can vary from 5 minutes to monthly averages (Bekker, 2007). Bekker (2007) proposes the following classification system (Table 3-2) for grading the accuracy and resolution of solar radiation data.

Table 3-2: South African irradiation data accuracy and resolution classification system (Bekker, 2007)

Accuracy	Accuracy grading	Resolution grading	Resolution
Regularly calibrated ground measurement stations, pyranometer accuracy < 1%, data accuracy < 10%	A	A	Daily measurements, 5- or 10-minute intervals
Estimates from hourly sunshine hour measurements	B	B	Daily measurements, 1-hour intervals
Satellite measurements	C	C	Monthly average, 1-hour intervals
Non-calibrated pyranometers or silicon-based irradiance meters	D	D	Daily or monthly average only

The data grade is written as accuracy:resolution. For example, non-calibrated pyranometer derived 1-hour interval data will be classified as D:B.

3.2 Data analysis

Six datasets were analysed for an estimation of the solar resource at Upington (28°4'S, 21°3'E), in the Northern Cape province of South Africa. The first dataset comprises hourly

pyranometer readings from the South African Weather Service (SAWS) measurement station in Upington (Kruger and Esterhuyse, 2005). The second data source is the NREL Climatological Solar Radiation (CSR) model for Africa (Solar and Wind Energy Resource Assessment, 2007). The third is the Surface meteorology and Solar Energy (SSE) resource from the NASA Atmospheric Science Data Center (NASA, 2008). The fourth consists of hourly Direct Normal Irradiance (DNI) readings taken from unspecified equipment at Olyfenhoutsdrif, near Upington (28°28.095'S, 21° 4.291'E) by Eskom's Sustainability and Innovation Department (Eskom, 2010b). The fifth set is a compilation of Direct Normal Irradiance and other meteorological data by Weather Analytics Inc developed for use in modelling (Khuen, 2011). The sixth dataset is a typical meteorological year obtained from the Centre for Renewable and Sustainable Energy Studies (CRSES) at Stellenbosch University.

3.2.1 SAWS pyranometer data

The SAWS (South African Weather Bureau (SAWB) at the time) employed a Kipp and Zonen CM5 Pyranometer to measure radiation intensity on a horizontal surface in the meteorological wavelength band of $\lambda = 0.3\ \mu m\ to\ 2.8\ \mu m$ from 1964 to 1992 which was a total of twenty-eight years. Global and diffuse radiation were measured hourly at local apparent solar time. Both global and diffuse components were measured in kilojoules per square metre per hour ($kJ/m^2\ /hr$).

Solar radiation measurements were managed by CB Archer who at the time was recognized as a dedicated and meticulous technician and scientist (Coetzee, 2009). According to Coetzee (2009), the SAWS network of sensors, which included those in Upington, was calibrated with a PMO6 absolute cavity radiometer developed at the Physikalisch-Meteorologisches Observatorium, Davos serving as the World Radiation Center (PMOD/WRC). The Upington instrument was calibrated every four years at the PMOD/WRC until 1995, ensuring traceability to the World Radiometric Reference (WRR) maintained by the World Meteorological Organisation.

The overall uncertainty in the WRR scale is reported by Myers (2003) to be 0.35%. There may be an additional 0.1% transfer uncertainty between the PMO6 absolute cavity radiometer at PMOD/WRC and the primary cavity radiometer used to calibrate the SAWS sensor network. Therefore, the uncertainty in the reference irradiance direct beam component measured with the primary cavity radiometer could be 0.45%.

Until early 1990 regular data submissions were made from the sensor network (including Upington) to the World Radiation Data Center (WRDC) in St. Petersburg. Power and Mills (2005) describe the measurements from the South African sensor network as high-quality with standardized instrumentation and calibration procedures. According to Power and Mills (2005) and Coetzee (2009) appropriate shadowband correction factors were applied to the pyranometers' diffuse radiation data and the uncertainty associated with the measured global and diffuse irradiance values is projected by Power and Mills (2005) to be less than 2%. On inspection, however, it was found that numerous days contained missing data and in some cases identical measurements were recorded for several consecutive hour-long periods, which casts doubt on the overall quality of the dataset. Although it is not possible to verify the accuracy of the measurements, it is unlikely that the uncertainty associated with the data falls within the expected 2%. This dataset can be classified as A:B.

3.2.2 NREL CSR model data for Africa

In 1995 NREL under the U.S. Department of Energy Resource Assessment Program, started the Data Grid Task. Maxwell, George, and Wilcox (1998) developed a Climatological Solar Radiation (CSR) Model which uses atmospheric condition information to accurately estimate global insolation (direct and diffuse) on a horizontal surface.

NREL states that, where possible, the data are validated with existing ground measurement station data. Maxwell *et al*., (1998) claim an accuracy of ±5% of a true measured value within a grid cell when input data are accurate.

The CSR model is a simplification of the Meteorological Statistical Model (METSTAT). It performs an iterative solar radiation energy calculation every 5 minutes from daybreak to sundown in a specific area one day each month when the daily-global extraterrestrial radiation (H_o) equals the monthly-averaged daily extraterrestrial radiation ($\overline{H}_o$) (Maxwell *et al*., 1998). Five-minute values are then summarised to arrive at a global, daily value using METSTAT algorithms. It is not known if data from Upington were used to validate the data in the model. This dataset can be graded as C:C.

3.2.3 NASA SSE global dataset

The NASA SSE global dataset contains 22 years (July 1983 to June 2006) of over 200 satellite-derived meteorology and solar energy metrics at a resolution of 1° by 1°. These metrics are averaged monthly.

Solar radiation data for SSE Release 6.0 were gathered from the NASA Science Mission Directorate's satellite and re-analysis research programs. Regression analysis of SSE versus the Baseline Surface Radiation Network (BSRN) monthly averaged values for global horizontal radiation, horizontal diffuse radiation, and direct normal radiation produce root mean squared error percentages of between 8.71% and 54.14%. A point of interest is that one of the BSRN measurement stations used to determine the accuracy of the SSE dataset was in De Aar, which is approximately 350 km from Upington and has very similar meteorological conditions. The work involved in the establishment and operation of the station is detailed by Esterhuyse (2004). A detailed description of the methodology used to arrive at the dataset is provided by NASA (2009). The SSE dataset can be graded C:B.

3.2.4 Eskom Sustainability and Innovation Department data

South African utility Eskom has made some measured solar data in the Northern Cape available to the public (Eskom, 2010b). These data were measured by their Sustainability and Innovation Department from November 2006 to 22 April 2010 and include Direct Normal Irradiance (in Olyfenhoutsdrif's case), wind speed and direction at 9m above ground, air temperature, relative humidity, and barometric pressure.

Although Eskom does not warrant the data, they are useful for checking against the other datasets evaluated here. Some of the stations have long gaps in their data logs (many missing data points) due to "downtime on the equipment" (Eskom, 2010b, 1) which are thought to be due to tracker and power supply problems. Despite significant periods of missing data this dataset can be graded D:B, and may even be graded A:B if proof of measurement instrument calibration is obtained from Eskom.

3.2.5 Weather Analytics data

Weather Analytics Incorporated provides "commercial grade" weather data for energy use profiling, modelling and management. One of their offerings is a typical meteorological year hourly time series dataset. The data are provided in either a Typical Meteorological Year (TMY) format or an EnergyPlus Weather (EPW) format. These formats are compatible with SAM.

The files are constructed using techniques approved by the United States Department of Energy (DOE) based on the most current 30 years of available data specific to the required location (Weather Analytics Inc., 2011). Weather Analytics term their data construction

technique the Sensor Point System. This system is based on the National Oceanic and Atmospheric Administration's (NOAA) National Centers for Environmental Prediction (NCEP) Climate Forecast System Reanalysis (CFSR) model (Weather Analytics Inc., 2011).

These files have value in providing a typical profile of a site in any given year and have been used as a building design aid. The files have limits though, as they do not profile the year to year range of climate and solar radiation variations very well (Khuen, 2011). This is better achieved with consecutive actual meteorological year data. This dataset can be graded as B:B.

3.2.6 CRSES data

The Centre for Renewable and Sustainable Energy Studies (CRSES) at Stellenbosch University has a METEONORM software license. The METEONORM computer program was developed by Meteotest in Switzerland as "a comprehensive climatological database for solar energy applications" (Meteotest, 2010a: 1). A typical meteorological year for Upington generated by METEONORM in EPW format was provided to attendees of the CRSES Solar Advisor Model CSP and PV Simulation Software Training on 1 June 2011 to 2 June 2011.

Meteotest (2010a) use ground measurements from stations in their global database. According to their listings Upington is station ID 4021. Thus it can be assumed that ground measurements were used as their input. For periods where ground measurements were not available a combination of neighbouring ground station measurements and satellite data are interpolated to produce the required results. The global radiation data used by METEONORM were quality controlled using six separate procedures including physical probability checks, time series analysis and cloud data comparison. Tests performed by Meteotest (2010a) to check the accuracy of their interpolation techniques yielded a monthly global radiation root mean square error of only nine percent. Therefore, this dataset may be graded as A:B.

3.3 Calculation methodology and results

3.3.1 SAWS pyranometer calculations

The first part of the calculation procedure was the analysis of the input data. Upon inspection of the dataset, it was found that eighteen of the twenty-eight years had between two and ninety-two days of missing measurements. The days with recorded and missing measurements are provided in Table 3-3. The method chosen to mitigate the uncertainty

introduced by the missing readings was to use only those years with fewer than five missing readings per month, of which there are eight.

Table 3-3: Radiometric analysis for Upington SAWS pyranometer data

Year	Days with recorded measurements	Days with missing measurements
1964	274	92
1965	344	21
1966	365	0
1967	365	0
1968	332	34
1969	344	21
1970	332	33
1971	361	4
1972	358	8
1973	361	4
1974	342	23
1975	349	16
1976	340	26
1977	355	10
1978	356	9
1979	359	6
1980	366	32
1981	365	0
1982	365	0
1983	334	31
1984	364	2
1985	365	28
1986	365	0
1987	365	0
1988	336	30
1989	365	0
1990	365	0
1991	363	2
1992	363	3

The second part of the calculation was to relate each hourly measurement of total and diffuse radiation to the fundamental geometric relationships described in Appendix A, including declination, solar time, hour angle, zenith angle and sunset hour angle. These were used to calculate hourly, daily and monthly extraterrestrial radiation from which hourly, daily and monthly clearness indices and diffuse fractions could be computed.

Hourly direct normal or beam radiation (I_b) was calculated as follows:

$$I_b = \frac{I - I_d}{\cos \theta_z} \tag{3.1}$$

where I is the total hourly solar radiation, θ_z is the zenith angle and I_d the hourly diffuse radiation. The use of an averaged value of θ_z for each hour interval introduces additional error but was considered unavoidable in producing results. Assuming a perfect tracking surface Equation 3.1 can be reduced to:

$$I_b = I - I_d \tag{3.2}$$

Daily- and monthly beam radiation (H_b and $\overline{H}_b$ respectively) were calculated using the method employed by Power and Mills (2005) on the same data as follows:

$$\begin{aligned} H_b &= H - H_d \\ \overline{H}_b &= \overline{H} - \overline{H}_d \end{aligned} \tag{3.3}$$

where H and $\overline{H}$ are the daily- and monthly total radiation respectively and H_d and $\overline{H}_d$ are the daily- and monthly diffuse radiation respectively.

It was found that estimating beam radiation using hourly, daily and monthly clearness indices (k_T, K_T and $\overline{K}_T$) produced very conservative results when compared to directly calculating beam radiation from the measurements.

In contrast, the calculated values of daily extraterrestrial radiation (H_o) using the method proposed by Duffie and Beckman (2006) produced a more optimistic results than straightforwardly averaging hourly extraterrestrial radiation (I_o) and forcing the negative values to zero. The difference in the two results was largest in the beginning and end of the year and smallest in the middle of the year towards August. The distribution of the difference was reminiscent of a normal distribution with least error normalized around the middle of the year and the largest errors being found on either extremes of each calendar year.

Daily direct normal radiation (DNR) per square metre was calculated by summing the hourly beam radiation over a 24 hour period and converting the measurements from *kJ/m^2/day* to *kWh/m^2/day*. These energy values were then averaged to yield a monthly daily average. Results are given in Figure 3-2.

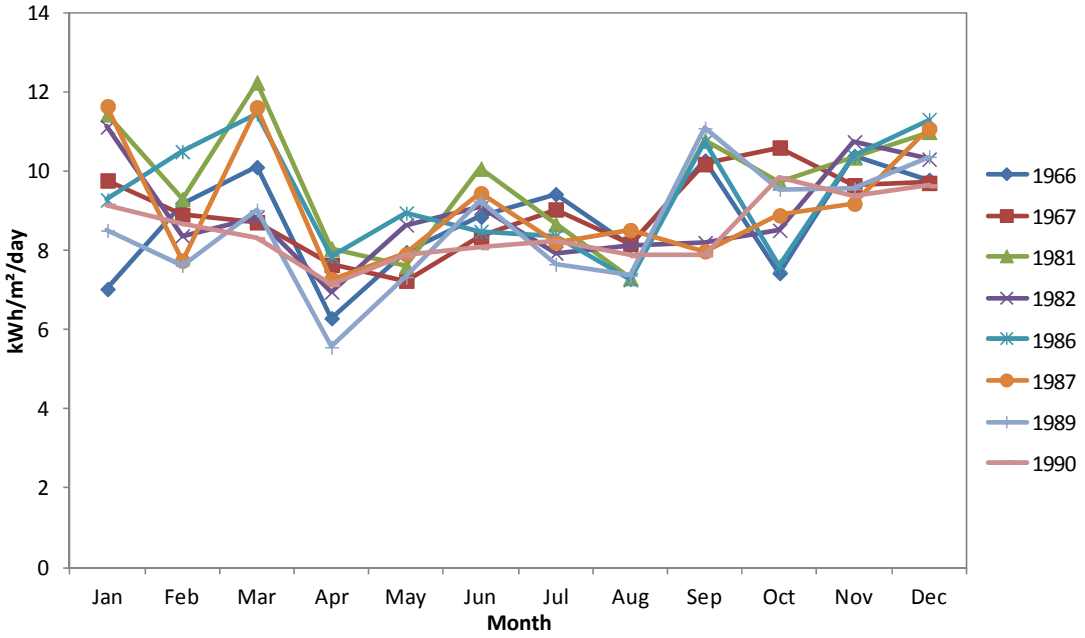

Figure 3-2: Monthly average daily direct normal radiation at Upington, measured by SAWS pyranometers

3.3.2 NREL CSR model calculations

The CSR model dataset is well laid-out and accessing final monthly averaged radiation values is uncomplicated. A 40 km by 40 km cell of interest is selected and its number is inserted in the model. The model then uses a database to find the associated monthly average radiation values as an annual average. The output of the model for the 40 km by 40 km cell including Upington is displayed in Figure 3-3 below.

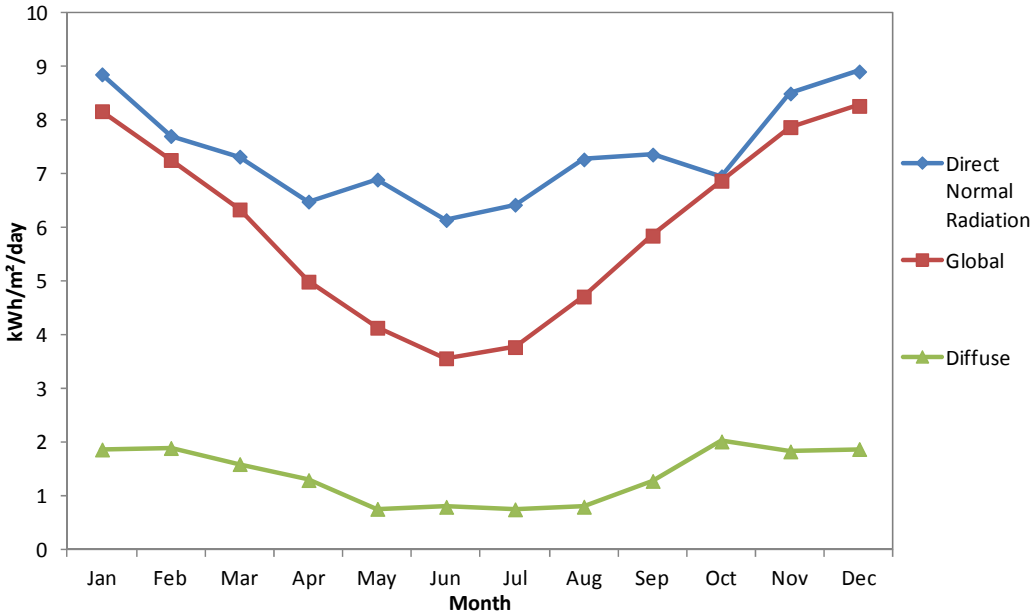

Figure 3-3: NREL CSR model monthly averaged daily solar energy

3.3.3 NASA SSE calculations

The different parameters of the SSE dataset were downloaded into Microsoft Excel for analysis. The resulting chart in Figure 3-4 gives the average monthly radiation data from 1983 to 2005.

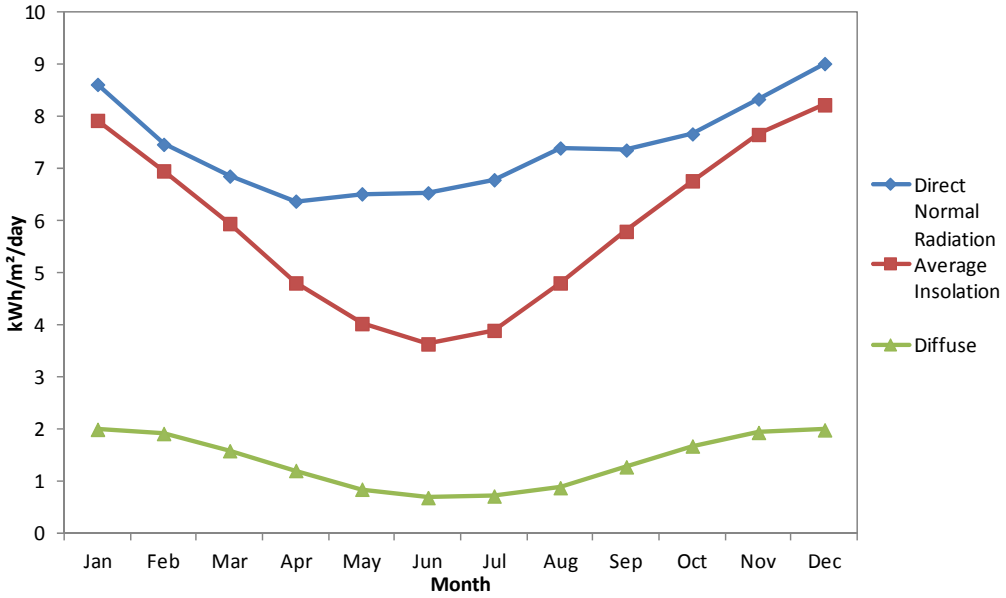

Figure 3-4: NASA SSE monthly averaged solar radiation

3.3.4 Eskom data calculations

The Eskom data were consolidated into spreadsheets containing the hourly Direct Normal Irradiance (DNI) for each year, from which daily and monthly averages were calculated. The 2006 measurements could not be used as they were only for November and December, and the same applied for the 2010 measurements as they only covered January to April. From January to June 2007 the measurement instrument was down, providing only intermittent data from September to December 2007.

As a result of this only the measurements from 2008 and 2009 were considered. Despite being more comprehensive than the other years of measured data, a meaningful number of data points were missing in these datasets. The number of missing data points appear to congregate around the winter months of June and July in both 2008 and 2009. June 2009 had 10 entire days without any data and 14 other days with incomplete data. Similarly July 2008 had 27 days with varying numbers of hourly data points missing in the record.

These findings were problematic since the average radiation presented here is determined cumulatively, so replacing missing data points with zero values to obtain a more accurate representation of the “as is” data results in a suppressed average. Hence, the more missing

data points the larger the variance between the actual DNI and the average calculated from the data set. A summary of the missing data in the set is provided in Table 3-4. This monthly averaged DNI was found to be 6.7 kWh/m^2/day, with the results shown in Figure 3-5. Introducing a synthetic average for missing values produces a more realistic result (Figure 3-6).

Table 3-4: Summary of missing measurements in Eskom dataset

Year	No. of days with incomplete measurements	No. of missing hourly readings	Months with missing readings	No. of days in month with missing readings
2008	30	298	June	2
			July	27
			September	1
2009	29	596	May	5
			June	24

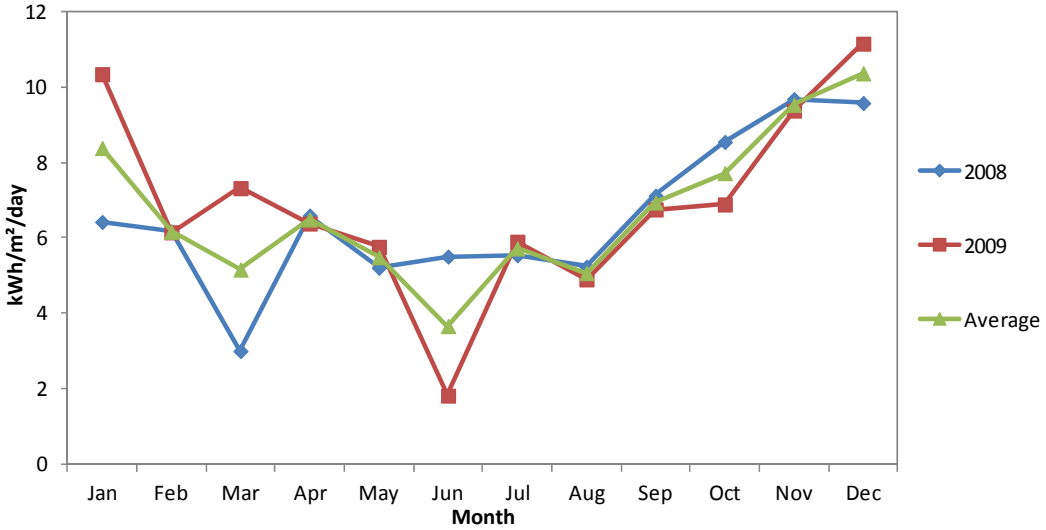

Figure 3-5: Eskom monthly averaged hourly DNI

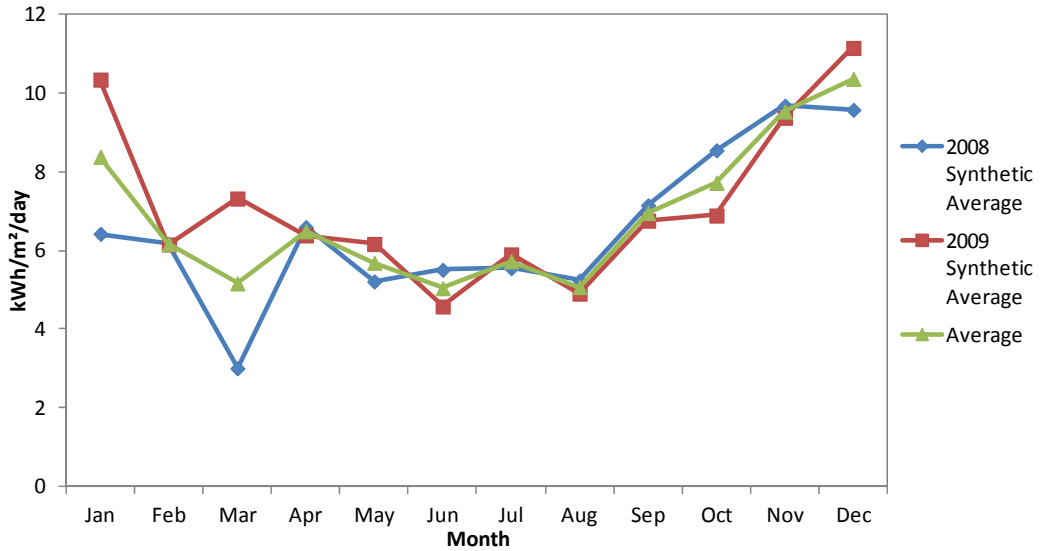

Figure 3-6: Eskom monthly averaged hourly DNI with synthetic averages inserted in missing hourly data points

These results show good agreement with both satellite and ground-based measurements. The average of these results was adopted as the quantitative result of this dataset.

3.3.5 Weather Analytics data calculations

The Weather Analytics data are in the EPW file format and were converted into a spreadsheet. The column headers for each meteorological measurement in the file were obtained from the Auxiliary EnergyPlus Programs document prepared by the University of Illinois and the University of California through the Ernest Orlando Lawrence Berkeley National Laboratory (2010).

Once the headings were assigned, the data were analysed with the same techniques used on the Eskom dataset. The results are displayed in Figure 3-7.

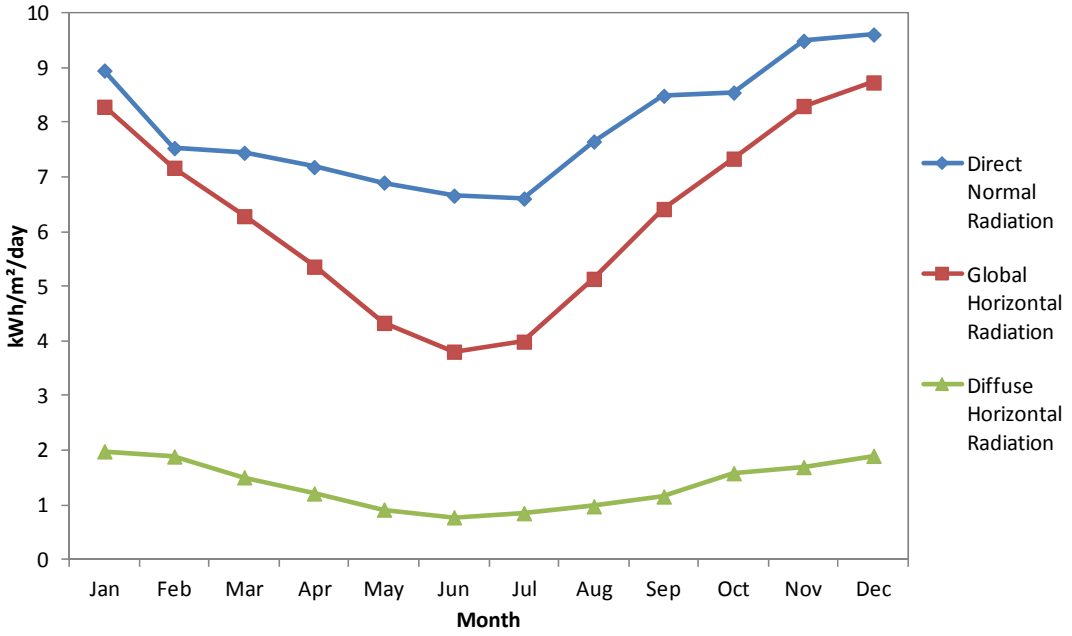

Figure 3-7: Weather Analytics monthly averaged daily solar energy

3.3.6 CRSES data calculations

The CRSES data are also in the EPW file format. Using the same technique as discussed above in section 3.3.5, the following results in Figure 3-8 were obtained from the METEONORM data provided by CRSES.

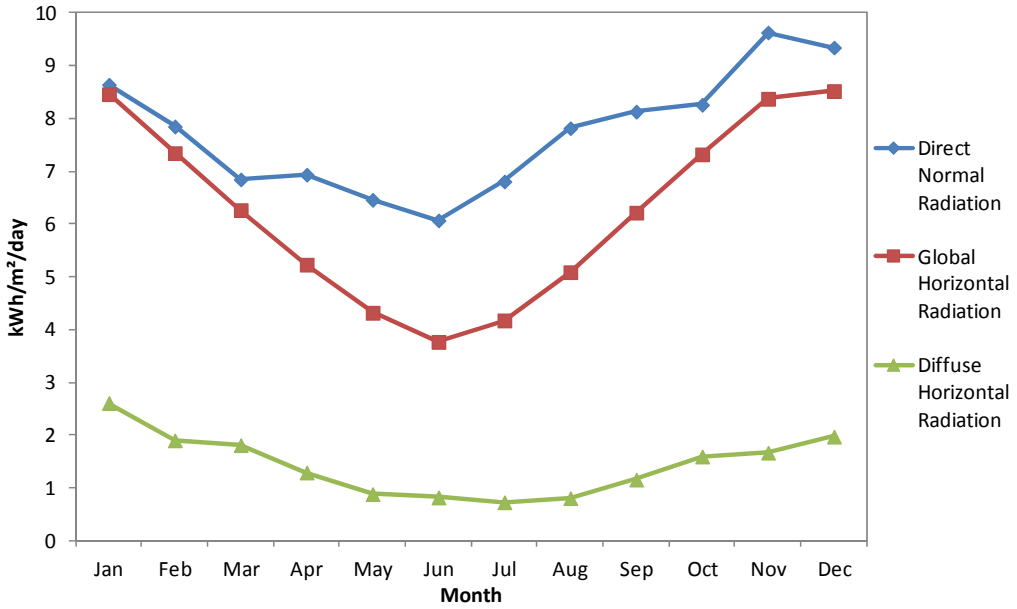

Figure 3-8: CRSES monthly averaged daily solar energy

3.3.7 Results

A comparison between the monthly average daily direct normal data obtained via the six approaches is given in Figure 3-9. Close agreement exists between the NASA, NREL, Weather Analytics and CRSES values with the SAWS readings giving noticeably higher DNR throughout the year, and the Eskom measurements providing significantly lower DNR during autumn and winter periods. All six curves show a reduction in radiation over the winter months, as expected. However, the degree of variability in the SAWS data again suggests higher random errors in the measurement process. Sources of uncertainty could include the inaccuracy of SAWS instruments, the use of an hourly averaged zenith angle to obtain DNR data from global and diffuse and the errors associated with calculating diffuse radiation with a shadow band. The unevenness in the Eskom measured data could arise from the relatively short period of data sampled (only 2 years), uncalibrated measuring instruments, instrument power supply problems, and unusually cloudy years during the period sampled. It is also possible that the Eskom instruments experienced two particularly cloudy years, particularly during the winter months; and that the actual values lie between the SAWS predictions and the Eskom measurements except for early summer where they agree and depart from the NASA, NREL, Weather Analytics and CRSES results. These results highlight the need for a greater number of calibrated permanent broadband monitoring stations throughout South Africa's sunbelt. Without high-quality data it is difficult to predict the performance of large-scale CSP plants either from a technical or economic perspective.

To arrive at a quantitative result after this analysis, each result was given a weighting from its dataset-grading according to Bekker's (2007) classification system. This weighting was used to generate a weighted average of the six datasets investigated. A second order polynomial was then used to describe the weighted average of all six datasets investigated. The curve approximated by this polynomial is a useful check when interpreting DNR data obtained from the Upington area.

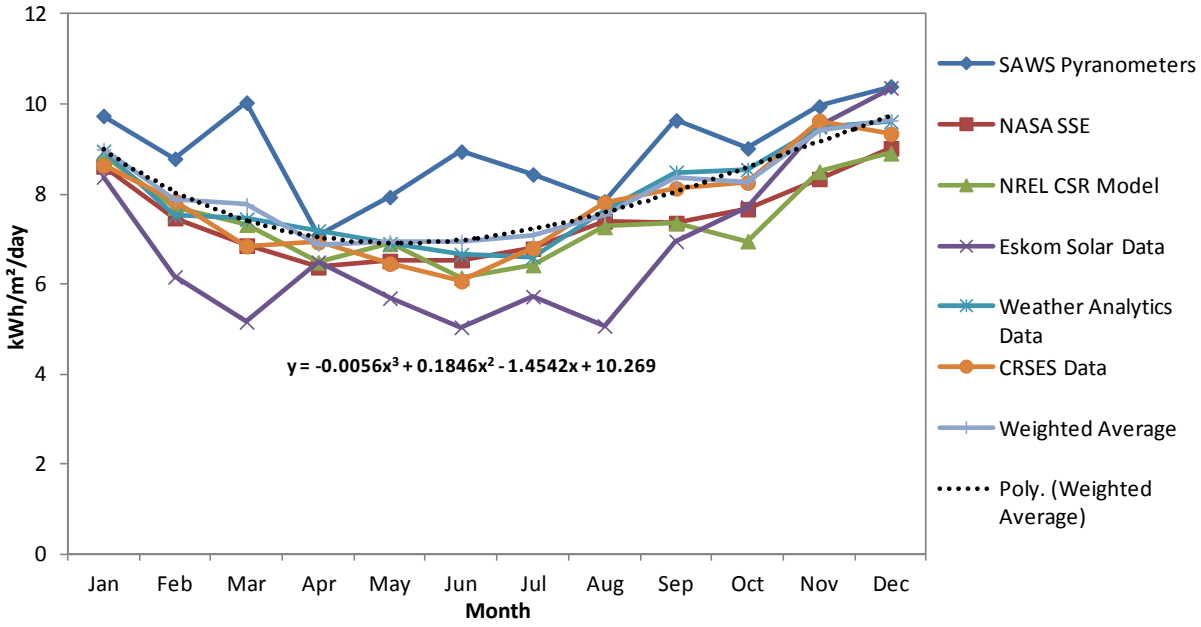

Figure 3-9: Results of monthly averaged daily direct normal radiation for Upington

Concentrating solar power technologies operate exclusively with DNR, therefore, it helps to compare the preliminary results for Upington to DNR levels at international locations where such power plants have been implemented. Using an average of the six predicted DNR levels, the South African solar resource compares extremely well with several international CSP sites (Table 3-5). The SEGS plants of southern California, for example, are frequently held up as examples of the green energy revolution since they have been in operation the longest and are regarded as having successfully demonstrated the bulk solar thermal power concept. Upington's monthly average DNR is between 3% and 37% higher than these and the other sites listed.

Table 3-5: Comparison of Upington radiometric data with existing CSP power plant sites

Site [Town, State/Province, Country]	Coordinates [Lat., Long.]	CSP power plants implemented	Monthly averaged daily DNR [kWh/m²/day]	Annual averaged DNR [kWh/m²/annum]
Upington, Northern Cape, South Africa	28°4'S, 21°3'E	None	7.72	2814.06
Daggett, California, USA	34°51'N, 116°49'W	SEGS I, II	7.5	2790
Kramer Junction, California, USA	35°00'N, 117°33'W	SEGS III-VII	7.09	2587.85
Harper Lake, California, USA	35°01'N, 117°20'W	SEGS VIII, IX	7.09	2587.85
Boulder City, Nevada, USA	35°48'N, 114°58'W	Solar One	6.92	2525.8
Plataforma Solar de Almería, Almería, Spain	37°5'N, 2°21'W	FRESDEMO, DISTAL II, EURODISH, PS10	5.68	2058.6

This result shows good agreement with a site assessment of the solar resource at Upington Solar Park performed by Suri *et al*. (2011). Suri *et al*. (2011) from GeoModel Solar correlated over four years (November 2006 to February 2011) of ground measurements from Eskom and Stellenbosch University with seventeen years (1994 to 2010) of SolarGIS satellite-derived solar radiation data to assess the DNR, GHI and Global Tilted Irradiance at the optimum angle of 28°. Their results are compared to findings of this study in Table 3-6.

Table 3-6: Comparison of Upington data with site assessment data from Suri *et al*. (2011)

Metric	Suri *et al*. (2011) data	Data from this study
Site [Town, Province, Country]	Upington Solar Park, Northern Cape, South Africa	Upington, Northern Cape, South Africa
Site coordinates [Lat., Long.]	28°32'33''S, 21°05'18''E	28°4'S, 21°3'E
Site elevation [m]	820 to 920	848
Monthly averaged daily DNR [kWh/m²/day]	7.72	7.72
Annual averaged DNR [kWh/m²/annum]	2816	2814.06

3.3.8 Modelling considerations

System Advisor Model simulation software requires certain input data to accurately model CSP systems. The first set of requirements is the location information listed in Table 3-7.

Table 3-7: Location information required by SAM

Data description	Units	Upington entries
Site identifier code/Station ID	N/A	4021
Station/Location name	N/A	Upington
Station state	N/A	Northern Cape
Site time zone (GMT)	Hours	+2
Site latitude	Degrees	-28.42
Site longitude	Degrees	21.2582
Site elevation	Metres	848

The second set of requirements is the meteorological data. SAM requires hourly data for one or a typical year of the measurements listed in Table 3-8.

Table 3-8: Meteorological data required by SAM

Data description	Units
Global Horizontal Insolation (GHI)	W/m²
Direct Normal Insolation (DNI)	W/m²
Direct Horizontal Insolation (DHI)	W/m²
Dry-bulb temperature	ºC
Dew-point temperature	ºC
Wet-bulb temperature	ºC
Wet-bulb temperature	ºC
Relative humidity	%
Atmospheric pressure	mbar
Wind speed	m/s
Albedo	unitless

The NASA SSE and NREL CSR datasets investigated in this chapter did not have the hourly DNI readings required by SAM excluding them from use as inputs to SAM.

The Weather Analytics data and the Meteonorm data provided by CRSES both had all the necessary meteorological data in order to successfully model CSP systems in Upington conditions.

The SAWS solar radiation data did not have accompanying hourly dry-bulb and dew-point temperature, relative humidity, atmospheric pressure, wind-speed, or albedo data.

The Eskom solar radiation data only had hourly direct normal insolation without any recorded direct horizontal or global horizontal insolation data.

To overcome these difficulties it was decided to augment the input weather files for the SAWS and Eskom solar radiation data with hourly meteorological data for Upington from the CRSES dataset.

Therefore the following datasets were used for modelling:

i. The SAWS GHI, DNI and DHI data augmented with Meteonorm data from CRSES,
ii. The Eskom DNI data augmented with Meteonorm data from CRSES,
iii. The Weather Analytics data,
iv. The Meteonorm data obtained from CRSES.

4. MODELLING AND RESULTS

4.1 Introduction

This chapter covers the modelling of the technologies discussed in the preceding chapters using SAM software. It starts with the simulation of each technology, after which a comparison is presented between one representative example of each technology.

4.2 Intra-technology simulation results

To provide an equitable platform for the comparison of the different technologies it was decided to fix certain global parameters listed in section 4.2.1. Once these parameters are defined, multiple cases for each technology are considered and the results of the simulation are discussed.

4.2.1 Global model parameters

Since the nameplate rating of the CSP plant planned to be built by Eskom was 100 MW, it was decided to make the nameplate electrical output of each technology modelled 100 MW_e. The same power dispatch schedule was assigned to each case of the simulation so that the performance of each technology under the required power dispatch regime determined the annual electric output in MWh.

It was also determined to use 6 hours of thermal storage for each applicable case to cater for South Africa's electricity usage profile where dominant peaks occur outside of peak DNI periods of the day. The motivation for selecting specific models within SAM is given in Table 4-1.

Table 4-1: SAM model choice decision register

Technology	SAM model available	Model chosen	Reason
Parabolic Trough	Parabolic Trough Physical	Parabolic Trough Physical	Not limited to components for which there is only measured data. Higher uncertainty though.
	Parabolic Trough Empirical		
Central Receiver	Power Tower Molten Salt	Power Tower Molten Salt	No energy storage option in Power Tower Direct Steam model.
	Power Tower Direct Steam		
Dish-Engine	Dish Stirling	Dish Stirling	Only one model available
CLFR	Linear Fresnel	Linear Fresnel	Only one model available

Four of the six datasets discussed in chapter 2 were used to evaluate each technology. These were the SAWS GHI, DNI and DHI data augmented with Meteonorm data from CRSES, the

Eskom DNI data augmented with METEONORM data from CRSES, the Weather Analytics data, and the Meteonorm data obtained from CRSES.

Each climate input file contained a minimum of the data listed in Table 3-8 in chapter 3 and each heading required 8760 hourly readings with no gaps for SAM to compute the annual performance of the plant.

Each system was specified with SAM's default CSP plant availability of 96%. The software then multiplies each hour's electrical output by 0.96 to account for plant downtime due to planned and unplanned maintenance. To summarise, the fixed and variable input parameters used in the intra-technology simulations are listed in Table 4-2.

Table 4-2: Fixed and variable input parameters for intra-technology comparison

Fixed parameters	**Units**	**Value**
Plant location	-	Upington, Northern Cape
Nameplate electrical output	MW_e	100
Power dispatch schedule	-	matched
Fossil fuel backup	-	Yes†
Hours of thermal storage	hours	6*†
Plant availability	%	96
Annual system degradation	%	1
Variable parameters	**Units**	**Values**
Climate input file	-	SAWS, Eskom, Weather Analytics, CRSES
Power cycle cooling method	-	Evaporative, Air-cooled

* Parameter not relevant for dish-engine model

† Parameter not relevant for CLFR model

With the above input parameters fixed, SAM generates certain direct outputs, which are then presented and used as a basis for deriving other metrics which are of interest to CSP developers (Table 4-3). These metrics are used to compare the relative strengths of each technology.

Table 4-3: Simulation outputs used for comparisons

Direct simulation outputs	**Units**
Net annual electric output	MWh
Generalised gross to net conversion factor	-
Annual power cycle water usage	m^3
Annual washing water usage	m^3
Total annual water usage	m^3
Total land area	acres converted to km^2
Derived simulation outputs	**Units**
Energy per m^3 of water	kWh/m^3
Energy per km^2 of land	GWh/km^2

4.2.1.1 System degradation

A 2009 NREL review of operations and maintenance data from the SEGS plants from 1989 to 2005 found that reflector and HCE failures accounted for 88% of total solar field component failure. Kutscher *et al.* (2010) state that reflector panel cracking or breaking due to wind damage were the biggest problems (58%), while HCE glass envelope breakage, vacuum loss, hydrogen infiltration and selective coating degradation were also significant failure items (30%). These failures result in plant performance degradation. A representation of these failures at an operational SEGS plant in Daggett, California is provided in Figure 4-1.

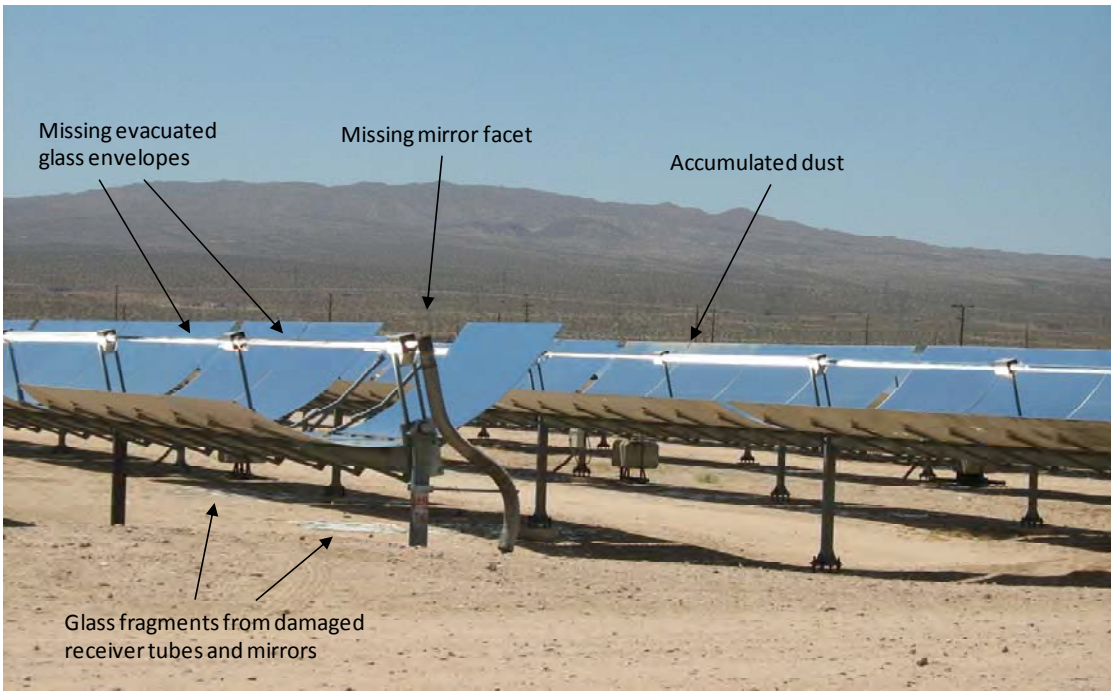

Figure 4-1: Illustration of damage to the collector field of an operational SEGS parabolic trough plant, including damaged mirror facets, missing HCE envelopes and poor cleaning maintenance. The plant is at Daggett, California.

Linear Fresnel plants may experience similar failures as the parabolic trough plants mentioned above. However, Areva Solar (2012) state that their low wind profile CLFR design should mitigate wind damage. Long term CLFR plant operation and maintenance data are not yet available.

Solar Two experienced heliostat tracking errors which could degrade plant performance (Stone and Jones, 1999). Heliostat mirror cleanliness is mentioned as a performance inhibitor in both Solar One (Kolb, 1991) and Solar Two (Pacheco and Gilbert, 1999), however, regular mirror washing as modelled below should prevent this problem. Pachecho and Gilbert (1999) mentioned molten salt isolation valve leaks in the receiver and steam generator system, fouling and plugging in the preheater tubes and degradation of the steam generator sump

insulation. These problems during the testing and evaluation program of Solar Two can be indicative of failures during plant operation. Long term operation and maintenance data from CRS plants are not yet available.

Brignoli and Bombelli (2009) performed tests on the EuroDish dish-engine system from 2002 to 2009. They found that conventional components of the EuroDish system were sources of failure. More dish-engine plant operational data are required to quantify performance degradation.

More performance degradation data are available for parabolic trough plants. This does not necessarily mean that they require more maintenance than the other technologies evaluated.

Considering the relatively low wind conditions in Upington (3.6 m/s annual average) in comparison to other CPS locations like Dagget, CA, USA (4.9 m/s annual average) it is expected that degradation from soiling will be modest. Due to a lack of system degradation information across the board, it was decided to specify the annual performance degradation of each system as 1% per year to keep the technologies compared on equal footing. SAM applies this rate to the system's annual electric output from year two onwards such that each year's annual output is 99% of the previous year's annual output over a 30 year period.

4.2.1.2 Thermal storage dispatch control

Identical thermal storage dispatch control settings were used for parabolic trough and power tower models. The power cycle dispatch control settings of the linear Fresnel model were matched to the parabolic trough and power tower settings. This aligned the periods when a fossil fueled backup boiler was used to augment the energy from the solar field entering the power block. The dish Stirling model does not use TES or a fossil fueled boiler to supplement plant output during periods of low insolation. The following settings were therefore not applied to the dish Stirling model.

South Africa's national load profile has dominant peaks in the morning (7am to 10am) and evenings (6 pm to 9 pm) (Eskom, 2010a); with the evening peaks being more pronounced (Meyer and van Niekerk, 2011). In winter peak demand increases (Eskom, 2011) but the load profile remains unchanged (Meyer and van Niekerk, 2011). Due to lower DNI levels and shorter days during the winter peak demand period and the pronounced evening peak, six full load hours of TES were selected for the parabolic trough and power tower models.

A thermal storage dispatch schedule was drawn up that matched the national load profile requirement and accounted for the seasonal differences in sunrise and sunset at Upington.

The following periods were defined in the thermal storage dispatch schedule given in Figure 4-2:

i. Period 1 (early morning to late afternoon) - Plant generates electricity at nameplate rating using solar field energy with fossil backup to cover cloud transients. TES is charged with excess solar field energy.

ii. Period 2 (11 pm to early morning) - Plant does not generate electricity. Some power is required to maintain HTF temperature, storage fluid temperature and other parasitic loads.

iii. Period 3 (early morning) - Plant generates electricity at nameplate capacity using solar field energy with fossil backup to cover low sunlight conditions.

iv. Period 4 (late afternoon) - Plant generates electricity at nameplate capacity using solar field energy with TES to cover low sunlight conditions. Backup boiler does not run.

v. Period 5 (late afternoon to 11 pm) - Plant generates electricity at nameplate capacity using TES energy.

The above description is adapted from a summary by Gilman (2012) of the requirements for this study.

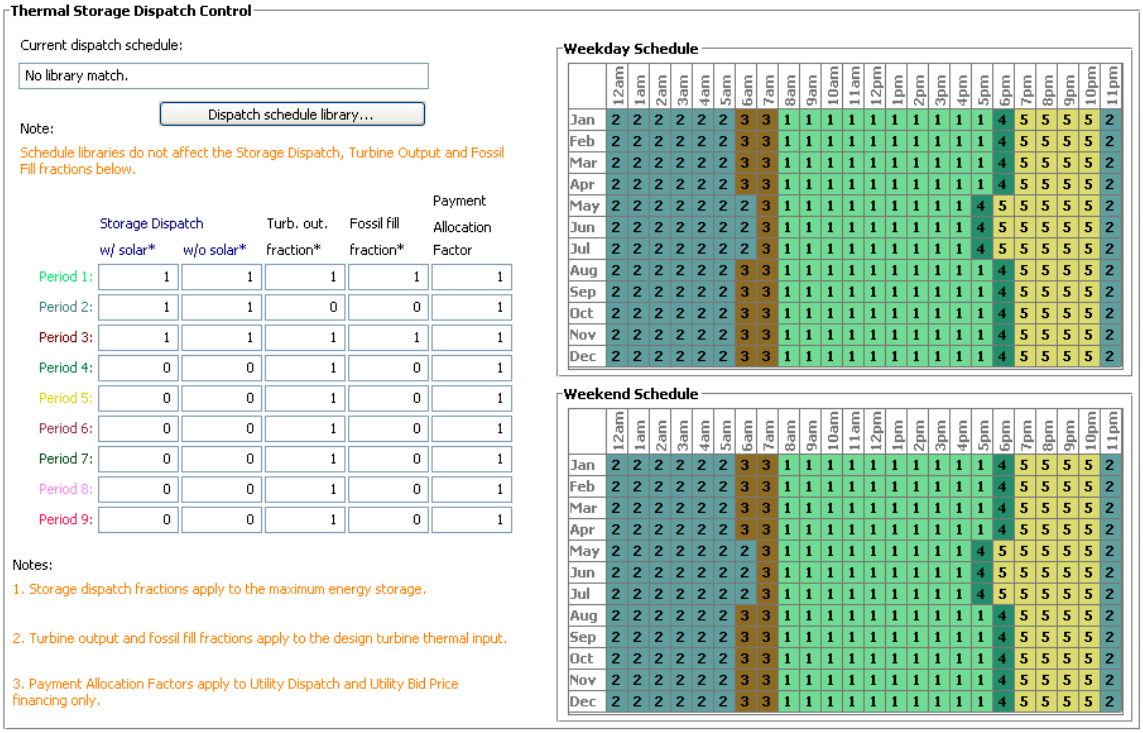

Figure 4-2: Thermal storage dispatch schedule

4.2.2 Parabolic trough simulation

The parabolic trough plant system modelled in this section is described in Figure 4-3. This is a standard configuration and very similar to the configuration proposed by Abengoa (2012a) for the !KaXu Solar One 100 MW trough project near Pofadder in the Northern Cape.

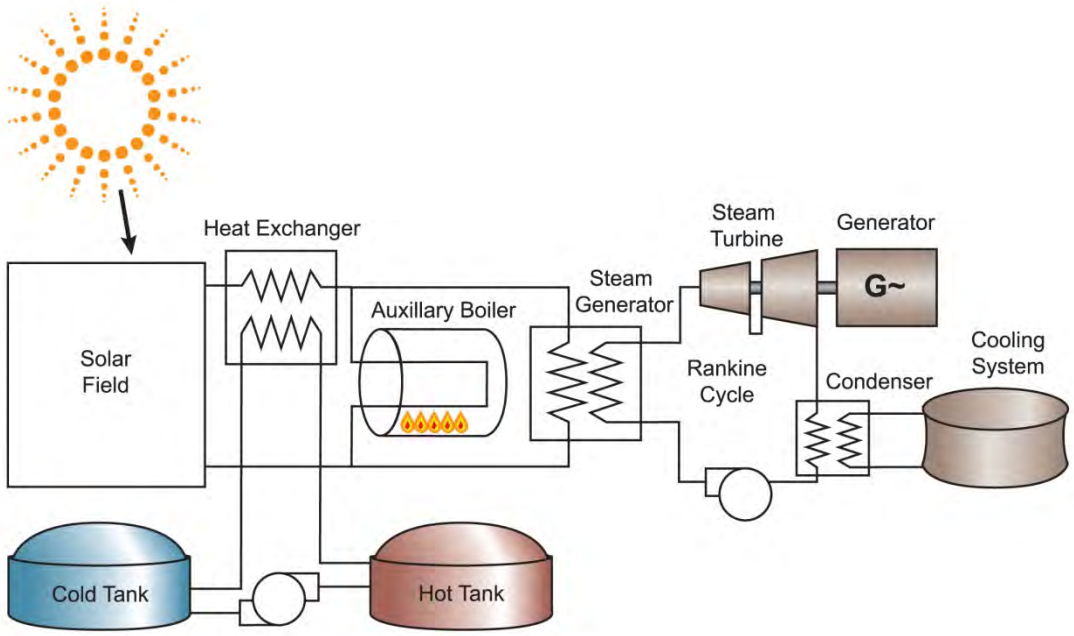

Figure 4-3: Parabolic trough plant schematic

The following sections describe the input parameters used to model a parabolic trough plant under Upington's weather conditions.

4.2.2.1 The solar field

SAM provides two methods of sizing the solar field. Method 1 allows the user to specify a solar multiple and SAM calculates the solar aperture to drive the power block at rated capacity. Method 2 allows the user to specify the solar field aperture independently of the power block rated capacity and SAM then calculates the solar multiple based on the user-entered solar field aperture.

Method 1 is more applicable in a greenfield project environment, whereas option 2 is applicable in a brownfield project environment where the solar field area is known. Method 1 was chosen for this case as this is a new plant being modelled. In order to arrive at an optimum solar multiple, a parametric simulation was run on an air-cooled power cycle parabolic trough plant with the CRSES input data. The SAM results are displayed in Figure 4-4.

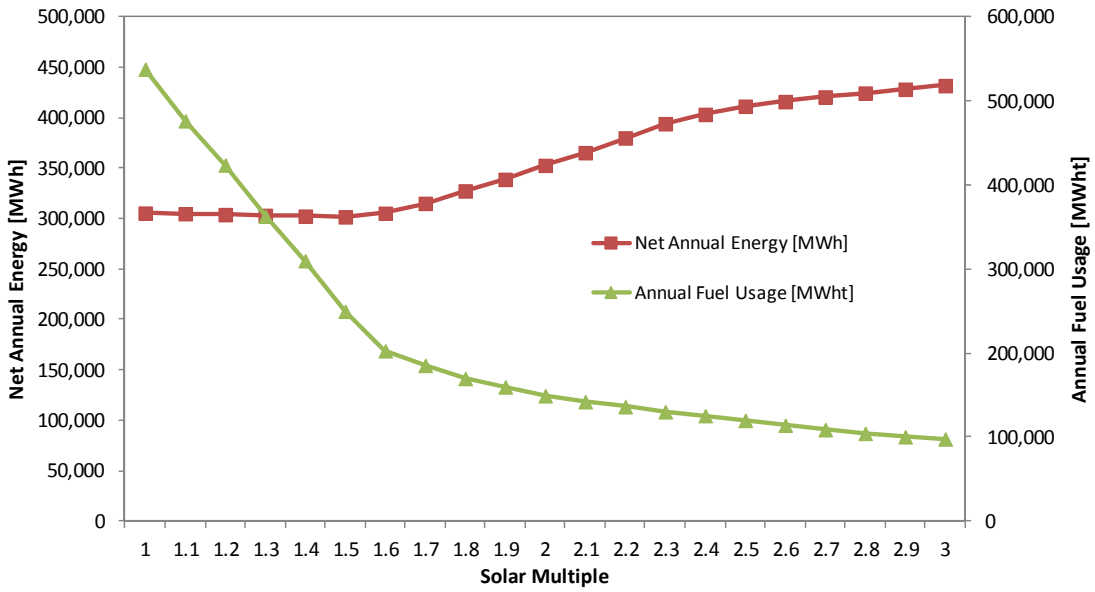

Figure 4-4: SAM result for parabolic trough solar multiple parametric simulation

The monotonically decreasing graph of annual electric output with respect to solar multiple means that there is no clear optimum. Auxiliary fuel usage was therefore used to inform the choice of the solar multiple, which was set at 2 to provide a compromise between annual output and system cost, and to limit auxiliary fuel usage.

Simultaneous partial defocusing was selected for the solar field to allow the collectors to move out of their optimum solar tracking position when the power block was receiving more energy from the solar field or TES system than required to run at rated capacity.

The HTF selected for this simulation was Therminol VP-1, due to its prominent use in recently built parabolic trough plants.

The model default of 12 collector and receiver assemblies termed SCA/HCE Assemblies in SAM were selected for each loop of the solar field. The non-solar field land area multiplier was left at the SAM default of 1.4 to cater for the power block and storage parts of the plant.

The annual water usage of the plant comes from various processes required for plant operation. One of the processes listed in the solar field component model is mirror washing. SAM suggests a cycle of 63 washes per annum and water usage per wash of 0.7 litres per square meter of solar field aperture. The field aperture of 860,010 m^2 calculated by SAM based on the solar multiple, results in an estimated annual water usage of over 37 million litres or 37,926 m^3 for this activity alone.

4.2.2.2 Solar collector assemblies

The physical trough model in SAM has six collector designs in its library. A description and summary of each collector's geometry are provided in Table 4-4. The EuroTrough ET150 was selected due to its light-weight, easy to assemble torque box design and large reflective aperture area which reduces the overall area required by the solar field.

Table 4-4: Collectors in SAM physical trough library

Collector name	Length of single module [m]	Number of modules per assembly	Length of collector assembly [m]	Aperture width of total structure [m]	Reflective aperture area [m²]
EuroTrough ET150	12.5	12	150	5.75	817.5
Luz LS-2	8.167	6	49	5	235
Luz LS-3	8.333	12	100	5.75	545
Solargenix SGX-1	8.333	12	100	5	470.3
AlbiasaTrough AT150	12.5	12	150	5.774	817.5
Siemens SunField 6	11.9	8	95.2	5.776	545

4.2.2.3 Heat collector elements

The physical trough model in SAM has four HCE designs in its library. A description and a summary of each receiver's parameters and SAM estimated design heat loss is provided in Table 4-5. Heat loss under design conditions is the noticeable difference between the receivers. Hence, the Schott PTR70 2008 receiver was chosen.

Table 4-5: Receivers in SAM physical trough library

Receiver name	Envelope absorptance	Envelope emittance	Envelope transmittance	Absorber absorptance	Bellows shadowing	Heat loss at design DNI and temperature [W/m]
Schott PTR70	0.02	0.86	0.963	0.96	0.96	190
Schott PTR70 2008	0.02	0.86	0.963	0.96	0.96	150
Solel UVAC 3	0.02	0.86	0.96	0.96	0.971	175
Siemens UVAC 2010	0.02	0.89	0.965	0.96	0.963	192

4.2.2.4 Power cycle

The power cycle component model used in the physical trough model is the same as that used in the power tower model. It contains a conventional steam Rankine cycle using either

evaporative- or air-cooling, and an optional fossil fuel fired backup boiler to heat the HTF when DNI levels do not provide enough energy to drive the power cycle at design load.

The design gross output of the power plant to achieve net output of 100 MW_e is 111 MW_e due to a gross to net conversion factor of 0.9.

One of the metrics in this component model affecting the water usage is the steam cycle blowdown fraction. This metric is the fraction of steam extracted from the steam mass flow rate through the power block that needs to be replaced with fresh power cycle makeup water. The power cycle suggests a conservative default value of 0.02 and multiplies the fraction by the hourly steam mass flow rate of the power cycle.

Both evaporative- and air-cooled power blocks were modelled for the parabolic trough plant in order to establish the plant's behaviour under differing cooling regimes. The cooling system used for the power block determines the annual water usage of the plant.

4.2.2.5 Thermal storage

The thermal storage component model uses a two-tank molten salt system as a basis. Solar salt was selected as the HTF following the practice of recently built parabolic trough plants (Bürkle and Müller-Steinhagen, 2009).

4.2.2.6 Parasitic power consumption

The parasitics component model accounts for the electrical power used by the tracking motors, the pumps transferring HTF from the receivers in the field to the power block, the pumps transferring HTF through the TES heat exchanger and the fixed electrical loads of the plant. The auxiliary heater and boiler loads are also accounted for in the component model.

4.2.3 Parabolic trough simulation results

Eight cases were considered in the parabolic trough simulation. Evaporative and air-cooled power cycles were considered for each of the four solar radiation input datasets. A high-level summary of the results is given in Table 4-6.

Table 4-6: SAM modelling results for parabolic trough technology

Upington								
Parabolic Trough Plant Simulation Results								
	Case 1	**Case 2**	**Case 3**	**Case 4**	**Case 5**	**Case 6**	**Case 7**	**Case 8**
Solar radiation data used	Weather Analytics	Weather Analytics	CRSES	CRSES	SAWS	SAWS	Eskom	Eskom
Power cycle cooling method	Evaporative	Air-cooled	Evaporative	Air-cooled	Evaporative	Air-cooled	Evaporative	Air-cooled
Net annual electric output [MWh]	403,145	398,477	407,165	401,839	351,032	349,539	348,924	347,498
Gross to net conv. factor	0.94	0.94	0.94	0.94	0.94	0.94	0.94	0.94
Annual power cycle water usage [m^3]	1,555,853	44,429	1,599,534	44,540	1,395,854	39,043	1,388,336	38,840
Annual washing water usage [m^3]	37,926	37,926	37,926	37,926	37,926	37,926	37,926	37,926
Total annual water usage [m^3]	1,593,778	82,356	1,637,749	82,467	1,433,782	76,970	1,426,262	76,767
Solar multiple	2	2	2	2	2	2	2	2
Aperture area [m^2]	860,010	860,010	860,010	860,010	860,010	860,010	860,010	860,010
Total land area [km^2]	3.141	3.141	3.165	3.141	3.141	3.141	3.141	3.141
Energy per m^3 of water [kWh/m^3]	252.9	4838.5	248.6	4872.7	244.8	4541.2	244.6	4526.7
Energy per km^2 of land [GWh/km^2]	128.4	126.9	128.7	127.9	111.8	111.3	111.1	110.6

From Table 4-6 it is clear that the electricity produced by this technology is proportional to its water usage. The power cycle cooling method affects the overall efficiency of the plant in terms of the gross to net conversion factor. Air-cooled parabolic trough plants produce an average of just under seventeen times more energy per cubic meter of water than evaporative cooled plants.

Using a row spacing of 15 m, SAM calculates the total area required for the solar field and then multiplies this by a non-solar field land area multiplier of 1.4 to obtain the total land area.

4.2.4 Central receiver simulation

The central receiver plant system modelled in this section is described in Figure 4-5. This is a standard molten salt central receiver configuration similar to the Solar Two configuration as noted by Pacheco and Gilbert (1999) and Pacheco *et al.* (2000).

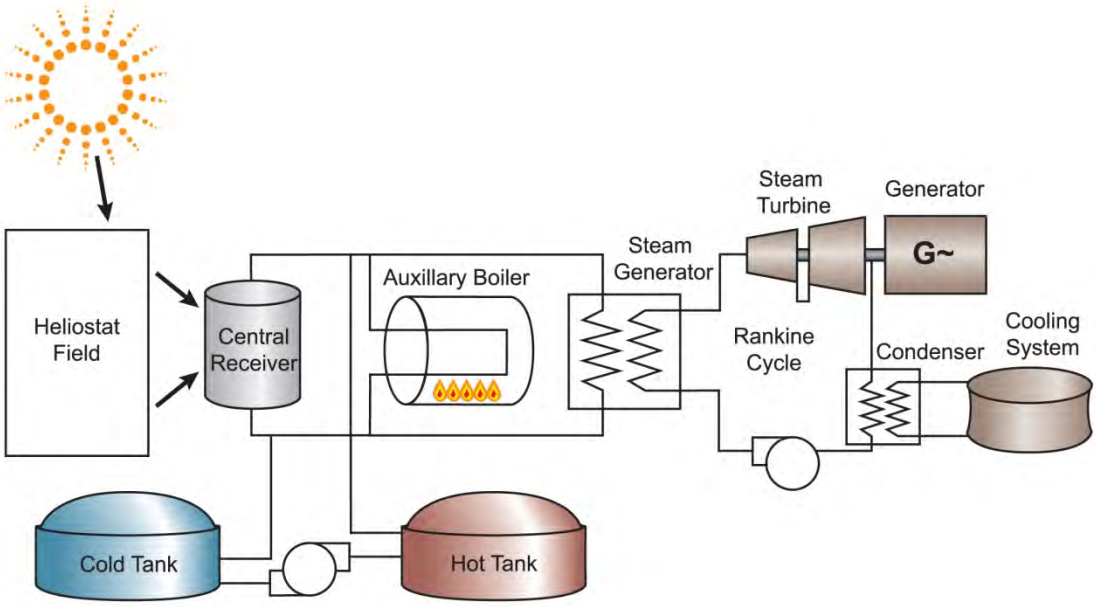

Figure 4-5: Central receiver plant schematic

The following sections describe the input parameters used to model a central receiver plant under Upington's weather conditions.

4.2.4.1 The heliostat field

SAM provides a circular field optimization wizard in the heliostat field component model of the power tower model. This wizard uses the receiver selected in the tower and receiver component model (either external or cavity) and then calculates optimal heliostat distribution, tower height and receiver dimensions. Apart from the receiver type, the solar multiple also influences this calculation significantly.

A solar multiple of 1.68 was selected to get the aperture area of the heliostat field as close as possible to the parabolic trough solar field to ease the comparison of power produced per square meter of aperture area. This resulted in a mirror area of 860,185 m^2 or 0.2% more than the aperture area of the parabolic trough plant based on optimisation calculations in SAM.

The heliostats are arranged in concentric circles around the central receiver tower. With the nearest set of heliostats being 129 m from the receiver tower and the furthest being 1291 m, the heliostat field is 61% larger than the parabolic trough solar field. However, a heliostat

field does not need as level a terrace as a parabolic trough solar field, which ensures a measure of flexibility despite its larger land requirement.

For mirror washing, the SAM documentation suggests 63 washes per annum and water usage per wash of 0.7 litres per square meter of solar field aperture. Considering the field aperture of 860,185 m^2, this results in an estimated annual water usage of over 37 million litres or 37,934 m^3 for this activity alone.

4.2.4.2 Tower and receiver

An important decision for a CRS is the type of receiver to be used. In order to facilitate the decision, the field optimization model was run for an external and cavity receiver and yielded the results in Table 4-7.

Table 4-7: External and cavity receiver metrics from field optimization model

Receiver type	Solar multiple	Tower height [m]	Receiver/internal panel height [m]	Receiver/aperture diameter/width [m]
External	1.9	183.33	21.33	13.33
Cavity	1.9	287.91	27.379	28

It is clear that the cost and construction risk is lower for an external receiver due to its lower tower height and more tightly dimensioned receiver. Hence, an external receiver was selected.

4.2.4.3 Power cycle

As mentioned in section 4.2.2.4 the power cycle component model for the physical trough model is the same used in the power tower model. A fossil fuel fired backup boiler was selected for this simulation, and the metrics described in section 4.2.2.4 remain valid.

4.2.4.4 Thermal storage

To permit comparison between the central receiver and parabolic trough technologies, the same two-tank molten salt TES system and dispatch philosophy as described in section 4.2.2.5 was used.

4.2.4.4 Parasitic power consumption

The power tower parasitics component model accounts for the electrical power used by the tracking motors of each heliostat, the pump transferring HTF to the power block from the receiver, the pumps transferring HTF through the TES heat exchanger and the fixed electrical loads of the plant. The piping losses between the receiver, TES system and power block, and the auxiliary heater and boiler loads are also accounted for in this component model.

4.2.5 Central receiver simulation results

Eight cases were considered in the central receiver simulation. Evaporative and air-cooled power cycles were considered for each of the four solar radiation input datasets. A high-level summary of the results is given in Table 4-8.

Table 4-8: SAM modelling results for central receiver technology

Upington								
Central Receiver Plant Simulation Results								
	Case 1	**Case 2**	**Case 3**	**Case 4**	**Case 5**	**Case 6**	**Case 7**	**Case 8**
Solar radiation data used	Weather Analytics	Weather Analytics	CRSES	CRSES	SAWS	SAWS	Eskom	Eskom
Power cycle cooling method	Evaporative	Air-cooled	Evaporative	Air-cooled	Evaporative	Air-cooled	Evaporative	Air-cooled
Net annual electric output [MWh]	412,886	409,500	404,692	404,181	322,288	321,549	335,673	334,905
Gross to net conv. factor	0.92	0.92	0.92	0.92	0.90	0.90	0.91	0.91
Annual power cycle water usage [m³]	1,327,238	33,031	1,324,103	32,449	1,099,683	26,777	1,123,618	27,383
Annual washing water usage [m³]	37,934	37,934	37,934	37,934	37,934	37,934	37,934	37,934
Total annual water usage [m³]	1,365,173	70,965	1,362,039	70,383	1,137,616	64,711	1,161,552	65,317
Solar multiple	1.68	1.68	1.68	1.68	1.68	1.68	1.68	1.68
Aperture area [m²]	860,185	860,185	860,185	860,185	860,185	860,185	860,185	860,185
Total land area [km²]	5.08	5.08	5.08	5.08	5.08	5.08	5.08	5.08
Energy per m³ of water [kWh/m³]	302.4	5770.5	297.1	5742.6	283.3	4969.0	289.0	5127.4
Energy per km² of land [GWh/km²]	81.3	80.6	79.7	79.6	63.4	63.3	66.1	65.9

The gross to net conversion factor of the central receiver system is less affected by the power cycle cooling method than the parabolic trough system. Similar electrical outputs for evaporative and air-cooled plants are achieved due to the higher temperatures obtainable by the central receiver. However, the proportionality of electricity output and water usage remains a strong feature of this technology. This technology presents lower annual water usage per unit of energy generated than parabolic trough technology at the expense of a larger land requirement, and a higher annual electrical energy output. Similarly to the parabolic trough model, air-cooled central receiver plants produce on average sixteen times more energy per cubic meter of water than evaporative cooled plants while evaporative plants produce an average of less than one percent more energy per square kilometer of land.

As mentioned earlier, the land requirement of the central receiver is significantly higher than the parabolic trough. However, due to the manner in which a central receiver concentrates DNR it is feasible to use land with more irregular features than can be allowed for in a parabolic trough installation. An example of this could be placing the tower in a valley and using the surrounding hills to position heliostats which would approximate to a discretised parabolic dish.

4.2.6 Dish-engine simulation

The dish-engine plant system modelled in this section is described in Figure 4-6.

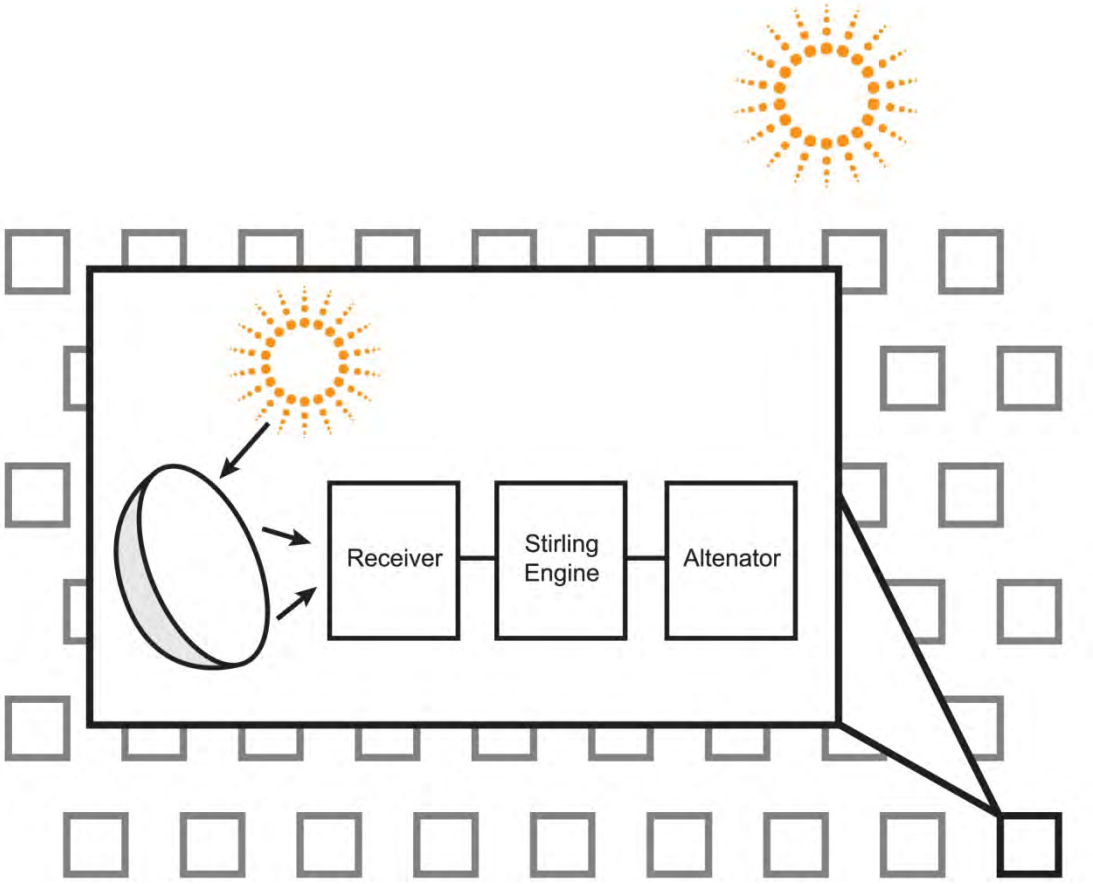

Figure 4-6: Dish-engine plant schematic

The dish-engine model in SAM is “rather complex and evolving” (System Advisor Model, 2010), hence SAM recommends the modelling only of the Stirling-engined parabolic dishes in its library and does not have a model for Brayton-engined parabolic dishes.

Despite Stirling Energy Systems (SES) filing for chapter 7 bankruptcy on 29 September 2011, their system was modelled as it provided plant power output comparable to the other technologies modelled in this study. The Wilkinson, Goldberg, and Associates, Inc. (WGA) dish Stirling system’s power output was too modest to be used in this simulation. The following sections describe the input parameters used to model a dish-engine plant under Upington’s weather conditions.

4.2.6.1 The solar field

The dish Stirling model’s solar field component has three elements. The first is the field layout which determines the number of collectors and total solar field area. The total number of collectors is obtained by multiplying the number of collectors on the North-South axis with

the number of collectors on the East-West axis, the assumption being that the solar field is square or rectangular in shape.

In the system properties element of SAM, a default wind stow speed of 16 m/s is specified, which is adjustable. Considering Upington's mean annual wind speed of approximately 3.6 m/s the plant is not expected to experience wind-speed related outages.

Array shading parameters is the third element. Here the North-South and East-West ground slope in degrees can be inserted if the site is not graded level. It was assumed that the site would have a level surface-bed so the default slopes of 0 degrees were left as is. The other metric considers the shading of the collector due to the Stirling engine's support arm. This is termed the slot gap. The slot gap width and slot gap height were left at the SAM default value of 1 m each.

4.2.6.2 The collector

In this component model, the parameters and performance of one dish-engine system are identified and applied to each dish-engine system in the field. Here the SES dish Stirling system projected and total mirror areas and reflectance are recorded in the mirror parameters element. The DNI value (in W/m^2) above which the cooling fan is required to operate, termed the insolation cut in for this WGA system is provided. This value is used to calculate the parasitic losses of each system.

4.2.6.3 The receiver

Only direct-illumination receivers are modelled by the software. SAM uses the aperture, insulation, absorber and cavity parameters to calculate the receiver's thermal losses which account for more than 50% of a dish-engine system's losses (System Advisor Model, 2011).

4.2.6.4 Stirling engine

Each engine in the SAM library has specific gross power output directly related to its input power from the collector and receiver models. A polynomial fit is applied to these engines using the Beale number power correlation (Fraser, 2008). This defines the gross output power of the Stirling engine from part load to full load. Fraser's (2008) Beale number curve fit polynomial ($Beale\#_{curve}$) can be described as follows with term description in Table 4-9:

$$Beale\#_{curve} = B_{CC} + B_{1st} \cdot P_{in,SE} + B_{2nd} \cdot {P_{in,SE}}^2 + B_{3rd} \cdot {P_{in,SE}}^3 + B_{4th} \cdot {P_{in,SE}}^4 \quad (4.1)$$

Table 4-9: Beale number curve terms

Term	Definition
B_{CC}	Beale constant coefficient
B_{1st}	Beale first-order coefficient
B_{2nd}	Beale second-order coefficient
B_{3rd}	Beale third-order coefficient
B_{4th}	Beale fourth-order coefficient
$P_{in,SE}$	Stirling engine input power from collector and receiver models

The values developed for the Stirling Energy Systems Stirling engine (Fraser, 2008) were used for this simulation.

4.2.6.5 Parasitic power consumption

The parasitic power consumption of each dish-engine system is subtracted from the gross output power of the engine ($P_{Gross,op}$) to arrive at the net system power (P_{Net}). Fraser (2008) describes it as follows:

$$P_{Net} = P_{Gross,op} - (P_{controls} + P_{fan} + P_{pump}) \quad (4.2)$$

Where the parasitic power consumption consists of the tracking controls ($P_{controls}$), the cooling fan (P_{fan}) and the cooling fluid pump (P_{pump}). The SAM values with a 50% ethylene glycol cooling fluid were used for this simulation.

4.2.7 Dish-engine simulation results

The discrete nature of dish-engine plants results in fewer output metrics as each dish is a self contained plant producing electrical energy into a grid, as opposed to a large thermal transport system providing heat to a singular steam-powered turbine. This results in the water used in the plant being restricted to cleaning water for the concentrators, which is not quantified by the model. Table 4-10 displays a high-level summary of the model results.

From Table 4-10 it is clear that the solar radiation input data determine the results as thermal storage is not used in Stirling-engined parabolic dish plants. The comparatively negligible water usage and substantially more efficient land utilisation are real benefits of this system. Using a 15 m separation on the North-South and East-West axis of each collector results in a very compact solar field in comparison to the parabolic trough and central receiver. The density of the solar field makes this plant more suitable for installations closer to urban areas than central receiver or parabolic trough plants.

Table 4-10: SAM modelling results for dish-engine technology

Upington				
Dish-Engine Plant Simulation Results				
	Case 1	**Case 2**	**Case 3**	**Case 4**
Solar radiation data used	Weather Analytics	CRSES	SAWS	Eskom
Collector power in [MWh], annual	1,015,020	988,634	643,980	877,841
Collector power out [MWh], annual	914,320	895,433	566,131	766,769
Receiver power in [MWh], annual	909,749	890,955	563,300	762,935
Receiver power out [MWh], annual	810,210	783,444	475,276	653,041
Gross field power [MWh], annual	253,225	244,888	147,268	202,468
Net annual electric output [MWh]	235,261	227,118	134,557	186,401
Annual washing water usage [m^3]	16,052	16,052	16,052	16,052
Number of dish-engines	4,000	4,000	4,000	4,000
Aperture area [m^2]	364,000	364,000	364,000	364,000
Total land area [km^2]	0.90	0.90	0.90	0.90
Energy per km^2 of land [GWh/km^2]	261.4	252.4	149.5	207.1

4.2.8 CLFR simulation

The CLFR plant system modelled in this section is described in Figure 4-7. This is a standard DSG CLFR configuration similar to the Novatec Biosol PE-1 plant in the Spanish town of Murcia, the variances being that this plant does not have steam storage and does use a backup fossil fuel boiler (Selig, 2009).

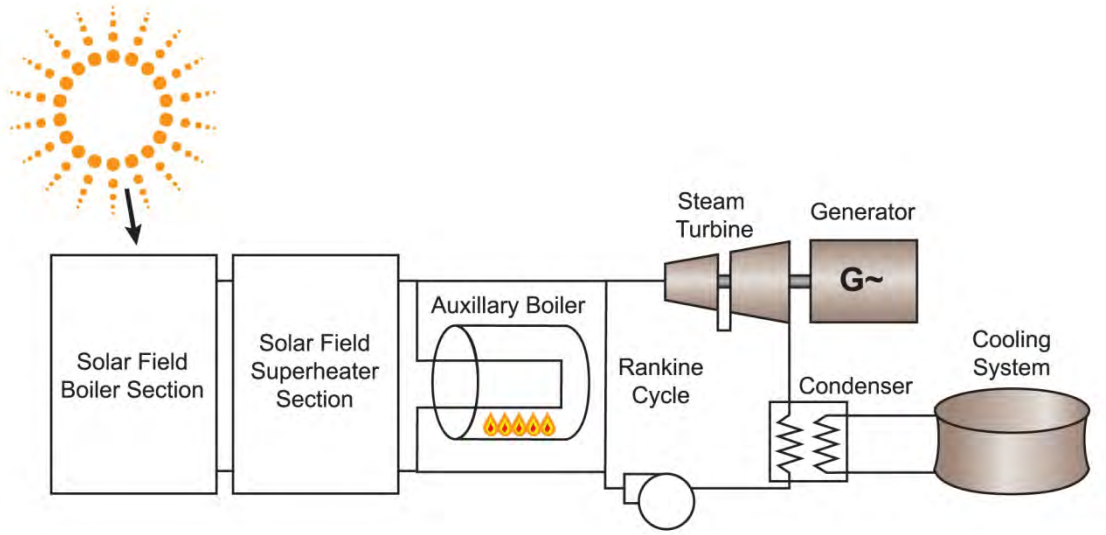

Figure 4-7: CLFR plant schematic

Version 2011.12.2 of SAM is the first to include a linear Fresnel model, and certain errors in the simulation were noted. For example the annual washing water result is zero despite a mirror washing regime being specified in the input. This result was calculated manually and included in the results table. The following sections describe the input parameters used to model a linear Fresnel plant under Upington's weather conditions.

4.2.8.1 The solar field

The linear Fresnel model also allows the solar field to be sized either by solar multiple (option 1) or solar field aperture (option 2). Option 1 was chosen for this case as this is a new plant being modelled. The default solar multiple of 1.79 was selected to provide an aperture area only 0.7% larger than that of the parabolic tough plant. This provides for ease of comparison with both parabolic trough and CRS.

The number of collector and receiver modules supplying the boiler and superheater were left at the default values in order not to change the solar field outlet temperature from the design value.

The energy required to heat the HTF, receiver components, piping, fittings and insulation during startup is accounted for by SAM with the "Thermal inertia per unit of solar field"

parameter. This was set at the default 2.7 kJ/K-m^2. The steam conditions at design DNI and temperature were left at the linear Fresnel model default values.

The linear Fresnel model has a default non-solar field land area multiplier of 1.6 yet the total land area of the plant still works out to less than half of the land area required for a parabolic trough plant. This is due to two reasons. Firstly the aperture area of a Fresnel collector is approximately the same as its collector area whereas the aperture area of a parabolic trough is only the projection of its collector area (Häberle *et al.*, 2002). Secondly the spacing required between parabolic trough collectors (15 m centre to centre in the SAM simulation) leaves a 9.25 m gap between collector rows, whereas the linear Fresnel reflectors are more densely packed. Häberle *et al.* (2002) provide a diagram comparing parabolic trough and linear Fresnel collector aperture area (*A*) and the gross land area (*B*). In Figure 4-8, the aperture area of the linear Fresnel collector is $\sum A_i$ and the gross land area $B = \sum A_i + \sum d_i$. With d_i being the space between primary collector mirrors.

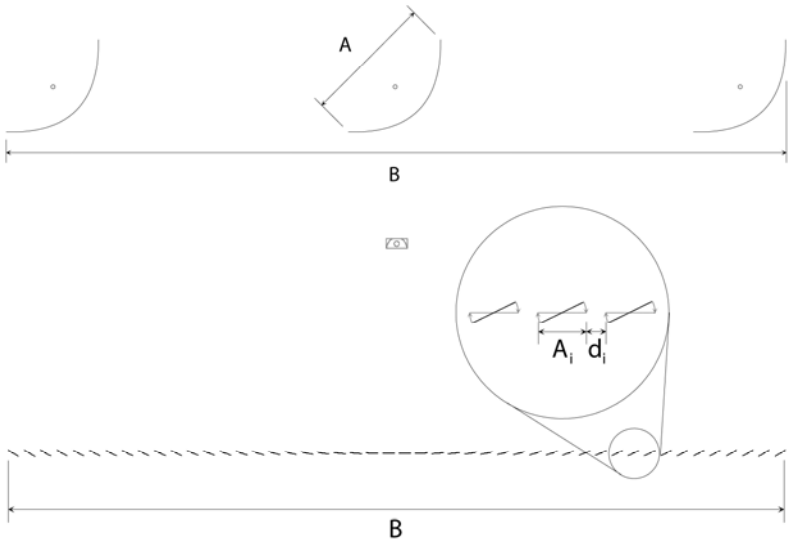

Figure 4-8: Parabolic trough (above) and linear Fresnel (below) collector aperture area and gross land area (Häberle *et al.*, 2002)

The mirror washing water usage in the solar field component model uses a default of 0.2 litres per square meter of solar field aperture at a washing cycle of 120 washes per annum. This value was changed to 0.7 litres per square meter of solar field aperture at a washing cycle of 63 washes per annum to bring it in line with the washing cycles used for the parabolic trough and central receiver plant models. Considering the approximate average field aperture of 862,848 m^2, this results in an estimated annual water usage of over 38 million litres or 38,052

m^3 for this activity. The field control parameters were set to the linear Fresnel model default values.

4.2.8.2 Collector and receiver

The collector and receiver component model allows differing boiler and superheater collector geometry. It was decided to keep the geometry the same for ease of installation and maintenance.

The collector geometry and optical performance element in the collector and receiver component model allows three methods of optical characterization, namely the solar position table method, the collector incidence angle table method or the incident angle modifiers method. The solar position table method with the default solar position/collector incidence angle table was selected as it defines the performance of the solar field at all sun positions for which the plant will operate. A polynomial fit heat loss model with SAM default coefficients was selected for the receiver.

4.2.8.3 Power cycle

The linear Fresnel power cycle component model, while similar to the physical trough and power tower power cycle component models, has a higher estimated gross to net electrical power conversion factor. The design gross output of the power plant to achieve net output of 100.58 MW_e is 107 MW_e due to a gross to net conversion factor of 0.94. As with the parabolic trough and central receiver options, a fossil fuel fired backup boiler was selected for this simulation.

The startup time of the power block in this model is less than the default time settings selected for the physical trough and power tower models. SAM suggests that 0.35 hours (21 minutes) are required for this plant while 0.5 hours (30 minutes) are required for the parabolic trough and central receiver options. This is due to the flat primary reflectors requiring less complicated solar tracking mechanisms and smaller physical movements to focus DNR onto the collector. This setting was thus left as is to observe how this benefit of the CLFR system impacts its net annual electric output.

A dispatch control component is included in the power cycle component of the linear Fresnel model as it does not have a TES component model. The dispatch schedule here was made identical to that shown in Figure 4-1 in section 4.2.2.5 for the fossil fill aspect.

4.2.8.4 Parasitic power consumption

The linear Fresnel parasitic losses component model calculates the total tracking power loss and the fixed parasitic loss. It also accounts for the auxiliary heater and boiler parasitic power consumption. The default values were selected for this simulation.

4.2.9 CLFR simulation results

Eight cases were considered in the CLFR simulation. Evaporative and air-cooled power cycles were considered for each of the four solar radiation input datasets. A high-level summary of the results is given in Table 4-11.

Table 4-11: SAM modelling results for linear Fresnel technology

Upington								
Linear Fresnel Plant Simulation Results								
	Case 1	**Case 2**	**Case 3**	**Case 4**	**Case 5**	**Case 6**	**Case 7**	**Case 8**
Solar radiation data used	Weather Analytics	Weather Analytics	CRSES	CRSES	SAWS	SAWS	Eskom	Eskom
Power cycle cooling method	Evaporative	Air-cooled	Evaporative	Air-cooled	Evaporative	Air-cooled	Evaporative	Air-cooled
Net annual electric output [MWh]	404,812	391,668	402,530	393,984	397,325	389,422	400,126	394,198
Gross to net conv. factor	0.96	0.94	0.96	0.94	0.95	0.93	0.95	0.94
Annual power cycle water usage [m³]	1,472,237	39,516	1,475,043	39,400	1,466,099	39,136	1,473,578	39,285
Annual washing water usage [m³]	38,052	38,052	38,052	38,052	38,052	38,052	38,052	38,052
Total annual water usage [m³]	1,510,289	77,568	1,513,095	77,452	1,504,151	77,188	1,511,630	77,337
Solar multiple	1.79	1.79	1.79	1.79	1.79	1.79	1.79	1.79
Aperture area [m²]	862,848	862,848	862,848	862,848	862,848	862,848	862,848	862,848
Total land area [km²]	1.381	1.381	1.381	1.381	1.381	1.381	1.381	1.381
Energy per m³ of water [kWh/m³]	268.0	5049.4	266.0	5086.8	264.2	5045.1	264.7	5097.2
Energy per km² of land [GWh/km²]	293.2	283.7	291.6	285.4	287.8	282.1	289.8	285.5

The linear Fresnel model commits the entire fossil fill contribution of the backup boiler to generating power at its nameplate capacity since it does not have a TES system. This results in a higher gross to net conversion factor due to less part-load condition periods being experienced by the power block. Thus the net annual electric output is very favourable. The problem with this is twofold. Firstly the CLFR result is artificially high and secondly the amount of fossil fuel used particularly in the winter months may exceed the 15% maximum as listed in the REFIT eligibility criteria (NERSA, 2011). In contrast, the parabolic trough and power tower models use the fossil fill contributions to assist in charging their respective TES systems. Hence the similar output of the parabolic trough and central receiver models.

4.3 Inter-technology comparisons

A comparison of the above technologies can best be achieved by constraining the assessment with the specific requirements of the site within the Northern Cape.

Upington is situated in the //Khara Hais Local Municipality within the Siyanda District Municipality in the Northern Cape (Municipal Demarcation Board, 2011). It borders the Orange River which is used extensively for the irrigation of the local agriculture industry.

According to the South African National Biodiversity Institute (SANBI) (2011) the //Khara Hais Local Municipality has two terrestrial ecosystems, namely the Nama-Karoo (71.65% of municipal land) and Savanna (28.35% of municipal land) biomes. It is expected that land within the Savanna biome with its higher annual rainfall will be occupied with commercial farms. It is undesirable to displace prime agricultural land with a power plant, hence a prudent site choice would be within the Nama-Karoo biome. This should make the EIA and Social Impact Assessment (SIA) approval process less cumbersome also.

With an annual average rainfall of between 100 mm and 520 mm (South African National Biodiversity Institute, 2011), the Nama-Karoo biome can be classified as an arid climate (Palmer and Ainslie, 2005). This implies that excessive water usage within the area must be eschewed. Hence, one of the constraining factors in the comparison was water usage.

While Upington is a major centre of trade and industry in the Northern Cape, the Northern Cape's population density is a capacious two to three people per square kilometer (Statistics South Africa, 2001). However, according to the 2001 Census results from Statistics South Africa, //Khara Hais Local Municipality has a population density of fifteen people per square kilometer. This is five times the norm for the province, but still suppressed when compared to the national average. This characteristic of the municipality suggests that land usage is not as much of a constraining factor as it would be in other areas of the country. However, it is never desirable to use more land than necessary for a power plant and optimum land usage is of importance to any development.

South Africa's domestic electricity load profile has dominant peaks in the morning (6 am to 8 am) and evenings (6 pm to 9 pm) (Davis *et al.*, 2011). This falls outside the peak energy generating hours of a solar thermal power plant. Therefore, thermal or another form of energy storage is required to service the evening peak demand. This also places an additional constraint on the technology comparison.

Another constraint, which occurs independently of the local conditions, is the overall efficiency of each system. Installing a suitable yet inefficient power plant will increase operating costs resulting in the utility and power user's expectations not being effectively met.

In order to standardize the comparison, it was decided to select the METEONORM solar radiation data obtained from the CRSES, as the methods used to obtain these data are well explained in the METEONORM handbooks provided by Meteotest (2010a and 2010b). The data construction technique of the Sensor Point System used by Weather Analytics Inc. is not in the public domain.

In summary, the constraints for the chosen cases of each available technology to compare were as follows, with the results given in Table 4-12.

i. METEONORM solar radiation data from CRSES to be used
ii. Only air-cooled power cycles to be considered due to water constraints
iii. Land utilization to be only a moderate deciding factor
iv. Energy storage to influence comparison strongly due to national load profile
v. Overall plant efficiency to be considered

Table 4-12: Inter-technology modelling results for a plant installed capacity of 100 MW_e

Upington				
Inter-technology Simulation Result Comparison for a 100 MW_e installed plant capacity				
	Parabolic Trough Plant	**Central Receiver Plant**	**Dish-Engine Plant**	**CLFR Plant**
Solar radiation data used	CRSES	CRSES	CRSES	CRSES
Power cycle cooling method	Air-cooled	Air-cooled	Radiator-cooled	Air-cooled
Net annual electric output [MWh]	401,839	404,181	227,118	393,984
Generalised gross to net conversion factor	0.94	0.92	0.97	0.94
Capacity factor [%]	45.9	46.1	25.9	44.7
Annual power cycle water usage [m^3]	44,540	32,449	Not modelled*	39,400
Annual washing water usage [m^3]	37,926	37,934	16,052	38,052
Total annual water usage [m^3]	82,467	70,383	16,052†	77,452
Solar multiple	2	1.68	Not applicable	1.79
Aperture area [m^2]	860,010	860,185	364,000	862,848
Total land area [km^2]	3.141	5.080	0.900	1.381
Energy per m^3 of water [kWh/m^3]	4,872.7	5,742.6	14,149	5,086.8
Energy per km^2 of land [GWh/km^2]	127.9	79.6	252.4	285.4

*Radiator cooling fluid water use not accounted for in SAM results.
† Excludes radiator cooling fluid water.

To examine the modelled power production and water usage of the four technologies over a year period, model results were graphed in Figure 4-9 and Figure 4-10 below.

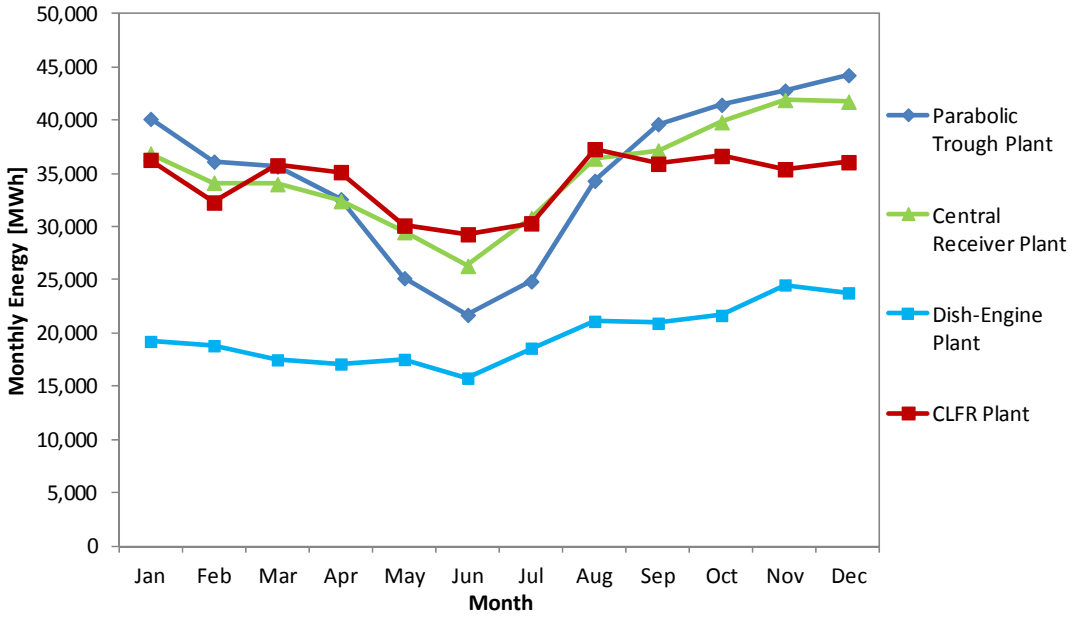

Figure 4-9: Modelled electrical output from parabolic trough, central receiver and dish-engine plants

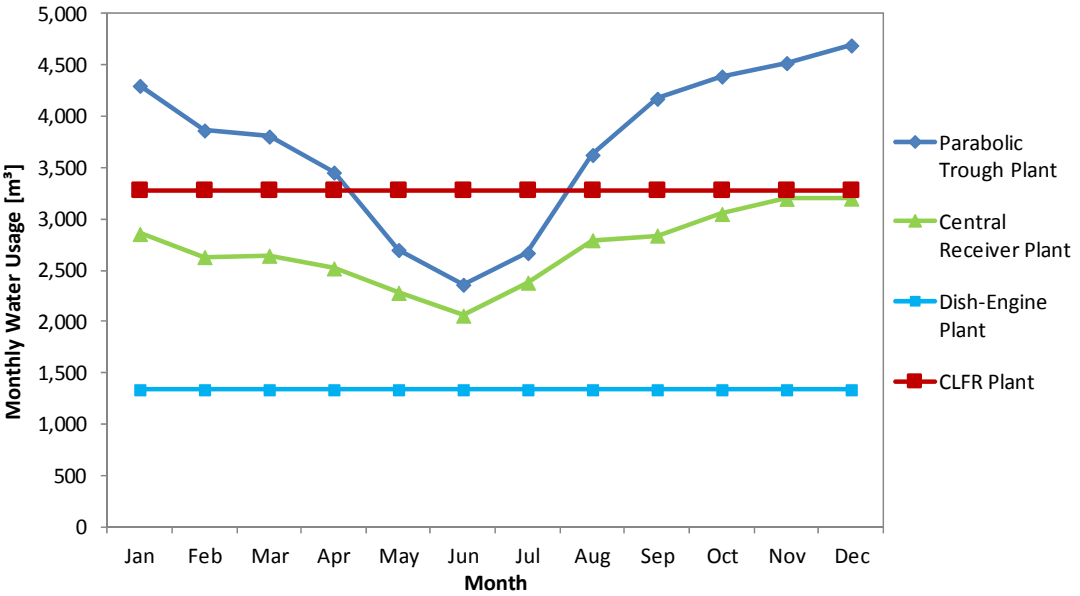

Figure 4-10: Modelled power block water usage from parabolic trough, central receiver and dish-engine plants

The results show that central receiver and parabolic trough technology provide more electrical energy than their CLFR and dish-engine counterparts. The linear Fresnel model did not have a monthly power cycle water usage figure, so the annual water usage from the model, and the manually calculated washing water usage were summed and averaged over the twelve months

to give an indication of the water usage. The central receiver and parabolic trough plant models produced similar net annual energy results. However, the parabolic trough plant used significantly more water annually than the central receiver plant (17.2% higher annual water usage). The water usage of the parabolic trough plant is its largest drawback.

The CLFR plant model produced more electrical energy than the dish-engine model. This additional energy was provided using more water and land area than the dish-engine array. Dish-engine technology exerts a much lighter load on the environment in terms of land usage and water consumption with a lower yet comparable power output.

To further aid the comparison, heat maps of the hourly net electric power output of each plant are given in Figure 4-11, Figure 4-12, Figure 4-13 and Figure 4-14.

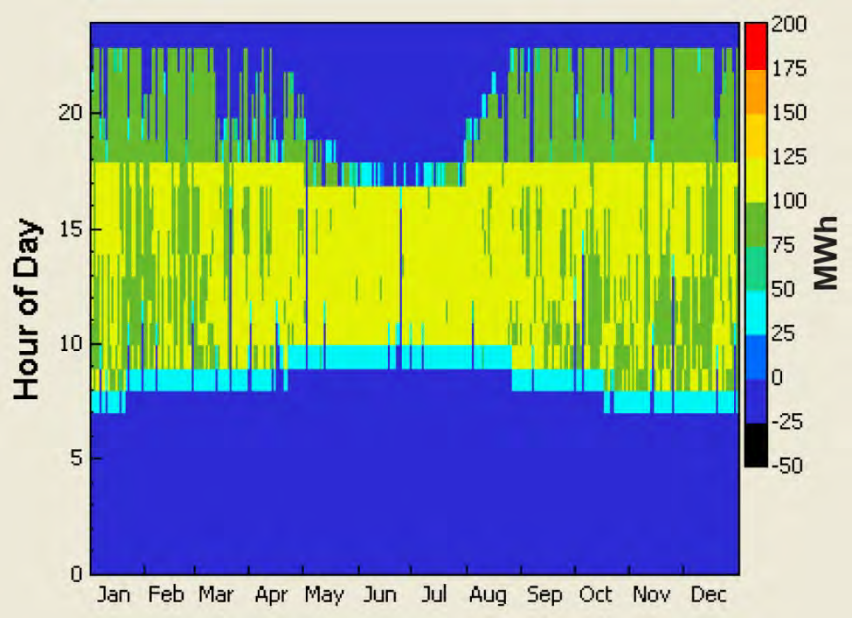

Figure 4-11: Net electric power output (MWh) of parabolic trough plant per hour of day

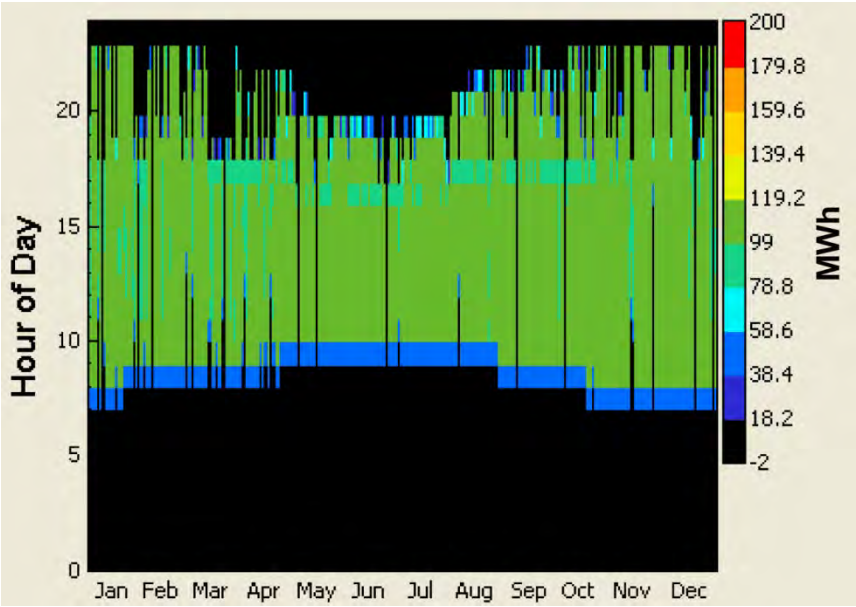

Figure 4-12: Net electric power output (MWh) of central receiver plant per hour of day

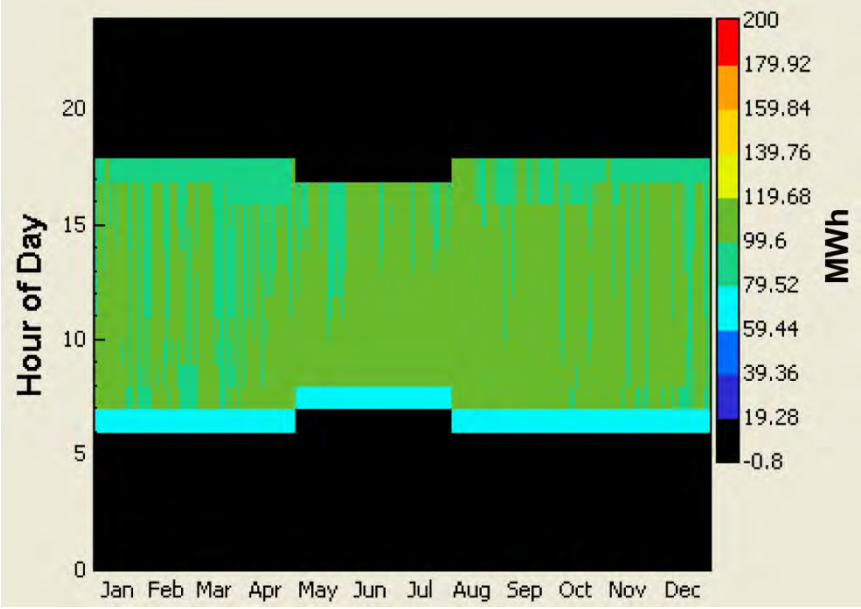

Figure 4-13: Net plant power output (MWh) of CLFR plant per hour of day

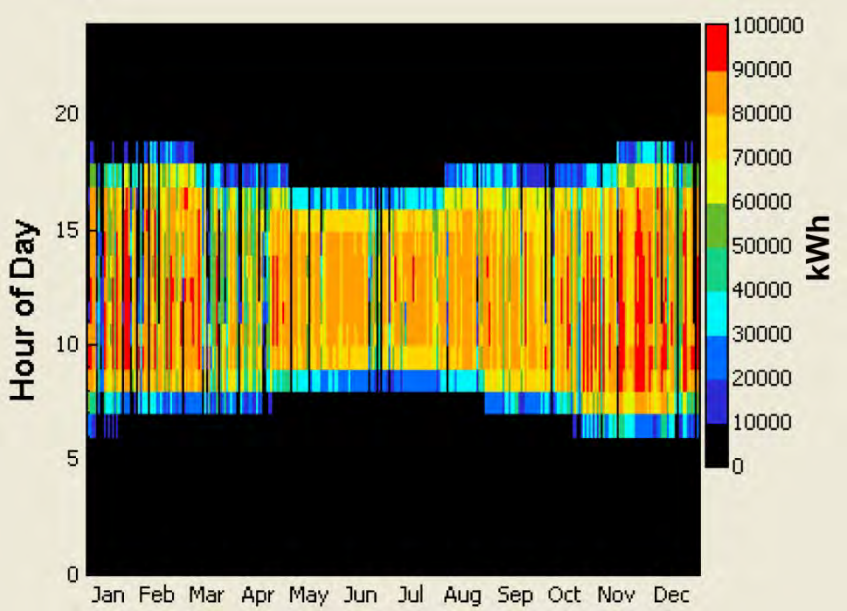

Figure 4-14: Hourly energy (kWh) of dish-engine plant per hour of day

The heat maps above allow each plant's electric output to be compared to the national load profile. The results show that central receiver technology best meets the evening load peak requirement of the national load profile. The CLFR plant does not match the national load profile as well as the central receiver- or parabolic trough plant. The parabolic trough plant does not seem to meet the evening load peak requirement as well as the central receiver plant during the winter months when South Africa experiences its seasonal peak in demand. The dish-engine plant provides limited power output partially covering the evening peak despite not having TES.

In general point focusing systems provide more electrical energy in the evenings than line focusing systems. Hence, point focusing systems are more suitable to meet the evening peak of the national load profile. SAM results for the system degradation input noted in section 4.2.1 are given in Figure 4-15.

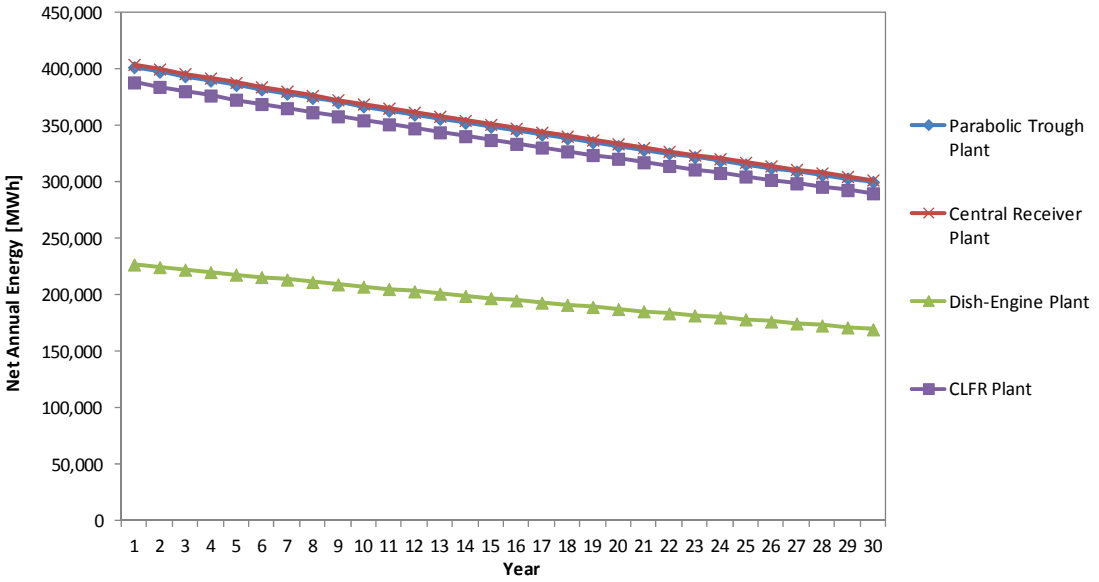

Figure 4-15: Effect of plant degradation on net annual energy

The results show a near linear reduction of net annual energy for each plant over a 30 year period. Actual degradation for each plant will differ from this model result and more operation and maintenance data are needed to model this aspect more accurately.

The central receiver model results were most favourable. The high annual energy output, low water consumption and national load profile matching proved considerable advantages and constitute a strong argument for its implementation. Its high land utilization for equivalent aperture area, as compared to its competitors, is a notable disadvantage.

The linear Fresnel model in SAM provided higher energy output than expected due to the manner in which it deployed its fossil fuel backup boiler. The non-TES direct steam application of CLFR technology is a drawback in the South African environment as it does not have the ability to match the national load profile. CLFR power block water usage is higher than central receiver power block. The plant's frugal land usage is an advantage.

Reducing the fossil fuel backup boiler contribution to zero for the parabolic trough, central receiver and linear Fresnel models, it is found that the output metrics of the linear Fresnel model compare as expected with those of more optically efficient parabolic trough and central receiver models (Table 4-13).

Table 4-13: Inter-technology modelling results without fossil fuel fired backup boiler

Upington				
Inter-technology Simulation Result Comparison for a 100 MW_e plant without fossil fuel fired backup boiler				
	Parabolic Trough Plant	**Central Receiver Plant**	**Dish-Engine Plant**	**CLFR Plant**
Solar radiation data used	CRSES	CRSES	CRSES	CRSES
Power cycle cooling method	Air-cooled	Air-cooled	Radiator-cooled	Air-cooled
Fossil fuel backup	No	No	No	No
Net annual electric output [MWh]	356,654	360,580	227,118	242,570
Overall power plant efficiency [%]	15.3	15.5	23.9	10.4
Generalised gross to net conversion factor	0.94	0.92	0.97	0.94
Capacity factor [%]	40.80%	41.10%	25.9	27.50%
Annual power cycle water usage [m^3]	39,610	29,008	Not modelled*	24,877
Annual washing water usage [m^3]	37,782	37,934	16,052	38,052
Total annual water usage [m^3]	77,392	66,942	16,052†	62,929
Solar multiple	2	1.68	Not applicable	1.79
Aperture area [m^2]	860,010	860,185	364,000	862,848
Total land area [km^2]	3.141	5.08	0.900	1.381
Energy per m^3 of water [kWh/m^3]	4,608.41	5,386.45	14,149	3,854.67
Energy per km^2 of land [GWh/km^2]	113.1	71.0	252.4	175.6

Removing fossil fuel backup illustrates how the higher optical efficiencies obtainable by the parabolic trough and central receiver affect their net annual electric output in contrast to the linear Fresnel model. The difference between the central receiver and linear Fresnel net annual electric output grows from 2.6% to 48.6% when fossil fuel backup is removed. Similarly the difference between the parabolic trough and linear Fresnel net annual electric output grows from 2% to 47%. The difference between the parabolic trough and central receiver net annual electric output increases from 0.6% to 1.1% when fossil fuel backup is removed. The comparatively higher overall efficiency and net annual electric output of the central receiver when fossil fuel backup is removed suggests that it is more suitable for projects with stringent fossil fuel backup requirements. One of NERSA's (2011) detailed eligibility criteria for a CSP plant is that it use no more than 15% fossil fuel input over an agreed period for morning startups and during cold days. This result suggests that the central receiver may most suitably meet this requirement.

The overall power plant efficiencies were calculated by applying the following formulae to the hourly data generated by the models:

$$\eta_{Parabolic\ Trough} = \frac{Net\ electric\ power\ output\ [MWh]}{Total\ incident\ thermal\ energy\ [MWh]} \quad (4.1)$$

$$\eta_{Central\ Receiver} = \frac{Net\ electric\ power\ output\ [MWh]}{Total\ incident\ thermal\ energy\ [MWh]} \quad (4.2)$$

$$\eta_{Dish-Engine} = \frac{Hourly\ Energy\ [kWh]}{Collector\ Power\ In\ [kWh]} \quad (4.3)$$

$$\eta_{CLFR} = \frac{Net\ plant\ power\ output\ [MWh]}{Total\ power\ incident\ on\ the\ field\ [MWh]} \quad (4.4)$$

The overall efficiency results agree with the literature cited in chapter 2 that Stirling dish-engine systems are most efficient overall and that the higher temperatures obtained by the central receiver result in it returning a higher efficiency than the parabolic trough and CLFR. The CLFR's lower optical efficiency (Figure 4-16) affects its overall efficiency significantly.

The parabolic trough model results reflect its ability to meet the evening peak load requirement of the national load profile. However, its higher annual water usage than competing technologies is a disadvantage.

The dish-engine results are promising, given the relatively low water consumption and land usage. However, the uncertainty regarding Stirling Energy Systems–the producers of the dish-engines modelled in this study–as well as this system's lack of TES which limits its ability to track the national load profile are both significant drawbacks to its implementation.

4.4 Validation of simulation results

A direct comparison between the CSP simulations conducted in this study and real plant performance is difficult because commercial performance data is seldom released, and no such facilities currently operate in South Africa. Nevertheless, a comparison between this work and similar studies done elsewhere is given below in an attempt to quantify the likely uncertainty of modeled results.

4.4.1 Parabolic trough result validation

García *et al*. (2011) performed a thorough literature survey of performance models for parabolic trough plants. They concluded that detailed comparisons with trough plant data are scarce, although they managed to obtain 42 summer days of actual data from the Andasol 2

plant in Granada, Spain. Their simulation displayed close agreement with actual data from the plant except for when the plant operator made decisions contrary to the simulation expectation. They also compared results to those of SAM and the daily gross electric energy generated differed on average by 2%. This lends confidence to the present work and suggests that parabolic trough simulations carried out in SAM may produce results that are accurate to within a few percent of the true performance.

The simulation model of García *et al*. (2011) was developed in Mathematica 7 software. The geographical and meteorological input data differ somewhat from this study since the Andasol 2 plant is in the Spanish province of Granada (northern hemisphere). A comparison of the key metrics is given in Table 4-14.

Table 4-14: Comparison of García *et al.* (2011) simulation metrics to those used in this study

Simulation Inputs	**García *et al.* (2011) simulation**	**This simulation**
Site	Aldeire y La Calahorra, Granada, Spain	Upington, Northern Cape, South Africa
Nameplate electrical output (gross/net) [MW_e]	50/49.9*	111/100
Hours of thermal storage	7.5	6
Solar collector assemblies	SKAL-ET	EuroTrough ET150
Heat collector elements	Half Schott PTR70 2008 Half Solel UVAC2 and UVAC3	Schott PTR70 2008
Heat transfer fluid	Therminol VP-1	Therminol VP-1
Solar field aperture Area [m^2]	510,120*	860,010
Power cycle cooling method	Evaporative	Air-cooled
Time-step between data points	10 min	1 hour
Simulation Outputs	**García *et al.* (2011) simulation**	**This simulation**
Annual electric output [MWh]	158,000*	401,839

*These values are provided by NREL (2011b) on the Andasol-2 plant and are not directly referred to by García et al. (2011).

Since García *et al*. (2011) could only obtain 42 days of plant data for comparison, they do not provide the annual metrics from their model. This makes a direct comparison of annual data difficult. Similar model components were used and from the information given by NREL (2011b), it can be seen that the annual output scales reasonably in terms of nameplate electrical output.

Wagner (2012) permits a more comprehensive analysis of simulation input and output data. The study includes a comparison of a DSG CLFR plant, a DSG central receiver plant, a molten salt central receiver plant and a Therminol HTF parabolic trough plant in SAM. The geographical and meteorological input data for the model was for Phoenix, Arizona in the USA. Fixing only dry cooling and no fossil backup, the other parameters were optimised to reach a fixed annual electric output of 300 GWh. This is in contrast to the approach taken in

this study where dry cooling, plant availability, nameplate electrical output, solar multiple, thermal storage and dispatch control were matched as closely as possible between the technologies and the annual electric output of each technology was compared in light of these constraints. Key metrics from the parabolic trough plant simulation of Wagner (2012) are given in Table 4-15. Results show similarity with the parabolic trough performance outputs of this study. The most notable difference is the capacity factor (that is the ratio of average plant electricity output to plant maximum rated electricity output) which the fossil fuel backup influences positively.

Table 4-15: Comparison of Wagner (2012) simulation metrics to those used in this study

Simulation Inputs	**Wagner (2012) parabolic trough simulation**	**This parabolic trough simulation**
Site	Phoenix, Arizona, USA	Upington, Northern Cape, South Africa
Nameplate electrical output (gross) [MW_e]	150	115
Fossil fuel backup	No	Yes
Solar multiple	1.46	2
Hours of thermal storage	1	6
Field aperture area [m^2]	850,302	860,010
Heat transfer fluid	Solar salt	Solar salt
Power cycle cooling method	Air-cooled	Air-cooled
Power cycle efficiency	0.378	0.3774
Boiler operating pressure [bar]	100	100
Simulation Outputs	**Wagner (2012) parabolic trough simulation**	**This parabolic trough simulation**
Annual water usage [m^3]	72,237	82,467
Capacity factor [%]	24.8	40.6
Annual electric output [MWh]	299,700	401,839

4.4.2 Central receiver result validation

A comparison of current and future costs of parabolic trough and central receiver plant technologies was performed in SAM by Turchi *et al.* (2010). While the projected Levelised Cost of Electricity (LCOE) of both technologies was found to be similar, the risks were considered as different for each technology. While the central receiver technology presented risk in terms of limited deployment and experience, parabolic trough technology required a technological breakthrough (via DSG) to achieve higher temperatures, which posed a technical risk. The study concluded that the higher operating temperatures of central receiver technology provided an efficiency advantage over parabolic troughs over the longer term.

The design and performance inputs of the 2015 baseline molten salt tower case presented by Turchi *et al*. (2010, pp.5-6) are compared to the inputs of this study in Table 4-16.

Table 4-16: Comparison of Turchi *et al.* (2010) simulation metrics to those used in this study

Simulation Inputs	Turchi et al. (2010) simulation	This simulation
Site	Daggett, California, USA	Upington, Northern Cape, South Africa
Nameplate electrical output (gross/net) [MW_e]	111/100	115/100
Solar multiple	1.8	1.68
Hours of thermal storage	6	6
Individual heliostat size [m^2]	148	148
Heliostat reflectance	0.95	0.90
Heat transfer fluid	Solar salt	Solar salt
Power cycle cooling method	Air-cooled	Air-cooled
Power cycle efficiency	0.416	0.425
Plant/System availability	91%	96%
Simulation Outputs	**Turchi et al. (2010) simulation**	**This simulation**
Capacity factor [%]	43	46.1
Annual electric output [MWh]	Not published	404,181

The assumptions used by Turchi *et al*. (2010) are similar to those used here except for the power cycle efficiency and plant availability which positively influence the capacity factor output from SAM, despite the lower solar multiple. Turchi *et al*. (2010) did not list the expected annual electric output from their simulations. However, the similarity of the capacity factor suggests that the simulation of the central receiver in this study is comparable to their findings.

A further comparison of this study's central receiver simulation with Wagner's (2012) molten salt central receiver plant simulation is helpful to further evaluate the results (Table 4-17).

Table 4-17: Comparison of Wagner (2012) simulation metrics to those used in this study

Simulation Inputs	Wagner (2012) simulation	This simulation
Site	Phoenix, Arizona, USA	Upington, Northern Cape, South Africa
Nameplate electrical output (gross) [MW_e]	55	115
Fossil fuel backup	No	Yes
Solar multiple	3.36	1.68
Hours of thermal storage	16	6
Field aperture area [m^2]	836,075	860,185
Heat transfer fluid	Solar salt	Solar salt
Power cycle cooling method	Air-cooled	Air-cooled
Power cycle efficiency	0.425	0.425
Boiler operating pressure [bar]	100	100
Simulation Outputs	**Wagner (2012) simulation**	**This simulation**
Annual water usage [m^3]	60,541	70,383
Capacity factor [%]	68.4	46.1
Annual electric output [MWh]	300,000	404,181

Results do not scale linearly due to the differences in nameplate electrical output, fossil fuel backup and hours of thermal storage. However, the interdependence of nameplate electrical output, hours of thermal storage and the resultant capacity factor is evident. That is, a plant

with a smaller power block and more thermal storage will annually produce electricity closer to its maximum nameplate rating than a plant with a larger power block and less thermal storage. Also clear is the direct relationship between annual electric output and annual water usage. The higher annual electric output from this study is attributable to a larger power block (reducing energy dumping during high DNR periods), fossil fuel backup (to cover cloud transients and low sunlight conditions in early morning periods) and a larger field aperture area.

4.4.3 Dish-engine result validation

Abbas *et al*. (2011) carried out an assessment of the technical and economic feasibility of a dish Stirling CSP plant for centralised electricity production in Algeria. They used a 100 MW plant as a reference case to evaluate the economic feasibility of three sites. Solar radiation and other meteorological data for each site were entered into a SAM model which was used to estimate the performance and cost of the 100 MW reference plant. The site with the highest DNI and hence the lowest LCOE was within the Tassili Oua-N-Ahaggar Desert in the province of Tamanrasset. When comparing performance data output from the SAM model with the results of this study, good agreement is demonstrated (Table 4-18).

Reddy *et al*. (2012) performed thermodynamic, annual performance and economic assessments of a 50 MW_e parabolic dish Stirling engine CSP plant in Jodhpur, India. The thermodynamic (exergetic) performance was evaluated using MathWorks MATLAB software. The Stirling engine was separately modelled using Engineering Equation Solver (EES). Finally, the annual performance and cost of the 50 MW_e plant was modelled using SAM. Their annual electric output figures scale linearly with the figures of this study. This suggests that a direct relationship exists between the number of collectors and the annual electric output of a dish-engine plant.

The simulation input parameters and output results of Abbas *et al*. (2011), Reddy *et al*. (2012) and this study are compared in Table 4-18. The input data are similar across the three cases, however the increased annual electric output for the Upington plant reflects the higher DNR levels available in the Northern Cape.

Table 4-18: Comparison of Abbas *et al*. (2011) and Reddy *et al*. (2012) simulations with this study

Simulation Inputs	Abbas *et al*. (2011) simulation	Reddy *et al*. (2012) simulation	This simulation
Site [Town, Province, Country]	Tassili Oua-N-Ahaggar Desert, Tamanrasset, Algeria	Jodhpur, Rajasthan, India	Upington, Northern Cape, South Africa
Site coordinates [Lat., Long.]	22°0.47' N, 5°0.31'E	26°29'N, 73°03'E	28°4'S, 21°3'E
Site elevation [m]	1377	243*	848
Monthly averaged daily DNR [kWh/m²/day]	7.26	5.77**	7.73†
Annual averaged DNR [kWh/m²/annum]	2691	2107.37**	2829.8†
Nameplate/Total capacity [MW_e]	100	50	100
Number of collectors	4000	2000	4000
Number of collectors, North-South	50	50	50
Number of collectors, East-West	80	40	80
Collector separation, North-South [m]	15	21.14	15
Collector separation, East-West [m]	15	21.14	15
Total solar field area [m^2]	900000	893800	900000
Collector/Concentrator/ aperture diameter [m]	10.57	10.57	10.57
Projected collector/concentrator/ glass area [m^2]	87.7	87.67	87.7
Total collector/ concentrator/aperture area [m^2]	91.01	91.01	91.0
Collector/Concentrator Mirror reflectance/ reflectivity	0.91	0.92	0.94
Focal length [m]	7.45	7.45	7.45
Receiver/Absorber aperture diameter [m]	0.2	0.2	0.184
Receiver operating temperature [°C]	720	720	720
Working fluid pressure (max) [MPa]	20	20	20
Stirling Engine Nameplate Capacity [kW_e]	25	25	25
Annual system degradation [%]	1	Not published	1
Simulation Outputs	**Abbas *et al*. (2011) simulation**	**Reddy *et al*. (2012) simulation**	**This simulation**
Annual electric output [MWh]	221,000	95,775.3	227,118

* Data obtained from Google Earth (2012) on the location provided and not directly referred to by Reddy *et al*. (2012).

† CRSES DNR values used in the final model in section 4.3.

** Figures obtained or calculated from NASA SSE data for site coordinates. Reddy *et al*. (2012) did not use these figures in their simulation as they assumed a DNR of 1000 W/m^2.

4.4.4 CLFR result validation

Gharbi *et al*. (2011) compared the annual optical efficiency of the concentrators of parabolic troughs and CLFRs using DNR data for the Hassi Rmel region of Algeria. They found the annual collector efficiency of the parabolic trough to be 55.8% while the CLFR returned a value of 45.8%. They conclude that the optical and thermal efficiency of the CLFR is lower because of the greater influence of the incidence angle and cosine factor on this type of collector when compared to that of the parabolic collector.

Giostri *et al*. (2011) compared the annual performance of commercial Fresnel collectors with parabolic trough collectors using Therminol VP-1 as the HTF. In addition they investigated a DSG case for the Fresnel collectors. Thermoflex software was used with the following design parameters to facilitate the comparison:

i. DNI of 900 W/m^2,
ii. Incidence angle equal to zero,
iii. Solar multiple equal to one,
iv. No thermal storage,
v. Net power output of 50 MW,
vi. Evaporative cooling.

The model was set up with an optical efficiency of 67% for the Fresnel collector based on manufacturer data from Novatec Biosol (2011). An optical efficiency of 75% was used for the parabolic trough collector based on Eurotrough ET100 information from Geyer *et al.* (2002). Using these parameters they found that at design conditions the optical, thermal and piping efficiencies of the parabolic trough collectors exceed those of the linear Fresnel collectors. The parasitic losses of the CLFR plant were lower than those of the parabolic trough plant. The overall efficiency of the parabolic trough plant was higher than that of the CLFR plant, resulting in the parabolic trough plant generating 3% more gross electrical power than the CLFR plant. The net power output per square meter of the CLFR plant was found to be higher than that of the parabolic trough plant, which agrees with the results obtained in this study.

Giostri *et al*. (2011) also performed an annual simulation for the location of Las Vegas, Nevada, USA in Thermoflex, with the input and output parameters shown in Table 4-19.

Table 4-19: Comparison of Giostri *et al*. (2011) simulations in Thermoflex to those of this simulation in SAM

Simulation Inputs	**Giostri *et al*. (2011) parabolic trough simulation**	**This parabolic trough simulation**	**Giostri *et al*. (2011) CLFR simulation**	**This CLFR simulation**
Simulation Software	Thermoflex	System Advisor Model	Thermoflex	System Advisor Model
Site [Town, Province, Country]	Las Vegas, Nevada, USA	Upington, Northern Cape, South Africa	Las Vegas, Nevada, USA	Upington, Northern Cape, South Africa
Site coordinates [Lat., Long.]	36°10'30"N, 115°08'11" W	28°4'S, 21°3'E	36°10'30"N, 115°08'11" W	28°4'S, 21°3'E
Average Temperature [°C]	19.8	21.5	19.8	21.5
Annual averaged DNR [kWh/m²/annum]	2592	2829.8†	2592	2829.8†
Nameplate/Total capacity [MW_e]	50	100	50	100
Power cycle cooling method	Evaporative	Air-cooled	Evaporative	Air-cooled
Solar multiple	1	2	1	1.79
Hours of thermal storage	0	6	0	0
Aperture area [m²]	235,899	860,010	268,596	862,848
Total land area [km²]	0.684	3.141	0.595	1.381
Simulation Outputs	**Giostri *et al*. (2011) parabolic trough simulation**	**This parabolic trough simulation**	**Giostri *et al*. (2011) CLFR simulation**	**This CLFR simulation**
Annual electric output [MWh]	97,818	401,839	74,454	393,984

† CRSES DNR values used in the final model in section 4.3.

Based on their results, Giostri *et al*. (2011) note that while the linear Fresnel collector is capable of collecting more solar energy than an equivalent parabolic trough collector, it fails to reflect that energy efficiently to the receiver. Therefore, particularly at high insolation incidence angles the CLFR plant is unable to match the parabolic trough plant's optical efficiency. This, in combination with the higher transverse angle losses of CLFR plants in winter, results in the lower annual electric output. These effects are modelled by SAM (Figure 4-16), however the fossil fuel backup of the modelled CLFR plant guarantees nominal power block output throughout most of the day, removing some of the advantage of the parabolic trough's higher optical efficiency.

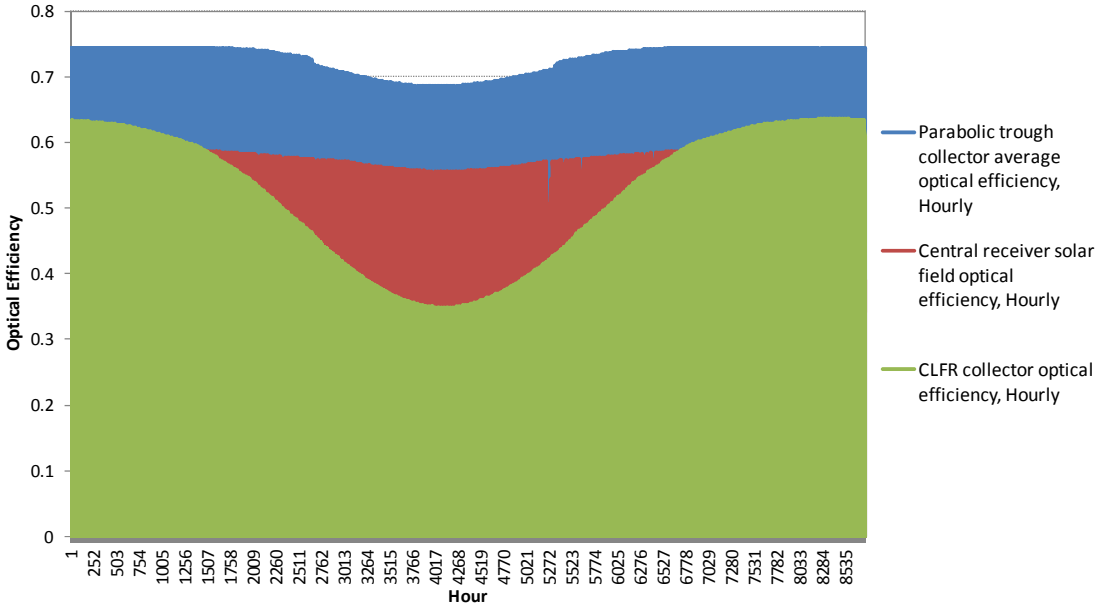

Figure 4-16: Average hourly optical efficiency of parabolic trough, central receiver and CLFR

Morin *et al*. (2012) performed a comparison of parabolic trough and CLFR power plants using ECOSTAR (developed by the DLR) and ColSim (Fraunhofer ISE in-house software). Meteorological input data for Daggett, California, USA were used for their annual performance simulations. Their approach was to optimize the aperture area of both technologies in order to match the LCOE. An average was taken from the ECOSTAR and ColSim results of Morin *et al*. (2012) and compared to this study in Table 4-20.

Table 4-20: Comparison of Morin *et al*. (2012) simulations in ECOSTAR and ColSim to this study

Simulation Inputs	**Morin *et al*. (2012) parabolic trough simulation**	**This parabolic trough simulation**	**Morin *et al*. (2012) CLFR simulation**	**This CLFR simulation**
Simulation Software	ECOSTAR and ColSim	System Advisor Model	ECOSTAR and ColSim	System Advisor Model
Site [Town, Province, Country]	Daggett, California, USA	Upington, Northern Cape, South Africa	Daggett, California, USA	Upington, Northern Cape, South Africa
Site coordinates [Lat., Long.]	34°51'N, 116°49'W	28°4'S, 21°3'E	34°51'N, 116°49'W	28°4'S, 21°3'E
Average Temperature [°C]	19.8	21.5	19.8	21.5
Annual averaged DNR [kWh/m²/annum]	2791	2829.8†	2791	2829.8†
Nameplate/Total capacity [MW_e]	50	100	50	100
Power cycle cooling method	Evaporative	Air-cooled	Evaporative	Air-cooled
Hours of thermal storage	0	6	0	0
Aperture area [m²]	269,000	860,010	371,000	862,848
Total land area [km²]	0.941	3.141	0.742	1.381
Simulation Outputs	**Morin *et al*. (2012) parabolic trough simulation**	**This parabolic trough simulation**	**Morin *et al*. (2012) CLFR simulation**	**This CLFR simulation**
Annual electric output [MWh]	110,500	401,839	93,500	393,984

† CRSES DNR values used in the final model in section 4.3.

Morin *et al*. (2012) noted that during periods of high insolation around solar noon the CLFR was forced to discard considerable excess energy due to its larger aperture area per receiver. They also observed that the optical losses inherent to the design of the CLFR reduce the amount of thermal energy delivered to the power block during early morning and late afternoon periods (high insolation incidence angles). This resulted in reduced operating time for the plant, which in turn led to the lower annual electric output of the CLFR plant in comparison to the parabolic trough plant.

In this study an identical fossil fill fraction was used across the parabolic trough, central receiver and CLFR models. This was required to match the power dispatch schedules. However, since the CLFR model does not have a TES system, it does not need to use a portion of the fossil fill fraction to charge TES system tanks. Therefore it used the complete fossil fill fraction to ensure nameplate electrical output is maintained throughout the day. Thus the backup fossil fuel boiler compensated for some of the optical losses which resulted in reduced operating time and electric output in the models of Morin *et al*. (2012). Setting the fossil fill fractions to zero across the board results in the CLFR and parabolic trough net annual electric output agreeing more closely with the result of Morin *et al*. (2012).

In sections 4.4.1 and 4.4.2 comparisons were carried out between the parabolic trough and central receiver CSP plants simulated in this study and those simulated by Wagner (2012) in SAM. Wagner (2012) describes the SAM model of the CLFR plant in more detail, noting the non-normal orientation of the primary reflectors towards incoming beam radiation as the primary optical loss of the CLFR. He also mentions the significant seasonal variation of optical performance of the CLFR. As mentioned in section 4.4.2 his modelling approach is different to the one adopted here. However, insight can be gained from the comparative results of his work despite this difference in approach. The results of his parabolic trough and CLFR models are compared to the results of this study in Table 4-21.

Table 4-21: Comparison of Wagner (2012) simulation metrics to those used in this study

Simulation Inputs	Wagner (2012) parabolic trough simulation	This parabolic trough simulation	Wagner (2012) CLFR simulation	This CLFR simulation
Site	Phoenix, Arizona, USA	Upington, Northern Cape, South Africa	Phoenix, Arizona, USA	Upington, Northern Cape, South Africa
Nameplate electrical output (gross) [MW_e]	150	115	158	107
Fossil fuel backup	No	Yes	No	Yes
Solar multiple	1.46	2	1.7	1.79
Hours of thermal storage	1	6	0	0
Field aperture area [m^2]	850,302	860,010	1,208,000	862,848
Heat transfer fluid	Solar salt	Solar salt	Water/steam	Water/steam
Power cycle cooling method	Air-cooled	Air-cooled	Air-cooled	Air-cooled
Power cycle efficiency	0.378	0.3774	0.38	0.38
Boiler operating pressure [bar]	100	100	110	110
Simulation Outputs	**Wagner (2012) parabolic trough simulation**	**This parabolic trough simulation**	**Wagner (2012) CLFR simulation**	**This CLFR simulation**
Annual water usage [m^3]	72,237	82,467	31,560	77,452
Capacity factor [%]	24.8	45.9	23.0	44.7
Annual electric output [MWh]	299,700	401,839	299,700	393,984

The results of Wagner's (2012) SAM simulation reflect the optical limitations of CLFR technology in comparison to parabolic trough technology. This is expressed by the much larger solar field aperture area required to obtain the same annual electric output. This study also reflects the higher aperture area required from a CLFR plant to obtain a similar nameplate electrical output to a parabolic trough.

Wagner's (2012) results also reflect the seasonal variation of CLFR optical performance via the lower capacity factor in comparison with the parabolic trough. Due to this study using fossil fuel backup, this seasonal variation was compensated for. With fossil fuel backup the parabolic trough plant capacity factor is 2.7% higher than the CLFR plant. Removing the fossil fuel backup, the CLFR plant capacity factor becomes 32.6% lower than the parabolic trough plant. This is similar to Wagner's (2012) result.

The CLFR plant model deploys its fossil fuel backup in such a manner that it compensates for some of its optical inefficiencies. Despite this, its resultant net annual electric output is still lower than the central receiver and parabolic trough plant models. Removing the fossil fuel backup results in the CLFR plant model producing 32.6% less net annual electric output than the parabolic trough plant model. These results agree on average with the work of Giostri *et al*. (2011) and Morin *et al*. (2012) as shown in Table 4-22.

Table 4-22: Estimation of annual electric output deviation

Simulation Output	**Giostri *et al.* (2011) parabolic trough simulation**	**Giostri *et al.* (2011) CLFR simulation**	**Percentage difference in parabolic trough and CLFR result**
Annual electric output [MWh]	97,818	74,454	31.4%
Simulation Output	**Morin *et al.* (2012) parabolic trough simulation**	**Morin *et al.* (2012) CLFR simulation**	
Annual electric output [MWh]	110,500	93,500	18.2%
Average difference between parabolic trough and CLFR annual electric output			**24.8%**
Simulation Output	**This parabolic trough simulation with fossil fuel backup**	**This CLFR simulation with fossil fuel backup**	**Percentage difference in parabolic trough and CLFR result**
Annual electric output [MWh]	401,839	393,984	2%
Simulation Output	**This parabolic trough simulation without fossil fuel backup**	**This CLFR simulation without fossil fuel backup**	**Percentage difference in parabolic trough and CLFR result**
Annual electric output [MWh]	356,654	242,570	47%
Average difference between parabolic trough and CLFR annual electric output			**24.5%**

5. DISCUSSION OF RESULTS

Two findings emerge from this study. Firstly the solar resource at Upington is exceptionally good compared with other CSP locations around the world, and the assessment conducted here shows good agreement with a recent assessment done by Suri *et al*. (2011). Secondly, given the solar resource at Upington, central receiver technology provides superior performance to parabolic trough, linear Fresnel, and dish-engine technology. The central receiver model produced between 2.6% and 44% higher annual electric output than the other models evaluated, and best matched the national load profile.

5.1 Solar resource assessment result

A simple average of the results obtained of the six meteorological datasets examined produced a monthly averaged daily DNR of 7.72 kWh/m²/day and an annual averaged DNR of 2814.1 kWh/m²/annum. This result showed good agreement with the results of Suri *et al*. (2011) of 7.72 kWh/m²/day and 2816 kWh/m²/annum. However, a grading was assigned to each dataset and the weighted average of the datasets examined produce a result of 7.98 kWh/m²/day and 2905.5 kWh/m²/annum. This is 3% higher than the result of Suri *et al*. (2011) and suggests that satellite-derived DNR data for Upington may underestimate the available resource.

Analysis of each dataset revealed that while ground measured DNR data were higher than satellite-derived data, missing readings from equipment resulted in large periods being omitted from the aggregation process. This raises the issue of quality ground measurement availability for Upington. More accurate ground measurements will result in more accurate solar system modelling.

The SAWS and Eskom ground measurement data problems were dealt with on a case by case basis resulting in the corrected data showing agreement with the other datasets examined. Using the more conservative simple average result it is found that the solar resource at Upington is 3% higher than the Daggett parabolic trough plant sites in California and 37% higher than the Plataforma Solar de Almería solar testing facility site. Using the weighted average, the DNR available at Upington is 6% higher than Daggett and 41% higher than Plataforma Solar de Almería.

These results indicate that the DNR at Upington is suitable for concentrating solar thermal technology projects to be implemented.

5.2 Modelling results

A key function of SAM is providing a uniform technology comparison framework. Comparisons of CSP technologies in SAM can be found in the literature, for example Turchi *et al*. (2010) and Wagner (2012). The analysis here differs somewhat from other work in the technologies compared, and modelling approach. The design parameters that were fixed for all the technologies are listed in Table 5-1.

Table 5-1: Fixed design parameters for this study

Parameter	Units	Value
Plant location	-	Upington, Northern Cape
Climate input file	-	CRSES
Nameplate electrical output	MW_e	100
Hours of thermal storage	hours	6*†
Plant availability	%	96
Power cycle cooling method	-	Air-cooled
Annual system degradation	%	1
Power dispatch schedule	-	matched
Fossil fuel backup	-	Yes†

* Parameter not relevant for dish-engine model

† Parameter not relevant for CLFR model

In addition to these parameters being held constant, the following parameters were matched as closely as possible:

i. Solar field aperture area,
ii. Solar multiple,
iii. Number of washes mirrors in the solar field received per annum.

Using these parameters, a comparison of the direct and derived simulation outputs in Table 4-3 was performed in chapter 4. These outputs, in combination with an assessment of how well each technology matches the national load profile, allow performance comparisons between the four technologies.

The following net annual electric output was predicted for each of the four technologies, using matched input parameters and the same climate input file: parabolic trough plant: 401,839 MWh, central receiver plant: 404,181 MWh, dish-engine plant: 227,118 MWh and CLFR plant: 393,984 MWh.

In a validation exercise it was found that the parabolic trough, central receiver, dish-engine and CLFR model outputs displayed agreement with results of similar research conducted elsewhere.

The parabolic trough model net annual electric output and water usage of 401,839 MWh and 82,467 m³ respectively compared reasonably with figures of 299,700 MWh and 72,237 m³ given by Wagner (2012). Despite a 30% smaller power block, this study's model produces 34.1% more annual electric output than the model of Wagner (2012). This can be attributed to the presence of fossil fuel backup, five more hours of thermal storage and a 0.8% larger field aperture area. The 34.1% higher annual output imposes a 14.2% higher annual water usage figure. This is a result of backup boiler water usage, longer power block operation due to larger thermal storage capacity and an additional 9,708 m^2 of mirror area requiring washing. The similarity of these results to the work of Wagner (2012), and the manner in which it linearly scales with the work of García *et al*. (2011), engenders confidence in the parabolic trough model evaluated here.

The central receiver model net annual electric output and water usage of 404,181 MWh and 70,383 m³ respectively are not easily comparable with the models of Turchi *et al*. (2010) and Wagner (2012). The central receiver model of Turchi *et al*. (2010) has very similar design metrics to the model in this study although the annual electric output is not published. Turchi *et al*. (2010) published a capacity factor of 43%, and this figure compares favourably with the result of 46.1% obtained here. The higher result is obtained from 2% higher power cycle efficiency and 5% higher plant availability model inputs. Comparisons with Wagner's (2012) results are more difficult. Wagner obtains net electric output of 300,000 MWh and water usage of 60,541 m³ annually using a power block that is 48% the size of the power block selected here, ten hours more thermal storage and a 3% smaller aperture area. This study's 35% higher annual electric output is attributable to a 109% larger power block (reducing energy dumping during high DNR periods), fossil fuel backup (to cover cloud transients and low sunlight conditions in early morning periods) and a 3% larger field aperture area. This higher annual output comes at the expense of a 16% higher annual water usage figure. Losses associated with running and cooling a larger steam turbine, backup boiler water usage and an additional 24,110 m^2 of mirror area contribute to this higher water usage figure.

While the central receiver results differ from Wagner's (2012), the design parameters readily account for those differences. A comparison to the capacity figure of Turchi *et al*. (2010) also suggests that the difference can be accounted for by simulation inputs. Hence the central receiver model result can be considered within range of the SAM simulation results obtained by Wagner (2012) and Turchi *et al*. (2010).

The dish-engine model net annual electric output of 227,118 MWh show good agreement with the Abbas *et al*. (2011) figures of 221,000 MWh. Abbas *et al*. (2011) used similar design

metrics to this study. The 3% higher annual output obtained in this study is attributable to 5.8% higher DNR in Upington and 3% higher collector reflectivity specified for this study. Reddy *et al.* (2012) obtained an annual electric output of 95,775 MWh from a 50% smaller dish-engine array. Reddy *et al.* (2012) are not clear on the meteorological data used in their SAM model. If Reddy *et al.* (2012) used Jodhpur annual DNR data then this result is in line with expectation as Jodhpur has 34% less DNR than Upington. Doubling the capacity of this dish-engine array results in 19% lower annual electric output than this study. This is in line with the annual electric output-DNR relationship observed between the results of Abbas *et al.* (2011) and this study.

The good agreement of this result with the work of Abbas *et al.* (2011) and the linearly proportional relationship of these results to those of Reddy *et al.* (2012), engender confidence in the dish-engine array model used here.

To avoid bias in the comparison, the same power dispatch schedule (section 4.2.1.2) was used for the parabolic trough, central receiver and CLFR models in SAM. The dish-Stirling model does not have a central power block so it cannot utilise fossil fuel backup or TES. Hence the power dispatch schedule could not be applied to the dish-Stirling model. The CLFR model does not have a TES system as the solar field generates steam directly. Wagner (2012) has recognized this shortcoming and has opted to pursue development of a CLFR model using a conventional HTF in the solar field. This model may be available in the next release of SAM. Currently the CLFR model uses its entire fossil fuel fill fraction to keep its steam turbine running at nameplate capacity. This compensates for the optical inefficiencies of the solar field during mornings and evenings, particularly in winter (see Figure 4-15). It also conceals the effects lower solar field optical efficiency has on turbine operation. Low solar field optical efficiency results in part-load operation of the turbine. This lowers turbine efficiency and results in a lower annual electric output. The parabolic trough and central receiver models use a portion of the fossil fill fraction to charge their TES tanks, which results in more part-load turbine operation than the CLFR model for the same input DNI. Therefore the parabolic trough and central receiver models are not able to commit as much of their fossil fill fraction to maintaining nominal power block operation as the CLFR model does. This diminishes some of the advantage of the parabolic trough and central receiver's higher optical efficiency. Removing fossil fuel backup from all three models resulted in the net annual output of the CLFR model becoming significantly lower than that of the parabolic trough and central receiver. The CLFR model output decreased from being 2% lower than the parabolic trough model to being 32.6% lower. Good agreement is shown between the average of these results and the work of Giostri *et al.* (2011) and Morin *et al.* (2012).

Comparing the results of each model, it is noted that the central receiver model provides the highest annual electric output. It produces 0.6% more than the parabolic trough (Figure 5-1) while using 14.7% less water annually (Figure 5-2). This result is in agreement with the analysis of Turchi *et al*. (2010) and Wagner (2012). The central receiver model also best met the evening and winter peak load requirements of the national load profile.

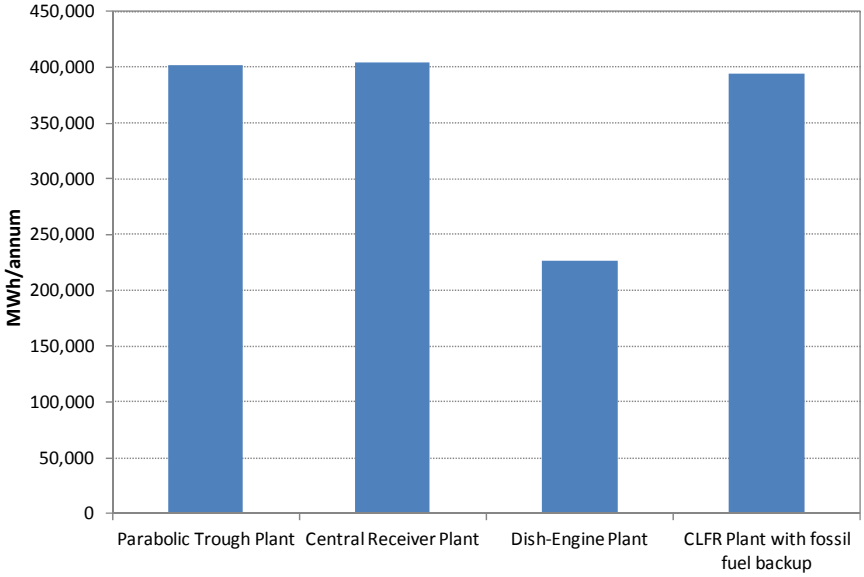

Figure 5-1: Inter-technology net annual electric output (MWh) comparison

The CLFR model produces 2% less annual electric output than the parabolic trough plant and 2.6% less than the central receiver when all have fossil fuel backup. Removing the fossil fuel backup from the CLFR, parabolic trough and central receiver models resulted in the CLFR net annual output being 32.6% lower than the parabolic trough and 48.6% lower than the central receiver model (Figure 5-2).

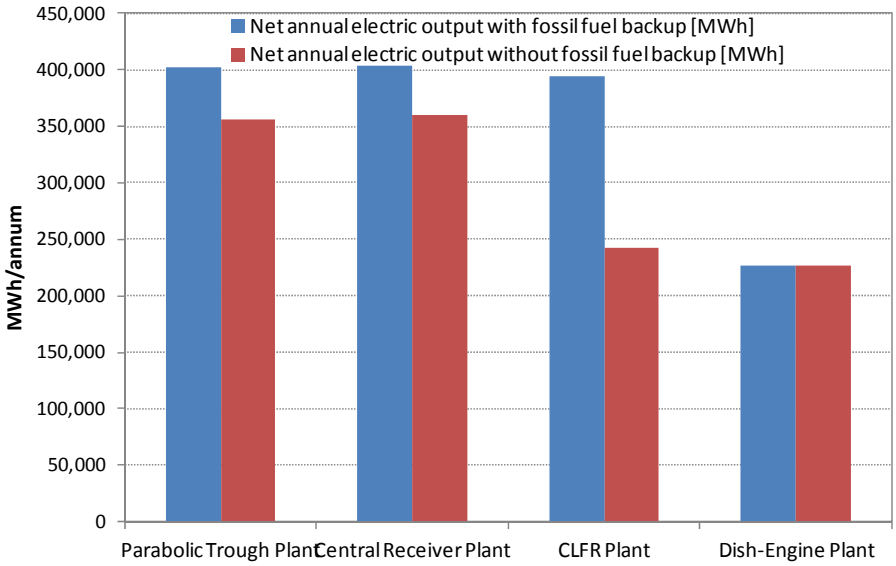

Figure 5-2: Comparison of contribution of fossil fuel backup to net annual electric output

The dish-engine model furnishes the highest overall efficiency of 23.9%. The CLFR overall efficiency is 32% lower than the parabolic trough and 33% lower than the central receiver model (Figure 5-3).

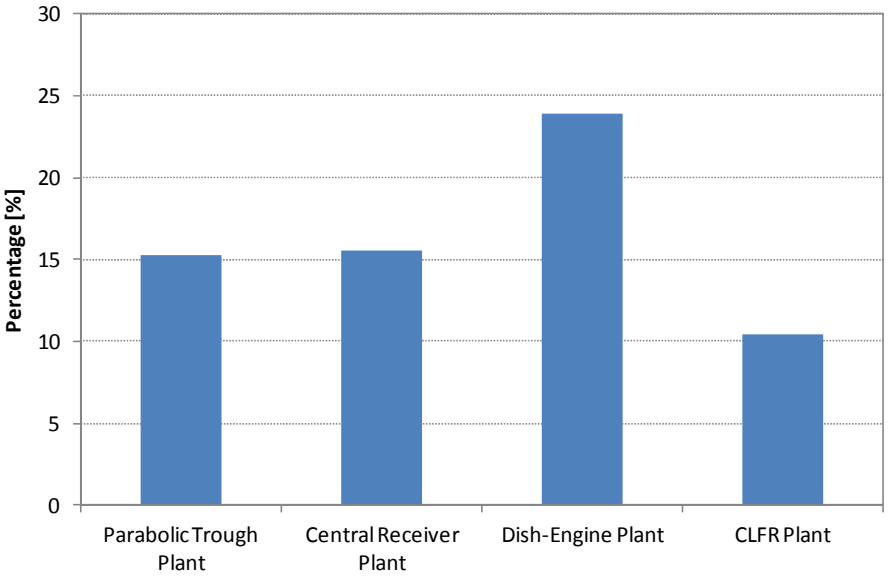

Figure 5-3: Comparison of overall power plant efficiency (%)

The dish-engine model produced 44% less electricity annually than the central receiver model (Figure 5-1) but it also used 77% less water excluding radiator cooling fluid water (Figure 5-4). Its annual electric output and water usage were 36% and 80% less than the parabolic trough model outputs respectively.

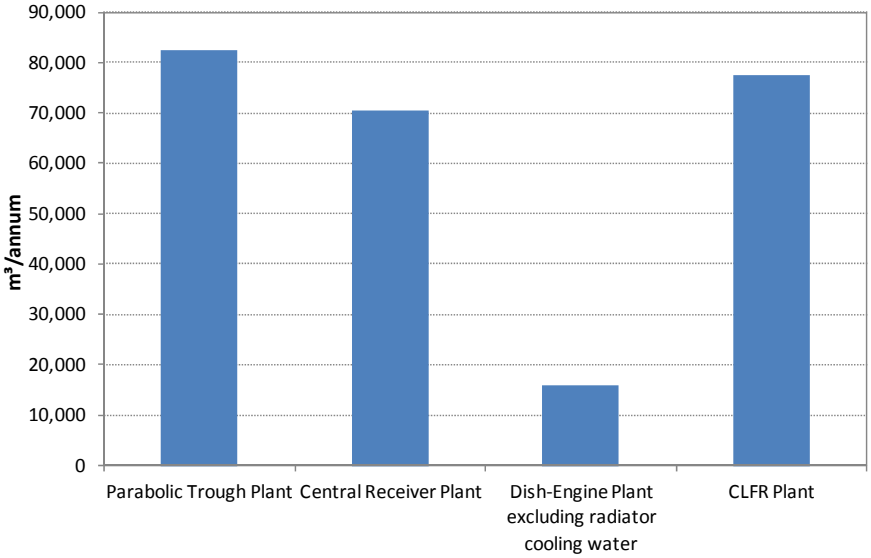

Figure 5-4: Inter-technology total annual water usage (m^3) comparison

Figure 5-5 shows the ratio of energy generated per cubic metre of water consumed for each power plant modelled. The dish-engine plant uses the least amount of water to produce energy while the central receiver is the second most efficient. Adding radiator cooling water usage to the water consumption of the dish-engine plant will reduce this ratio.

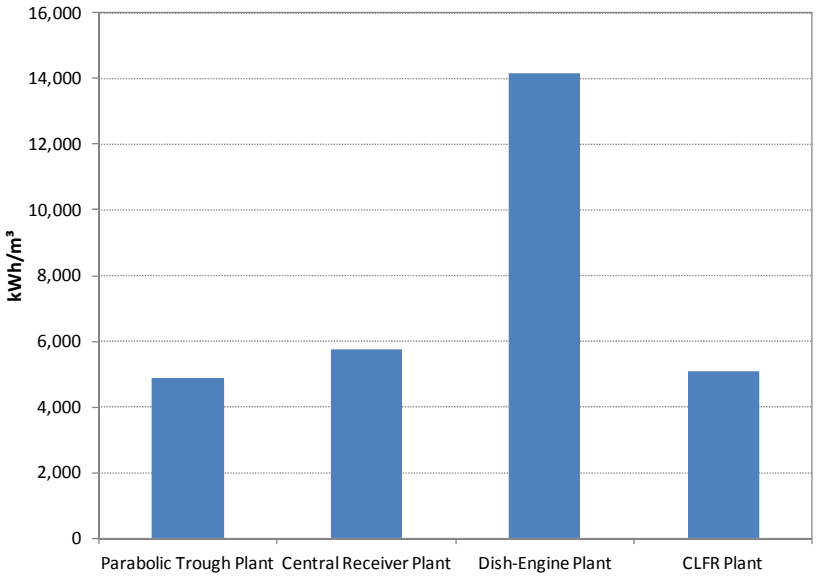

Figure 5-5: Inter-technology comparison of energy produced per cubic metre of water used in kWh/m^3

Considering the potential for local manufacture of major plant components, it appears that CLFR technology presents the highest potential for substantial local manufacture of its components (Table 5-2). Its flat primary reflectors, static, non-vacuum receiver and standard steam cycle power block pose low technical risk to local manufacturers. van Niekerk (2009) asserts that linear Fresnel components can be easily manufactured locally. Parabolic trough technology appears hampered in this regard with its curved glass collectors, vacuum receivers and flexible piping required to transport high temperature HTF. The Southern Africa Solar Thermal and Electricity Association (SASTELA) (2012) notes that local manufacture of curved collectors will only be feasible when local parabolic trough plant installations reach 500 MW. Similarly, local manufacture of parabolic trough receiver tubes becomes feasible with local trough installations reaching 200 MW (van Niekerk, 2009). Due to the modular design of dish-engine plants, developers may find benefit in sourcing complete dish-engines and only sourcing materials for the plant infrastructure locally. Central receivers present potential because flat heliostats can be manufactured locally. The heliostat field is the largest contributor to the capital cost of the plant, up to as much as 60% of the total cost according to van Niekerk (2009). Hence local content can make up the majority of the capital expenditure on such a project. The receiver and its associated piping are required to sustain very high

temperatures with steep gradients. This may present a barrier to local manufacture, however, thermal coal power plant suppliers may be able to provide for this.

Regarding modularity and scalability of each plant to generate more than 100 MW_e, the dish-engine plant appears most suitable. Provided there is enough land available, the number of dish-engines in the field can be doubled. The land area would require terracing and an electrical infrastructure upgrade (cabling and substation expansion). For parabolic troughs, adding to the solar field involves interconnection of the piping and more powerful or additional HTF pumps. This increases the parasitic load of the plant. To increase the output the steam turbine has to either be replaced by a larger unit or a second unit has to be installed. For CLFRs adding another circuit has similar effects as mentioned for parabolic troughs unless an entirely parallel circuit is installed. To upgrade the capacity of a central receiver plant the receiver, turbine and associated piping must be upgraded. This requires significant downtime of the plant. However, eSolar (2009) build modular and scalable central receiver plants with multiple tower-receivers. This concept allows for easier expansion of a central receiver plant.

The effect of plant degradation on the net annual energy of each plant modelled was discussed in section 4.3. Part of this discussion is the ease with which the components of each technology can be replaced. The solar field is permanently exposed to the elements. Direct sun, wind, storms, and dramatic temperature differences at different times of day result in the weathering or damage of components. While each technology has a stow position for its collectors to avoid damage to the reflective surfaces, breakages do occur.

Replacing the primary reflectors of a CLFR plant appears most convenient as the mirrors are flat and close to the ground. Replacing the receiver will require a crane and rigging or a boom-lift. Replacing the mirror surface on a parabolic trough is more challenging because of the shape of the glass and the height of the collector from the ground. Its receiver will also require a crane and rigging or a boom-lift to access. Large dish-engines tend to require boom-lifts to replace mirrors at the top of the collector dish. The receiver and Stirling engine can be accessed with a ladder if the dish-engine is moved into an adequate maintenance position. Heliostats in a central receiver solar field can vary in size. The large heliostats modelled in this study will require a ladder or boom-lift to access the highest points, but with flat surfaces it should be easy to replace a mirror facet. The central receiver tower should be designed to allow for maintenance platforms at the required heights. Routine maintenance is not problematic if the design allows for this, however replacement of larger components on the receiver would require a crane and rigging.

Table 5-2: Potential for local manufacture of major CSP components

Major component	Parabolic trough	Central receiver	Dish-engine	CLFR
Collector	Curvature of mirror a potential challenge for local manufacture	Flat heliostats and support structure can be manufactured locally	Curvature of dish may be a challenge unless a multi-faceted collector is used	Flat primary reflectors and support structure can be manufactured locally
Receiver	Precision manufacturing to ensure vacuum in annulus may be a challenge	Precision design required for high temperatures and steep temperature gradients may be a challenge	Precision design required for high temperatures and steep temperature gradients may be a challenge	No vacuum required and insulation can be procured locally
Tracking system	Single axis tracking systems can be locally designed and manufactured	Dual axis tracking is more complicated but still not a challenge for local design and manufacture	Dual axis tracking is more complicated but still not a challenge for local design and manufacture	Single axis tracking systems can be locally designed and manufactured
Solar field piping	Flexible portions of piping may be troublesome to fabricate locally but most standard piping can be procured locally	Precision receiver piping may be troublesome as leaks in this system have to be avoided	No solar field piping unless a central cooling tower is used. Electrical cabling can be procured locally	Flexible portions not required as receiver is static. Standard piping can be procured locally
Thermal Energy Storage	Construction of tanks, piping and pumps should not be problematic. Ensuring tight quality control to avoid leaks may be a challenge	Construction of tanks, piping and pumps should not be problematic. Ensuring tight quality control to avoid leaks may be a challenge	Not applicable	Not applicable
Power block	Construction of complete power block including dry-air coolers is not new to local industry, however turbines and many ancillaries may be foreign sourced	Construction of complete power block including dry-air coolers is not new to local industry, however turbines and many ancillaries may be foreign sourced	Stirling engines will most likely be foreign sourced	Construction of complete power block including dry-air coolers is not new to local industry, however turbines and many ancillaries may be foreign sourced

On balance, the central receiver technology is the leading candidate because it generates more electricity annually than the other technologies in a fashion that best meets the national load profile. That is it most efficiently converts the solar resource at Upington to usable electricity during periods of peak demand. Its heliostat field, the most expensive component of the plant, can be manufactured locally. Retrofitting damaged heliostat field mirrors is easier than trough or dish-engine mirrors. Thus from a technical performance perspective a central receiver CSP plant is most suitable as a bulk electricity generator in the Upington area.

6. CONCLUSION AND RECOMMENDATIONS

South Africa relies nearly exclusively on coal to meet its electricity demand. The REFIT provides a platform for CSP technologies to be introduced into the nation's bulk power generation scheme and it is certain that concentrating solar thermal and PV technology will contribute to South Africa's future generating capacity. Solar thermal technology has a unique advantage in being able to store energy in heat form and dispatch it as required. This allows CSP technology to cater for South Africa's dominant evening load peak.

The objective of this study was to assess which CSP technology, from a technical performance perspective, is most suitable for bulk power generation given the solar resource available in Upington. To answer part of this question, an investigation of the solar resource available at Upington was performed. The investigation suggests that Upington's monthly averaged daily DNR is between 7.72 kWh/m²/day and 7.98 kWh/m²/day. This compares favourably with DNR levels at current CSP sites like Daggett in California (7.5 kWh/m²/day) and Plataforma Solar de Almería (5.68 kWh/m²/day) in Spain. Upington is therefore a suitable location for concentrating solar thermal technology projects to be implemented.

To answer the balance of the question, four competing CSP technologies were investigated: the parabolic trough, CLFR, central receiver and dish-engine. Each technology was simulated using System Advisor Model and the central receiver model produced the highest annual electric output (404,181 MWh), while best matching the national load profile. It compared well with the parabolic trough, CLFR and dish-engine model results of 401,839 MWh, 393,984 MWh and 227,118 MWh respectively. The central receiver's higher operating temperatures make it more suitable for a Brayton cycle, and with shale gas exploration occurring in the Northern Cape, it could be hybridised to provide base load power generation capability. If shale gas reserves in the area are not exploited, the central receiver provides even higher output without fossil fuel co-firing in comparison to the parabolic trough and CLFR technologies. The central receiver's overall efficiency is only exceeded by the dish-engine model. The possibility of manufacturing heliostats locally can boost the local content of such an installation up to 60% of the overall cost. The slope of a central receiver plant site can exceed what is allowable for a comparable parabolic trough and CLFR plant. Ease of maintenance of a central receiver heliostat field is only surpassed by that of a CLFR installation.

From a purely technical perspective, the results of this study support the argument for implementing the central receiver at Upington and confirm Eskom's decision to do so. It is

recognised that an economic comparison of these technologies may not result in the same conclusion. While financial considerations may ultimately decide the selection of a technology, a clear understanding of the technical performance of the various options is vital to the process. Such metrics are given in chapters 4 and 5.

This work provides a platform for more detailed analysis of each CSP technology. An investigation solely focused on modelling central receiver technology in Upington could yield useful results based on the preliminary work performed here. This study also provides a basis for feasibility-level studies for concentrating solar thermal power plants in the Upington area of the Northern Cape.

REFERENCES

Abbas, M., Boumeddane, B., Said, N., Chikouche, A., 2011. Dish Stirling technology: A 100 MW solar power plant using hydrogen for Algeria. *International Journal of Hydrogen Energy*, 36 (2011), pp.4305-4314.

Abengoa Solar, 2010. *Solutions to Global Climate Change: Photovoltaic Technology Plants.* [pdf] Seville: Abengoa Solar. Available at: <http://www.abengoasolar.com/corp/export/sites/solar/resources/pdf/en/Sevilla_PV.pdf> [Accessed 13 March 2010].

Abengoa Solar, 2012. *NERSA !KaXu Solar One license application – public hearing: Postmasburg, 6 March 2012.* [pdf] Centurion: Abengoa Solar. Available at: <http://www.nersa.org.za/Admin/Document/Editor/file/Consultations/Electricity/Presentations/Ka%20Xu%20Solar%20One%20(Pty)%20Limited.pdf> [Accessed 26 September 2012].

Andraka, C.E., Powell, M.P., 2008. Dish Stirling Development for Utility-Scale Commercialization. *14th Biennial CSP SolarPACES Symposium*. Las Vegas, NV USA. 4-7 March 2008. Almería: Solar Power and Chemical Energy Systems.

Areva-Solar, 2012. *Our Technology and Features.* [online] Available at: <http://www.areva.com/EN/solar-198/arevasolarour-technology.html#tab=tab5> [Accessed 15 January 2012].

Bansal, R.C., 2000. Subsection 11.2 Renewable Energy Technologies in Section 11 Alternate Sources of Power. In: D.G. Fink and H.W. Beaty, eds. 2000. *Standard Handbook for Electrical Engineers*. 14th ed. New York: McGraw-Hill, pp.11-5–11-6.

Bekker, B., 2007. Irradiation and PV array energy output, cost, and optimal positioning estimation for South Africa. *Journal of Energy in Southern Africa,* 18 (2), pp.16-25.

Bernhard, R., Hein, S., de Lalaing, J., Eck, M., Eickhoff, M., Pfänder, M., Morin, G., Häberle, A., 2008. Linear Fresnel Collector Demonstration on the PSA Part II – Commissioning and First Performance Tests. *14th Biennial CSP SolarPACES Symposium*. Las Vegas, NV USA. 4-7 March 2008. Almería: Solar Power and Chemical Energy Systems.

Bernhard, R., de Lalaing, J., Kistner, R., Eck, M., Eickhoff, M., Feldhoff, J.F., Heimsath, A., Hülsey, H., Morin, G., 2009. Linear Fresnel Collector Demonstration at the PSA – Operation and Investigation. *SolarPACES 2009: Electricity, fuels and clean water powered by the sun*. Berlin, Germany. 15-18 September 2009. Almería: Solar Power and Chemical Energy Systems.

Bevacqua, B., Prakash, R., Gamble, C., 2008. Extending Organic Heat Transfer Fluid Life in Aging Solar Energy Generation Systems. *14th Biennial CSP SolarPACES Symposium*. Las Vegas, NV USA. 4-7 March 2008. Almería: Solar Power and Chemical Energy Systems.

Bradshaw, R.W., Siegel, N.P., 2008. Molten Nitrate Salt Development for Thermal Energy Storage in Parabolic Trough Solar Power Systems. *Proceedings of Energy Sustainability 2008.* Jacksonville, Florida USA. 10-14 August 2008. New York: American Society of Mechanical Engineers.

Brignoli, V., Bombelli, D., 2009. An easy Software to Estimate the Production of the Eurodish Solar Generator in Italy. *SolarPACES 2009: Electricity, fuels and clean water powered by the sun*. Berlin, Germany. 15-18 September 2009. Almería: Solar Power and Chemical Energy Systems.

Buck, R., Heller, P., Koch, H., 1996. Receiver Development for a Dish-Brayton System. *Proceedings of the 1996 International Solar Energy Conference*. San Antonio, TX USA 31 March to 3 April 1996. New York: American Society of Mechanical Engineers.

Burgaleta, J.I., Arias, S., Salbidegoitia, I.B., 2009. Operative Advantages of a Central Tower Solar Plant with Thermal Storage System. *SolarPACES 2009: Electricity, fuels and clean water powered by the sun*. Berlin, Germany. 15-18 September 2009. Almería: Solar Power and Chemical Energy Systems.

Bürkle, D., Müller-Steinhagen, H., 2009. *Andasol 1: The largest solar power station officially inaugurated.* [online] Available at: <http://www.dlr.de/en/DesktopDefault.aspx/tabid-13/135_read-17179/> [Accessed 31 July 2009].

Cameron, C.P., Boyson, W.E., Riley D.M., 2008. Comparison of PV System Performance-Model Predictions with Measured PV System Performance. *33rd IEEE PVSC*. San Diego, CA USA. 11-16 May 2008. New York: Institute of Electrical and Electronics Engineers.

Cameron, C., Cornelius, C., 2007. *A Systems-Driven Approach to Solar Energy R&D*. Sandia Paper 2007-3296C. Albuquerque (NM): Sandia National Laboratories.

Coetzee, G., 2009. *Discussion on Calibration of South African Weather Service Pyranometers.* [email] (Personal communication, 29 June 2009).

Cogentrix, 2012. *Cogentrix Energy's Alamosa Solar Generating Plant Begins Commercial Operation.* [online] Available at: <http://www.cogentrix.com/news.aspx>
[Accessed 24 September 2012].

Cohen, G.E., Kearney, D.W., Kolb, G.J., 1999. *Final Report on the Operation and Maintenance Improvement Program for Concentrating Solar Power Plants*. Sandia Report SAND99-1290. Albuquerque (NM): Sandia National Laboratories.

Davis, S., Prier, M., Cohen, B., Hughes, A., Nyatsanza K., 2011. *Measuring the rebound effect of energy efficiency initiatives for the future: A South African case study*. ENERGY RESEARCH CENTRE. Cape Town: University of Cape Town.

Department of Energy (DoE), Republic of South Africa, 2009. *Notice: Electricity Regulation Act, 2006: Determination Regarding the Integrated Resource Plan and New Generation Capacity*. Government Gazette, 31 December 2009. [online] Available at: <http://www.energy.gov.za> [Accessed 1 July 2012].

Department of Energy (DoE), Republic of South Africa, 2011. *Government Notice: Department of Energy: Electricity Regulation Act No.4 of 2006: Electricity Regulations on the Integrated Resource Plan 2010 - 2030*. Government Gazette, 6 May 2011. [online] Available at: <http://www.energy.gov.za> [Accessed 1 July 2012].

Department of Energy (DoE), Republic of South Africa, 2012. *Renewable Energy Independent Power Producer Procurement Programme.* [online] Available at: <http://www.energy.gov.za> [Accessed 11 July 2012].

Department of Minerals and Energy (DME), Republic of South Africa, 2003. *White Paper on Renewable Energy, November 2003*. [online] Available at: <http://www.dme.gov.za> [Accessed 7 October 2008].

Dudley, V.E., Evans, L.R., 1995. *Test Results Industrial Solar Technology Parabolic Trough Solar Collector*. Springfield (VA): National Technical Information Service.

Dudley, V.E., Kolb, G.J., Sloan, M., Kearney, D., 1994. *Test Results SEGS LS-2 Solar Collector*. Springfield (VA): National Technical Information Service.

Duffie, J.A., Beckman W.A., 2006. *Solar Engineering of Thermal Processes*. 3rd ed. Hoboken (NJ): John Wiley & Sons, Inc.

Eck, M., Eickhoff, M., Fontela, P., Laing, D., Meyer-Grünefeldt, M., Möllenhoff, M., Nölke, M., Vives, F.O., Riffelmann, K.J., Sanchez-Biezma, A., Bahl, C., 2009. Test and Demonstration of the Direct Steam Generation (DSG) at 500°C. *SolarPACES 2009: Electricity, fuels and clean water powered by the sun*. Berlin, Germany. 15-18 September 2009. Almería: Solar Power and Chemical Energy Systems.

Eskom, 2007. *Electricity: Costs and Benefits. Eskom Fact Sheet. Generation Communication. GFS 0014 Revision 4.* [doc] Sunninghill: Eskom. Available at:
<http://www.eskom.co.za/content/ES%200004ElectrCostBenefRev4.doc>
[Accessed 5 January 2009].

Eskom, 2010a. *Integrated Report 2010: Eskom: On the path to recovery*. [pdf] Sunninghill: Eskom. Available at:
< http://financialresults.co.za/2010/eskom_ar2010/downloads/eskom_ar2010.pdf >
[Accessed 27 September 2012].

Eskom, 2010b. *Release of Eskom Solar and Met Data*. [online] Available at:
<http://www.eskom.co.za/live/content.php?Item_ID=16103&Revision=en/4>
[Accessed 2 November 2010].

Eskom, 2011. *Eskom: partnering for a sustainable future: Integrated Report 2011.* [pdf] Sunninghill: Eskom. Available at:
< http://financialresults.co.za/2011/eskom_ar2011/downloads/eskom-ar2011.pdf >
[Accessed 27 September 2012].

Eskom, Bohlweki Environmental, 2006. *Environmental Impact Assessment – Scoping Phase: Proposed Construction of a Concentrating Solar Power (CSP) Plant and Related Infrastructure: Northern Cape.* [online] Available at: <http://www.eskom.co.za>
[Accessed 28 August 2008].

eSolar, 2009. *Sierra SunTower: A New Blueprint for Solar Energy.* [pdf] Burbank (CA): eSolar. Available at: <http://www.esolar.com/sierra_fact_sheet.pdf>
[Accessed 26 September 2012].

Esterhuyse, D.J., 2004. *Establishment of the South African baseline surface radiation network station at De Aar*. MSc. (Meteorology) Pretoria: University of Pretoria.

ExxonMobil, 2011. *2012 The Outlook for Energy: A View to 2040*. 5959 Las Colinas Boulevard, Irving, Texas 75039-2298. [online] Available at: <http://www.exxonmobil.com>
[Accessed 19 December 2011].

Feldhoff, J.F., Birnbaum, J., Fichtner, M., Hirsch, T., Jöcker, M., Pitz-Paal, R., Zimmermann, G., 2009. Steam Temperature Stability in a Direct Steam Generation Solar Power Plant. *SolarPACES 2009: Electricity, fuels and clean water powered by the sun*. Berlin, Germany. 15-18 September 2009. Almería: Solar Power and Chemical Energy Systems.

Flagsol, Solar Millenium LLC, Department of Energy United States of America, 2010. *Advanced High Temperature Trough Collector Development CSP Program Review.* Washington (DC): U.S. Department of Energy. Available at: <http://www1.eere.energy.gov/solar/.../csp_prm2010_solar millenium.pdf>
[Accessed 21 December 2011].

Fluri, T.P., Von Backström, T.W., 2008. Performance analysis of the power conversion unit of a solar chimney power plant. *Solar Energy*, 82 (2008), pp.999-1008.

Forristall, R., 2003. *Heat Transfer Analysis and Modelling of a Parabolic Trough Solar Receiver Implemented in Engineering Equation Solver*. Springfield (VA): National Technical Information Service.

Forsberg, C.W., Peterson, P.F., Zhao, H., 2007. High-Temperature Liquid-Fluoride-Salt Closed-Brayton-Cycle Solar Power Towers. *Journal of Solar Energy Engineering*, 129, pp.141-146.

Fraser, P.R., 2008. *Stirling Dish System Performance Prediction Model*. MSc. (Mechanical Engineering). Madison: University of Wisconsin – Madison.

Gallup, D.R., Kesseli, J.B., 1994. *A Solarized Brayton Engine Based on Turbo-Charger Technology and the DLR Receiver*. Springfield (VA): National Technical Information Service.

Gamble, C., Schopf, M., 2009. Optimization Opportunities for Therminol® VP-1 Heat Transfer Fluid in Concentrating Solar Power Facilities. *SolarPACES 2009: Electricity, fuels and clean water powered by the sun*. Berlin, Germany. 15-18 September 2009. Almería: Solar Power and Chemical Energy Systems.

García, I.L., Álvarez, J.L., Blanco, D., 2011. Performance model for parabolic trough solar thermal power plants with thermal storage: Comparison to operating plant data. *Solar Energy*, 85 (2011), pp.2443-2460.

García, X., 2000. *Overall Energetic Comparison of DSG and Oil-Based Parabolic Trough Systems with Rankine Cycles for Electricity Generation*. Almería (Spain): CIEMAT.

German Energy Agency (DENA), 2009. *Renewables Made in Germany: The German solar thermal power plant industry*. [online] Available at: <http://www.renewables-made-in-germany.com/en/solar-thermal-power-plants/> [Accessed 6 January 2009].

Geyer, M., Lüpfert, E., Osuna, R., Esteban, A., Schiel, W., Schweitzer, A., Zarza, E., Nava, P., Langenkamp, J., Mandelberg, E., 2002. EUROTROUGH - Parabolic Trough Collector Developed for Cost Efficient Solar Power Generation. *11th SolarPACES: International Symposium on Concentrating Solar Power and Chemical Energy Technologies.* Zurich, Switzerland. 4-6 September 2002. Almería: Solar Power and Chemical Energy Systems.

Gharbi, N., Derbal, H., Bouaichaoui, S., Said, N., 2011. A comparative study between parabolic trough collector and linear Fresnel reflector technologies. *Energy Procedia 6* (2011) 565–572.

Gilman, P., Blair, N., Mehos, M., Christensen, C., Janzou, S., Cameron, C., 2008. *Solar Advisor Model User Guide for Version 2.0.* Springfield (VA): National Technical Information Service.

Gilman, P., 2012. *Thermal Storage Dispatch Control for Physical Trough Model.* [email] (Personal communication, 4 January 2012).

Giostri, A., Binotti, M., Silva, P., Macchi, E., Manzolini, G., 2011. Comparison of Two Linear Collectors in Solar Thermal Plants: Parabolic Trough vs. Fresnel. *Proceedings of the ASME 2011 5th International Conference on Energy Sustainability*. Washington, DC, USA. 7-10 August 2011. New York: American Society of Mechanical Engineers.

Google Earth 6.2. 2012. *SH 61, Rajasthan, India* 26°29'N, 73°03'E, elevation 243m. Available through: <http://www.google.com/earth/index.html>
[Accessed 2 September 2012].

Goswami, D.Y., Kreith, F., and Kreider, J.F., 2000. *Principles of Solar Engineering*. 2nd ed. Philadelphia: Taylor & Francis.

Häberle, A., Zahler, C., Lerchenmüller, H., Mertins, M., Wittwer, C., Trieb, F., Dersch, J., 2002. The Solarmundo line focussing Fresnel collector. Optical and thermal performance and cost calculations. *11th SolarPACES: International Symposium on Concentrated Solar Power and Chemical Energy Technologies.* Zurich, Switzerland. 4-6 September 2002. Almería: Solar Power and Chemical Energy Systems.

Heller, P., Pfänder, M., Denk, T., Tellez, F., Valverde, A., Fernandez, J., Ring, A., 2006. Test and Evaluation of a Solar Powered Gas Turbine System. *Solar Energy,* 80 (10), pp.1225-1230.

Herrmann, U., Nava, P., 2005. Trapping the sun's rays – The development of the SKAL-ET150 parabolic trough collector. *DLR Nachrichten 109 – Special Issue Solar Research.* January 2005: 34-37.

Herrmann, U., Nava, P., 2006. Thermal Storage Concept for a 50 MW Trough Power Plant in Spain. *Trough Workshop in Lake Tahoe* February 2006: 34-37.

Hoyer, M., Riffelmann, K.J., Benitez, D., Nava, P., 2009. Performance and Cost Comparison of Linear Fresnel and Parabolic Trough Collectors. *SolarPACES 2009: Electricity, fuels and clean water powered by the sun*. Berlin, Germany. 15-18 September 2009. Almería: Solar Power and Chemical Energy Systems.

Hulstrom, R. ed. 1989. *Solar Resources*. Massachusetts: MIT Press.

Infinia Corporation, 2011. *Powerdish by Infinia.* [online] Available at: <http://powerdish.com> [Accessed 14 December 2011].

International Energy Agency (IEA), 2011. *CO_2 Emissions from Fuel Combustion – Highlights. 2011 Edition. IEA Statistics.* [pdf] Paris: International Energy Agency. Available at: <http://www.iea.org/co2highlights/co2highlights.pdf> [Accessed 30 June 2012].

Iqbal, M., 1983. *An Introduction to Solar Radiation*. Toronto: Academic.

Jorgensen, G., 2001. *Summary Status of Most Promising Candidate Advanced Solar Mirrors (Testing and Development Activities) Milestone report to DOE*. Springfield (VA): National Technical Information Service.

Kearney, D.W., 2007. Parabolic Trough Collector Overview. *Parabolic Trough Workshop 2007*. Golden, CO, USA.

Kelly, B., 2006a. *Nexant Parabolic Trough Solar Power Plant Systems Analysis Task 1: Preferred Plant Size January 20, 2005 — December 31, 2005*. Springfield (VA): National Technical Information Service.

Kelly, B., 2006b. *Nexant Parabolic Trough Solar Power Plant Systems Analysis Task 2: Comparison of Wet and Dry Rankine Cycle Heat Rejection January 20, 2005 – December 31, 2005*. Springfield (VA): National Technical Information Service.

Kelly, B., Herrmann, U., Hale, M.J., 2001. Optimization Studies for Integrated Solar Combined Cycle Systems. *Proceedings of Solar Forum 2001 Solar Energy: The Power to Choose*. Washington, DC USA. 21-25 April 2001. New York: American Society of Mechanical Engineers.

Khuen, C., 2011. *Discussion on creating epw/tmy files.* [email] (Personal communication, 13 June 2011).

Kistler, B.L., 1986. A User's Manual for DELSOL3: *A Computer Code for Calculating the Optical Performance and Optimal System Design for Solar Thermal Central Receiver Plants.* Sandia National Laboratory, Albuquerque, NM. SAND86-8018.

Klein, S.A., 1977. Calculation of Monthly Average Insolation on Tilted Surfaces. *Solar Energy*, 19 (1977), pp.325-329.

Kolb, G.J., 1991. *The Design of Future Central Receiver Power Plants based on Lessons Learned from the Solar One Pilot Plant.* Springfield (VA): National Technical Information Service.

Kreider, J.F., 2006. Chapter 20 Solar Energy Applications in *Mechanical Engineering Handbook*. John Wiley and Sons. 663-701.

Kreith, F., Kreider, J.F., 1978. *Principles of Solar Engineering*. Washington (DC): McGraw-Hill Co.

Kröger, D.G., 2011. *SUNSPOT: Stellenbosch University Solar Power Thermodynamic cycle.* [pdf] Stellenbosch: Stellenbosch University. Available at: <http://blogs.sun.ac.za/sterg/files/2011/05/SUNSPOT-2.pdf> [Accessed 2 October 2012].

Kruger, A.C., Esterhuyse, D.J., 2005. *Sunshine and Cloudiness*. Climate of South Africa: WS46. Pretoria: South African Weather Service.

Kuckelkorn, T., Benz, N., Dreyer, S., Schulte-Fischedick, J., Moellenhoff, M., 2009. Advances in Receiver Technology for Parabolic Trough Collectors – A step forward towards higher efficency and longer lifetime. *SolarPACES 2009: Electricity, fuels and clean water powered by the sun*. Berlin, Germany. 15-18 September 2009. Almería: Solar Power and Chemical Energy Systems.

Kurtz, S., 2012. *Opportunities and Challenges for Development of a Mature Concentrating Photovoltaic Power Industry*. Springfield (VA): National Technical Information Service.

Kutscher, C., Mehos, M., Turchi, C., Glatzmaier, G., Moss, T., 2010. *Line-Focus Solar Power Plant Cost Reduction Plan.* Springfield (VA): National Technical Information Service.

Laing, D., Bahl, C., Bauer, T., Lehmann, D., Steinmann, W., 2009. Thermal Energy Storage for Direct Steam Generation. *SolarPACES 2009: Electricity, fuels and clean water powered by the sun*. Berlin, Germany. 15-18 September 2009. Almería: Solar Power and Chemical Energy Systems.

Langenkamp, J., 1998. *Revised LEC Projections and Discussion of Different DGS Benefits*. Almería (Spain): CIEMAT.

Lew D., Milligan, M., Jordan, G., Freeman, L., Miller, N., Clark, K., Piwko, R., 2009. How do Wind and Solar Power Affect Grid Operations: The Western Wind and Solar Integration Study. *8th International Workshop on Large Scale Integration of Wind Power and on Transmission Networks for Offshore Wind Farms.* Bremen, Germany. 14–15 October 2009.

Luzzi, A., Lovegrove, K., 2004. Solar Thermal Power Generation in *Encyclopedia of Energy, Volume 5*. Amsterdam: Elsevier. 669-683

Mancini, T.R., 1994. *An Overview: Component Development for Solar Thermal Systems*. Springfield (VA): National Technical Information Service.

Maxwell, E.L., George, R.L., Wilcox, S.M., 1998. A Climatological Solar Radiation Model. *Proceedings of the 1998 American Solar Energy Society Annual Conference*. Albuquerque, NM USA. 14-17 June 1998. Boulder: American Solar Energy Society.

Meteotest, 2010. *METEONORM Version 6.0 – Handbook part I: Software.* Fabrikstrasse 14, CH-3012 Bern, Switzerland. [online] Available at: <http://www.meteonorm.com> [Accessed 14 December 2011].

Meteotest, 2010. *METEONORM Version 6.0 – Handbook part II: Theory*. Fabrikstrasse 14, CH-3012 Bern, Switzerland. [online] Available at: <http://www.meteonorm.com> [Accessed 14 December 2011].

Meyer, A.J., van Niekerk, J.L., 2011. Roadmap for the Deployment of Concentrating Solar Power in South Africa. *SolarPACES 2011: Concentrating Solar Power and Chemical Energy Systems.* Granada, Spain. 20-23 September 2011. Almería: Solar Power and Chemical Energy Systems.

Mills, D.R., Morrison G.L., 2000. Compact Linear Fresnel Reflector Solar Thermal Powerplants. *Solar Energy,* 68 (3), pp.263-283.

Mills, D.R., Morrison, G., Le Liévre, P., 2003. Multi-Tower Line Focus Fresnel Arrays. *Proceedings of the 2003 International Solar Energy Conference.* Hawaii Island, Hawaii USA. 16-18 March 2003. New York: American Society of Mechanical Engineers.

Mills, D., 2004. Advances in solar thermal electricity technology. *Solar Energy,* 76 (2004), pp.19-31.

Mills, D., Morrison, G.L., Le Liévre, P., 2004a. Design of a 240 MWe Solar Thermal Power Plant. *ISES Eurosun 2004 Conference* Freiburg, Germany 20-24 June 2004. Freiburg: International Solar Energy Society.

Mills, D.R., Le Liévre, P., Morrison, G.L., 2004b. First Results from Compact Linear Fresnel Reflector Installation. *Solar 2004 Proceedings – Australia and New Zealand Solar Energy Society 42nd Annual Conference* Perth, Australia 30 November to 3 December 2004. Frenchs Forest: Australia and New Zealand Solar Energy Society.

Moens, L., Blake, D.M., 2005. Advanced Heat Transfer and Thermal Storage Fluids. *Proceedings of the 2005 International Solar Energy Conference.* Orlando, Florida, USA. 6-12 August 2005. New York: American Society of Mechanical Engineers.

Morin, G., Dersch, J., Platzer, W., Eck, M., Häberle, A., 2012. Comparison of Linear Fresnel and Parabolic Trough Collector power plants. *Solar Energy*, 86 (2012), pp.1–12.

Müller-Steinhagen, H., Trieb, F., 2004. Concentrating solar power: A review of the technology. *Ingenia*, Issue 18, February: 1-8.

Municipal Demarcation Board, 2011. *Municipal Outer Boundary Redetermination (DEMs)*. [online] Available at: <http://www.demarcation.org.za/pages/default_new.html>
[Accessed 27 November 2011].

Myers, D.R., 2003. Solar Radiation Modelling and Measurements for Renewable Energy Applications: Data and Model Quality. *International Expert Conference on Mathematical Modelling of Solar Radiation and Daylight—Challenges for the 21st Century* Edinburgh, Scotland 15–16 September 2003. National Renewable Energy Laboratory: Golden.

National Aeronautics and Space Administration (NASA), 2009. *Surface meteorology and Solar Energy (SSE) Release 6.0 Methodology*. *Version 2.4 January 30, 2009*. [pdf] Langley: National Aeronautics and Space Administration. Available at: <http://eosweb.larc.nasa.gov/sse/documents/SSE6Methodology.pdf> [Accessed 7 July 2009].

National Energy Regulator of South Africa (NERSA), 2007. *Electricity Supply Statistics for South Africa 2005*. [pdf] Pretoria: National Energy Regulator of South Africa. Available at: <http://www.nersa.org.za/Admin/Document/Editor/file/News%20and%20Publications/Publications/Current%20Issues/Electricity%20Supply%20Statistics/2007%20Nersa%20ESS%20Booklet_o.pdf> [Accessed 6 January 2009].

National Energy Regulator of South Africa (NERSA), 2009a. *South Africa Renewable Energy Feed-in Tariff (REFIT) Regulatory Guidelines 26 March 2009*. [online] Available at: <http://www.remtproject.org/Document.aspx> [Accessed 11 July 2012].

National Energy Regulator of South Africa (NERSA), 2009b. *Renewable Energy Feed – In Tariff Guidelines*. [online] Available at: <http://www.remtproject.org/Document.aspx> [Accessed 11 July 2012].

National Energy Regulator of South Africa (NERSA), 2009c. *Renewable Energy Feed – In Tariffs Phase II*. [online] Available at: <http://www.remtproject.org/Document.aspx> [Accessed 11 July 2012].

National Energy Regulator of South Africa (NERSA), 2011. *Review of Renewable Energy Feed - In Tariffs*. [online] Available at: <http://www.remtproject.org/Document.aspx> [Accessed 11 July 2012].

National Renewable Energy Laboratory (NREL), 2011a. *Concentrating Solar Power Projects: Kimberlina Solar Thermal Power Plant*. [online] Available at: <http://www.nrel.gov/csp/solarpaces/project_detail.cfm/projectID=37> [Accessed 28 November 2011].

National Renewable Energy Laboratory (NREL), 2011b. *Concentrating Solar Power Projects: Andasol-2*. [online] Available at: <http://www.nrel.gov/csp/solarpaces/project_detail.cfm/projectID=4> [Accessed 1 September 2012].

Nobesol Levante, 2008. *Olmedilla de Alarcón (España)*. [online] Available at: <http://www.nobesol.com/?seccion=4&subseccion=2&contenido=40>
[Accessed 26 May 2010].

NOVATEC BIOSOL AG, 2011. *PE 1 – World's first Fresnel Solar Power Plant in commercial operation.* [pdf] Karlsruhe: Novatec Solar. Available at: <http://www.novatecsolar.com/files/mne0911_pe1_broschure_english.pdf>
[Accessed 9 September 2012].

Ortega, J.I., Burgaleta, J.I., Tellez, F.M., 2006. *Central receiver system (CRS) solar power plant using molten salt as heat transfer fluid.* SENER / CIEMAT publication,
Madrid, Spain.

Pacheco, J.E., Gilbert, R., 1999. *Overview of Recent Results of the Solar Two Test and Evaluations Program.* Springfield (VA): National Technical Information Service.

Pacheco, J.E., Reilly, H.E., Kolb, G.J., Tyner, C.E., 2000. *Summary of the Solar Two Test and Evaluation Program.* Springfield (VA): National Technical Information Service.

Pacheco, J.E., Showalter, S.K., Kolb, W.J., 2001. Development of a Molten-Salt Thermocline Thermal Storage System for Parabolic Trough Plants. *Proceedings of Solar Forum 2001 Solar Energy: The Power to Choose*. Washington, DC USA. 21-25 April 2001. New York: American Society of Mechanical Engineers.

Palmer, A.R., Ainslie, A.M., 2005. Chapter 3 GRASSLANDS OF SOUTH AFRICA in J.M. Suttie, S.G. Reynolds and C. Batello (editors) *GRASSLANDS of the WORLD*. Food and Agriculture Organization of the United Nations: Rome 2005. ISBN 92-5-105337-5.

Philibert, C., 2004. Case Study 1: Concentrating Solar Power Technologies. *International Energy Technology Collaboration and Climate Change Mitigation. OECD Environment Directorate. International Energy Agency (IEA).* Paris: OECD/IEA.

Pitz-Paal, R., 2008. Chapter 10 Concentrating Solar Power in T.M. Letcher (editor) *Future Energy: Improved, Sustainable and Clean Options for Our Planet*. Amsterdam: Elsevier. 171-192.

Power, H.C., Mills, D.M., 2005. Solar Radiation Climate Change over Southern Africa and an Assessment of the Radiative Impact of Volcanic Eruptions. *International Journal of Climatology*, 25, pp.295-318.

Prabhu, E., 2006. *Solar Trough Organic Rankine Electricity System (STORES) Stage 1: Power Plant Optimization and Economics November 2000 — May 2005*. Springfield (VA): National Technical Information Service.

Price, H., Lüpfert, E., Kearney, D., Zarza, E., Cohen, G., Gee, R., Mahoney R., 2002. Advances in Parabolic Trough Solar Power Technology. *Journal of Solar Energy Engineering*, 124, pp.109-125.

Pye, J., 2008. *Compact Linear Fresnel Reflector*. [online] Available at: <http://pye.dyndns.org/> [Accessed 6 January 2009].

Reddy, S.V., Kaushik, S.C., Tyagi, S.K., 2012. Exergetic analysis and performance evaluation of parabolic dish Stirling engine solar power plant. *International Journal of Energy Research.* [e-journal] (2012), Available through: Wiley Online Library <wileyonlinelibrary.com> [Accessed 24 August 2012].

ReflecTech, Inc., 2009. *ReflecTech Mirror Film*. 18200 West Highway 72, Arvada, CO 80007 303.330.0399. [online] Available at: <http://www.ReflecTechSolar.com> [Accessed 8 June 2009].

Relloso, S., Castañeda, N., Domingo, M., 2008. New Senertrough Collector Development in Collaboration with Key Components Suppliers. *14th Biennial CSP SolarPACES Symposium*. Las Vegas, NV USA. 4-7 March 2008. Almería: Solar Power and Chemical Energy Systems.

REN21 Renewable Energy Policy Network for the 21st Century, 2011. *Renewables 2011 Global Status Report.* [online] Available at: <http://www.ren21.net/REN21Activities/Publications/GlobalStatusReport/GSR2011/tabid/56142/Default.aspx> [Accessed 21 December 2011].

Rodríguez-García, M.M., Marquez-Payés, J.M., Biencinto, M., Adler, J.P., Díez, L.E., 2009. First Experimental Results of a Solar PTC Facility. *SolarPACES 2009: Electricity, fuels and clean water powered by the sun*. Berlin, Germany. 15-18 September 2009. Almería: Solar Power and Chemical Energy Systems.

Rojas, E., Zarza, E., Fernández-García, A., González, L., 2008. Towards A Standardized Characterization Of Parabolic Trough Collectors. *14th Biennial CSP SolarPACES Symposium*. Las Vegas, NV USA. 4-7 March 2008. Almería: Solar Power and Chemical Energy Systems.

Romero, M., Buck, R., Pacheco, J.E., 2002. An Update on Solar Receiver Systems, projects, and Technologies. *Journal of Solar Energy Engineering*, 124, pp.98-108.

Schwarzbözl, P., Buck, R., Sugarmen, C., Ring, A., Crespo, J.M., Altwegg, P., Enrile, J., 2006. Solar gas turbine systems: Design, cost and perspectives. *Solar Energy*, 80 (10), pp.1231-1240.

Selig, M., 2009. *PE1 – First Fresnel solar power plant in operation: Experiences and Outlook.* [presentation] NOVATEC BIOSOL. [online] Available at: <http://www.fundaciongasnaturalfenosa.org/SiteCollectionDocuments/Actividades/Seminarios/MURCIA%20220909/2-%20Martin%20Selig%20Novatec-BioSol-gasnatural.pdf> [Accessed 1 October 2012].

South African Renewable Energy Resource Database (SARERD), 2006. *Sarerd – Solar Radiation*. [online] Available at: <http://www.sabregen.co.za/sarerd%20database/solar.htm> [Accessed 6 January 2009].

Southern Africa Solar Thermal and Electricity Association (SASTELA), 2012. *SA's first solar plants.* [online] Available at: <http://www.sastela.org/services.html> [Accessed 29 September 2012].

Scott, B., Lee, J., 2006. *Saguaro Solar Power Plant, Red Rock, Arizona*. POWER Magazine, August 2006. [online] Available at: <http://www.powermag.com/issues/cover_stories/Saguaro-Solar-Power-Plant-Red-Rock-Arizona_468.html> [Accessed 20 July 2009].

Siemens AG, Energy Sector, 2008. *Steam turbines for solar thermal power plants*. Freyeslebenstrasse 1, 91058 Erlangen, Germany. [online] Available at: <http://www.siemens.com/energy> [Accessed 20 July 2009].

SkyFuel, Inc., 2009. *SkyTrough™ Parabolic Trough Concentrator*. [pdf] Albuquerque, NM: SkyFuel, Inc. Available at: <http://www.skyfuel.com/downloads/brochure/SkyFuelSkyTroughBrochure%28SkyFuel%29August2008.pdf> [Accessed 26 August 2009].

Solar and Wind Energy Resource Assessment (SWERA) Data Archive, 2007. *Solar: monthly and annual average direct normal (DNR), global horizontal (GHI), latitude tilt, and diffuse data and GIS data at 40km resolution for Africa from NREL.* [online] Available at: <http://swera.unep.net/index.php?id=35&idx=333> [Accessed 20 August 2009].

Solargenix Energy, Power Plant Division, 2004. *Trough Concentrator Development.* Solargenix Energy Headquarter, 1378 McNeill Road, Sanford, NC 27330. [online] Available at: <http://www.solargenix.com/power_plant_tech.cfm> [Accessed 28 February 2011].

South African National Biodiversity Institute. 2011. *Municipal Biodiversity Summary Project*. [Online] Available at: <http://bgis.sanbi.org/municipalities/summaries.asp?muni=NC083> [Accessed 27 November 2011].

Stassen, G., 1996. *Towards a Renewable Energy Strategy for South Africa.* Ph. D. (Architecture). Pretoria: University of Pretoria.

Statistics South Africa. 2001. Census 2001 Digital Census Atlas. [online] Available at: <http://www.statssa.gov.za/census2001/digiatlas/index.html> [Accessed 27 November 2011]

Stine, W.B., Diver, R.B., 1994. *A Compendium of Solar Dish/Stirling Technology*. Springfield (VA): National Technical Information Service.

Stone, K.W., Jones, S.A., 1999. *Analysis of Solar Two Heliostat Tracking Error Sources.* Sandia National Laboratory, Albuquerque, NM, and The Boeing Company, Huntington Beach, CA. SAND99-0239C.

Suri, M., Cebecauer, T., Skoczek, A., Betak, J., 2011. *Site Assessment of Solar Resource: Upington Solar Park: Province Northern Cape, South Africa.* GeoModel Solar, Bratislava, Slovakia. Reference No. 58-01/2011 rev. 2.

System Advisor Model. 2010. Version 2010.11.9

System Advisor Model. 2011. Version 2011.12.2

Thompson, R., 2010. *Discussion on recent visits to Siemens Concentrating Solar Power, Abengoa, Solar Millenium, Flagsol, eSolar and Sky-Fuel.* [Conversation] (Personal communication, 16 April 2010).

Tiwari, G.N., 2002. *Solar Energy: Fundamentals, Design, Modelling and Applications.* New Delhi: Narosa Publishing House.

Turchi C.S., Ma, Z., Erbes, M., 2011. Gas Turbine/Solar Parabolic Trough Hybrid Designs. *ASME Turbo Expo 2011*. Vancouver, Canada. 6-10 June 2011.

Turchi, C., Mehos, M., Ho, C.K., Kolb, G.J., 2010. Current and Future Costs for Parabolic Trough and Power Tower Systems in the US Market. *SolarPACES 2010*. Perpignan, France. 21-24 September 2010. Almería: Solar Power and Chemical Energy Systems.

United Nations Statistics Division, 2004. *Carbon dioxide emissions (CO_2), metric tons of CO_2 per capita (CDIAC).* [online] Available at: <http://mdgs.un.org/unsd/mdg/SeriesDetail.aspx?srid=751> [Accessed 5 January 2009].

University of Illinois, University of California, Ernest Orlando Lawrence Berkeley National Laboratory. 2010. *Auxiliary EnergyPlus Programs*. Springfield (VA): National Technical Information Service.

Van Niekerk, W., 2009. *Drivers for CSP in the Northern Cape: Growth, Jobs and Poverty Alleviation.* [presentation] Centre for Renewable and Sustainable Energy Studies. Stellenbosch University.

Van Wyk, J., Weidema, J., Fikela, N., 2006. *Digest of South African Energy Statistics 2006*. Pretoria: Department of Minerals and Energy, Directorate: Energy Planning and Development. ISBN: 0-9584376-4-5.

Vázquez, J., Castañeda, N., 2008. Senertrough. The Collector for Extresol-1. 600 Meters Loop Test in Andasol-1 and Test Unit Description. *14th Biennial CSP SolarPACES Symposium*. Las Vegas, NV USA. 4-7 March 2008. Almería: Solar Power and Chemical Energy Systems.

Vázquez, J., Castañeda, N., Castañeda, D., 2009. First Commercial Application of Senertrough Collector: High Performance at Reduced Cost. *SolarPACES 2009: Electricity,*

fuels and clean water powered by the sun. Berlin, Germany. 15-18 September 2009. Almería: Solar Power and Chemical Energy Systems.

Wagner, M.J., 2008. *Simulation and Predictive Performance Modelling of Utility-Scale Central Receiver System Power Plants.* MSc. (Mechanical Engineering). Madison: University of Wisconsin – Madison.

Wagner, M.J., 2012. Results and Comparison from the SAM Linear Fresnel Technology Performance Model. *2012 World Renewable Energy Forum.* Denver, CO USA. 13-17 May 2012.

Wagner, M.J., Gilman, P., 2011. *Technical Manual for the SAM Physical Trough Model.* Springfield (VA): National Technical Information Service.

Weather Analytics Incorporated, 2011. *Products & Applications.* [online] Available at: <http://www.weatheranalytics.com/globaltmy.html> [Accessed 11 December 2011].

Wizard Power Pty Limited, 2011. *Dishes*. [online] Available at: <http://www.wizardpower.com.au/index.php?option=com_content&view=article&id=12&Itemid=13> [Accessed 31 October 2011].

Wizard Power Pty Limited, 2011. *Mirrors*. [online] Available at: <http://www.wizardpower.com.au/index.php?option=com_content&view=article&id=14&Itemid=15> [Accessed 31 October 2011].

Wolff, G., Gallego, B., Tisdale, R., Hopwood, D., 2008. CSP concentrates the mind. *renewable energy focus*, January/February 2008: 43.

Zahler, C., Berger, M., Häberle, A., Louw, J., Schwind, T., 2009. Mirroxx Fresnel Process Heat Collectors for Industrial Applications and Solar Cooling. *SolarPACES 2009: Electricity, fuels and clean water powered by the sun*. Berlin, Germany. 15-18 September 2009. Almería: Solar Power and Chemical Energy Systems.

Zarza, E., Valenzuela, L., León, J., Weyers, H.D., Eickhoff, M., Eck, M., Hennecke, K., 2001. The DISS Project: Direct Steam Generation in Parabolic Troughs Operation and Maintenance Experience Update on Project Status. *Proceedings of Solar Forum 2001 Solar Energy: The*

Power to Choose. Washington, DC USA. 21-25 April 2001. New York: American Society of Mechanical Engineers.

Zobaa, A., 2006. Subsection 11.4 Photovoltaics in Section 11 Alternate Sources of Power in *Standard Handbook for Electrical Engineers*. McGraw-Hill. 11-18 – 11-23.

APPENDIX A: THE SOLAR RESOURCE

Introduction

In this appendix some basic concepts of the solar resource and solar energy engineering are reviewed. Duffie and Beckman's *Solar Engineering of Thermal Processes* (2006) was used as a baseline for the equations and astronomical data in this chapter. Where possible the geometric relations, equations and indices are contextualised to the Upington location.

The sun is composed of gaseous matter with an interior temperature estimated at between $8x10^6$ K and $40x10^6$ K. It has a diameter of $1.39x10^9$ m and is, on average, $1.495x10^{11}$ m from the earth. The sun's effective or equivalent black body temperature is reported to be between 5760 K (Goswami, *et al*., 2000) and 5777 K (Duffie and Beckman, 2006; Tiwari, 2002). Goswami, *et al*. (2000), suggest that the earth intercepts approximately $1.7x10^{14}$ kW of the $3.8x10^{23}$ kW of energy emitted by the sun. The distance between the sun and the earth varies by 1.7% due to the peculiarity of the earth's elliptical orbit about the sun (Duffie and Beckman, 2006). At the mean sun-earth distance of $1.495x10^{11}$ m, the sun subtends an angle of 32 minutes (Duffie and Beckman, 2006). A planar representation of the sun-earth geometry is displayed in Figure 2-1.

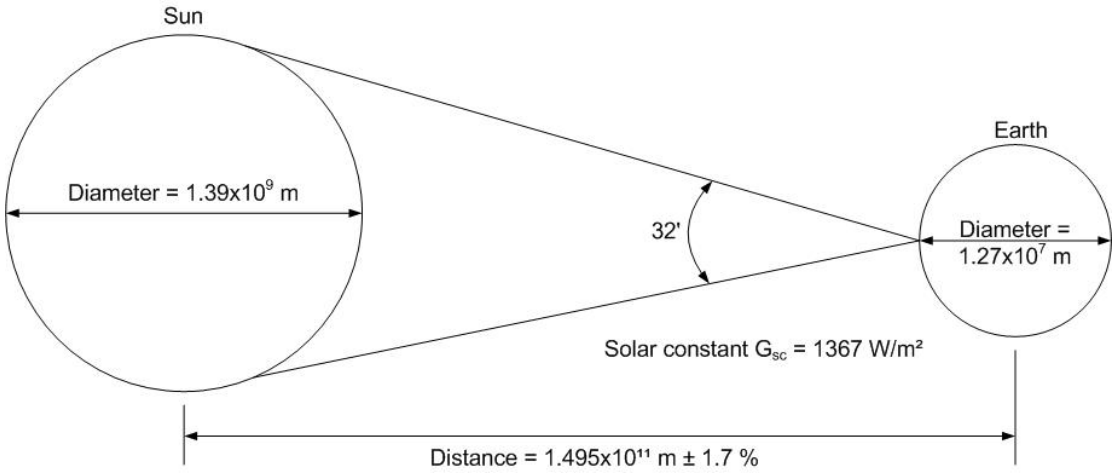

Figure A1: Sun-earth relationships (Modified from Duffie and Beckman, 2006)

The solar constant, G_{sc} sometimes referred to as I_o in certain references, is defined as

> "the energy from the sun per unit time received on a unit area of a surface perpendicular to the direction of propagation of the radiation at mean earth distance outside the atmosphere."
> (Duffie and Beckman, 2006: 5)

Many estimates of the solar constant have been reported over the years and the World Radiation Center (WRC) chose a value of 1367 W/m² with an uncertainty of 1%. Knowing the spectral distribution of the solar constant is helpful. The WRC standard spectral irradiance curve compiled from space and high-altitude measurements is provided in Figure A2.

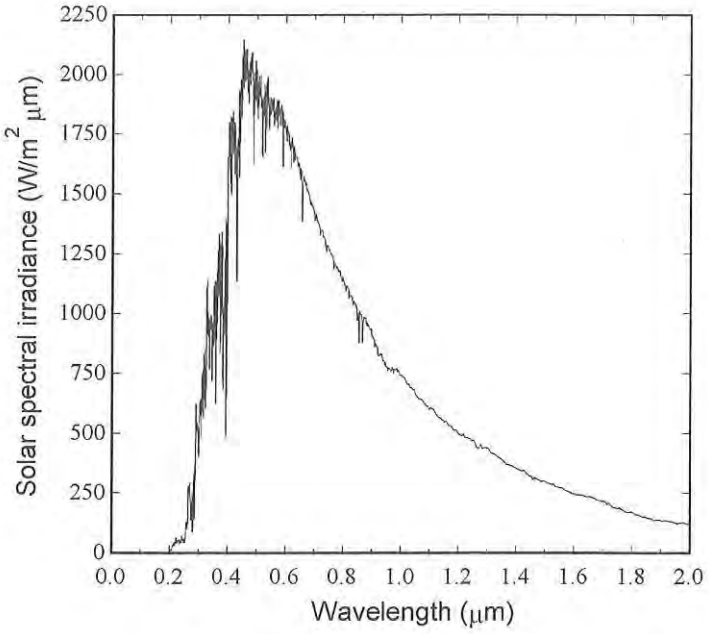

Figure A2: The WRC standard spectral irradiance curve at average earth-sun distance (Duffie and Beckman, 2006)

From the curve it is clear that the wavelength range of 0.25 μm to 3.0 μm includes most of the energy radiated by the sun. Hence, this portion of the sun's electromagnetic radiation is of primary importance. The solar radiation that reaches the earth varies due to internal effects within the sun and due to variations in the earth-sun distance (Duffie and Beckman, 2006). The earth-sun variation leads to deviation of extraterrestrial radiation flux in the range of ±3.3% or ±3.4% as suggested by Goswami, *et al.* (2000). A simple equation to calculate this variance, with adequate accuracy for the required calculations is given by Equation A.1.

$$G_{on} = G_{sc}\left(1 + 0.033cos\frac{360n}{365}\right) \tag{A.1}$$

G_{on} equals the extraterrestrial radiation striking a plane at a right angle to the radiation on the *n*th day of any given year. A more accurate result can be given by Equation A.2 developed by Spencer (1971) as cited by Iqbal (1983).

$$G_{on} = G_{sc}(1.000110 + 0.034221cosB + 0.001280sinB + 0.000719cos2B + 0.000077sin2B) \tag{A.2}$$

where B is given by

$$B = (n-1)\frac{360}{365} \tag{A.3}$$

When comparing the two equations over a sample year, say 2009, it is noted that the variance is slight as shown in Figure A3.

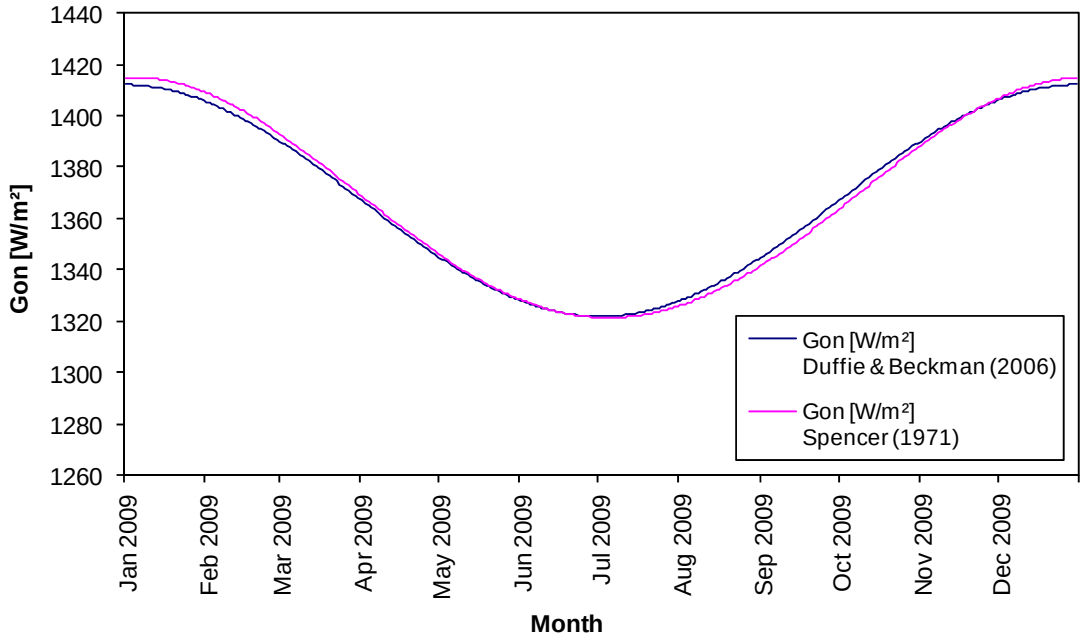

Figure A3: Variation of extraterrestrial solar radiation with time of year

In addition to these two variances, solar radiation received at the earth's surface is affected by two more important phenomena: atmospheric scattering by dust, air molecules and water as well as atmospheric absorption by CO_2, O_3, and H_2O. A detailed review of these interactions is presented by Iqbal (1983).

Geometric relationships of beam radiation

For meaningful calculations of solar radiation to be performed, a few geometric relationships between the sun and a plane should be understood. In order to obtain a global reference point, the latitude of a given plane is required. This latitude (ϕ) is defined as the angular location south or north of the equator, with south being negative. Latitude ranges between -90°and 90°. The latitudes of the measurement stations in Upington where the data were obtained to model the four systems in this study are -28.4° and -28.566°. Another "global" metric is declination (δ); defined as the spatial relation of the sun at solar noon and the plane of the equator. Declination is computed with the approximate equation of Cooper (1969) as cited by Duffie and Beckman (2006):

$$\delta = 23.45sin\left(2\pi\frac{284+n}{365}\right) \tag{A.4}$$

where the value is in degrees, and the day of year is n (i.e. n =1 for January 1, n = 33 for February 2, etc.). Declination moves from -23.45° on 21 December through +23.45° on 21 June of the next year and returning to -23.45° on that year's 21 December.

A more accurate equation with an error of less than 0.035° by Spencer (1971) as cited by Iqbal (1983) is provided below.

$$\delta = \left(\frac{180}{\pi}\right)(0.006918 - 0.399912cosB + 0.070257sinB - 0.006758cos2B + 0.000907sin2B - 0.002697cos3B + 0.00148sin3B) \tag{A.5}$$

Kreider (2006) presents the following equation which yields results more accurate than Cooper's equation yet not as accurate as Spencer:

$$sin\delta = 0.398cos[0.986(n-173)] \tag{A.6}$$

Viewing the results of all three equations on one plot (Figure A4) is useful in understanding the variation of declination through the year and the slight difference in results from each equation.

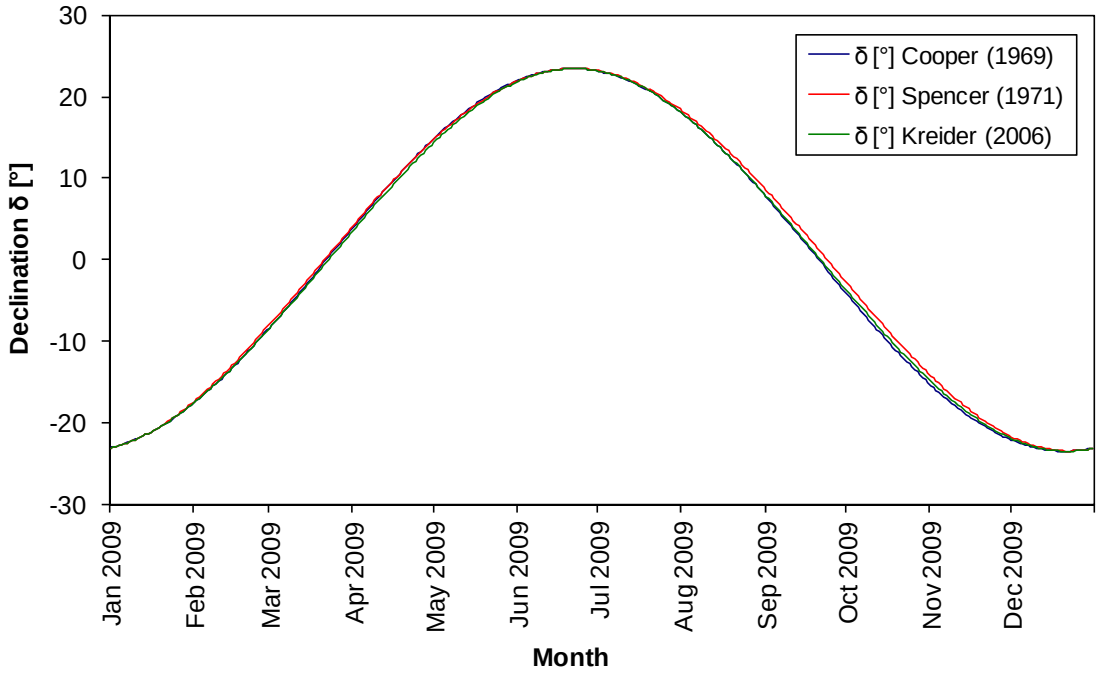

Figure A4: Annual declination variation

The plane of any solar collector may be in any particular orientation relative to the earth at given time. The relationships are defined in terms of the beam solar radiation from the sun directed at the plane. A few useful angles are designated in Figure A5.

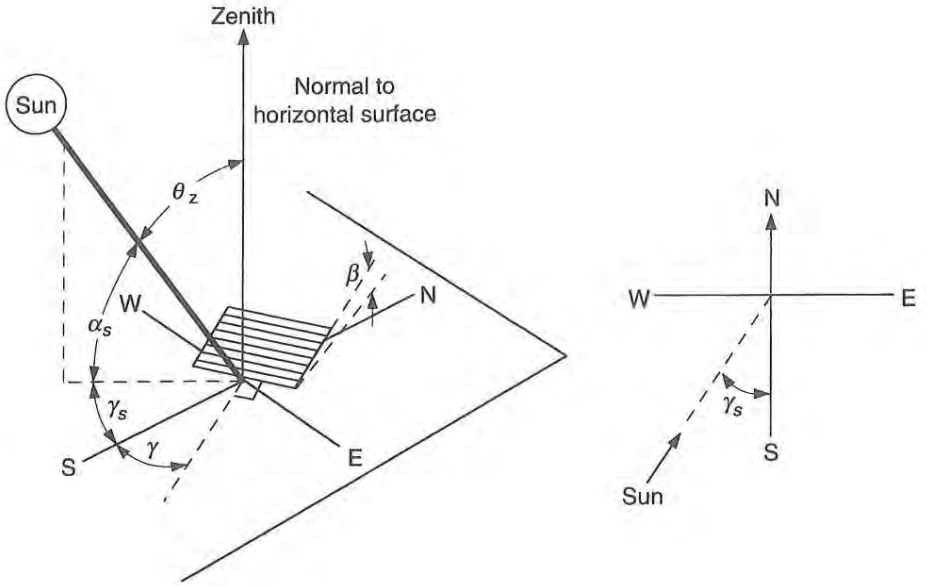

Figure A5: Geometric relationships between a plane and incoming beam radiation and solar azimuth angle in plan view (Duffie and Beckman, 2006)

The following definitions summarized from Duffie and Beckman (2006) describe the geometric relationships in Figure A5 above.

i. Slope (β) is the angle between the horizontal and the plane of the surface in question and can range between 0° and 180°. If β is greater than 90° then some of the plane is facing the ground.
ii. Surface azimuth angle (γ) is the deviation of the projection of the normal to the surface from the local longitude on a horizontal plane with south being zero, west positive and east negative. The surface azimuth angle can lie between -180° and 180°.
iii. Hour angle (ω) is the displacement of the sun east or west of the local longitude due to the 15° per hour rotation of the earth on its axis, with the morning being negative and the afternoon positive. Solar time is taken from the position of the sun in the sky. Solar noon is when the sun reaches its zenith in the sky. The solar hour angle is zero at solar noon and changes by 15 degrees per hour from solar noon. For instance at 8 a.m. solar time the hour angle is equal to –60° (8 a.m. is 4 hours from noon – 4 times 15 is equal to 60, with a negative sign since it is morning).
iv. The angle of incidence (θ) is the angle between the normal of a surface and the incident beam radiation on it.

The angles describing the position of the sun in the sky are:

i. The zenith angle (θ_z) is the angle between the normal of a horizontal surface and the sun, in other words, the angle between the beam radiation striking a horizontal surface and the vertical.
ii. The solar altitude angle (α_s) is the complement of the zenith angle, that is, the angle between the beam radiation striking a horizontal surface and the horizontal.
iii. The solar azimuth angle (γ_s) is the angle between the sun and south, when looking at a surface from above (plan view). If the sun is east of south the angle is negative. If the sun is west of south the angle is positive.

These angles relate to each other usefully. The angle of incidence, θ, may be quantified in terms of the other angles as follows:

$$\begin{aligned}\cos\theta = {} & \sin\delta\sin\phi\cos\beta - \sin\delta\cos\phi\sin\beta\cos\gamma + \cos\delta\cos\phi\cos\beta\cos\omega \\ & + \cos\delta\sin\phi\sin\beta\cos\gamma\cos\omega + \cos\delta\sin\beta\sin\gamma\sin\omega\end{aligned} \tag{A.7}$$

The above equation can be simplified under certain ordinarily occurring circumstances. One of the cases of interest is a horizontal surface during the day. In this case the zenith angle, θ_z, must be between 90° and 0° as the sun moves from one horizon through its zenith to the other horizon.

In this situation, $\beta = 0$, and the above equation simplifies to

$$\cos\theta_z = \cos\phi\cos\delta\cos\omega + \sin\phi\sin\delta \tag{A.8}$$

The calculation of hourly radiation on the tilted surface of a collector from estimates or measurements of hourly radiation on a horizontal surface is required to design or measure the performance of a solar power plant. A means of converting the data available for global and diffuse radiation on a horizontal surface to beam and diffuse on the plane of the collector is required. The geometric factor R_b, provides a ratio of beam radiation on a tilted surface and beam radiation on the horizontal at any instant. It can be calculated by appropriate use of the two equations above.

The ratio is:

$$R_b = \frac{\cos\theta}{\cos\theta_z} \tag{A.9}$$

In order to calculate radiation received at the earth's surface, a convenient normalizing radiation level is required. This normalizing factor is the theoretically possible radiation available if there were no atmosphere, namely extraterrestrial radiation.

A method of calculating extraterrestrial radiation will allow the estimation of average solar radiation and determination of the distribution of sunshine and cloudiness from measurements of total solar radiation on a horizontal surface.

Considering a horizontal plane outside the atmosphere, the solar radiation impinging it at any instant is the solar radiation given by Equation A.1 divided by R_b:

$$G_o = G_{sc}\left(1 + 0.033\cos\frac{360n}{365}\right)\cos\theta_z \tag{A.10}$$

Combining this equation with the fifth equation in this section yields G_o on a horizontal surface at any instant between sunrise and sunset:

$$G_o = G_{sc}\left(1 + 0.033\cos\frac{360n}{365}\right)\left(\cos\phi\cos\delta\cos\omega + \sin\phi\sin\delta\right) \tag{A.11}$$

Frequently the daily extraterrestrial radiation on a horizontal surface, H_o is required to calculate daily solar radiation. By integrating the above equation over the period from sunrise to sunset, H_o is acquired. If G_{sc} is in W/m^2, then H_o in J/m^2 is given by:

$$H_o = \frac{24 \times 3600 G_{sc}}{\pi}\left(1 + 0.033\cos\frac{360n}{365}\right) \times \left(\cos\phi\cos\delta\sin\omega_s + \frac{\pi\omega_s}{180}\sin\phi\sin\delta\right) \quad \text{(A.12)}$$

ω_s is the sunset hour angle in degrees, given by the following Equation:

$$\cos\omega_s = -\tan\phi\tan\delta \quad \text{(A.13)}$$

Another useful ratio, the clearness index, is the ratio of solar radiation at the surface of the earth and extraterrestrial radiation. It is most useful to consider clearness indices over a period of time. The most granular data used in this study consider radiation over the period of an hour, and is subsequently summed up into days and then into months. The clearness indices for each of these periods are defined below:

The hourly clearness index, k_T, is:

$$k_T = \frac{I}{I_o} \quad \text{(A.14)}$$

Where I_o is given by:

$$I_o = \frac{12 \times 3600}{\pi} G_{sc}\left(1 + 0.033\cos\frac{360n}{365}\right) \times \left[\cos\phi\cos\delta(\sin\omega_2 - \sin\omega_1) + \frac{\pi(\omega_2 - \omega_1)}{180}\sin\phi\sin\delta\right] \quad \text{(A.15)}$$

and I is the total hourly solar radiation measured on a horizontal surface.

The daily clearness index, K_T, is defined as the ratio of a particular day's radiation to the extraterrestrial radiation for that day. It is given by:

$$K_T = \frac{H}{H_o} \quad \text{(A.16)}$$

The monthly average clearness index, $\bar{K}_T$, is:

$$\bar{K}_T = \frac{\bar{H}}{\bar{H}_o} \quad \text{(A.17)}$$

where $\bar{H}$ is the average monthly daily solar radiation on a horizontal surface and $\bar{H}_o$ is the monthly averaged daily extraterrestrial solar radiation. $\bar{K}_T$ values vary due to site location and season. The literature suggests the variance lies between 0.3 for a very overcast climate to 0.8

for a very sunny climate. The National Aeronautics and Space Administration (NASA) Surface meteorology and Solar Energy (SSE) dataset provides a monthly average clearness index for Upington of 0.65. Calculating $\overline{K}_T$ from the hourly pyranometer readings from the South African Weather Service (SAWS) measurement station in Upington results in an average value of 0.69.

The I, H, $\overline{H}$ data used to calculate the clearness indices above are from measurements of total solar radiation on a horizontal surface, which tend to be pyranometer measurements. Pyranometers are instruments which measure global (beam plus diffuse) and diffuse radiation. Most available ground-station-measured solar radiation data are obtained from these instruments. Hulstrom (1989) and Duffie and Beckman (2006) provide a detailed discussion of the detection mechanisms and calibration standards of pyranometers in use. One of the datasets used in this study was collected by Kipp and Zonen Model CM5 pyranometers.

APPENDIX B: SOLAR DATA CALCULATIONS

This appendix contains data and calculations for quantifying the solar resource at Upington, using the six data sources discussed in chapter 3. A summary of the spreadsheets created in Microsoft Excel to perform the calculations and error checks is provided.

SAWS calculations

As the dataset and the calculations performed in it were too large to incorporate in this appendix, a summary of the results of the calculations is provided in the tables below. The full dataset is included on the CD provided with the dissertation.

Table B1: Average daily H_b energy per month [kWh/m²/day]

Average Daily H_b Energy per month [kWh/m²/day]										
	1966	1967	1980	1981	1982	1985	1986	1987	1989	1990
Jan	4.898	6.786	7.417	7.919	7.763	6.214	6.604	8.049	6.014	6.865
Feb	6.018	5.971	5.873	6.316	5.648	6.633	6.819	5.189	5.486	5.839
Mar	5.505	4.717	4.650	5.691	4.869	5.421	5.032	5.516	5.234	5.265
Apr	3.471	4.180	4.611	4.518	3.855	3.727	4.387	3.977	3.105	4.08
May	3.067	3.105	3.962	3.344	3.684	3.44	3.911	3.511	3.363	3.607
Jun	2.563	2.768	2.738	3.33	3.056	3.406	2.806	3.122	3.215	2.898
Jul	3.434	3.443	3.563	3.385	3.145	3.487	3.271	3.183	3.064	3.3
Aug	3.955	4.123	3.176	3.58	4.153	4.223	3.689	4.304	3.796	4.094
Sep	5.069	4.709	4.613	5.804	4.427	5.036	4.789	4.209	4.721	4.891
Oct	4.627	6.376	7.672	5.993	5.568	4.857	4.838	5.587	5.896	6.244
Nov	7.082	6.634	6.813	7.171	7.438	6.028	6.875	6.418	6.578	6.888
Dec	7.037	6.847	7.554	7.892	7.172	6.558	7.978	7.729	7.412	7.26

Table B2: Average DNI per month [kWh/m²/day]

Average DNI per month [kWh/m²/day]										
	1966	1967	1980	1981	1982	1985	1986	1987	1989	1990
Jan	7.029	9.768	10.173	11.435	11.119	8.100	9.276	11.641	8.508	9.148
Feb	9.193	8.895	8.706	9.301	8.374	10.083	10.497	7.745	7.624	8.677
Mar	10.104	8.715	9.055	12.238	8.843	13.095	11.447	11.615	9.022	8.3
Apr	6.294	7.643	8.014	8.050	6.956	6.502	7.849	7.278	5.562	7.145
May	7.959	7.240	8.999	7.606	8.647	7.708	8.946	7.906	7.331	7.869
Jun	8.851	8.339	7.912	10.067	9.083	9.874	8.483	9.446	9.251	8.074
Jul	9.424	9.039	9.088	8.663	7.937	9.019	8.368	8.206	7.654	8.228
Aug	8.132	8.176	5.996	7.307	8.112	8.165	7.268	8.516	7.366	7.872
Sep	10.272	10.179	7.194	10.771	8.200	8.783	10.757	7.984	11.086	7.893
Oct	7.431	10.600	12.873	9.714	8.510	7.215	7.622	8.889	9.543	9.84
Nov	10.385	9.646	9.694	10.349	10.742	8.479	10.376	9.184	9.551	9.387
Dec	9.782	9.707	9.585	10.995	10.306	8.271	11.307	11.077	10.364	9.636
Annual	8.738	8.996	8.941	9.708	8.902	8.774	9.350	9.124	8.572	8.506

Table B3: Total annual DNI [kWh/m²/annum]

	1966	1967	1980	1981	1982	1985	1986	1987	1989	1990
Annual DNI	3095	3284	3267	3544	3241	3200	3399	3337	3076	2987

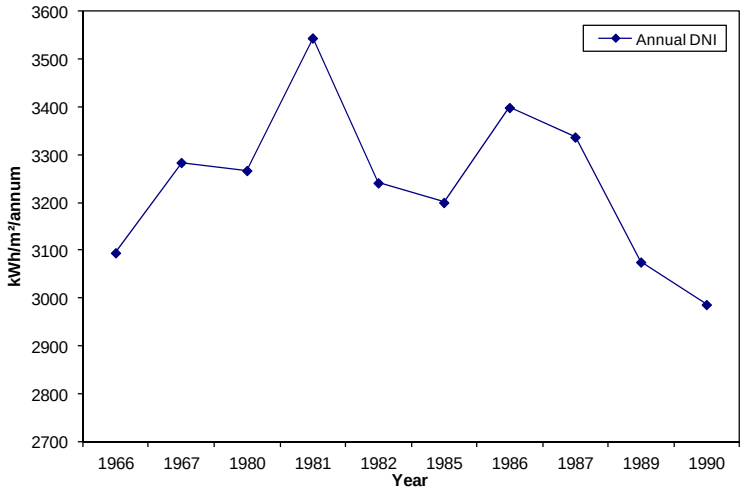

Figure B1: Total annual DNI [kWh/m²/annum]

Table B4: Average monthly DNI [kWh/m²/day]

	Jan	Feb	Mar	Apr	May	Jun	Jul	Aug	Sep	Oct	Nov	Dec
1966	7.029	9.193	10.104	6.294	7.959	8.851	9.424	8.132	10.272	7.431	10.385	9.782
1967	9.768	8.895	8.715	7.643	7.24	8.339	9.039	8.176	10.179	10.600	9.646	9.707
1981	11.435	9.301	12.238	8.05	7.606	10.067	8.663	7.307	10.771	9.714	10.349	10.995
1982	11.119	8.374	8.843	6.956	8.647	9.083	7.937	8.112	8.2	8.510	10.742	10.306
1986	9.276	10.497	11.447	7.849	8.946	8.483	8.368	7.268	10.757	7.622	10.376	11.307
1987	11.641	7.745	11.615	7.278	7.906	9.446	8.206	8.516	7.984	8.889	9.184	11.077
1989	8.508	7.624	9.022	5.562	7.331	9.251	7.654	7.366	11.086	9.543	9.551	10.364
1990	9.148	8.677	8.3	7.145	7.869	8.074	8.228	7.872	7.893	9.840	9.387	9.636
Ave	9.741	8.788	10.036	7.097	7.938	8.949	8.44	7.844	9.643	9.019	9.952	10.397

NREL CSR calculations

The NREL CSR model required a cell ID and then provided the results based on the cell ID entered. The cell was located on the map provided, and the results for the cell located in the Upington area are provided below.

Table B5: Average monthly direct, global, latitude tilt and diffuse irradiance [Wh/m²/day]

Enter Cell Id ->	**1402285**																
	Return Cell	Longitude	Latitude														
Month				Jan	Feb	Mar	Apr	May	Jun	Jul	Aug	Sep	Oct	Nov	Dec	Annual
Direct	1402285	21.083	-28.59	8859	7710	7325	6488	6899	6143	6430	7274	7364	6959	8502	8912	7405
Global	1402285	21.083	-28.58	8173	7264	6341	4997	4138	3569	3776	4720	5854	6876	7876	8272	5988
Latitude Tilt	1402285	21.083	-28.59	7424	7237	7176	6489	6155	5632	5817	6509	7020	7196	7376	7320	6779
Diffuse	1402285	21.083	-28.59	1869	1897	1598	1299	763	800	754	802	1283	2019	1833	1878	1399

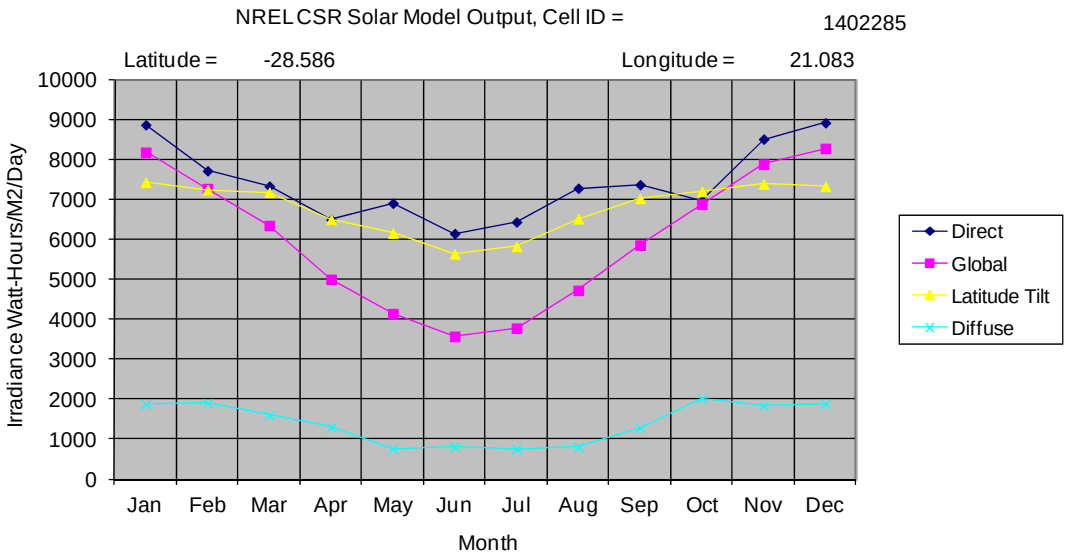

Figure B2: Average monthly direct, global, latitude tilt and diffuse irradiance [Wh/m²/day]

NASA SSE calculations

Once the desired data were obtained from the NASA SSE website they were organised in the following tables and graphs.

Table B6: Monthly averaged insolation incident on a horizontal surface [kWh/m^2/day]

Monthly Averaged Insolation Incident On A Horizontal Surface (kWh/m^2/day)													
Year	Jan	Feb	Mar	Apr	May	Jun	Jul	Aug	Sep	Oct	Nov	Dec	Annual
1983	n/a	n/a	n/a	n/a	n/a	n/a	3.49	4.85	5.67	6.87	7.09	7.68	n/a
1984	8.5	7.6	5.72	4.67	3.7	3.25	3.82	4.48	5.94	6.84	8.07	8.78	5.94
1985	7.6	6.19	6.06	4.59	3.89	3.34	3.64	4.65	5.73	6.56	7.37	7.72	5.61
1986	7.77	7.73	5.86	4.51	3.82	3.1	3.39	4.15	5.56	6.38	7.43	8.41	5.66
1987	8.59	6.99	6.13	4.36	3.7	3.25	3.45	4.51	5.22	6.76	7.44	8.36	5.73
1988	8.01	6.39	5.34	4.28	3.52	3.51	3.96	4.15	5.6	7.21	7.14	7.46	5.55
1989	7.56	6.75	6.05	3.98	3.71	3.2	3.93	4.93	5.45	7.07	7.8	8.64	5.76
1990	8.09	7.27	6	4.35	4.3	3.54	3.88	4.88	5.81	7.32	7.9	8.1	5.95
1991	7.51	7.23	5.59	5.1	4.31	3.48	3.98	5.03	5.37	6.54	7.46	7.4	5.74
1992	8.31	6.97	6.25	4.84	4.48	3.82	4.11	4.97	5.95	6.99	8.2	8.96	6.15
1993	8.24	6.95	5.75	4.64	4.22	3.78	3.74	4.76	6.32	6.58	7.62	8.42	5.91
1994	7.44	6.4	6.08	4.89	4.18	3.76	4.13	4.93	5.73	6.88	7.53	8.87	5.9
1995	8.24	7.24	5.53	5.28	4	3.73	4.07	5.14	5.42	6.83	7.5	8.04	5.91
1996	7.54	7.01	6.22	4.99	4.22	3.85	3.74	5.1	6.04	6.32	7.26	8.53	5.9
1997	7.7	7.08	5.85	5.47	4.08	3.64	4.06	5.07	6.14	6.76	8.52	7.88	6.01
1998	8.08	6.82	5.79	5.51	4.17	3.96	3.8	4.72	6.08	7.24	8.18	8.24	6.05
1999	7.82	7.16	6.09	5.18	3.61	3.79	3.94	5.17	5.93	6.7	8.02	7.38	5.89
2000	7.49	6.67	5.93	5.2	4.45	3.84	4.08	4.91	5.57	6.7	7.85	8.01	5.89
2001	8.3	7.13	6.54	4.67	4.33	3.83	3.91	4.96	5.75	7.11	6.88	8.2	5.96
2002	8.09	7.29	5.9	4.75	3.92	3.75	4.15	4.73	6.29	6.89	7.95	8.21	5.99
2003	7.96	6.62	6.31	4.74	4.08	4.01	4.13	4.83	5.5	6.12	8.09	8.81	5.93
2004	7.77	6.86	6.04	5.02	4.09	3.85	4.11	5.06	6.09	6.58	7.2	8.58	5.94
2005	7.78	6.78	5.83	4.83	3.92	3.68	4.27	4.69	6.15	6.48	7.75	8.58	5.89
1983 - 2005	7.93	6.96	5.95	4.81	4.03	3.64	3.9	4.81	5.8	6.77	7.66	8.23	5.87
Min % Dif	-6	-11	-10	-18	-13	-15	-13	-14	-10	-10	-10	-10	-12
Max % Dif	8	10	9	13	10	9	8	7	8	7	10	8	9

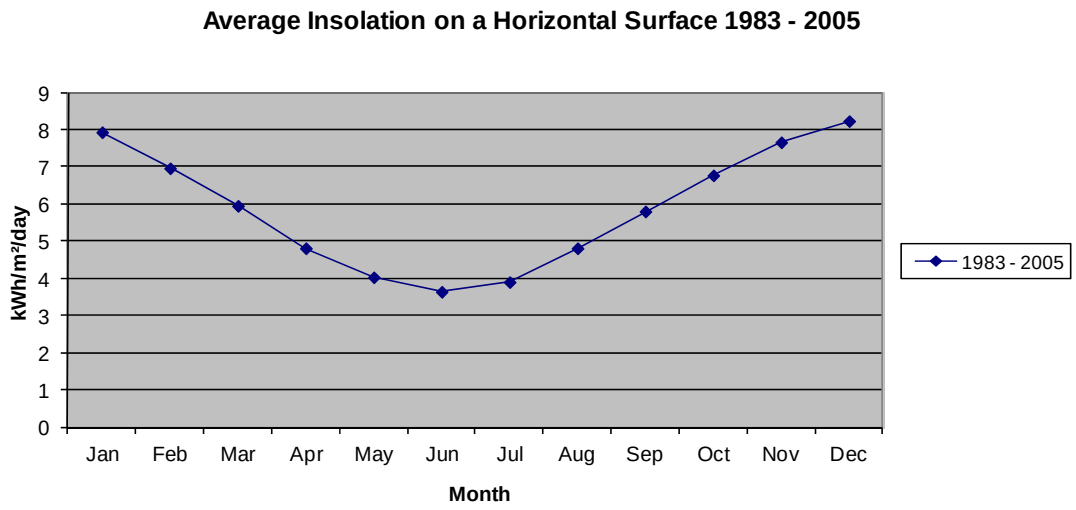

Figure B3: Monthly averaged insolation incident on a horizontal surface [kWh/m^2/day]

Table B7: Monthly averaged insolation clearness index [0 to 1.0]

Monthly Averaged Insolation Clearness Index (0 to 1.0)													
Year	Jan	Feb	Mar	Apr	May	Jun	Jul	Aug	Sep	Oct	Nov	Dec	Annual
1983	n/a	n/a	n/a	n/a	n/a	n/a	0.61	0.7	0.65	0.66	0.61	0.63	n/a
1984	0.71	0.69	0.6	0.61	0.6	0.6	0.66	0.64	0.68	0.66	0.7	0.73	0.66
1985	0.64	0.56	0.64	0.6	0.63	0.62	0.63	0.67	0.66	0.63	0.64	0.64	0.63
1986	0.65	0.7	0.62	0.58	0.62	0.57	0.59	0.6	0.64	0.62	0.64	0.69	0.63
1987	0.72	0.63	0.64	0.56	0.6	0.6	0.6	0.65	0.6	0.65	0.64	0.69	0.63
1988	0.67	0.58	0.56	0.56	0.57	0.65	0.69	0.59	0.64	0.69	0.62	0.62	0.62
1989	0.63	0.62	0.64	0.52	0.6	0.59	0.68	0.71	0.63	0.68	0.67	0.71	0.64
1990	0.68	0.66	0.63	0.57	0.7	0.65	0.68	0.7	0.67	0.71	0.68	0.67	0.67
1991	0.63	0.66	0.59	0.66	0.7	0.64	0.69	0.72	0.62	0.63	0.64	0.61	0.65
1992	0.7	0.63	0.66	0.63	0.73	0.7	0.71	0.71	0.68	0.67	0.71	0.74	0.69
1993	0.69	0.63	0.61	0.6	0.69	0.7	0.65	0.68	0.73	0.63	0.66	0.7	0.66
1994	0.62	0.58	0.64	0.64	0.68	0.69	0.72	0.7	0.66	0.66	0.65	0.73	0.67
1995	0.69	0.66	0.58	0.68	0.65	0.69	0.71	0.74	0.63	0.66	0.65	0.66	0.67
1996	0.63	0.64	0.65	0.65	0.69	0.71	0.65	0.73	0.69	0.61	0.63	0.7	0.67
1997	0.65	0.64	0.62	0.71	0.66	0.67	0.71	0.72	0.7	0.65	0.74	0.65	0.68
1998	0.68	0.62	0.61	0.72	0.68	0.73	0.66	0.68	0.7	0.7	0.71	0.68	0.68
1999	0.66	0.65	0.64	0.67	0.59	0.7	0.69	0.74	0.69	0.65	0.69	0.61	0.66
2000	0.63	0.61	0.63	0.68	0.72	0.71	0.71	0.7	0.64	0.65	0.68	0.66	0.67
2001	0.7	0.65	0.69	0.61	0.7	0.71	0.68	0.71	0.66	0.69	0.59	0.68	0.67
2002	0.68	0.66	0.62	0.62	0.64	0.69	0.72	0.68	0.72	0.67	0.69	0.68	0.67
2003	0.67	0.6	0.66	0.62	0.66	0.74	0.72	0.69	0.64	0.59	0.7	0.73	0.67
2004	0.65	0.62	0.64	0.66	0.67	0.71	0.71	0.72	0.7	0.63	0.62	0.71	0.67
2005	0.65	0.62	0.62	0.63	0.64	0.68	0.74	0.67	0.71	0.63	0.67	0.71	0.66
1983 - 2005	0.67	0.63	0.63	0.63	0.66	0.67	0.68	0.69	0.67	0.65	0.66	0.68	0.66
Min Dif	-0.04	-0.07	-0.06	-0.11	-0.08	-0.1	-0.09	-0.1	-0.07	-0.06	-0.07	-0.07	-0.08
Max Dif	0.06	0.07	0.06	0.09	0.07	0.07	0.06	0.05	0.06	0.05	0.07	0.06	0.07

Table B8: Monthly averaged beam radiation (averaged insolation incident on a horizontal surface multiplied by insolation clearness index)

Monthly Averaged Beam Radiation (Averaged Insolation Incident On A Horizontal Surface*Insolation Clearness Index)												
Year	Jan	Feb	Mar	Apr	May	Jun	Jul	Aug	Sep	Oct	Nov	Dec
1983 - 2005	5.31	4.38	3.75	3.03	2.66	2.44	2.65	3.32	3.89	4.4	5.06	5.6

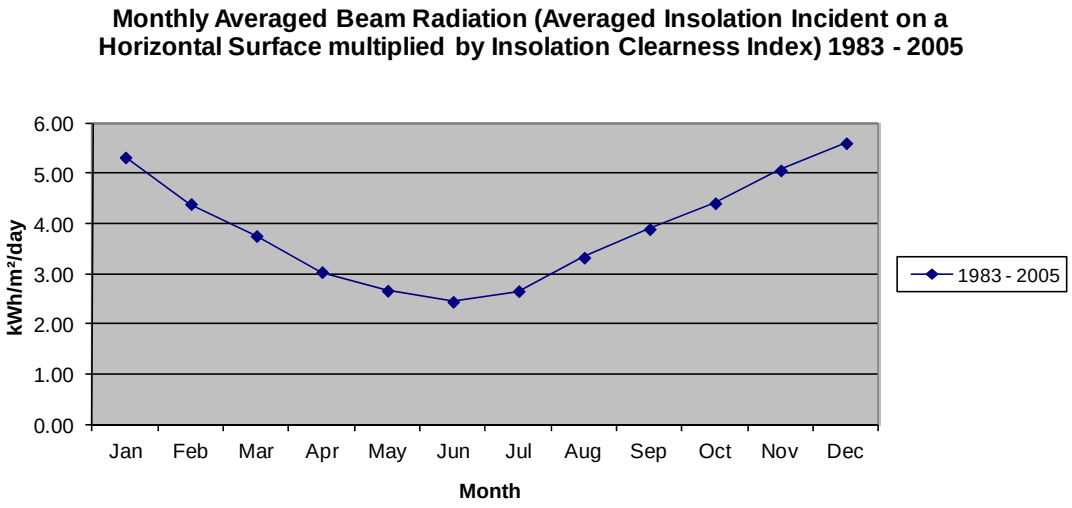

Figure B4: Monthly averaged beam radiation (averaged insolation incident on a horizontal surface multiplied by insolation clearness index)

Table B9: Monthly averaged direct normal radiation [kWh/m^2/day]

Monthly Averaged Direct Normal Radiation (kWh/m^2/day)													
Lat -28.4 Lon 21.3	Jan	Feb	Mar	Apr	May	Jun	Jul	Aug	Sep	Oct	Nov	Dec	Annual Average
22-year Average	8.62	7.47	6.86	6.38	6.52	6.54	6.79	7.4	7.36	7.67	8.34	9.02	7.42

Table B10: Monthly averaged insolation incident on a horizontal surface [kWh/m^2/day]

Monthly Averaged Insolation Incident On A Horizontal Surface (kWh/m^2/day)													
Lat -28.4 Lon 21.3	Jan	Feb	Mar	Apr	May	Jun	Jul	Aug	Sep	Oct	Nov	Dec	Annual Average
22-year Average	7.93	6.96	5.95	4.8	4.03	3.63	3.89	4.82	5.78	6.78	7.66	8.21	5.86

Table B11: Monthly averaged diffuse radiation incident on a horizontal surface [kWh/m^2/day]

Monthly Averaged Diffuse Radiation Incident On A Horizontal Surface (kWh/m^2/day)												
Year	Jan	Feb	Mar	Apr	May	Jun	Jul	Aug	Sep	Oct	Nov	Dec
1983 - 2005	5.93	5.04	4.36	3.59	3.18	2.94	3.17	3.94	4.5	5.1	5.72	6.22

Table B12: Monthly averaged diffuse radiation incident on a horizontal surface [kWh/m^2/day]

Monthly Averaged Diffuse Radiation Incident On A Horizontal Surface (kWh/m^2/day)													
Lat - 28.4 Lon 21.3	Jan	Feb	Mar	Apr	May	Jun	Jul	Aug	Sep	Oct	Nov	Dec	Annual Average
22-year Average	2	1.92	1.59	1.21	0.85	0.69	0.72	0.88	1.28	1.68	1.94	1.99	1.39
Minimum	1.69	1.57	1.33	0.87	0.61	0.48	0.58	0.68	1.01	1.42	1.52	1.62	1.11
Maximum	2.2	2.17	1.8	1.47	1.05	0.91	0.94	1.17	1.51	1.93	2.23	2.32	1.64
22-year Average K	0.66	0.63	0.62	0.62	0.65	0.66	0.67	0.68	0.66	0.65	0.66	0.67	0.65
Minimum K	0.62	0.56	0.56	0.51	0.57	0.57	0.58	0.59	0.6	0.59	0.59	0.6	0.58
Maximum K	0.72	0.7	0.68	0.71	0.72	0.73	0.72	0.73	0.72	0.7	0.73	0.73	0.72

Table B13: Monthly averaged direct normal radiation [kWh/m^2/day]

Monthly Averaged Direct Normal Radiation (kWh/m^2/day)												
Year	Jan	Feb	Mar	Apr	May	Jun	Jul	Aug	Sep	Oct	Nov	Dec
1983 - 2005	8.62	7.47	6.86	6.38	6.52	6.54	6.79	7.4	7.36	7.67	8.34	9.02

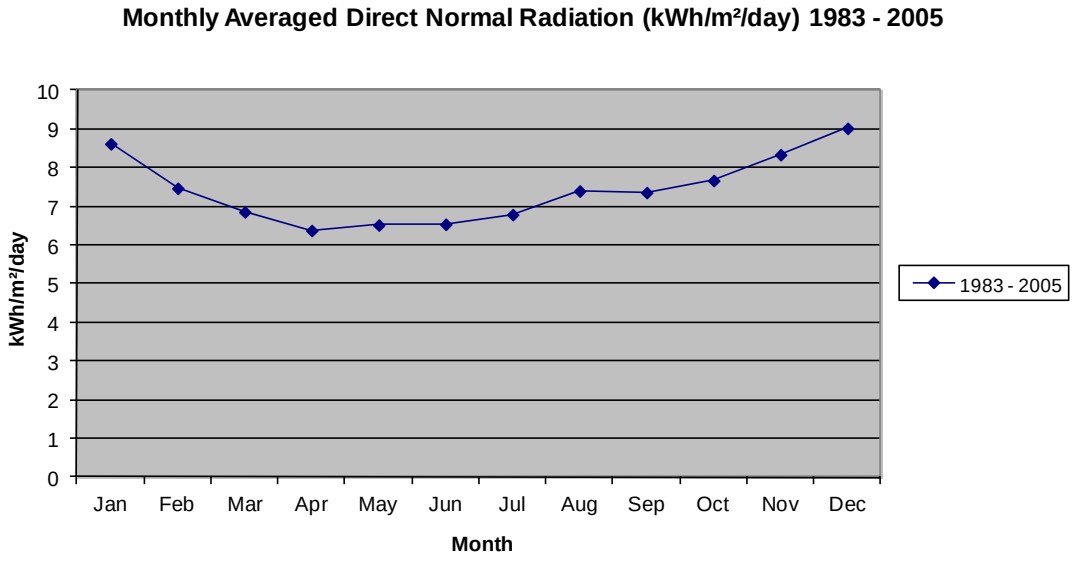

Figure B5: Monthly averaged direct normal radiation [kWh/m^2/day] 1983 - 2005

Table B14: Monthly averaged average, diffuse and direct normal radiation

Year	Jan	Feb	Mar	Apr	May	Jun	Jul	Aug	Sep	Oct	Nov	Dec	
Average Insolation	7.93	6.96	5.95	4.81	4.03	3.64	3.9	4.81	5.8	6.77	7.66	8.23	
Diffuse	2	1.92	1.59	1.21	0.85	0.69	0.72	0.88	1.28	1.68	1.94	1.99	Sum
Direct Normal Radiation	8.62	7.47	6.86	6.38	6.52	6.54	6.79	7.4	7.36	7.67	8.34	9.02	88.97
Monthly	267.22	209.16	212.66	191.4	202.12	196.2	210.49	229.4	220.8	237.77	250.2	279.62	2707.04

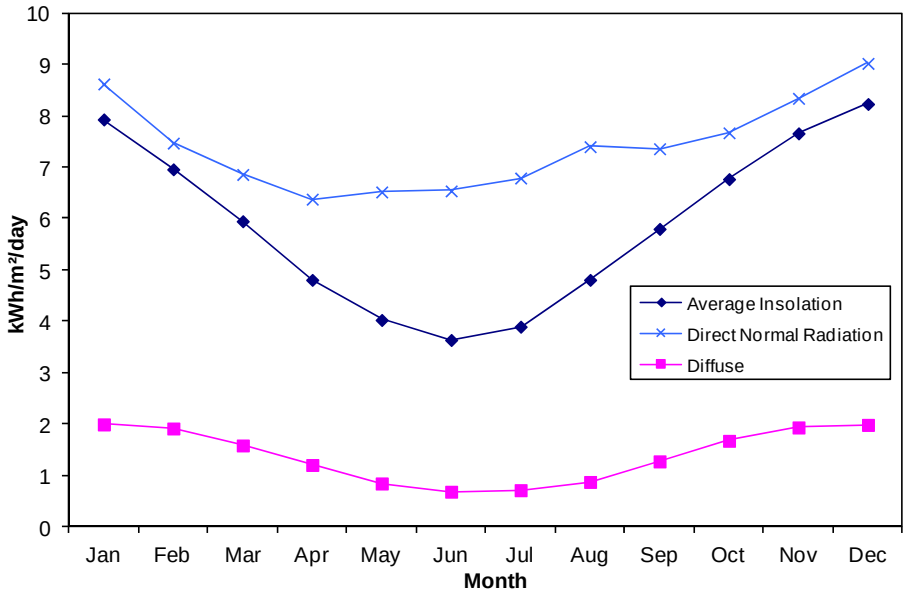

Figure B6: Monthly averaged average, diffuse and direct normal radiation [kWh/m^2/day]

Eskom data calculations

The Eskom data required numerous checks and manipulations to transform them into a final usable form. The tables below show the results of the calculations performed for every hour for each year of data.

Summary of data as-is:

Table B15: Summary of Eskom 2007, 2008 and 2009 monthly averaged DNI data as-is

	Jan	Feb	Mar	Apr	May	Jun	Jul	Aug	Sep	Oct	Nov	Dec
2007	0.008	0	0	0	0	0	5.403	1.449	0	5.711	9.744	1.741
2008	6.426	6.177	3.006	6.596	5.214	5.509	5.545	5.238	7.121	8.547	9.682	9.576
2009	10.343	6.152	7.322	6.384	5.766	1.826	5.903	4.906	6.759	6.891	9.377	11.149
Average	5.592	4.11	3.443	4.327	3.66	2.445	5.617	3.864	4.627	7.05	9.601	7.489

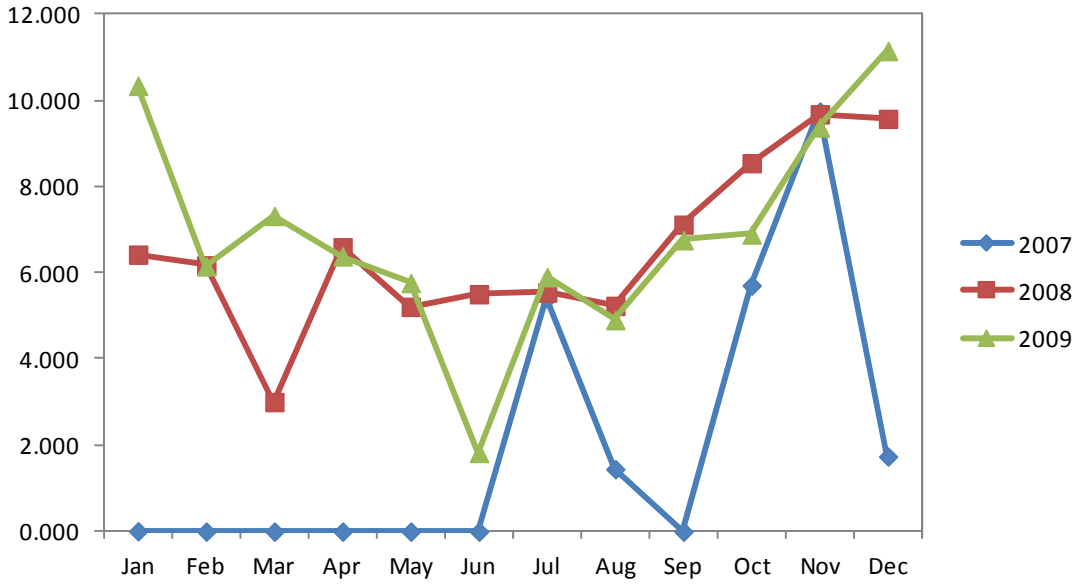

Figure B7: Summary of Eskom 2007, 2008 and 2009 monthly averaged DNI data as-is

The second part was correcting the years of usable data. The DNI data for 2007 were discarded. The DNI data for 2008 and 2009 were then analysed and all the missing datapoints were inserted with a zero value. Summary of corrected data:

Table B16: Summary of Eskom 2008 and 2009 corrected monthly averaged DNI data

	Jan	Feb	Mar	Apr	May	Jun	Jul	Aug	Sep	Oct	Nov	Dec
2008	6.426	6.177	3.0063	6.596	5.214	5.509	5.545	5.238	7.121	8.547	9.682	9.576
2009	10.343	6.152	7.3221	6.384	5.766	1.826	5.903	4.906	6.759	6.891	9.377	11.149
Average	8.384	6.165	5.1642	6.490	5.49	3.667	5.724	5.072	6.94	7.719	9.53	10.363

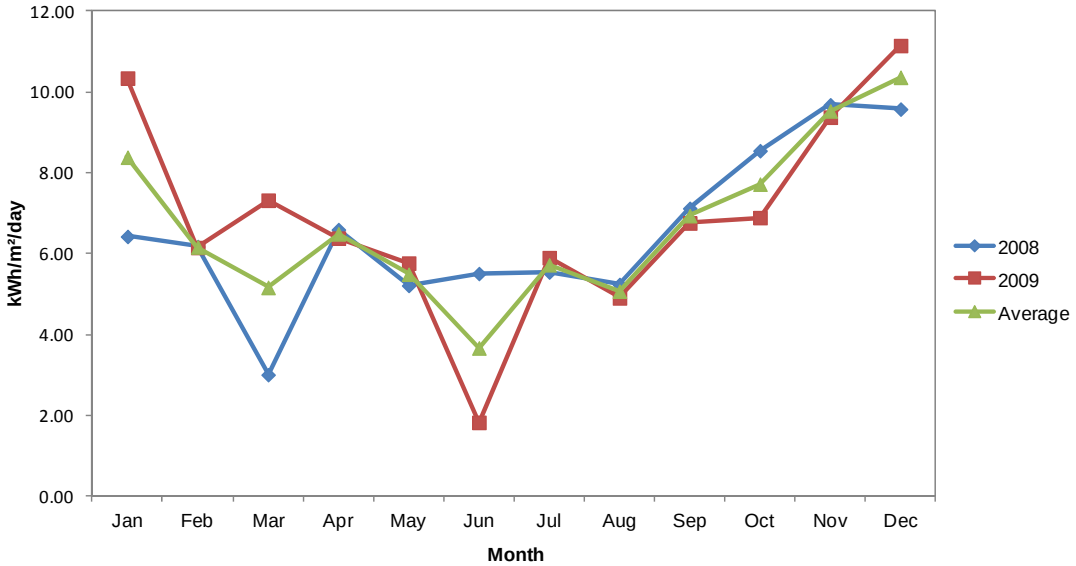

Figure B8: Summary of Eskom 2008 and 2009 corrected monthly averaged DNI data

The third part was introducing a synthetic average to replace the zero DNI values in the DNI data for 2008 and 2009. The first step of this process was generating an average hourly DNI value for each hour of the specific month with missing measurements. This step was done for

five months – June 2008, July 2008, September 2008, May 2009 and June 2009. Once the averages were computed they were used to replace all the zero value place holders for missing measurements in the annual calculation. Comparison of corrected data and data with synthetic (artificial) average:

Table B17: Summary of Eskom 2008 and 2009 corrected and artificially averaged monthly averaged DNI data

	Jan	Feb	Mar	Apr	May	Jun	Jul	Aug	Sep	Oct	Nov	Dec
2008 Corrected	6.426	6.177	3.0063	6.596	5.214	5.509	5.545	5.238	7.121	8.547	9.682	9.576
2009 Corrected	10.343	6.152	7.3221	6.384	5.766	1.826	5.903	4.906	6.759	6.891	9.377	11.149
2008 Artificial Average	6.426	6.177	3.0063	6.596	5.214	5.51	5.55	5.238	7.15	8.547	9.682	9.576
2009 Artificial Average	10.343	6.152	7.3221	6.384	6.166	4.578	5.903	4.906	6.759	6.891	9.377	11.149
Average	8.384	6.165	5.1642	6.49	5.59	4.356	5.725	5.072	6.947	7.719	9.53	10.363

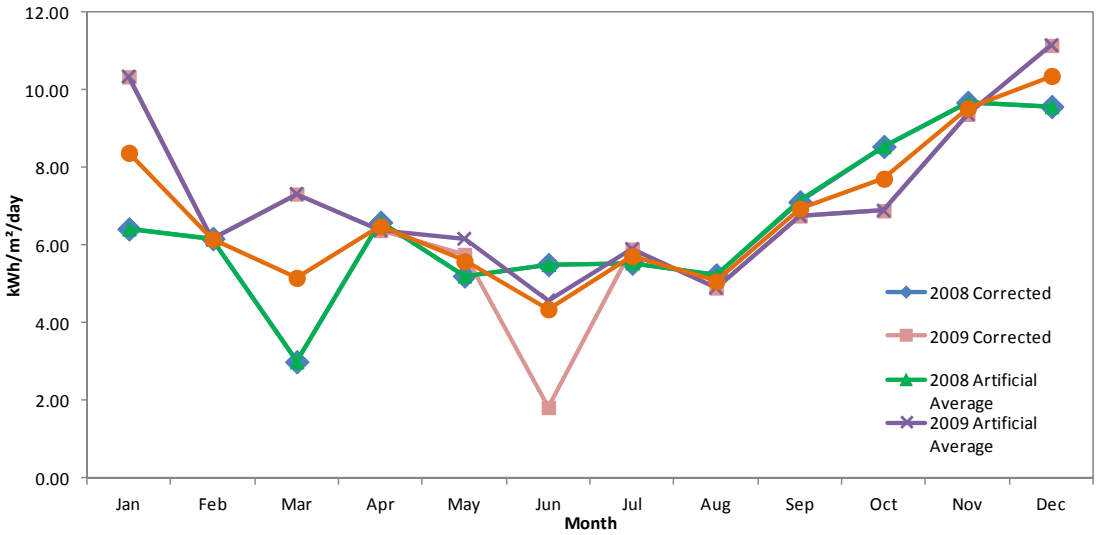

Figure B9: Summary of Eskom 2008 and 2009 corrected and artificially averaged monthly averaged DNI data

Summary of data with synthetic average:

Table B18: Summary of Eskom 2008 and 2009 synthetically averaged monthly averaged DNI data

	Jan	Feb	Mar	Apr	May	Jun	Jul	Aug	Sep	Oct	Nov	Dec
2008 Synthetic Average	6.426	6.177	3.006	6.596	5.214	5.51	5.55	5.238	7.15	8.547	9.682	9.576
2009 Synthetic Average	10.343	6.152	7.322	6.384	6.166	4.578	5.903	4.906	6.759	6.891	9.377	11.149
Average	8.384	6.165	5.164	6.49	5.69	5.044	5.727	5.072	6.955	7.719	9.53	10.363

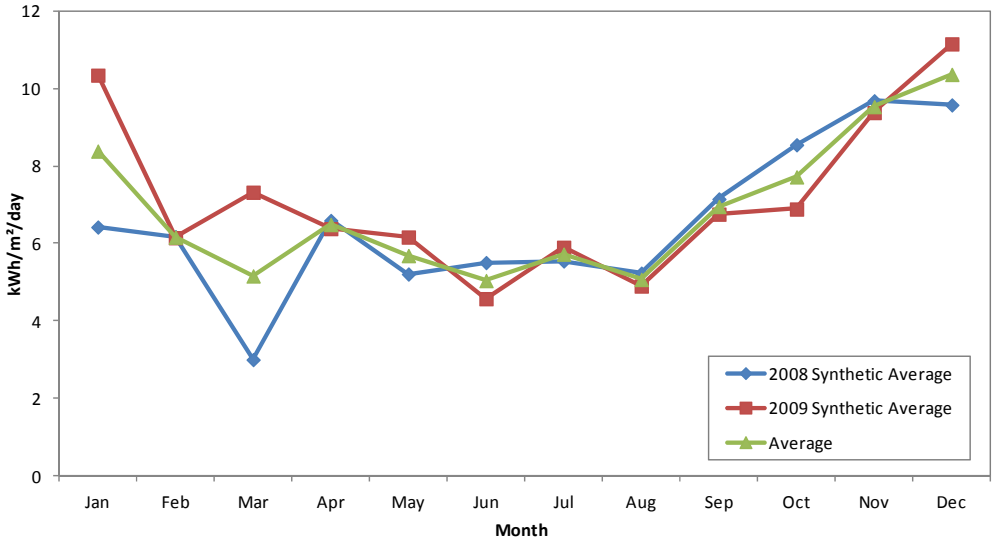

Figure B10: Summary of Eskom 2008 and 2009 synthetically averaged monthly averaged DNI data

Weather Analytics data calculations

The global horizontal radiation, direct normal radiation and diffuse radiation provided by Weather Analytics Inc. were summed into monthly averages. A summary of the calculation follows. These data were used for Figure 3-7 in section 2.3.5.

Table B35: Summary of Weather Analytics monthly averaged GHI, DNI and DHI

Weather Analytics	Jan	Feb	Mar	Apr	May	Jun	Jul	Aug	Sep	Oct	Nov	Dec
Global Horizontal Radiation	8.29	7.174	6.287	5.363	4.335	3.805	3.989	5.139	6.417	7.34	8.305	8.734
Direct Normal Radiation	8.954	7.533	7.448	7.185	6.902	6.661	6.608	7.653	8.490	8.55	9.497	9.612
Diffuse Horizontal Radiation	1.982	1.888	1.506	1.21	0.915	0.773	0.85	0.975	1.155	1.581	1.693	1.898

CRSES data calculations

The METEONORM calculated global horizontal radiation, direct normal radiation and diffuse radiation provided by CSRES were summed into monthly averages. A summary of the calculation follows. These data were used for Figure 3-8 in section 2.3.6.

Table B39: Summary of CRSES monthly averaged GHI, DNI and DHI

CRSES	Jan	Feb	Mar	Apr	May	Jun	Jul	Aug	Sep	Oct	Nov	Dec
Global Horizontal Radiation	8.461	7.345	6.264	5.231	4.32	3.768	4.174	5.088	6.216	7.320	8.374	8.52
Direct Normal Radiation	8.64	7.848	6.846	6.935	6.458	6.069	6.806	7.817	8.130	8.26	9.63	9.344
Diffuse Horizontal Radiation	2.609	1.902	1.81	1.292	0.883	0.82	0.728	0.806	1.158	1.595	1.668	1.971

APPENDIX C: CLIMATE INPUT FILE DESCRIPTION

The climate input files required by SAM to simulate the technologies investigated in this study require a year of hourly readings of certain meteorological measurements. Four datasets were used to model each of the four technologies evaluated in this study. The measurements or data estimates used in these four climate input files are available on the included CD. A sample of the data format is provided below. This sample contains only the header information and the first two days of data of each file. The complete climate input file used in the SAM simulations is on the included CD. The data in each climate file may be used to create a TMY3 file in SAM for further modelling and analysis.

Table C1: Header information and first two days of METEONORM climate input file from CSRES

		Latitude {N+/S-}	Longitude {E+/W-}	TimeZone {+/- GMT}	Elevation {m}						
LOCATION	Upington	-28.42	21.2582	2	848						
DESIGN CONDITIONS	0										
TYPICAL/EXTREME PERIODS	0										
		Ground Temp Depth {m}									
GROUND TEMPERATURES	1	1									
Jan {C}	Feb{C}	Mar {C}	Apr {C}	May {C}	Jun {C}	Jul {C}	Aug {C}	Sept {C}	Oct {C}	Nov {C}	Dec {C}
23.6	25.1	25.6	25.1	23.6	21.6	19.5	18	17.5	18	19.5	21.6
HOLIDAYS/DAYLIGHT SAVINGS	No										
COMMENTS 1	METEONORM Version 6.0										
		Number of Intervals per Hour	DP Name/Descr	DP Start Day of Week	DP Start Day	DP End Day					
DATA PERIODS (DPs)	1	1	Data	Sunday	1-Jan	31-Dec					

Date	Hour	Global Horizontal Radiation {Wh/m2}	Direct Normal Radiation {Wh/m2}	Diffuse Horizontal Radiation {Wh/m2}	Dry Bulb Temp {C}	Dew Point Temp {C}	Relative Humidity {%}	Pressure {mbar}	Wind Speed {m/s}	Albedo {.01}
Saturday, January 01, 2005	1	0	0	0	27.9	22.7	73	918	2.4	-99
Saturday, January 01, 2005	2	0	0	0	28.9	22.7	69	918	2	-99
Saturday, January 01, 2005	3	0	0	0	28.3	22.7	72	918	1.8	-99
Saturday, January 01, 2005	4	0	0	0	28.7	22.7	70	918	2	-99
Saturday, January 01, 2005	5	0	0	0	28.9	22.7	69	918	2	-99
Saturday, January 01, 2005	6	1	0	1	29	22.7	69	918	2.3	-99
Saturday, January 01, 2005	7	109	196	78	30.2	22.7	64	918	1.9	-99
Saturday, January 01, 2005	8	71	0	71	30.6	22.7	63	918	2.5	-99
Saturday, January 01, 2005	9	66	0	66	30.7	22.7	62	918	2.3	-99
Saturday, January 01, 2005	10	237	19	223	31.5	22.7	60	918	3.6	-99
Saturday, January 01, 2005	11	79	0	79	31.2	22.7	61	918	3.2	-99
Saturday, January 01, 2005	12	386	42	346	32.7	22.7	56	918	3.2	-99
Saturday, January 01, 2005	13	823	311	514	34.9	22.7	49	918	3.4	-99
Saturday, January 01, 2005	14	492	82	412	35.5	22.7	48	919	3.8	-99
Saturday, January 01, 2005	15	740	325	447	36.9	18.7	34	919	3.4	-99
Saturday, January 01, 2005	16	646	376	353	37.8	14.7	26	919	4.5	-99
Saturday, January 01, 2005	17	370	126	292	37.3	18.7	34	919	3.6	-99
Saturday, January 01, 2005	18	217	60	191	35.6	22.7	47	919	3.8	-99
Saturday, January 01, 2005	19	109	115	84	34.9	22.7	49	919	3.2	-99
Saturday, January 01, 2005	20	16	0	16	35.2	22.7	49	920	3.4	-99
Saturday, January 01, 2005	21	0	0	0	33.3	22.7	54	920	3.4	-99
Saturday, January 01, 2005	22	0	0	0	33	22.7	55	920	2.5	-99
Saturday, January 01, 2005	23	0	0	0	31.8	22.7	59	920	2.1	-99
Saturday, January 01, 2005	24	0	0	0	30.5	22.7	63	920	1.9	-99
Sunday, January 02, 2005	1	0	0	0	28.9	22.7	69	921	1.7	-99
Sunday, January 02, 2005	2	0	0	0	27.2	22.7	76	921	2.7	-99
Sunday, January 02, 2005	3	0	0	0	26.3	22.7	80	921	4.3	-99
Sunday, January 02, 2005	4	0	0	0	25.4	21.8	80	921	3.8	-99
Sunday, January 02, 2005	5	0	0	0	24.8	21.1	80	921	3.6	-99
Sunday, January 02, 2005	6	0	0	0	24.6	21	80	921	3	-99
Sunday, January 02, 2005	7	137	639	37	26	22.3	80	922	3.4	-99
Sunday, January 02, 2005	8	387	881	64	28.1	22.7	72	922	2.4	-99
Sunday, January 02, 2005	9	641	997	78	30.5	22.7	63	922	2.8	-99
Sunday, January 02, 2005	10	859	1040	92	32.8	18.7	43	922	3	-99
Sunday, January 02, 2005	11	1053	926	245	35	14.7	30	922	3.8	-99
Sunday, January 02, 2005	12	722	267	466	35.6	10.7	22	923	3.4	-99
Sunday, January 02, 2005	13	754	200	555	36	7.5	17	923	4.8	-99
Sunday, January 02, 2005	14	688	153	539	36.1	7.5	17	923	5.2	-99
Sunday, January 02, 2005	15	650	183	485	36.1	8.4	18	923	4.3	-99
Sunday, January 02, 2005	16	544	205	385	35.8	8.8	19	923	5	-99
Sunday, January 02, 2005	17	445	242	296	35.3	9.1	20	924	4.3	-99
Sunday, January 02, 2005	18	278	156	212	34.3	10.3	23	924	4.5	-99
Sunday, January 02, 2005	19	116	151	84	33	9.2	23	924	2.8	-99
Sunday, January 02, 2005	20	2	0	2	31.6	9.9	26	924	2.1	-99
Sunday, January 02, 2005	21	0	0	0	29.9	12.7	35	924	1.6	-99
Sunday, January 02, 2005	22	0	0	0	28.2	13.5	40	924	1.2	-99
Sunday, January 02, 2005	23	0	0	0	26.6	12.9	43	925	0.9	-99
Sunday, January 02, 2005	24	0	0	0	24.9	13.5	49	925	0.6	-99

Table C2: Header information and first two days of Weather Analytics climate input file

		Latitude {N+/S-}	Longitude {E+/W-}	TimeZone {+/- GMT}	Elevation {m}
LOCATION	Upington	-28.566	21.25	2	826
DESIGN CONDITIONS	0				
TYPICAL/EXTREME PERIODS	0				
GROUND TEMPERATURES					
HOLIDAYS/DAYLIGHT SAVINGS	No				
COMMENTS 1	Weather Analytics - Sensor Point System data - based on the NOAA/NCEP Climate Forecast System Reanalysis (CFSR) model				

		Number of Intervals per Hour	DP Name/Descr	DP Start Day of Week	DP Start Day	DP End Day
DATA PERIODS (DPs)	1	1	Data	Sunday	1-Jan	31-Dec

Date	Hour	Global Horizontal Radiation {Wh/m2}	Direct Normal Radiation {Wh/m2}	Diffuse Horizontal Radiation {Wh/m2}	Dry Bulb Temp {C}	Dew Point Temp {C}	Relative Humidity {%}	Pressure {mbar}	Wind Speed {m/s}	Albedo {.01}
Sunday, January 01, 1995	1	0	0	0	14.6	1.4	43	915	5	999
Sunday, January 01, 1995	2	0	0	0	14.2	2.3	52	916	6	999
Sunday, January 01, 1995	3	0	0	0	13	4.4	59	915	5	999
Sunday, January 01, 1995	4	0	0	0	11.6	5	66	916	4	999
Sunday, January 01, 1995	5	0	0	0	10.9	5.6	72	916	3	999
Sunday, January 01, 1995	6	0	0	0	13.9	5.9	60	917	4	999
Sunday, January 01, 1995	7	112	377	52	17.2	6.2	48	917	4	999
Sunday, January 01, 1995	8	351	744	77	20	6.1	37	917	3	999
Sunday, January 01, 1995	9	597	871	105	23	4.8	26	916	2	999
Sunday, January 01, 1995	10	818	929	133	26.5	2.4	17	916	1	999
Sunday, January 01, 1995	11	995	1001	122	28.9	-0.5	13	915	1	999
Sunday, January 01, 1995	12	1115	1025	131	30.4	-2.3	10	914	2	999
Sunday, January 01, 1995	13	1168	1032	141	31.4	-4.1	9	913	2	999
Sunday, January 01, 1995	14	1148	1041	134	31.3	-5.6	8	913	3	999
Sunday, January 01, 1995	15	1061	1038	125	32.1	-7.4	7	912	3	999
Sunday, January 01, 1995	16	909	1017	116	32	-7.8	7	912	4	999
Sunday, January 01, 1995	17	705	980	101	30.8	-7.9	8	912	4	999
Sunday, January 01, 1995	18	467	890	88	26.8	-7.9	10	912	3	999
Sunday, January 01, 1995	19	218	654	75	20.8	-7.3	14	913	3	999
Sunday, January 01, 1995	20	24	74	23	18.6	-7.4	16	914	3	999
Sunday, January 01, 1995	21	0	0	0	17.1	-7.8	18	915	3	999
Sunday, January 01, 1995	22	0	0	0	15.3	-7.7	19	915	2	999
Sunday, January 01, 1995	23	0	0	0	14.2	-7.9	20	914	2	999
Sunday, January 01, 1995	24	0	0	0	13.5	-8.4	20	914	2	999
Monday, January 02, 1995	1	0	0	0	12.9	-8.8	21	914	2	999
Monday, January 02, 1995	2	0	0	0	12.6	-9.2	24	914	2	999
Monday, January 02, 1995	3	0	0	0	11.6	-7.7	26	914	2	999
Monday, January 02, 1995	4	0	0	0	10.9	-7.3	28	914	2	999
Monday, January 02, 1995	5	0	0	0	11.4	-6.7	30	915	2	999
Monday, January 02, 1995	6	0	0	0	17.3	-5.7	22	916	3	999
Monday, January 02, 1995	7	111	402	48	21.3	-4.6	19	916	3	999
Monday, January 02, 1995	8	351	793	61	24.8	-3.4	15	917	4	999
Monday, January 02, 1995	9	598	919	79	28.4	-3.3	11	917	3	999
Monday, January 02, 1995	10	819	975	102	30.7	-5.1	8	917	3	999
Monday, January 02, 1995	11	997	1005	122	32.7	-6.4	7	916	3	999
Monday, January 02, 1995	12	1116	1028	130	34.3	-7	6	915	3	999
Monday, January 02, 1995	13	1167	1032	141	35.4	-5.8	6	914	3	999
Monday, January 02, 1995	14	1148	1040	134	35.1	-4.7	5	915	4	999
Monday, January 02, 1995	15	1061	1037	125	35.4	-4.9	5	914	5	999
Monday, January 02, 1995	16	907	1016	115	34.9	-4.6	6	913	5	999
Monday, January 02, 1995	17	704	979	99	33.5	-5.1	6	914	5	999
Monday, January 02, 1995	18	466	890	87	29.3	-6.5	8	914	3	999
Monday, January 02, 1995	19	218	656	75	22.3	-8.2	12	914	3	999
Monday, January 02, 1995	20	24	81	23	18.7	-8.4	14	916	2	999
Monday, January 02, 1995	21	0	0	0	16.8	-9.2	15	916	2	999
Monday, January 02, 1995	22	0	0	0	16.3	-9.6	15	917	2	999
Monday, January 02, 1995	23	0	0	0	16.7	-10.2	15	916	3	999
Monday, January 02, 1995	24	0	0	0	16.9	-10.2	15	916	3	999

Table C3: Header information and first two days of SAWS GHI, DNI & DHI data with METEONORM data climate input file

		Latitude {N+/S-}	Longitude {E+/W-}	TimeZone {+/- GMT}	Elevation {m}
LOCATION	Upington	-28.42	21.2582	2	848
DESIGN CONDITIONS	0				
TYPICAL/EXTREME PERIODS	0				
		Ground Temp Depth {m}			
GROUND TEMPERATURES	1	1			

Jan {C}	Feb{C}	Mar {C}	Apr {C}	May {C}	Jun {C}	Jul {C}	Aug {C}	Sept {C}	Oct {C}	Nov {C}	Dec {C}
23.6	25.1	25.6	25.1	23.6	21.6	19.5	18	17.5	18	19.5	21.6

HOLIDAYS/DAYLIGHT SAVINGS	No					
COMMENTS 1	SAWS GHI, DNI & DHI and METEONORM Data from CRSES for all other required inputs					
		Number of Intervals per Hour	DP Name/Descr	DP Start Day of Week	DP Start Day	DP End Day
DATA PERIODS (DPs)	1	1	Data	Sunday	1-Jan	31-Dec

Date	Hour	Global Horizontal Radiation {Wh/m2}	Direct Normal Radiation {Wh/m2}	Diffuse Horizontal Radiation {Wh/m2}	Dry Bulb Temp {C}	Dew Point Temp {C}	Relative Humidity {%}	Pressure {mbar}	Wind Speed {m/s}	Albedo {.01}
Saturday, January 01, 2005	1	0	0	0	27.9	22.7	73	918	2.4	-99
Saturday, January 01, 2005	2	0	0	0	28.9	22.7	69	918	2	-99
Saturday, January 01, 2005	3	0	0	0	28.3	22.7	72	918	1.8	-99
Saturday, January 01, 2005	4	0	0	0	28.7	22.7	70	918	2	-99
Saturday, January 01, 2005	5	0	0	0	28.9	22.7	69	918	2	-99
Saturday, January 01, 2005	6	62	43	19	29	22.7	69	918	2.3	-99
Saturday, January 01, 2005	7	262	204	59	30.2	22.7	64	918	1.9	-99
Saturday, January 01, 2005	8	480	385	95	30.6	22.7	63	918	2.5	-99
Saturday, January 01, 2005	9	685	548	137	30.7	22.7	62	918	2.3	-99
Saturday, January 01, 2005	10	867	733	134	31.5	22.7	60	918	3.6	-99
Saturday, January 01, 2005	11	993	845	148	31.2	22.7	61	918	3.2	-99
Saturday, January 01, 2005	12	1038	849	189	32.7	22.7	56	918	3.2	-99
Saturday, January 01, 2005	13	1012	790	222	34.9	22.7	49	918	3.4	-99
Saturday, January 01, 2005	14	977	815	161	35.5	22.7	48	919	3.8	-99
Saturday, January 01, 2005	15	844	695	148	36.9	18.7	34	919	3.4	-99
Saturday, January 01, 2005	16	633	482	152	37.8	14.7	26	919	4.5	-99
Saturday, January 01, 2005	17	437	320	117	37.3	18.7	34	919	3.6	-99
Saturday, January 01, 2005	18	239	158	81	35.6	22.7	47	919	3.8	-99
Saturday, January 01, 2005	19	59	26	33	34.9	22.7	49	919	3.2	-99
Saturday, January 01, 2005	20	0	0	0	35.2	22.7	49	920	3.4	-99
Saturday, January 01, 2005	21	0	0	0	33.3	22.7	54	920	3.4	-99
Saturday, January 01, 2005	22	0	0	0	33	22.7	55	920	2.5	-99
Saturday, January 01, 2005	23	0	0	0	31.8	22.7	59	920	2.1	-99
Saturday, January 01, 2005	24	0	0	0	30.5	22.7	63	920	1.9	-99
Sunday, January 02, 2005	1	0	0	0	28.9	22.7	69	921	1.7	-99
Sunday, January 02, 2005	2	0	0	0	27.2	22.7	76	921	2.7	-99
Sunday, January 02, 2005	3	0	0	0	26.3	22.7	80	921	4.3	-99
Sunday, January 02, 2005	4	0	0	0	25.4	21.8	80	921	3.8	-99
Sunday, January 02, 2005	5	0	0	0	24.8	21.1	80	921	3.6	-99
Sunday, January 02, 2005	6	61	34	27	24.6	21	80	921	3	-99
Sunday, January 02, 2005	7	276	209	67	26	22.3	80	922	3.4	-99
Sunday, January 02, 2005	8	475	371	104	28.1	22.7	72	922	2.4	-99
Sunday, January 02, 2005	9	671	559	112	30.5	22.7	63	922	2.8	-99
Sunday, January 02, 2005	10	887	738	149	32.8	18.7	43	922	3	-99
Sunday, January 02, 2005	11	961	803	158	35	14.7	30	922	3.8	-99
Sunday, January 02, 2005	12	1056	882	175	35.6	10.7	22	923	3.4	-99
Sunday, January 02, 2005	13	1011	837	174	36	7.5	17	923	4.8	-99
Sunday, January 02, 2005	14	941	725	217	36.1	7.5	17	923	5.2	-99
Sunday, January 02, 2005	15	756	555	200	36.1	8.4	18	923	4.3	-99
Sunday, January 02, 2005	16	597	440	157	35.8	8.8	19	923	5	-99
Sunday, January 02, 2005	17	426	325	101	35.3	9.1	20	924	4.3	-99
Sunday, January 02, 2005	18	220	157	63	34.3	10.3	23	924	4.5	-99
Sunday, January 02, 2005	19	55	30	24	33	9.2	23	924	2.8	-99
Sunday, January 02, 2005	20	0	0	0	31.6	9.9	26	924	2.1	-99
Sunday, January 02, 2005	21	0	0	0	29.9	12.7	35	924	1.6	-99
Sunday, January 02, 2005	22	0	0	0	28.2	13.5	40	924	1.2	-99
Sunday, January 02, 2005	23	0	0	0	26.6	12.9	43	925	0.9	-99
Sunday, January 02, 2005	24	0	0	0	24.9	13.5	49	925	0.6	-99

Table C4: Header information and first two days of Eskom DNI data with METEONORM data climate input file

		Latitude {N+/S-}	Longitude {E+/W-}	TimeZone {+/- GMT}	Elevation {m}
LOCATION	Upington	-28.42	21.2582	2	848
DESIGN CONDITIONS	0				
TYPICAL/EXTREME PERIODS	0				
		Ground Temp Depth {m}			
GROUND TEMPERATURES	1	1			

Jan {C}	Feb{C}	Mar {C}	Apr {C}	May {C}	Jun {C}	Jul {C}	Aug {C}	Sept {C}	Oct {C}	Nov {C}	Dec {C}
23.6	25.1	25.6	25.1	23.6	21.6	19.5	18	17.5	18	19.5	21.6

HOLIDAYS/DAYLIGHT SAVINGS	No					
COMMENTS 1	Eskom DNI and METEONORM Data from CRSES for all other required inputs					
		Number of Intervals per Hour	DP Name/Descr	DP Start Day of Week	DP Start Day	DP End Day
DATA PERIODS (DPs)	1	1	Data	Sunday	1-Jan	31-Dec

Date	Hour	Global Horizontal Radiation {Wh/m2}	Direct Normal Radiation {Wh/m2}	Diffuse Horizontal Radiation {Wh/m2}	Dry Bulb Temp {C}	Dew Point Temp {C}	Relative Humidity {%}	Pressure {mbar}	Wind Speed {m/s}	Albedo {.01}
Saturday, January 01, 2005	1	0	0	0	27.9	22.7	73	918	2.4	-99
Saturday, January 01, 2005	2	0	0	0	28.9	22.7	69	918	2	-99
Saturday, January 01, 2005	3	0	0	0	28.3	22.7	72	918	1.8	-99
Saturday, January 01, 2005	4	0	0	0	28.7	22.7	70	918	2	-99
Saturday, January 01, 2005	5	0	0	0	28.9	22.7	69	918	2	-99
Saturday, January 01, 2005	6	1	0	1	29	22.7	69	918	2.3	-99
Saturday, January 01, 2005	7	109	1	78	30.2	22.7	64	918	1.9	-99
Saturday, January 01, 2005	8	71	106	71	30.6	22.7	63	918	2.5	-99
Saturday, January 01, 2005	9	66	182	66	30.7	22.7	62	918	2.3	-99
Saturday, January 01, 2005	10	237	442	223	31.5	22.7	60	918	3.6	-99
Saturday, January 01, 2005	11	79	484	79	31.2	22.7	61	918	3.2	-99
Saturday, January 01, 2005	12	386	502	346	32.7	22.7	56	918	3.2	-99
Saturday, January 01, 2005	13	823	517	514	34.9	22.7	49	918	3.4	-99
Saturday, January 01, 2005	14	492	516	412	35.5	22.7	48	919	3.8	-99
Saturday, January 01, 2005	15	740	137	447	36.9	18.7	34	919	3.4	-99
Saturday, January 01, 2005	16	646	321	353	37.8	14.7	26	919	4.5	-99
Saturday, January 01, 2005	17	370	503	292	37.3	18.7	34	919	3.6	-99
Saturday, January 01, 2005	18	217	482	191	35.6	22.7	47	919	3.8	-99
Saturday, January 01, 2005	19	109	436	84	34.9	22.7	49	919	3.2	-99
Saturday, January 01, 2005	20	16	339	16	35.2	22.7	49	920	3.4	-99
Saturday, January 01, 2005	21	0	89	0	33.3	22.7	54	920	3.4	-99
Saturday, January 01, 2005	22	0	0	0	33	22.7	55	920	2.5	-99
Saturday, January 01, 2005	23	0	0	0	31.8	22.7	59	920	2.1	-99
Saturday, January 01, 2005	24	0	0	0	30.5	22.7	63	920	1.9	-99
Sunday, January 02, 2005	1	0	0	0	28.9	22.7	69	921	1.7	-99
Sunday, January 02, 2005	2	0	0	0	27.2	22.7	76	921	2.7	-99
Sunday, January 02, 2005	3	0	0	0	26.3	22.7	80	921	4.3	-99
Sunday, January 02, 2005	4	0	0	0	25.4	21.8	80	921	3.8	-99
Sunday, January 02, 2005	5	0	0	0	24.8	21.1	80	921	3.6	-99
Sunday, January 02, 2005	6	0	0	0	24.6	21	80	921	3	-99
Sunday, January 02, 2005	7	137	13	37	26	22.3	80	922	3.4	-99
Sunday, January 02, 2005	8	387	241	64	28.1	22.7	72	922	2.4	-99
Sunday, January 02, 2005	9	641	377	78	30.5	22.7	63	922	2.8	-99
Sunday, January 02, 2005	10	859	438	92	32.8	18.7	43	922	3	-99
Sunday, January 02, 2005	11	1053	476	245	35	14.7	30	922	3.8	-99
Sunday, January 02, 2005	12	722	500	466	35.6	10.7	22	923	3.4	-99
Sunday, January 02, 2005	13	754	516	555	36	7.5	17	923	4.8	-99
Sunday, January 02, 2005	14	688	524	539	36.1	7.5	17	923	5.2	-99
Sunday, January 02, 2005	15	650	526	485	36.1	8.4	18	923	4.3	-99
Sunday, January 02, 2005	16	544	525	385	35.8	8.8	19	923	5	-99
Sunday, January 02, 2005	17	445	513	296	35.3	9.1	20	924	4.3	-99
Sunday, January 02, 2005	18	278	486	212	34.3	10.3	23	924	4.5	-99
Sunday, January 02, 2005	19	116	434	84	33	9.2	23	924	2.8	-99
Sunday, January 02, 2005	20	2	335	2	31.6	9.9	26	924	2.1	-99
Sunday, January 02, 2005	21	0	88	0	29.9	12.7	35	924	1.6	-99
Sunday, January 02, 2005	22	0	0	0	28.2	13.5	40	924	1.2	-99
Sunday, January 02, 2005	23	0	0	0	26.6	12.9	43	925	0.9	-99
Sunday, January 02, 2005	24	0	0	0	24.9	13.5	49	925	0.6	-99

APPENDIX D: SYSTEM ADVISOR MODEL INPUT PARAMETERS

SAM background

Solar Advisor Model was developed to meet the United States (US) Department of Energy (DOE) Office of Solar Energy Technologies' need of a system modelling tool (Cameron and Cornelius, 2007). The model is based on the validated TRNSYS time-series simulation program developed at the University of Wisconsin (Wagner and Gilman, 2011). Using hourly meteorological resource data, TRNSYS is able to simulate the performance of PV, CSP and water heating systems (Wagner and Gilman, 2011). Adding customised components to the TRNSYS engine allowed the modelling of wind, geothermal and biomass power systems. As such the name was then changed from Solar Advisor Model to System Advisor Model (SAM). A concise summation of SAM's capability is provided by Wagner and Gilman (2011) below.

> "The System Advisor Model provides a consistent framework for analyzing and comparing power system costs and performance across the range of solar technologies and markets, from photovoltaic (PV) systems for residential and commercial markets to concentrating solar power and large PV systems for utility markets."
> (Wagner and Gilman, 2011: 1)

Parabolic trough models

Eight cases of the parabolic trough plant were modelled to evaluate evaporative and air-cooled plants under the four DNI datasets. Each model was set up identically except for the power cycle cooling method and climate input file. The major inputs used in each component model of the physical trough model are listed in the following sections.

Solar Field

The solar field collects insolation and converts it into heat. It typically consists of a common cold header pipe that transports cool HTF (above freezing point) through solar collector assembly (SCA) loops, and a common hot header pipe which collects the heated HTF from the SCA loops and transports it to the power block of the plant.

System Advisor Model models the performance of each SCA individually in the field and can allow for up to four differing collector and receiver unit configurations in one plant model (Wagner and Gilman, 2011). A new solar plant will typically use only one collector and

receiver combination to reduce construction and maintenance complexity and cost. Hence, one SCA was selected: the EuroTrough ET150. It was selected because of its light-weight and easy to assemble torque box design, and large reflective aperture area- which reduces the overall area required by the solar field.

In SAM the solar field can be sized using either the solar multiple (option 1) or specifying the solar field aperture independently of the power block rated capacity (option 2). When option 2 is selected SAM calculates the solar multiple based on the user-entered solar field aperture.

Method 1 was chosen as this was a new plant being modelled. A parametric simulation described in section 4.2.2.1 was run on an air-cooled power cycle parabolic trough plant with the CRSES input data to determine the optimal solar multiple. This solar multiple was used for each parabolic trough case.

Three solar field mass flow rate conditions can be experienced during plant operation. Ideal mass flow rate, mass flow rate below the minimum allowable value, and mass flow rate above the maximum.

When the solar field is not absorbing sufficient energy to heat the HTF even at the minimum allowable mass flow rate and the flow rate descends below this value, SAM resets the mass flow rate to the minimum value and recalculates the outlet temperature of the solar field (Wagner and Gilman, 2011). Wagner and Gilman (2011) report that this results in the solar field outlet temperature falling below the design value.

When the solar field is absorbing excess energy, such that it needs to have a mass flow rate higher than the maximum value to avoid overheating the HTF, then defocusing the collectors is necessary. System Advisor Model allows three methods of defocusing the collectors: full defocusing, partial sequenced defocusing and partial simultaneous defocusing (Wagner and Gilman, 2011). Partial simultaneous defocusing was selected to allow for quick refocusing when absorbed energy decreased to safer levels and to ensure that the HTF did not risk being overheated. Using sequenced defocusing allows for more annual electric output but operates the HTF at elevated temperatures. These elevated temperatures produce high boiling degradation products within Therminol VP-1 and reduce its service life (Gamble and Schopf, 2009). The benzene content of Therminol VP-1 makes it preferable to utilize it as long as possible before considering disposal (Bevacqua *et al.*, 2008).

Gamble and Schopf (2009, p. 1) from Solutia Inc claim that Therminol VP-1 is “the most thermally stable organic heat transfer fluid available”. Analyzing 15 years of Therminal VP-1 samples from a CSP plant they found very little change in the fluid’s thermal conductivity. This combined with its prominent use in recently built parabolic trough plants motivated the selection of Therminol VP-1 for each simulation.

Dirt on the mirrors of the solar field significantly reduce the energy absorbed from the solar field. System Advisor Model suggests a cycle of 63 washes per annum and water usage per wash of 0.7 litres per square meter of solar field aperture. This equates to a wash of the solar field collector mirrors and HCEs every five or six days using approximately 604,296 litres of water. This washing schedule was used due to the moderately windy conditions at Upington.

The area allocated for the power block, TES tanks, electrical distribution system, header piping system, control room and plant servitudes was 483,437 m^2 using the SAM default non-solar field land area multiplier of 1.4.

Collectors (SCAs)

Table 4-2 in section 4.2.2.2 displays the comparative reflective areas for each SCA in the SAM library. By choosing an SCA with a large aperture area the amount of loops require to produce the heat required by a 100 MW_e power block are reduced. This then reduces the head requirement on the field HTF pumps which are the largest contributor to parasitic losses of the plant (Wagner and Gilman, 2011). Hence, the EuroTrough ET150 was selected.

System Advisor Model determines the solar flux on each collector using the climate input file data, sun position, and derating values. The physical trough model also calculates row shadowing which occurs in the morning and evening when the zenith angle is large. Other losses also accounted for are IAM, end spillage, and when wind speeds call for the SCAs to move into the stow position. Constant losses like mirror reflectance, tracking error, mirror soiling and geometry defects are also modelled. Wagner and Gilman (2011, p. 27)

Receivers (HCEs)

The HCE model in SAM allows for the modeling of four different receiver types in the same plant. Within each type, four varying conditions can be defined. For example in an extreme case, a single plant may contain four different HCE models, with each model containing some HCEs with broken glass others with lost vacuum in their annulus, some with more dirt on their surface than others and others intact. This detail is suitable for modeling a running plant with detailed operation and maintenance data. As this is a new plant which will most likely

have a single type of HCE to reduce maintenance complexity and cost, only one type of HCE was selected. The Schott PTR70 2008 from the SAM library as it had the lowest heat loss at design.

Power Cycle

The Rankine power cycle in SAM models the following components:

> "the turbine(s), condenser, condensate pump, feedwater pump(s), deaerator(s), feedwater heater(s), preheater heat exchanger, boiler, superheater heat exchanger, and reheat heat exchanger(s)."
> (Wagner and Gilman, 2011: 52)

In the plant capacity section of the power cycle interface SAM subtracts 10% from the gross electric output to account for the parasitic losses. The resulting net electric power output is 90% of the gross electric output.

The power block section provides values for rated cycle efficiency, design inlet temperature, design outlet temperature and boiler operating pressure under design conditions. The fossil backup boiler lower heating value efficiency was set to 0.9 as suggested in SAM. System Advisor Model suggests a steam cycle blowdown fraction of 0.013 for wet-cooled systems and 0.016 for dry cooled systems. A value of 0.02 was used uniformly throughout to minimize build-up of minerals, scales and solids in the power block equipment.

The plant control section lists the plant operation metrics. A low resource power cycle standby period of two hours was allowed to cater for large cloud transients. Twenty percent of rated thermal power was set as a requirement for starting or keeping the power block on standby. The time required for the plant to start producing electricity from start or standby thermal power was set as 30 minutes as suggested by SAM. The power cycle heat exchanger was set up to let HTF flow through for power generation once it reached a minimum temperature of 300ºC. The turbine was set to operate at a maximum overdesign rating of 105% its nameplate rating. It was also set not to operate at below 25% its nameplate rating. Fixed pressure turbine inlet pressure control was used.

For every climate input file an evaporative- and air-cooled power cycle was modelled. This necessitated a separate case being setup for each set of weather data used.

For evaporative-cooled power cycles the average wet bulb temperature from the climate input file being used was used as the ambient temperature at design. “The temperature rise of the cooling water across the condenser under design conditions” (System Advisor Model, 2011), was set at the 10ºC recommended by SAM. The temperature difference between the wet bulb temperature and the water cycling at the condenser inlet was set to 5ºC as recommended by SAM. The minimum condenser pressure was set at 1.25 inches of mercury as specified by SAM for evaporative-cooled systems.

For air-cooled power cycles the average dry bulb temperature from the climate input file being used was used as the ambient temperature at design. “The pressure-drop ratio across the air-cooled condenser heat exchanger” (System Advisor Model, 2011), was set at the 1.0028 recommended by SAM. The temperature difference between the dry bulb temperature and the condenser inlet (turbine outlet) was set to 16ºC as recommended by SAM. The minimum condenser pressure was set at 2 inches of mercury as specified by SAM for air-cooled systems.

Thermal Storage

Six full load hours of TES were selected to cater for the South African national load profile’s evening dominant peak (6pm to 9pm) (Davis *et al.*, 2011). Using two tanks each capable of storing the entire storage HTF volume required for six hours of full load operation, SAM calculates the storage volume required in m^3 and thermal capacity in MW_{th}. One tank stores the hot storage HTF and the other stores the cold storage HTF.

The storage system modelled in this study was an indirect storage system, hence the storage HTF is different from the solar field HTF. This is due to the cost of Therminol VP-1 being too high for use in the plant and in the storage tanks. The storage HTF is heated by the solar field HTF via a heat exchanger. Solar salt was selected as storage HTF in order to limit the costs of the plant.

The fossil dispatch mode was set to minimum backup level in order to limit the use of the backup boiler which would reduce fossil fuel costs.

The thermal storage dispatch control philosophy was as stated in section 4.2.1.2.

Parasitics

System Advisor Model subtracts the electrical parasitic load from the gross electric output of the power cycle in each hour of simulation.

The piping thermal loss coefficient, which accounts for the losses incurred from the header, inter-receiver, runner and crossover piping was set at the default value.

The tracking power losses were set to the SAM default value of 125 W per SCA, which is then multiplied by the number of SCAs in the solar field to arrive at the total tracking loss.

The pumping power coefficient required to pump the storage HTF from one tank to another through the solar field-to-TES heat exchanger was set at the SAM suggested value of 0.15 kJ/kg. This value is then multiplied by the mass flow rate into and out of the tanks to determine the pumping power required for the TES system.

The pumping power coefficient required to pump the solar field HTF through the solar field-to-TES heat exchanger and then through the power cycle heat exchanger was set at the SAM suggested value of 0.55 kJ/kg. This value is then multiplied by the mass flow rate through the TES and power cycle heat exchangers to determine the pumping power required for the TES system.

The facilities required within the plant to support maintenance staff such as buildings, control rooms, and plant lighting draw an electrical load from the output of the plant. The building and control room part of this load will be HVAC, water heating, and IT infrastructure power requirements. This load is catered for in the “Fraction of rated gross power consumed at all times” coefficient in SAM. System Advisor Model then multiplies this fraction with the gross power output of the plant to determine this parasitic load in MW_e. The design point total for this aspect was 0.6105 MW_e.

The auxiliary fossil fueled heater required for the backup boiler is modelled using a polynomial equation that calculates this parasitic load as a function of the fossil fuelled boiler’s energy production. The SAM suggested coefficients were used to model this parasitic load.

Central receiver models

Eight cases of the central receiver plant were modelled to evaluate evaporative and air-cooled plants under the four DNI datasets. Each model was set up identically except for the power cycle cooling method and climate input file. The major inputs used in each component model of the power tower model are listed in the following sections.

Heliostat field

The heliostat field and tower receiver have to be optimized as a complete system. This is because the height and geometry of the receiver determine the distribution of heliostats around it.

System Advisor Model uses an optimisation wizard to optimise the heliostat field size and corresponding receiver tower height. The wizard is based on the DELSOL3 code developed by Kistler (1986) at Sandia National Laboratory. The DELSOL3 code is incorporated into SAM with the Power Tower Generation Program (PTGen) described by Wagner (2008). Using primarily the solar multiple, heliostat dimensions, plant nameplate capacity and type of receiver specified (external or cavity), the optimization wizard runs through an iterative process to arrive at an optimum. This optimum includes the number of heliostats, layout of the heliostat field and height of the receiver tower. The solar multiple was set to provide an aperture area as close as possible to that of the parabolic trough plant modelled. A solar multiple of 1.68 provided an aperture area of within 0.4% of the aperture area of the parabolic trough plant.

The heliostat field page also allows users to specify heliostat properties. For this simulation, large 12.2 m by 12.2 m square heliostats were used. System Advisor Model makes the assumption that each heliostat has a two-axis tracking motor. A mirror reflectance and soiling value of 0.9 was selected as it provided a conservatively weighted average of the mirrors that could be used on the heliostats. Heliostat availability was set at 0.99 to allow for 1 percent of the heliostats in the field to be maintained at any time. The SAM default image error value was used to account for “tracking imprecision, foundation motion, mirror waviness, panel alignment problems, atmospheric refraction and tower sway” (System Advisor Model, 2011). The heliostats were set to move into the stow position when the wind speed from the climate input file went above 15 m/s.

A washing cycle of 63 washes per annum and water usage per wash of 0.7 litres per square meter of solar field aperture were used to keep this water usage component in line with the

parabolic trough. This equates to a wash of the solar field heliostat mirrors every five or six days using approximately 602,130 litres of water. This washing schedule was used due to the moderately windy conditions at Upington.

Due to the heliostat field requiring more area than a parabolic trough solar field of equivalent aperture area the non-solar field land area multiplier was set to 1.3. Since no piping system was required for the heliostat field only the power block, TES tanks, electrical distribution system, control room and plant servitudes were required to be allowed for.

Tower and receiver

The most important metric in the tower and receiver page is whether the receiver will be external or within a cavity. This determines the dimensions, thermodynamic characteristics, HTF flow and tower height of the receiver.

The external receiver was selected and the optimisation wizard calculated the following properties for it:

Receiver height:	19.91 m
Receiver diameter:	12.44 m
Number of panels:	20

The receiver coating emittance was set to 0.88 and SAM assumes this stays constant over the range of wavelengths received from the heliostat field. The SAM suggested receiver thermodynamic characteristics were used in the simulations. A 60% $NaNO_3$ and 40% KNO_3 salt HTF was selected to be used in the receiver as this was a direct TES system and a similar storage HTF to the solar salt used in the parabolic trough simulation was required for ease of comparison. Type AISI316 stainless steel is used for the receiver piping because of its resistance to corrosion. This is a requirement with the salt HTF cycling through it. The design operation of the receiver was set up such that the flow rate to the receiver would not drop below 25% of the maximum flow rate and when it exceeded 120% of the maximum SAM would defocus the heliostats.

Power Cycle

The Rankine power cycle component model in SAM is identical for the parabolic trough and power tower models. The settings in both simulations were set-up as closely as possible with the exceptions noted below.

The design gross output required from the turbine had to be 115 MW_e as opposed to 111 MW_e used for the parabolic trough plant because SAM estimates higher parasitic losses in operating a central receiver plant. This was reflected in the power tower plant gross to net conversion factor of 0.87 as opposed to 0.9 for the parabolic trough plant.

Due to the higher design temperatures attainable by the central receiver the power cycle design efficiency is 13% higher than that of the parabolic trough power cycle. The minimum required startup temperature for the central receiver power cycle is 200ºC higher than that required for the parabolic trough.

For every climate input file an evaporative- and air-cooled power cycle was modelled. This necessitated a separate case being setup for each set of weather data used. The evaporative- and air-cooled settings were identical to that of the parabolic trough case.

Thermal Storage

The same settings used in the parabolic trough TES component model were used for the central receiver model. The most notable difference is that the central receiver plant utilised a direct storage system as opposed to the indirect system used in the parabolic trough case. All other settings were matched to the parabolic trough case except those noted below. The initial HTF temperature was 574ºC for the central receiver and 300ºC for the parabolic trough. The thermal storage dispatch control philosophy used was as stated in section 4.2.1.2.

Parasitics

The parasitic loads for the central receiver were similar to that of the parabolic trough apart from the following items.

The energy required for each heliostat to startup and track are itemised separately and measured in kW_e. A value of 0.025 kW_e is required for the startup hour and 0.055 kW_e for each hour that the heliostat is tracking the sun.

The pumping and piping losses are measured from the receiver towards the TES system and power block. Although the piping layout is different, the TES configuration would be very similar which resulted in SAM using the same loss values as the parabolic trough case.

Dish-engine models

Four cases of the dish-engine plant were modelled to evaluate power output for each of the four DNI datasets. Each model was set up identically except for the climate input file. The major inputs used in each component model of the dish Stirling model are listed in the following sections.

Solar Field

The solar field of a dish-engine plant is a network of autonomously tracking dish-engine systems.

The field layout used in this simulation was an array 50 dish-engine systems wide (in the North-South direction) and 80 systems long (in the East-West direction). This provided a total of 4000 dish-engine systems in the plant. The North-South and East-West spacing between each dish was 15 m. This resulted in a solar field area of 0.9 km^2.

Since a new plant is being modelled it is expected that the solar field area will be graded level. This will result in no array shading parameters based on ground slope. The wind stow speed of the collector dish of each system is 16 m/s. System Advisor Model calculates the capacity of the plant by summing the nameplate capacity of each dish-engine system in the solar field. Hence, the 4000 25 kW_e dish-engine systems should produce 100 MW_e.

Collector

The dish collector used on this system had a total mirror area of 91 m^2 of which 87.7 m^2 was projected onto the receiver aperture. An average mirror reflectance of 0.94 was used to account for the different solar mirrors that could be used on the collector.

The cooling system fan was set to operate when the DNR went above 200 W/m^2.

Receiver

The receiver aperture receives solar radiation from the collector but also loses heat to the atmosphere via convection and radiation losses. Its diameter can vary between 0.14 m and 0.2 m. It was set to 0.184 m in this simulation.

The insulation of the receiver housing was set to 75 mm as used by the SES and WGA receivers. The insulation thermal conductivity used to calculate the conduction losses was set to 0.006 W/mK as stated in the SES and WGA reference input values.

The absorptance of the 0.6 m^2 absorber was set to 0.9.

Fraser (2008) cited Harris (1985) as stating that receiver cavity geometry has less than a 3% impact on annual thermal receiver performance. The cavity geometry of the SES receiver was used in this simulation.

Stirling engine

The nameplate capacity of the Stirling engine used for each dish-engine system is 25 kW_e. The engine setup of the SES engine was used in this simulation. The set of Beale number coefficients developed by Fraser (2008) and described in section 4.2.6.4 were used.

Parasitics

The tracking control and cooling systems make up the parasitic load of each dish-engine system. The tracking system is estimated to use an average of 150 W. The cooling system load depends on the DNR being received and varies hourly with the DNR in climate input file.

CLFR models

Eight cases of the CLFR plant were modelled to evaluate evaporative and air-cooled plants under the four DNI datasets. Each model was set up identically except for the power cycle cooling method and climate input file. The major inputs used in each component model of the linear Fresnel model are listed in the following sections.

Solar Field

The CLFR solar field is similar to the parabolic trough solar field in how it contains both collectors and receivers.

This solar field was set up with a recirculated boiler loop flow configuration. Twelve collector receiver modules (called boiler units) were connected in series in the boiler section. Four collector receiver modules (called superheater units) of identical geometry to the boiler units were connected in series in the superheater section

The solar multiple was set to provide an aperture area as close as possible to that of the parabolic trough plant modelled. A solar multiple of 1.79 provided an aperture area of within 0.05% of the aperture area of the parabolic trough plant.

Since the solar field boils feed water to produce steam directly, its steam outlet temperature is higher than that of the HTF leaving the parabolic trough plant. A field outlet temperature of 440ºC is suggested by SAM for the selected number of boiler and superheater units in this simulation.

A washing cycle of 63 washes per annum and water usage per wash of 0.7 litres per square meter of solar field aperture were used to keep this water usage component in line with the parabolic trough. This equates to a wash of the solar field mirrors and receivers every five or six days using approximately 603,994 litres of water. This washing schedule was used due to the moderately windy conditions at Upington.

Due to the solar field requiring less area than a parabolic trough solar field of equivalent aperture area the non-solar field land area multiplier was set to 1.6.

An advantage of the CLFR solar field is that it is only required to move into stow position at windpeeds of above 20 m/s. This means that this plant will be able to operate when the other plants modelled in this study have to be shut down.

Collector and Receiver

The collector and receiver geometry for the boiler and superheater circuits was kept identical for ease of installation and maintenance.

The polynomial fit heat loss model selected for the receiver produced the following aggregate weighted losses:

Average field temperature difference at design:	313.5ºC
Heat loss at design:	462 W/m
Receiver thermal derate:	0.96
Receiver optical derate	1
Collector optical loss at normal incidence:	0.64

Power Cycle

The Rankine power cycle component model in SAM is identical for the parabolic trough and linear Fresnel models. The settings in both simulations were set-up as closely as possible with the exceptions noted below.

The design gross output required from the turbine had to be 107 MW_e as opposed to 111 MW_e used for the parabolic trough plant because SAM estimates lower parasitic loss in operating a CLFR plant. This was reflected in the power tower plant gross to net conversion factor of 0.94 as opposed to 0.9 for the parabolic trough plant.

The turbine inlet pressure for this power block was 10% higher than that of the parabolic trough power plant.

For every climate input file an evaporative- and air-cooled power cycle was modelled. This necessitated a separate case being setup for each set of weather data used. The evaporative- and air-cooled settings were identical to that of the parabolic trough case.

Parasitics

The parasitic loads for the CLFR plant were similar to that of the parabolic trough apart from the following item.

The tracking power loss was calculated per square meter of solar field.

APPENDIX E: SYSTEM ADVISOR MODEL RESULTS

Parabolic trough model results

In addition to the annual results tabled in chapter 6, monthly energy values and water consumption figures were obtained from the SAM physical trough model. These results are tabled below.

Table E1: Parabolic trough model monthly results

Case 1			
Location	Solar Radiation Data Used	Technology	Power Cycle Cooling Method
Upington	Weather Analytics Inc.	Parabolic Trough Plant	Evaporative
Month	Gross Electric Output (MWh)	Monthly Energy (MWh)	Water Usage (m^3)
Jan	46,373	43,573	166,455
Feb	36,832	34,616	133,089
Mar	41,076	38,652	147,062
Apr	34,870	33,037	122,441
May	25,632	24,314	89,958
Jun	22,086	20,906	76,299
Jul	23,943	22,741	82,121
Aug	34,945	33,277	118,361
Sep	42,606	40,365	144,467
Oct	44,265	41,806	153,231
Nov	43,356	40,928	151,697
Dec	48,438	45,729	170,672
Case 2			
Location	Solar Radiation Data Used	Technology	Power Cycle Cooling Method
Upington	Weather Analytics Inc.	Parabolic Trough Plant	Air-cooled
Month	Gross Electric Output (MWh)	Monthly Energy (MWh)	Water Usage (m^3)
Jan	45,969	42,873	4,614
Feb	36,365	33,939	3,660
Mar	40,753	38,056	4,077
Apr	35,086	32,954	3,504
May	25,863	24,252	2,624
Jun	22,235	20,772	2,276
Jul	24,007	22,499	2,448
Aug	35,187	33,096	3,509
Sep	42,817	40,086	4,230
Oct	44,211	41,308	4,397
Nov	43,221	40,404	4,300
Dec	47,928	44,844	4,789
Case 3			
Location	Solar Radiation Data Used	Technology	Power Cycle Cooling Method
Upington	CRSES	Parabolic Trough Plant	Evaporative
Month	Gross Electric Output (MWh)	Monthly Energy (MWh)	Water Usage (m^3)

Jan	43,622	40,863	160,495
Feb	39,149	36,773	144,815
Mar	38,285	36,003	141,299
Apr	34,697	32,803	124,920
May	26,735	25,341	94,081
Jun	23,130	21,941	80,284
Jul	26,385	25,107	90,765
Aug	36,380	34,607	124,034
Sep	42,297	40,077	145,460
Oct	44,509	42,001	156,412
Nov	46,116	43,509	164,057
Dec	47,839	45,105	172,913
Case 4			
Location	Solar Radiation Data Used	Technology	Power Cycle Cooling Method
Upington	CRSES	Parabolic Trough Plant	Air-cooled
Month	Gross Electric Output (MWh)	Monthly Energy (MWh)	Water Usage (m^3)
Jan	42,984	40,116	4,297
Feb	38,610	36,113	3,863
Mar	38,083	35,652	3,803
Apr	34,694	32,583	3,453
May	26,820	25,159	2,699
Jun	23,169	21,711	2,361
Jul	26,460	24,866	2,669
Aug	36,503	34,310	3,624
Sep	42,266	39,626	4,172
Oct	44,312	41,445	4,388
Nov	45,661	42,776	4,519
Dec	47,178	44,225	4,691
Case 5			
Location	Solar Radiation Data Used	Technology	Power Cycle Cooling Method
Upington	SAWS	Parabolic Trough Plant	Evaporative
Month	Gross Electric Output (MWh)	Monthly Energy (MWh)	Water Usage (m^3)
Jan	43,238	40,477	159,652
Feb	35,426	33,353	131,763
Mar	32,613	30,747	121,870
Apr	27,367	25,849	99,602
May	23,009	21,725	82,020
Jun	20,482	19,356	71,835
Jul	21,386	20,213	74,516
Aug	27,615	26,215	95,367
Sep	29,994	28,508	105,113
Oct	37,845	35,866	134,334
Nov	42,553	40,075	152,512
Dec	46,079	43,275	167,271

Case 6			
Location	Solar Radiation Data Used	Technology	Power Cycle Cooling Method
Upington	SAWS	Parabolic Trough Plant	Air-cooled
Month	Gross Electric Output (MWh)	Monthly Energy (MWh)	Water Usage (m^3)
Jan	43,057	40,185	4,305
Feb	35,273	33,069	3,547
Mar	32,727	30,736	3,296
Apr	27,575	25,893	2,775
May	23,292	21,788	2,367
Jun	20,594	19,225	2,120
Jul	21,632	20,195	2,213
Aug	27,931	26,217	2,809
Sep	30,249	28,456	3,033
Oct	38,026	35,730	3,791
Nov	42,529	39,822	4,221
Dec	45,824	42,786	4,565
Case 7			
Location	Solar Radiation Data Used	Technology	Power Cycle Cooling Method
Upington	Eskom	Parabolic Trough Plant	Evaporative
Month	Gross Electric Output (MWh)	Monthly Energy (MWh)	Water Usage (m^3)
Jan	41,139	38,560	151,896
Feb	29,776	27,912	111,440
Mar	30,811	28,889	115,746
Apr	29,338	27,652	107,226
May	22,477	21,207	80,441
Jun	20,285	19,142	71,155
Jul	21,587	20,391	75,231
Aug	25,399	24,108	88,457
Sep	34,215	32,361	118,643
Oct	39,033	36,787	137,917
Nov	44,498	41,933	158,967
Dec	47,243	44,523	171,218
Case 8			
Location	Solar Radiation Data Used	Technology	Power Cycle Cooling Method
Upington	Eskom	Parabolic Trough Plant	Air-cooled
Month	Gross Electric Output (MWh)	Monthly Energy (MWh)	Water Usage (m^3)
Jan	40,914	38,487	4,100
Feb	29,609	27,638	2,994
Mar	30,907	28,873	3,121
Apr	29,566	27,710	2,966
May	22,741	21,250	2,315
Jun	20,397	19,014	2,101
Jul	21,840	20,374	2,233
Aug	25,672	24,085	2,599

Sep	34,500	32,277	3,437
Oct	39,182	36,610	3,894
Nov	44,467	41,617	4,403
Dec	46,998	44,041	4,677

Central receiver model results

In addition to the annual results tabled in chapter 6, monthly energy values and water consumption figures were obtained from the SAM molten salt power tower model. These results are tabled below.

Table E2: Central receiver model monthly results

Case 1			
Location	Solar Radiation Data Used	Technology	Power Cycle Cooling Method
Upington	Weather Analytics Inc.	Central Receiver Plant	Evaporative
Month	Gross Electric Output (MWh)	Monthly Energy (MWh)	Water Usage (m^3)
Jan	46,113	42,503	135,116
Feb	35,663	32,743	105,379
Mar	39,909	36,662	117,183
Apr	36,006	33,138	102,990
May	31,201	28,826	88,397
Jun	28,627	26,500	79,457
Jul	30,104	27,838	83,276
Aug	37,450	34,641	103,360
Sep	42,275	39,244	117,366
Oct	43,542	40,291	123,426
Nov	45,070	41,820	128,476
Dec	49,646	45,884	142,812
Case 2			
Location	Solar Radiation Data Used	Technology	Power Cycle Cooling Method
Upington	Weather Analytics Inc.	Central Receiver Plant	Air-cooled
Month	Gross Electric Output (MWh)	Monthly Energy (MWh)	Water Usage (m^3)
Jan	45,594	41,781	3,250
Feb	35,268	32,205	2,525
Mar	39,725	36,309	2,825
Apr	36,237	33,094	2,566
May	31,468	28,795	2,247
Jun	28,783	26,363	2,057
Jul	30,225	27,649	2,159
Aug	37,727	34,540	2,665
Sep	42,506	39,110	2,989
Oct	43,564	39,984	3,076
Nov	45,045	41,477	3,177
Dec	49,297	45,255	3,494

Case 3			
Location	Solar Radiation Data Used	Technology	Power Cycle Cooling Method
Upington	CRSES	Central Receiver Plant	Evaporative
Month	Gross Electric Output (MWh)	Monthly Energy (MWh)	Water Usage (m^3)
Jan	40,386	37,041	121,082
Feb	37,146	34,144	111,859
Mar	37,129	33,866	111,896
Apr	35,364	32,319	103,868
May	31,868	29,416	90,775
Jun	28,690	26,386	80,110
Jul	33,218	30,761	92,300
Aug	39,287	36,352	109,146
Sep	40,084	37,153	112,710
Oct	43,166	39,902	124,013
Nov	45,448	42,107	132,112
Dec	45,555	42,108	134,232
Case 4			
Location	Solar Radiation Data Used	Technology	Power Cycle Cooling Method
Upington	CRSES	Central Receiver Plant	Air-cooled
Month	Gross Electric Output (MWh)	Monthly Energy (MWh)	Water Usage (m^3)
Jan	40,185	36,870	2,855
Feb	36,969	34,129	2,630
Mar	37,248	33,992	2,643
Apr	35,639	32,402	2,519
May	32,215	29,492	2,282
Jun	28,909	26,319	2,059
Jul	33,618	30,816	2,381
Aug	39,718	36,401	2,793
Sep	40,436	37,161	2,840
Oct	43,349	39,807	3,050
Nov	45,456	41,898	3,197
Dec	45,347	41,734	3,200
Case 5			
Location	Solar Radiation Data Used	Technology	Power Cycle Cooling Method
Upington	SAWS	Central Receiver Plant	Evaporative
Month	Gross Electric Output (MWh)	Monthly Energy (MWh)	Water Usage (m^3)
Jan	39,481	36,001	119,302
Feb	32,637	29,507	99,349
Mar	32,112	28,892	98,092
Apr	28,076	24,867	83,717
May	23,368	20,602	68,207
Jun	21,187	18,558	60,717
Jul	22,232	19,578	63,315
Aug	28,404	25,303	80,299

Sep	30,076	27,119	86,238
Oct	34,994	31,727	102,205
Nov	38,744	35,403	113,942
Dec	41,699	38,159	124,300
Case 6			
Location	Solar Radiation Data Used	Technology	Power Cycle Cooling Method
Upington	SAWS	Central Receiver Plant	Air-cooled
Month	Gross Electric Output (MWh)	Monthly Energy (MWh)	Water Usage (m^3)
Jan	39,314	35,953	2,806
Feb	32,491	29,274	2,332
Mar	32,243	28,923	2,310
Apr	28,281	24,934	2,022
May	23,638	20,685	1,708
Jun	21,310	18,474	1,557
Jul	22,492	19,608	1,633
Aug	28,708	25,333	2,052
Sep	30,315	27,107	2,161
Oct	35,126	31,655	2,500
Nov	38,736	35,208	2,745
Dec	41,477	37,795	2,952
Case 7			
Location	Solar Radiation Data Used	Technology	Power Cycle Cooling Method
Upington	Eskom	Central Receiver Plant	Evaporative
Month	Gross Electric Output (MWh)	Monthly Energy (MWh)	Water Usage (m^3)
Jan	40,489	37,134	122,029
Feb	27,353	24,759	83,821
Mar	28,762	25,828	88,261
Apr	30,257	27,536	90,183
May	25,127	22,910	72,977
Jun	20,436	18,419	58,374
Jul	23,813	21,788	67,624
Aug	27,036	24,446	76,792
Sep	32,124	29,494	91,287
Oct	37,594	34,537	108,854
Nov	42,966	39,737	125,675
Dec	46,531	43,072	137,741
Case 8			
Location	Solar Radiation Data Used	Technology	Power Cycle Cooling Method
Upington	Eskom	Central Receiver Plant	Air-cooled
Month	Gross Electric Output (MWh)	Monthly Energy (MWh)	Water Usage (m^3)
Jan	40,328	37,021	2,874
Feb	27,221	24,558	1,967
Mar	28,843	25,829	2,073
Apr	30,476	27,608	2,171

May	25,426	23,011	1,825
Jun	20,560	18,337	1,499
Jul	24,084	21,807	1,740
Aug	27,319	24,466	1,959
Sep	32,406	29,495	2,299
Oct	37,749	34,458	2,667
Nov	42,977	39,546	3,029
Dec	46,348	42,723	3,280

Dish-engine model results

In addition to the annual results tabled in chapter 6, monthly energy values and water consumption figures were obtained from the SAM dish Stirling model. These results are tabled below.

Table E3: Dish-engine model monthly results

Case 1		
Location	Solar Radiation Data Used	Technology
Upington	Weather Analytics Inc.	Dish-Engine Plant
Month	Gross Electric Output (MWh)	Monthly Energy (MWh)
Jan	22,637	21,954
Feb	18,518	17,938
Mar	20,300	19,602
Apr	18,934	18,290
May	18,851	18,193
Jun	17,704	17,093
Jul	18,255	17,649
Aug	20,944	20,268
Sep	22,950	22,224
Oct	23,202	22,440
Nov	25,196	24,445
Dec	25,734	24,970
Case 2		
Location	Solar Radiation Data Used	Technology
Upington	CRSES	Dish-Engine Plant
Month	Gross Electric Output (MWh)	Monthly Energy (MWh)
Jan	19,977	19,229
Feb	19,464	18,825
Mar	18,207	17,494
Apr	17,777	17,107
May	18,129	17,533
Jun	16,316	15,775
Jul	19,206	18,588
Aug	21,812	21,112

Sep	21,663	20,932
Oct	22,436	21,668
Nov	25,317	24,534
Dec	24,586	23,786
Case 3		
Location	Solar Radiation Data Used	Technology
Upington	SAWS	Dish-Engine Plant
Month	Gross Electric Output (MWh)	Monthly Energy (MWh)
Jan	17,301	16,565
Feb	13,579	12,936
Mar	13,266	12,613
Apr	8,970	8,431
May	8,055	7,558
Jun	6,337	5,939
Jul	7,434	6,989
Aug	9,617	9,110
Sep	11,678	11,111
Oct	14,337	13,648
Nov	17,444	16,746
Dec	19,252	18,518
Case 4		
Location	Solar Radiation Data Used	Technology
Upington	Eskom	Dish-Engine Plant
Month	Gross Electric Output (MWh)	Monthly Energy (MWh)
Jan	19,900	19,054
Feb	13,401	12,811
Mar	12,789	12,122
Apr	15,452	14,785
May	14,561	13,940
Jun	11,973	11,393
Jul	14,518	13,913
Aug	12,615	11,993
Sep	16,838	16,157
Oct	19,439	18,708
Nov	24,336	23,484
Dec	26,647	25,809

CLFR model results

In addition to the annual results tabled in chapter 6, monthly energy values and water consumption figures were obtained from the SAM linear Fresnel model. These results are tabled in this section. Only the monthly energy metric output was provided by the linear Fresnel model.

Table E3: CLFR model monthly results

Case 1	
Location	Upington
Solar Radiation Data Used	Weather Analytics Inc.
Technology	Linear Fresnel Plant
Power Cycle Cooling Method	Evaporative
Month	Monthly Energy (MWh)
Jan	37,774
Feb	33,679
Mar	37,418
Apr	36,215
May	30,354
Jun	29,262
Jul	30,249
Aug	37,462
Sep	36,709
Oct	37,925
Nov	36,756
Dec	37,877
Case 2	
Location	Upington
Solar Radiation Data Used	Weather Analytics Inc.
Technology	Linear Fresnel Plant
Power Cycle Cooling Method	Air-cooled
Month	Monthly Energy (MWh)
Jan	35,820
Feb	32,101
Mar	35,996
Apr	35,146
May	29,865
Jun	29,052
Jul	30,162
Aug	36,967
Sep	35,755
Oct	36,375
Nov	34,968
Dec	35,783
Case 3	
Location	Upington
Solar Radiation Data Used	CRSES
Technology	Linear Fresnel Plant
Power Cycle Cooling Method	Evaporative
Month	Monthly Energy (MWh)
Jan	37,194

Feb	33,530
Mar	36,722
Apr	35,722
May	30,377
Jun	29,241
Jul	30,284
Aug	37,483
Sep	36,544
Oct	37,867
Nov	36,702
Dec	37,636
Case 4	
Location	Upington
Solar Radiation Data Used	CRSES
Technology	Linear Fresnel Plant
Power Cycle Cooling Method	Air-cooled
Month	Monthly Energy (MWh)
Jan	36,276
Feb	32,271
Mar	35,753
Apr	35,122
May	30,101
Jun	29,285
Jul	30,313
Aug	37,282
Sep	35,907
Oct	36,638
Nov	35,398
Dec	36,054
Case 5	
Location	Upington
Solar Radiation Data Used	SAWS
Technology	Linear Fresnel Plant
Power Cycle Cooling Method	Evaporative
Month	Gross Electric Output (MWh)
Jan	37,099
Feb	33,184
Mar	36,402
Apr	35,057
May	30,062
Jun	29,097
Jul	30,094
Aug	36,486
Sep	35,588

Oct	37,169
Nov	36,265
Dec	37,378
Case 6	
Location	Upington
Solar Radiation Data Used	SAWS
Technology	Linear Fresnel Plant
Power Cycle Cooling Method	Air-cooled
Month	Gross Electric Output (MWh)
Jan	36,199
Feb	31,946
Mar	35,457
Apr	34,528
May	29,848
Jun	29,201
Jul	30,192
Aug	36,405
Sep	35,041
Oct	36,013
Nov	35,001
Dec	35,819
Case 7	
Location	Upington
Solar Radiation Data Used	Eskom
Technology	Linear Fresnel Plant
Power Cycle Cooling Method	Evaporative
Month	Gross Electric Output (MWh)
Jan	37,341
Feb	33,051
Mar	36,333
Apr	35,655
May	30,197
Jun	29,214
Jul	30,237
Aug	36,532
Sep	36,181
Oct	37,443
Nov	36,584
Dec	38,030
Case 8	
Location	Upington
Solar Radiation Data Used	Eskom
Technology	Linear Fresnel Plant
Power Cycle Cooling Method	Air-cooled

Month	Gross Electric Output (MWh)
Jan	37,384
Feb	33,145
Mar	35,530
Apr	35,071
May	29,932
Jun	29,264
Jul	30,278
Aug	36,427
Sep	35,552
Oct	36,380
Nov	35,272
Dec	36,389